IMINE-DONOR COMPLEXES WITH GROUP 6 AND GROUP 11 TRANSITION METALS: COORDINATION AND DYNAMICS

by

LEIGH-ANNE DE JONGH

Thesis submitted in fulfilment of the requirements for the degree of

Master of Chemistry in the Faculty of Science at Stellenbosch University

SUPERVISOR: DR. S. CRONJE

CO-SUPERVISOR: PROF. H.G. RAUBENHEIMER

DECEMBER 2008

Declaration

By submitting this thesis electronically, I declare that the entirety of the work contained therein is my own, original work, that I am the owner of the copyright thereof (unless to the extent explicitly otherwise stated) and that I have not previously in its entirety or in part submitted it for obtaining any qualification.

Date: December 2008

SUMMARY

In this study the coordination of ligands with several coordination sites, 2-aminoazoles (2-amino-4-methylthiazole), 2-aminobenzothiazole, 2-aminobenzoimidazole and 2-aminothiazoline and a biguanidine (*N*-(2-methylphenyl)imidodicarbonimidic diamide) to soft metal centres [gold(I) (group 11), chromium(0) (group 6) and tungsten (0) (group 6)] was investigated. The aminoazoles have three coordination sites, an exocyclic amine nitrogen, an endocyclic imine nitrogen and an endocyclic thioether sulphur. The biguanidine ligand has three sites for deprotonation, one central amine and two imine nitrogens, and at least five sites available for nitrogen coordination.

Reaction of the 2-aminoazoles with $Au(C_6F_5)(tht)$ yielded the unexpected homoleptically rearranged bis(pentafluorophenyl)gold(I) complexes with various cations including a 2-aminoazolium and lithium cation. The exception was provided by 2-aminothiazoline which substituted tht in $Au(C_6F_5)(tht)$ to yield the known product $Au(C_6F_5)$(2-aminothiazoline). The full characterisation of this compound was completed by the determination of its molecular structure. The compound is linear and the Au-C and Au-N bond lengths are in good agreement with literature values reported for related compounds. Endocyclic imine nitrogen (borderline hard) coordination of the 2-aminothiazoline to gold(I) did not alter the ligand's bond lengths and angles substantially. Different combinations of intermolecular forces govern the crystal lattice organisation in the solid state. These include aurophilic interactions, π-π interactions and hydrogen bonding.

It could be argued that the Au(I) centre is hardened by the C_6F_5 group but coordination of the 2-aminoazole ligands to $Au(PPh_3)^+$ units by reaction with $Au(PPh_3)NO_3$ showed the same preference for the endocyclic imine nitrogen donor. A series of new complexes, (2-amino-4-methylthiazole)(triphenylphosphine)gold(I) nitrate, **6**, (2-aminobenzothiazole) (triphenylphosphine)gold(I), nitrate, **7** and (2-aminobenzimindazole)(triphenylphosphine) gold(I) nitrate, **10A** and **10B**, were characterised by single crystal X-ray structure determinations, IR and NMR spectroscopy and FAB-MS spectrometry. The labilising *trans* influence of the 2-aminoazole ligands was clearly demonstrated by the elongation of the Au-P bond. The geometry at the gold(I) centres is linear, Au-N bond lengths are similar to previously reported values and the structural parameters of the 2-aminoazole

ligands do not differ significantly from the uncoordinated 2-aminoazoles. The unexpected two-coordinated silver complex, bis(2-aminobenzothiazole)silver(I), **8**, nitrate, was also isolated from the reaction mixture of (2-aminobenzothiazole) (triphenylphosphine)gold(I) nitrate, **7**. The small amount of silver present was obtained, when $Au(PPh_3)Cl$ was treated with an excess of $AgNO_3$ to afford starting material $Au(PPh_3)NO_3$. The molecular structure of this compound was determined.

Again the reaction of 2-aminothiazoline and $Au(PPh_3)NO_3$ provided an exception. An interesting and unusual ring opening of the heterocyclic ligand occuring *via* possible deprotonation and proton migration produced a mercapto-ethyl-cyanamide ligand coordinating through the sulphur atom. The molecular structure determination of the product, **9**, revealed the presence of an intramolecular aurophilic interaction. The solid state assembly of the above compound is governed by intermolecular aurophilic interaction, π-stacking and hydrogen bonding.

The isolated 2-aminoazole compounds show the same coordination preference as for gold(I), when reacted with the soft group 6 metal centres. They are coordinated to the fragments, $(CO)_5Cr$ and $(CO)_5W$, *via* the borderline hard imine donor despite the presence of a soft thioether in the ligand. The new complexes, (2-aminobenzimidazole) pentacarbonylchromium(0), **12**, (2-amino-1-methyl-benzimidazole)pentacarbonyl-chromium, **13**, (2-aminobenzothiazole)pentacarbonylchromium, **14**, (2-amino benzothiazole)pentacarbonyltungsten(0), **17**, (2-aminobenzimidazole)pentacarbonyl-tungsten(0), **18** and (2-aminothiazoline)pentacarbonyltungsten, **19**, were all fully characterised and the molecular structures of **12-14** and **17-19** were determined. In the solid-state it was evident that different combinations of intermolecular forces determine the crystal lattice organisation.

The biological activity displayed by metformin together with the known anti-cancer potential of (phosphine)gold(I) compounds and cationic gold(I) compounds provided the impetus for the preparation and characterisation of gold(I) and gold(III) complexes of the metformin analogue, *N*-(2-methylphenyl)imidodicarbonimidic diamide. The molecular structure of an interesting dinuclear bridged gold(I) compound, bis[μ_2-bis(diphenyl phosphino)]methane(nitrato)digold(I) (**20**) co-crystallised with deuterated methanol, bis(pentafluorophenyl)gold(I) complexes with imonium cations (**21**, **21A**) and a new

gold(III) complex, *cis*-dichloro(*N*-(2-methylphenyl)imidodicarbonimidic diamide)gold(III), **22**, were determined. The bonding parameters of the backbone of *N*-(2-methylphenyl)imidodicarbonimidic diamide do not differ significantly from those in the free ligand and the solid state packing shows that intermolecular Au···Au interaction, π-stacking and hydrogen bonding determine the crystal lattice organisation.

OPSOMMING

In hierdie studie is die voorkeur koördinasie-posisies van 2-aminoasool ligande soos 2-amino-4-metieltiasool, 2-aminobensotiasool, 2-aminobensimidasool en 2-aminotiasolien en ‘n biguanidien, *N*-(2-metielfeniel)imidodikoolstofimidiese diamied aan verskeie sagte metaalkerne soos goud(I) (groep 11), chroom(0) (groep 6) en wolfram(0) (groep 6), ondersoek. Die 2-aminoasool ligande beskik oor drie koördinasieposisies, o.a. ‘n eksosikliese amien, endosikliese imien en ‘n endosikliese thioeter terwyl die biguanidien ligand oor drie deprotoneringsposisies, o.a. die sentrale amien en twee imien stikstowwe, en minstens vyf moontlike koördinasieposisies beskik.

Die reaksie van die 2-aminoasole met $Au(C_6F_5)(tht)$ produseer komplekse wat ‘n homoleptiese herrangskiking ondergaan om bis(pentafluorofeniel)goud(I) met ‘n verskeidenheid van katione, o.a. 2-aminoasolium en litium te lewer. Die 2-aminotiasolien het die tht in $Au(C_6F_5)(tht)$ gesubsitueer om ‘n $Au(C_6F_5)$(2-aminotiasolien) kompleks te lewer en is dus die enigste uitsondering op die reël. Die bepaling van molekulêre struktuur was nodig om volledige karaterisering te voltooi. Die komplekse is lineêr met Au-C en Au-N bindings lengtes wat ooreenstem met beskikbare literatuurwaardes van soortgelykte produkte. Die koördinasie van 2-aminotiasolien *via* die endosikliese imien stikstof atoom laat die bindingslengtes en -hoeke van die ligand onveranderd. Dis duidelik dat verskillende kombinasies van intermolekulêre kragte soos aurofiliese interaksies, π-π pakking en waterstofbindings die kristalroosterorganisasie in die vaste toetsand bepaal.

Dit kan verwag word dat the Au(I) atoom simbiotiesverhard word deur die teenwoordigheid van die C_6F_5 groep maar koördinasie van die 2-aminoasool ligand aan die $AuPPh_3$ eenheid, deur die reaksie met $Au(PPh_3)NO_3$ uit te voer, toon dieselfde voorkeur vir die endosikliese imien stikstof donor. ’n Reeks nuwe komplekse, (2-amino-4-metieltiasool)(trifenielfosfien)goud(I) nitraat, **6**, (2-aminobensotiasool)(trifeniel-fosfien)goud(I) nitraat, **7** en (2-aminobensimindasool)(trifenielfosfien)goud(I) nitraat, **10A** en **10B** is ten volle gekarakteriseer deur KMR-, IR- en FAB-MS analises sowel as enkelkristal X-straaldiffraksie struktuurbepalings. Interessante strukturele karaktereinskappe onthul deur die ondersoek van die komplekse in die vaste toestand, sluit

in die labiliserende *trans* invloed van die 2-aminoasool ligande op die trifenielfosfien ligande in. Hierdie verskynsel is duidelik vanuit die waargenome Au–P bindingsverlengings. Die geometrie rondom die Au(I) kerne is lineêr en die Au-N bindingslengtes stem ooreen met gerapporteerede strukturele parameters en waardes vir 2-aminoasool in die literatuur en onthul dat koördinasie van die vry ligande aan ’n goud(I)-kern nie tot noemenswaardige veranderinge in die bindings lengtes en hoeke van die ligande aanleiding gee nie. Die ongewone twee gekoördineerde silver(I) kompleks, bis(2-aminobensotiasool)silver(I) nitraat, **8**, is uit die reaksiemengsel wat (2-amino-bensotiasool)(trifenielfosfien)goud(I) nitraat, **7**, bevat geisoleër en die molekulêre struktuur daarvan is bepaal.

Die 2-amniotiasolien is weerens die uitsondering op die reël, in die reaksie daarvan met $Au(PPh_3)NO_3$, word‘n unieke ringopening van die heterosikliese ligand waargeneem word. Die ringopening onstaan moontlik deur deprotonering en protonmigrasie om ‘n nuwe ligand, 2-merkapto-etiel-sianamied te lewer, wat deur die swaelatoom koördineer en sodoende ’n interessante verskynsel lewer. Die molekulêre struktuur van die produk, **9**, verskaf inligting aangaande intramolekulêre aurofiliese interaksies. Vanuit die vaste toestand pakking van die kompleks blyk dit dat verskillende kombinasies van intermolekulêre kragte die organisasie van die kristalrooster bepaal. Dit sluit swak intermolekulêre aurofiliese interaksies, π-π interaksies en waterstofbindings in.

Die geisolëerde 2-aminoasoolkomplekse toon dat dieselfte koördinasievoorkeur wat waargeneem is by goud(I) weereens ter sprake is by die koördinasie aan sagte groep 6 metaalkerne. Die ligande koördineer aan die fragmente $(CO)_5Cr$ en $(CO)_5W$ *via* die grensgeval harde imien stikstof alhoewel die sagte tioeter-groep ook beskikbaar is vir koordinasie. Die nuwe komplekse, (2-aminobensimidasool)pentakarbonielchroom(0), **12**, (2-amino-1-metiel-bensimidasool)pentakarbonielchroom(0), **13**, (2-aminobensotiasool) pentakarbonielchroom, **14**, (2-aminobensotiasool)pentakarbonieltungsten(0), **17**, (2-aminobensimidasool)pentakarbonieltungsten(0), **18** en (2-aminotiasolien)pentakarboniel tungsten, **19** is almal volledig gekarakteriseer en molekulêre strukture van **12**-**14** en **17**-**19** is bepaal. Die vaste toestand pakking van die komplekse word bepaal deur verskillende kombinasies van intermolekulêre kragte.

Die biologiese aktiwiteit van metformin en fosfiengoud(I) asook spesifiek kationiese goud(I) verbindings se anti-kankeraktiwiteit het as aansporing gedoen vir die bereiding en karakterisering van goud(I)- en goud(III)komplekse van die metformin analoog, *N*-(2-metielfeniel)imidodikoolstofimidiese diamied. Die molekulêre struktuur van 'n interessante, bikernige gebrugte goud(I) kompleks, bis[μ_2-bis(difenielfosfien)]metaan(nitrato)digoud(I), **20**, wat met gedeutereerde metanol gekristaliseer het is bepaal. Twee *bis*(pentafluorofeniel)goud(I) komplekse met imonuim katione (**21**, **21A**) en die nuwe goud(III)kompleks, *cis*-dichloro(*N*-(2-methylphenyl)imidodikoolstofimidiese diamied)gold(III) chloried **22**, is bepaal. Die bindingsparameters van die ruggraat van die *N*-(2-metielfeniel)imidodikoolstofimidiese diamied verskil nie merkwaardig van die vry ligand nie en pakking in die kristalrooster toon die teenwoordigheid van Au···Au interaksies, π-π interaksies en waterstofbindings aan.

To my parents that supported me

To my supervisors that encouraged me

And

To my friends and co-workers that were always there for me

The flask is our canvas…
the periodic table is our paint.

ACKNOWLEDGEMENTS

There are people that have meant a great deal to me during this study and who have made this year a rewarding and enriching experience. I would like to mention the following people in particular:

First of all I would like to thank my parents for their sustained love and support throughout my studies and for always providing me with a never-ending sea of opportunities.

All my friends for providing support and healthy distractions, especially Storm and Leigh for being the best gym buddies ever. Zaskia for being the only person that is crazy enough to swim in the winter with me and for always putting a smile on my face - it was priceless.

Dr. Cronje, for your important contribution to this study, all your support and good advice. Prof. Raubenheimer, for your kind interest in this study as well as your indispensable advice, suggestions and ideas. All the members of the organometallic chemistry group for creating a stimulating and pleasant working environment. Adelé, for providing us with non-academic reading material every Tuesday and your friendship. Elzet, for your patience and for being approachable whenever for whatever. Christoph, for all your patience during the collection of X-Ray data and refinement. Bertie, for all your crazy stories. Summer for appreciating everything and for just being you. Again I would like to thank Christoph, for X-ray data collections and refinements.

Jean and Elsa for excellent NMR services and kindness. Mr. Ward for your speedy service, friendly smiles and interesting conversations in the passage. Mrs. May for your kindness and patience.

I would also like to welcome the newest member of our chemistry family, baby Cronje, Béatrice.

Finally, for financial support, I would like to thank the National Research Foundation and Stellenbosch University.

Certain aspects of the work in this study have already been presented in the form of:

A poster presentation by the author at the SACI Inorganic Conference 2007, Langebaan, Western Cape, 8-12 th July 2007, titled "Amino-azole and biguanide complexes of Au(I) and Cr(0)."

Publication: L.A. de Jongh, C.E. Strasser, S. Cronje, H.G. Raubenheimer, "*Bis(diphenylphosphino)]methane-digold(I) perdeuteromethanol nitrate*". *Acta Crystallogr.,* **2007**, *E63(8)*, m2137.

CONTENTS

CHAPTER 3

Novel 2-aminoazole complexes of chromium(0) and tungsten(0)

CHAPTER 4

Preparation and characterisation of novel gold(I) and gold(III) complexes containing *N*-(2-methylphenyl)imidodicarbonimidic diamide

ABBREVIATIONS

	Å	Ångstrom (10^{-10} m)
	amt	2-aminothiazoline
	Ar	Aromatic
	bipy	bipyridine
	Cys	Cystine
	ºC	Degrees Centigrade
	DMSO	Dimethyl sulfoxide
	dppm	Bis(diphenylphosphino)methane
	decomp.	Decomposition
	ES	Electron Spray
	FT	Fourier Transform
	His	Hystidine
	IR	Infrared
	L	Ligand
	M_f	Molecular formula
	M_r	Relative molecular mass
	Me	Methyl
	m.p.	Melting point
	MS	Mass spectrometry
	n.a.	Not applicable
	n.o.	Not observed
	pfp	Pentafluorophenyl
	R	Alkyl, aryl or hydrogen group
	rt	Room temperature
	^{t}Bu	Tertiary butyl
	^{t}BuIm	Tertiary butylimidazole
	TLC	Thin Layer Chromatography
	THF	Tetrahydrofuran
	tht	Tetrahydrothiophene
NMR	bs	Broad singlet
	d	Doublet
	dd	Doublet of doublets
	δ	Chemical shift (ppm)
	J	Coupling constant (Hz)
	m	Multiplet
	MHz	Megahertz
	ppm	Parts per million
	q	Quartet
	s	Singlet
	t	Triplet
	Δ	difference
MS	FAB-MS	Fast atom bombardment mass spectrometry
	EI-MS	Electron impact mass spectrometry
	M^+	Molecular ion
	m/z	Mass/charge ratio
IR	ν	Stretching vibration
	δ^{b}_{oop}	out of plane bending
	δ^{b}	bending vibration

st	Strong
w	weak
m	medium

Chapter 1

The coordination chemistry of gold(I), gold (III), chromium(0) and tungsten(0).

1.1 Brief introduction to gold chemistry

Gold has the electronic ground state configuration of [Xe] [$4f^{14}$] [$5d^{10}$] $6s^1$, giving rise to gold(I) compounds with the closed shell configuration [$5d^{10}$], which is analogous to the situation in copper(I) [$3d^{10}$] and silver(I) [$4d^{10}$]. Gold(I) complexes are traditionally obtained from predominantly soft donor ligands, these complexes are normally two coordinated, but examples where complexes adopt three- or four coordination are known. These phenomena where Au^+ is reluctant to accept more than two ligands, i.e. its poor acceptor character, are at variance with the properties of it's Cu^+ and Ag^+ congeners and are an indication of the gold valence orbitals modified by relativistic effects.[1] Gold is known to display unique chemical behaviour compared to other transition metals. It not only possesses the highest oxidation potential, but also the highest electron affinity of all metal atoms. These distinctive characteristics have been rationalised through the concept of relativistic effects, which reach a maximum for this noble metal. The unusual redox properties were first attributed to lanthanide contraction which extends over the whole of the 5d block and beyond Hf-Hg and Tl-Bi but this did not explain the maxima of the redox potential and electron affinity displayed by the gold atom.[2] Thus the lanthanide contraction along with relativistic effects is the only rational explanation to describe this maximum at the gold atom. The relativistic effect can be summarised as the contraction of the s-orbital and the expansion of the d-orbitals, thus reducing the energy separation between the s- and d-orbitals which constitute the valence shell. The magnificent colour of bulk gold can be ascribed to this small energy gap. The $5d^{10}$ electrons are no longer chemically inert and can participate in bonding, although in a lesser bond contribution. The resulting smaller energy gap between the 5d and 6s and the modified spin-orbital effects, afford hybrid orbitals suitable for the formation of strong bonds in several geometries which allows for the formation of energetically more favourable complexes of

[1] H. Schmidbaur, *Gold Bull.* **2000**, *33*, 3.
[2] H. Schmidbaur, S. Cronje, B. Djordjevic, O. Schuster, *Chem. Phys*. **2005**, *311*, 151.

gold centres with the higher oxidation states of Au^{III} and Au^{V}. Bonding between gold(I) centres, with equal charge, can also now be better understood in light of these considerations.[3]

The molecular chemistry of gold is very interesting since gold can exist in a variety of oxidation states, ranging from -1 to 5. Of these states, only Au(0), Au(I) and Au(III) are stable in aqueous biological environments and are dominated by Au(I) and Au(III). The Au^{+} complexes are generally found to be two-coordinated complexes with linear geometry. The ligands can be neutral (L) or anionic (X^{-}) affording a general type of complex which is cationic, neutral or anionic[2] (Scheme 1.1).

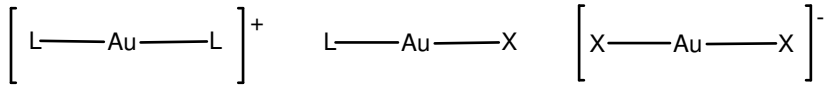

Scheme 1.1: Two-coordinated gold(I) complexation patterns.

Gold(III) mostly exhibits a square-planar geometry.[4] Many ligands form stable complexes with Au(III), thus leading to a range of complexes with a variety of chemical and physical properties.[5] Au(III) has ground state configuration [Xe] [$4f^{14}$] [$5d^{8}$], thus making it a low spin d^{8}, diamagnetic species which coordinates with ligands to form mostly four-coordinate square-planar complexes.[5] The gold(III) complex, $HAuCl_4$, has been shown to be an inhibitor of avian myeloblast and reverse transcriptase at concentrations that are non-toxic to HeLa cells.[6] The high oxidation power of Au(III) complexes limits the number of nucleophiles for which ligand substitution can be investigated without encountering complications associated with redox reactions.[7] Certain soft nucleophiles can act as reducing agents to reduce Au(III) to Au(I) and Au(III) forms complexes more readily with harder ligands than Au(I).

Most of the time gold metal forms a bond with another atom by simply formally donating an electron to attain an extremely stable electronic state. Conventional wisdom states that

[3] M.C. Gimeno, A. Laguna in: *Comprehensive Coordination Chemistry II*, *Vol. 6* (Eds. J.A. McCleferty and T.J. Meyer), Elsevier Pergamon, Oxford, **2004**, p. 911.
[4] C.F. Shaw III, *Chem. Rev.* **1999**, *99*, 2589.
[5] C.F. Shaw III in: *Gold Progress in Chemistry, Biochemistry and Technology* (Ed. H. Schmidbaur), John Wiley & Sons, Ltd., **1999**, Chichester, p. 260.
[6] S.P. Fricker in: *The chemistry of organic derivatives of gold and silver* (Eds. S. Patai, Z. Rappaport), John Wiley & Sons, Ltd, **1999**, p. 641.
[7] F.J. Monlien, L. Helm, A. Abou-Hamdan, A.E. Merbach, *Inorg. Chim. Acta*, **2002**, *331*, 257.

atoms in such a state should not engage in any further external bonding but Schmidbaur showed through accumulated experimental evidence,[8] while state of the art quantum chemical calculations were performed by Pyykkö,[9] that there is evidence of strong metal-metal interaction between gold centres in metal complexes.

The implementation of solid-state analyses, *via* the single crystal X-ray diffraction technique has revealed interesting supramolecular interactions between gold centres, which have attracted a particular amount of attention in recent years, and are still pertinent in studies which are presently undertaken. These interactions can be further divided into intermolecular- (i.e between gold centres in two different molecules) and intramolecular Au···Au (within the same molecule) interactions. These weak interatomic attractive forces are mostly between d^{10} gold atoms, were initially interpreted using semi-empirical molecular orbital calculations in terms of electron donation from a filled d-orbital on one metal centre to an empty p-orbital on a second and *vice versa*.[10] However, more sophisticated *ab initio* calculations revealed that these bonding effects do not contribute significantly to the bonding energies calculated at the Hartree–Fock level and the origin of this stabilisation is electronic and corresponds to effects similar to those found in van der Waals molecules like Mg_2 and Ar_2[11] which are enhanced in case of gold by relativistic effects.[12] Pyykkö has attributed these interactions to correlation effects enhanced by relativistic effects,[13] where the relativistic effect can be summarised as the already mentioned contraction of the outer s-orbital and the expansion of the d-orbitals which reduces the energy separation between the valence shells of gold. The quantum definition of aurophilic bonding describes Au···Au interaction as an effect based largely on electron correlation of the closed-shell components, somewhat similar to van der Waals interactions, but usually stronger and therefore cautiously addressed as "super van der Waals interactions." The Au···Au separation (2.8-3.3 Å) is longer than the sum of the metallic radii but shorter than the sum of the estimated van der Waal radii of gold (3.60Å).[14]

---

[8] H. Schmidbaur in: *Gold: Progress in Chemistry Biochemistry and Technology* (Ed. H. Schmidbaur), John Wiley & Sons Ltd., Chichester, **1999**, p. 259.
[9] P. Pyykkö, *Chem. Rev*., **1997**, *97***,** 579.
[10] P.K. Mehrotra, R. Hoffmann, *Inorg. Chem*., **1978**, *17*, 2187.
[11] J. Li, P. Pyykkö, *Inorg. Chem*., **1993**, *32*, 2630.
[12] P. Pyykkö, N. Rudenburg, *J.Chem. Soc., Chem. Comm*., **1993**, 1812.
[13] P. Pyykkö, *Angew. Chem. Int. Ed. Engl.,* **2004**, *43*, 4412.
[14] D. Micheal, P. Mingos, *J. Chem.Soc., Dalton Trans*, **1996**, 561.

The strength of aurophilic interaction can be thought of as intermediate between a conventional covalent or ionic bond and a van der Waals interaction. The strength of aurophilic interactions have been estimated by NMR experiments to be of the same order of magnitude as that of a typical hydrogen bond (29-33 kJ/mol).[15] These Au···Au interactions also often play a determining role in the molecular configurations and crystal lattice organisation of gold(I) complexes.[16,17]

The chemistry of gold is dominated by the typically linear gold(I) and square-planar gold(III) derivatives. Among the gold complexes, those with gold(I) centres are the most widespread and will largely be the focus of the study.

The aim of this chapter is not to represent a comprehensive overview of the vast literature available on the topic of gold chemistry, but to present some of the reasons for using gold derivatives with N, P and S donor ligands. The emphasis will be placed on N donors since my study is mostly aimed at investigating nitrogen containing ligands with multiple bonding sites. Although gold chemistry has made advances in a wide number of fields, this chapter will deal with its medicinal applications. Additional information appears in the introductory section of each of the following chapters.

1.2 Interesting developments in gold chemistry

1.2.1 Sulphur donor ligands in gold chemistry

Of all of the sulphur-containing gold complexes that have shown potential as drugs, the phosphine(thiolate)gold(I) complexes are of particular interest owing to their relation to the gold-based drug auranofin, which is utilised in the treatment of rheumatoid arthritis (Scheme 1.2).[18]

[15] H. Schmidbaur, W. Graf, W. Müller, G. Müller, *Angew. Chem. Int,. Ed. Engl.* **1988**, *27*, 417.
[16] M.C. Gimeno, A. Laguna, *Gold Bull.* **2003**, *36*, 83.
[17] C.E. Strasser, W. Gabrielli, C. Esterhuysen, O.B. Schuster, S.D. Nogai, S. Cronje, H.G. Raubenheimer, *New. J. Chem*., **2008,** *32*, 138.
[18] P.J. Barnard, M.V. Baker, S.J. Berners-Price, D.A. Day, *J. Inorg. Biochem.,* **2004**, *98*, 1642.

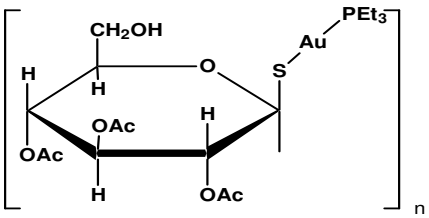

Scheme 1.2: Auranofin the current drug being used in the treatment of rheumatoid arthritis.

The thioethers, dimethylsulfide and tetrahydrothiophene (Scheme 1.3), are weak σ-donors and are readily displaced by ligands with superior donor abilities. The gold(I) and gold(III) complexes containing dialkyl sulphides (SMe_2) or tetrahydrothiophenes (SC_4H_8) have frequently been used as versatile precursors in the synthesis of new gold complexes, since they are generally stable at room temperature and their sulphur containing ligand can readily be replaced by other neutral or anionic ligands.[19, 20, 21, 22] In this study $[Au(C_6F_5)(tht)]$ was employed as a precursor complex because of the labile nature of tetrahydrothiophene.

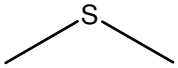

dimethylsulfide

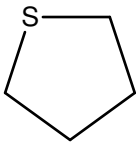

tetrahydrothiophene

Scheme 1.3: The thioethers often used as ligands in precursor gold complexes.

Although the generalisation that gold(I) prefers S-donor to N-donor ligands is sometimes made, Cronje and co-workers[23] have recently shown that gold(I) centres, when provided with a choice between borderline-hard imine and soft endo- and exocyclic thioether ligands, prefer imine coordination. This finding is confirmed by the emerging number of gold(I) imine and amine complexes prepared by substitution of thioether ligands.

[19] R.Usón, A. Laguna, J. Vincente, *J. Organomet. Chem.,* **1977**, *131*, 471;
[20] R.Usón, A. Laguna, M. Laguna and E. Fernandez, *J. Chem. Soc., Dalton Trans*., **1982**, 1971.
[21] M.R. Awang, G.A. Carriedo, J.A.K. Howard, K.A. Mead, I. Moore, C.M. Nunn, F.G.A. Stone, *J. Chem. Soc., Chem. Commun.*, **1983**, 964.
[22] J. Coetzee, W.F. Gabrielli, K. Coetzee, O. Schuster, S.D. Nogai, S. Cronje, H.G Raubenheimer, *Angew. Chem. Int. Ed*., **2007**, 46, 2497
[23] S. Cronje, H. G. Raubenheimer, H.S.C. Spies, C. Esterhuysen, H. Schmidbaur, A. Schier, G. J. Kruger, *Dalton Trans.* **2003**, 2859.

1.2.2 Phosphorus donor ligands in gold chemistry

Most of the gold complexes described in literature are those that contain phosphorus donors. The phosphorus donor ligand forms stable complexes with metal centres in both high and low oxidation states. Gold(I) has a d^{10} configuration which is capable of retro-donation to both an anti-bonding orbital on a phenyl ring and the empty d-orbital on a phosphorus atom in a phosphine ligand. Nicolas[24] implemented ^{19}F NMR spectra to obtain information about π-interaction in a series of tertiary phosphine gold phenyl complexes. The ^{19}F NMR π-acceptor parameters measure the amount of π-interaction between gold and phenyl but it is not correct to assign the overall change measured to the π-interaction only. The changes in σ-donor power of the phosphine will alter the energy difference between the gold-d orbital and the anti-bonding phenyl orbital and thus affect the π-interaction. The σ-effect will not be discussed since it is not known if π-interaction is a result of an increase or decrease in σ-electron donation. The results are based purely on π-interactions and determined using only the chemical shift of the *meta*- and *para*-phenylcarbons in (fluorophenyl)(phosphine)gold complexes in ^{19}F NMR spectra. The difference between the *meta* and *para* chemical shifts is the π-acceptor parameter (Δ). The larger the value of Δ the greater the gold-phenyl π-interaction and hence the smaller the back-donation to the phosphine, while a small Δ implies good π-acceptor character for the phosphine. The results show that the π-acceptor order of phosphines is: $(PhO)_3P$ > $(C_6F_5)Ph_2P$ > Ph_3P ≈ Ph_2 ≈ *para*-$(MeC_6H_4)_3P$ > $PhMe_2P$ ≈ Et_3P ≈ Bu_3P and this agrees with the tendency of electron-withdrawing groups on phosphorus which increase with π-acceptor strength. A variety of gold(I) complexes with the general form $Au(X)(PR_3)$ have been described and recently their potential in medical applications investigated. The bis-chelated diphosphinegold(I) complex $[Au(dppe)_2]Cl$ [dppe = 1,2-bis(diphenylphosphino) ethane] is known to possess anti-tumour activity against a broad range of tumour models.[25]

Two classes of phosphine complexes show anti-tumour activity:[26]

1) neutral two-coordinated gold(I)
2) tetrahedral cationic bischelated gold(I) complexes related to $[Au(dppe)_2]^+$.

---

[24] D.I. Nicholas, *J. Chem. Soc.*, **1970**, 1216.
[25] M.V. Baker, P.J. Barnard, S. J. Berners-Price, S.K. Brayshaw, J.L. Hickey, B.W. Skelton, A.H. White, *Dalton Trans.,* **2006**, 3708.
[26] P.J. Barnard, M.V. Baker, S.J. Berners-Price, B.W. Skelton, A.H. White, *Dalton Trans.,* **2004**, 1038.

1.2.3 Nitrogen donor ligands in gold chemistry

The study of N donor ligands integrated in gold(I) complexes have not been reported extensively. This can be attributed to the previously accepted incompatibility of the soft gold(I) centre and hard to borderline-hard nitrogen donors which supposedly produce complexes of limited stability.[27] Until recently the examples of N-donors in gold(I) complexes in the literature were limited to amine complexes derived from aliphatic and aromatic amines, azoles and others, which were stabilised by inert phosphine ligands. Since the stability of nitrogen containing complexes could be problematical, additional stabilisation needs to be provided. This additional stabilisation is observed in the solid state as intermolecular bonding, i.e. aurophilic interactions or hydrogen bonding. These interactions may compete with each other or co-exist to synergistically stabilise the nitrogen donor complex as was recently shown by Laguna and co-workers.[28] As mentioned previously, Cronje and co-workers[23] have recently shown that gold(I) centres prefer imine coordination when provided with a choice between borderline-hard imine and soft thioether ligands.

1.3 Medicinal applications of gold compounds

Certain gold(I) complexes are known to show anti-malarial activity, anti-HIV activity, antitumour activity, anti-infective activity and are used in the treatment of rheumatoid arthritis.[6] Gold-based drugs are regarded as pro-drugs, they are metabolised and then chemically changed into active forms in the body after administration.[29]

Rheumatoid arthritis is a disease of the joints, with no known cause or cure. It is progressively debilitating due to joint erosion with its concomitant pain and difficulty in movement. The first stage of treatment is non-steroidal anti-inflammatory drugs (NSAID) which reduces inflammation and pain associated with this disease but these do not stop the progression of the disease. The second stage of treatment is disease modifying anti-rheumatoid drugs (DMARD). These drugs are used to slow down the biological process of this disease and guide inflammatory disease into remission.[30] The current DMARD drugs used includes three gold-based drugs, sodium

[27] M.C. Gimeno, A. Laguna in: *Comprehensive Coordination Chemistry II*, *Vol. 6* (Eds. J.A. McCleferty, T.J. Meyer), Elsevier Pergamon, Oxford**, 2004**, p. 1034.
[28] A. Codina, E.J. Fernández, P.G. Jones, A. Laguna, J.M. López-de-Luzuriaga, M. Monge, M.E. Olmos, J. Pérez, M.A. Rodriguez, *J. Am. Chem. Soc*. **2002**, *124*, 6781.
[29] E.R.T. Tiekink, *Crit. Rev. Oncol. Hematol.* **2002**, *42*, 225.
[30] A.A. Mohamed, H.E. Abdou, J. Chen, A.E. Bruce, M.R.M. Bruce, *Comm. Inorg. Chem.* **2002**, *23*, 321.

aurothiomalate (myochrysine), aurothioglucose (solganol), both injectable gold drugs, and [(tetra-O-acetyl-β-D-(glucopyranosyl)thio](triethylphosphine)gold(I)] (auranofin); orally administered (Scheme 1.4).

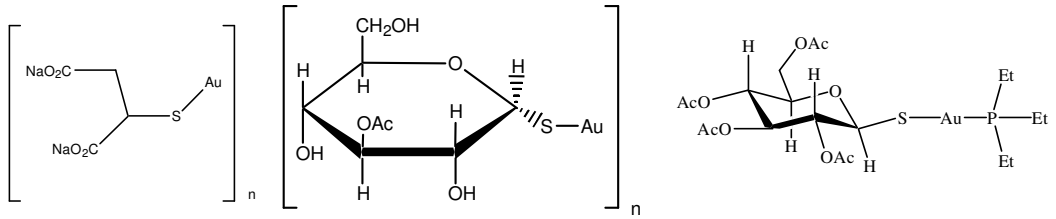

Myochrysine *Solganol* *Auranofin*

Scheme 1.4: Gold-based drugs available in treatment of rheumatoid arthritis.

The disadvantage is that the drugs, myochrysine and solganol, should be injected into the site of inflammation.

The most widely used anti-cancer drug is a Pt(II) complex, cisplatin. Au(III) complexes are isoelectronic and isostructural to platinum(II) complexes, thus similarities in electron configuration and structural characteristics exist, and Au(III) complexes might have potential as anti-tumour agents. Au(III) complexes are generally much more reactive than Pt(II) complexes but toxicity is still problematic.[25] These factors have contributed to a vast amount of research in gold(III) chemistry.

The mitochondria play an important role in the absorption of these gold complexes, since the mitochondria are responsible for regulated programmed cell death and the selective death of carcinoma cells. Mitochondrial dissipation assays conducted on rat liver mitochondria, revealed a significant variation in the degree at which gold compounds enter the cell and thus there is a direct relationship between the swelling of mitochondria and gold uptake.[21] Furthermore, the selective absorption of cationic gold compounds for normal cells is controlled by the lipohilicity/hydrophilicity ratio. The gold complexes can be adjusted to suit the lipohilicity/hydrophilicity ratio by modification through the ligand.

The low tumour selectivity of the available cancer drugs keeps the search to find the "super drug" that can target drug-resistant tumour cells alive. In chapter 2 a study of

imine coordinated gold(I) complexes containing a PPh_3 (since phosphine ligands have displayed biological activity) is reported while in Chapter 4 the incorperation of the *N*-(2-methylphenyl)imidodicarbonimidic diamide (because biguanidines, like metformin, display biological activity for the therapeutic treatment of pain and anxiety, was invesigated.[31,32]

1.4 Introduction to the group 6 metals, tungsten and chromium.

Tungsten metal has an outer electron configuration of $5d^5\ 6s^1$ and is known to exist in oxidation states from -1 to +6 with latter being the most common. Since the metal has such a high melting point, its primary application for many years was as a filament for incandescent lamps. Currently the interest has shifted towards alloys containing tungsten for use in high temperature applications.[33]

Chromium metal has an outer electron configuration of $3d^5\ 4s^1$ and forms complexes in oxidation states of -2 to +6.[34] The greater part of the chromium ore is reduced by heat with coal to give 'ferrochrome', used in manufacture of alloy steels while CrO_3 solutions are employed in the electroplating of chromium on other metals to impart wear resistance and for decorative purposes.

The group 6 metals typically exhibit metallic bcc structures and in the massive state are lustrous, silvery and, when pure, fairly soft. When comparing chromium to vanadium, chromium has a lower melting point and enthalpy of atomisation. The phenomena implies that 3d electrons are now beginning to enter the inert electron core and are less readily delocalised by the formation of metal bonds.[34]

The stable, colourless, crystalline hexacarbonyls, $M(CO)_6$ (M= Cr, W), with the metal in oxidation state 0, are octahedral and diamagnetic as anticipated from the 18-electron rule. The replacement of one or more of the carbonyl groups by a better σ-donor, π-donor or σ-

[31] P. Morain, C. Abraham, B. Portevin, G. De Nanteuil, *Mol. Pharmacol*., **1994**, 46, 732.
[32] W.M. Watkins, J.D. Chutlay, D.G. Sixsmith, H.C. Spencer, R.E. Howells*, J. Phar. Pharmacol*., **1987**, *39*, 261.
[33] Z. Dori in: *Comprehensive Coordination Chemistry: The Synthesis, Reactions, Properties & Applications of Coordination Compounds* (Ed. G .Wilkinson), Pergamon Press, Oxford, **1987**, p. 973.
[34] P.A. Lay, A. Levina in: *Comprehensive Coordination Chemistry II*, *Vol. 4* (Eds. J.A. McCleverty, T.J. Meyer), Elsevier Pergamon, Oxford **2004**, p. 313.

donor / π-acceptor ligand is possible, giving rise to a host of complexes of the general form $[M(CO)_{6-x}L_x]$(charges omitted) (eq 1) or $[M(CO)_{6-2x}(L\text{-}L)_x]$ with L= NO^+, NH_3, CN^-, PF_3 or L-L=bipy, butadiene.

$$M(CO)_6 + xL \longrightarrow M(CO)_{6-x}L_x + xCO \qquad (1)$$

In the discussion of the different ligand types, that follow, focus is directed towards nitrogen coordinated ligands incorporated into metal carbonyl complexes.

1.4.1 σ-Donor ligands

As a result of the M(0) oxidation state, where M= Cr or W, and the fact that σ-donor ligands cannot help dissipate the electron build-up on the metal it appears that at least 3CO groups must remain coordinated to the metal to accept the electron density on the metal. The nitrogen ligands that can be classified as σ-donor ligands are: NEt_3[35] (with x =1, 2), NH_2Cy,[36] MeCN[37] (with x = 1, 2,3), dien,[38] en,[39] 1,3-$Ph_2N_3^-$ [40]or NCS^-.[41]

The IR spectra of $[Cr(CO)_{6-x}(L_x)]$ complexes reveal that with an increase in x more electron density has to be accepted by the remaining carbonyls. In this manner the electron population in the CO π*-orbital increases and leads to a decrease in the M-C bond order and an increase in the C-O stretching vibration frequency, ν(CO).

1.4.2 σ-Donor / π-acceptor ligands.

Such ligands have the capability to donate electrons to the metal and accept electrons back from the metal into $t_{2g}(\pi)$-type orbitals of relatively high energy. These ligands are capable of substituting more than three CO-groups in the $M(CO)_6$ complexes and the value of x varies between four to six for excellent π-acceptor ligands like PF_3. Nitrogen

[35] W. Strohmeier, K. Gerlack, D. von Hobe, *Chem. Ber.*, **1961**, *94*, 164.
[36] C.S. Kraihanzel, F.A. Cotton, *Inorg. Chem.*, **1963**, *2*, 533.
[37] I.W. Stolz, G.R. Dobson, R.K. Sheline, *Inorg. Chem.,* **1963**, *2*, 323.
[38] H. Berhrens, W. Klerk, *Z. Anorg. Allg. Chem.*, **1957**, *292*, 151.
[39] R.B. King, K.C. Nianan, *Inorg. Chem.*, **1957**, *14*, 271.
[40] A. Wojcicki, M.F. Farona, *J. Inorg. Nucl. Chem.*, **1975**, *14*, 1717.
[41] J.K. Ruff, *Inorg. Chem.,* **1969**, *8*, 86.

ligands that can be classified as σ-donor /π acceptor group include py[42], bipy[39], phen[39] terpy[43] and NO.[44]

1.4.3 π-Acceptor nitrogen ligands.

Ligands in this group are capable of stabilizing low valent central metals without the aid of attached carbonyls. The two ligands that are isoelectronic to CO and are excellent π-acceptors are nitrosonium (NO^+) or aryl and alkyl-diazonium ions (N_2R^+). Another group of N donor π-acceptors are members of the α-diimine group (Scheme 1.5). These ligands accept π-electron density from the chromium into the C=N π*-orbitals and are moderately good π-acceptors.

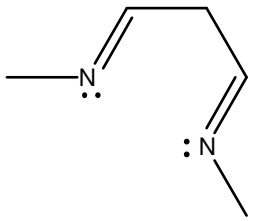

Scheme 1.5: An α-diimine group.

1.5 Recent development involving 2-aminoazole ligands

Intermolecular hydrogen bond interactions are proposed to be significant for the biological activity of molecules involved in biochemical processes in living cells and thus the analyses of crystal systems are very important. Yeşilel and co-workers[45] investigated the above mentioned aspects by analysing the supramolecular squarate and hydrogen squarate compounds with 4-amino-1,2,4-triazole, 2-aminothiazole and 2-aminobenzimidazole. They described three organic amine squarate salts; 4-amino-*4H*-1,2,4-triazolium hydrogensquarate, bis(2-aminothiazolium) squarate and bis(2-amino-*1H*-benzo[*d*]imidazolium) squarate. These organic amine molecules link the sqaurate ions *via* N-H···O hydrogen bonds. Shimizu and co-workers [46] recently patented a 2-

[42] E.W. Abel, M.A. Bennett, G. Wilkinson, *J.Chem. Soc*., **1959**, 2323.
[43] H. Beherens, N. Anders, *Z. Naturforsch., Teil B*, **1964**, *19*, 767.
[44] S.K. Satija, B.I Swanson, *Inorg. Synth*., **1976**, *16*, 1.
[45] O.Z. Yeşilel, M. Odabaşoğlu, O. Büyükgüngör, *J. Mol. Struct*., *874*, **2008**, 151.
[46] K. Shimizu, T. Miyagai, N. Kikuchi, *PCT Int. Appl*.,**2006**, 57.

aminobenzimidazole derivative for potential medical use. This derivative is effective for the treatment of a disease which is caused by abnormal serum acid level and is represented by the general formula in Scheme 1.6.

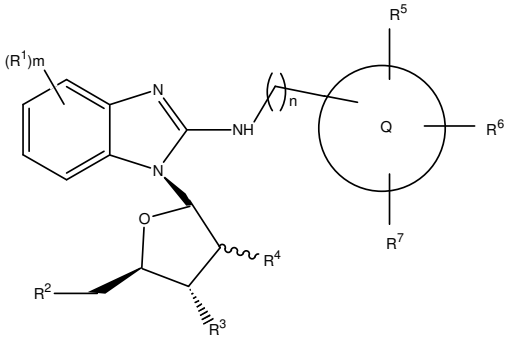

Scheme 1.6: The 2-aminobenzimidazole derivative for potential medical use (where R^1 represents a halogen atom, m is an integer between 0 and 2, n is an integer from 1 to 2, R^2=OH, R^3 and R^4 dependently represent H or OH, the ring Q represents a heterocyclic or bicyclic hydrocarbon, R^5 and R^6 independently represent a cyano group and R^7 represents H, a halogen or a (hetro)aryl group).

1.6 Research objectives and thesis outline.

In the past[7] nitrogen coordinated gold(I) complexes, were considered to be unstable but presently more of these nitrogen coordinated complexes are being isolated. Cronje and co-workers[14] proved that coordination *via* nitrogen is possible even if a soft sulphur atom is available. However the preference of gold(I) for the softer sulphur atom is mostly observed.[7] In this thesis, I aim to investigate the site of coordination of 2-aminoazoles to gold(I), chromium(0) and tungsten(0) in **Chapter 2** and **Chapter 3.** A series of 2-aminoazole ligands, namely 2-aminobenzothiazole, 2-amino-1-methylbenzimindazole, 2-aminobenzimindazole, 2-aminothiazoline and 2-amino-4-methylthiazole,which have more than one possible coordination site (soft sulphur atoms, hard and borderline-hard nitrogen atoms) were employed.

The investigation was planned with reference to the preparation and the structural characteristics, analytical and physical properties, thus full characterisation of the new compounds with the implementation of techniques such as FT-IR spectroscopy, NMR spectroscopy, FAB-MS spectrometry and single crystal X-Ray diffraction.

The results obtained from the coordination of the series of ligands to gold(I) are reported in **Chapter 2** which expands the number of imine coordinated gold(I) complexes and also again emphasizes the importance of the valued gold(I) precursor complexes, $Au(C_6F_5)(tht)$ and $Au(PPh_3)NO_3$. **Chapter 2** provides us with an overview over unexpected homoleptically rearranged products containing $Au(C_6F_5)_2^-$ and various 2-aminoazolium cations or the lithium cations and the successful synthesis and complete characterisation of a series of novel (phosphine)gold(I) complexes derived from the series of 2-aminoazole ligands.

The interesting results obtained in **Chapter 2** inspired the work reported in **Chapter 3** but now using soft metal centres, chromium(0) and tungsten(0), with the implementation of $CO_5Cr(thf)$ and $CO_5W(thf)$ as precursor complexes. The full characterisation of these novel complexes was obtained. **Chapter 3**, thus provides an overview of a series of new 2-aminoazole complexes of chromium(0) and tungsten(0).

As a second part to this thesis, we planned to study the coordination preference of a biguanidine, *N*-(2-methylphenyl)imidodicarbonimidic diamide, upon coordination to gold(I) and gold(III). In **Chapter 4** we investigated the reaction and coordination of *N*-(2-methylphenyl)imidodicarbonimidic as ligand to gold(I) and gold(III). This is a structural study, and it does for the most part involve the analysis of crystal structures obtained throughout our research, and the interpretation of these results.

To summarise the thesis outline: In **Chapter 2**, we will report the investigation of the complex nature of 2-aminoazole ligands upon coordination to gold(I). The new structures of the gold complexes will be analyzed and discussed. Information obtained and tendencies observed in **Chapter 2** were further expanded in **Chapter 3** by the employment of the same series of 2-aminoazole ligands in the preparation of a series of novel chromium- and tungsten complexes. The focus of the area will be on the coordination preference displayed by the 2-aminoazole ligands used in the syntheses of the above mentioned metal complexes which will be analysed and the structures discussed in detail. **Chapter 4** focused on the complexation of *N*-(2-methylphenyl)imidodicarbonimidic diamide (biologically active) with gold(I) and gold(III).

Chapter 2

Aminoazole complexes of gold(I): Coordination and dynamics

2.1 Introduction

In recent years a great interest to study the coordination chemistry of gold with nitrogen donor ligands has emerged especially since the breakthrough discovery that hard donors such as primary,[1,3] secondary[2,3]and tertiary[3] amines and even ammonia[4] can astonishingly form stable complexes with gold(I). The study of imine[5] complexes, with this metal, followed subsequently.

The ability of gold(I), as a naturally soft metal centre, to coordinate to both soft- and hard ligands is well established in the literature.[6] As mentioned previously, in relation to its affinity for sulphur and phosphine donor ligands, gold(I) has a moderate tendency to form complexes with nitrogen donor ligands. The tendencies displayed by gold atoms to aggrate *via* intermolecular and intramolecular aurophilic interactions often induce additional stability in the complexes, resulting in interesting and unpredictable crystal structures in the solid-state. The gold(I) complexes derived from neutral nitrogen donor ligands are predominantly of the type X-Au-L, where X constitutes a halide or pseudo halide anion and L represents a neutral, Lewis base containing nitrogen.

It was initially thought that the affinity of gold(I) for nitrogen was very low and most gold-nitrogen bonds were of limited stability.[7] Schmidbaur *et al.*[8] proved that this affinity is increased if more than one gold atom is present at the nitrogen centre. The polyauration seems to be much more facile than in the introductory step of the

[1] K. Angermaier, H. Schmidbaur, *J. Chem. Soc*., *Dalton Trans.* **1995**, 559.
[2] A. Grohmann, H. Schmidbaur, *Inorg. Chem*. **1992**, *31*, 3378.
[3] J. Vicente, M.-T. Chicote, R. Guerro, P.G. Jones, *J. Chem. Soc*., *Dalton Trans*. **1995**, 1205.
[4] J. Yau, D.M.P. Mingos*, J.Chem. Soc., Dalton Trans*. **1997**, 1103.
[5] W. Schneider, A. Bauer, H. Schmidbaur, *J.Chem. Soc., Dalton Trans.*, **1997**, 415.
[6] J. Strahle, in *Gold*: *Progress in Chemistry, Biochemistry and Tegnology* (Ed H. Schmidbaur), John Wiley & Sons Ltd., Chichester, **1999**, 311.
[7] M.C. Gimeno, A. Laguna in: *Comprehensive Coordination Chemistry II*, *Vol. 6* (Eds. J. A. McCleverty , T. J. Meyer), Elsevier Pergamon, Oxford, **2004**, p.1034
[8] A. Grohmann, J. Riede, H. Schmidbaur, *J. Chem. Soc., Dalton Trans*., **1991**, 783.

metallation of nitrogen.[2] Previous results in gold chemistry had revealed that, as the size of the nitrogen-centred metal increases, so does the stability of the cluster products that form. Most two-coordinated compounds of type L-Au-X display Au···Au interactions but the strength of these interactions are influenced by electronic effects. It was alleged that the extent to which Au···Au interactions are effected, is controlled by electronic effects which depend on the substitutents L and X. Some of the experimental results and theoretical calculations[9] show that the tendency observed is, that the low group electronegativity in the soft ligand shortens the Au···Au distance accompanied with an increase in bond energy. A more recent study by Schmidbaur and co-workers[10] revealed that even within a series the model is contradictory. The more obvious reason for this contradiction is that steric effects play the most vital role since the weak Au···Au interaction is effortlessly overruled by steric repulsions and other components like packing forces.

A study by Schmidbaur and Angermaier[10] endeavoured to investigate the supramolecular aggregation, intramolecular and intermolecular, of nitrogen centered gold cluster cations $[\{Au(PR'_3)\}_nNR_{4-n}]^+$ for different values of n - and for different subsituents R' and R (Scheme 2.1).

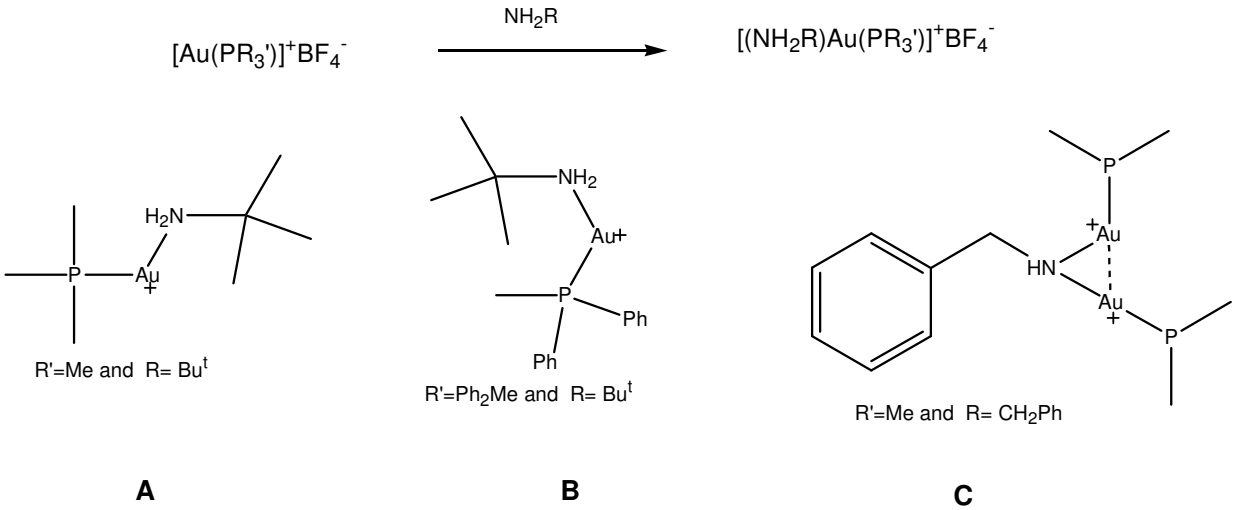

Scheme 2.1: Nitrogen centered gold cluster cations, $[\{Au(PR'_3)\}_nNR_{4-n}]$, with different values of n and different substituents R and R'.

[9] P. Pyykkö, J. Li , N. Runeberg, *Chem. Phys. Lett*., **1994**, *218*, 133.
[10] K. Angermaier, H. Schmidbaur, *J.Chem. Soc., Dalton Trans*. **1995**, 559.

The structures of complexes **A** and **B** show primary amines as donor ligands which are two-coordinated to the gold(I) with the tertiary phosphine as secondary ligand. The intermolecular aurophilic interaction is observed only in complex **A** [Au···Au 3.047(1) Å]. It is absent in complex **B** because of the sterically bulky Bu^t and $MePh_2P$ groups which prevent close metal-metal contact. Complex **C** contains a typical benzylamino group bearing two Me_3PAu^+ substituents at a quaternary nitrogen centre. The Au-N-Au angle is smaller than that of a normal tetrahedron, at 99.9(3)º because of the Au···Au interaction observed, which resembles $[(AuL_2)_2OR]^+$, $[(AuL_2)_2SR]^+$ and $[(AuL_2)_2SeR]^+$ which are valence isoelectronic to **C**.

Cronje and co-workers[11] have also confirmed this preference of gold(I) compounds to coordinate to neutral nitrogen donors above neutral thioether donors in their study to expose the ligand preference of the $[AuC_6F_5]$ centre. Results have shown that the soft acid centre Au^+, in a series of ligand substitutions, displays the following order in decreasing preference: C=S > R_2NH (hard base) >>>C=N-(borderline base) > RSR (soft base). This disagrees with the conventional classification of soft and hard acids and bases which indicates a decreasing preference C=S > RSR (soft base) >>C=N-(borderline base) > R_2NH (hard base). It can be argued that AuC_6F_5 ligand hardens the $[AuC_6F_5]$ centre thus it was necessary to also investigate the coordination site preference on a $[AuPPh_3^+]$ centre.

Recently Shukla and co-workers [12] have shown that coordination of the 2-aminobenzimidazole to some halogen-dimethylsulphoxide/tetramethylenesulphoxide-ruthenium(I) and ruthenium(III) occurs through the imine nitrogen which agrees with our observations in this chapter.

The idea for the implementation of PPh_3AuNO_3 as a starting material with nitrogen containing ligands results from the fact that gold(I) phosphine complexes are renowned for showing potential as anti-tumour agents.[13] These include compounds such as $[Au(Cl)(PEt_3)]$, $[Au(dppe)_2]Cl$ [where dppe = 1,2-bis(diphenylphosphino)ethane] and Auranofin, the latter is, however, more valued for

[11] S. Cronje, H.G. Raubenheimer, H.S.C. Spies, C. Esterhuysen, H. Schmidbaur, A. Schier, G.J. Kruger, *Dalton Trans*., **2003**, 2859.
[12] S.N. Shukla, P. Gaur, H. Kaur, M. Prasad, *J. Coord. Chem*., **2007**, *60*, 1047.
[13] E.R.T. Tiekink, *Gold Bull.* **2003**, *36*, 117.

its role in the treatment of rheumatoid arthritis.

Gold(I) complexes can also be stabilized by thiolate or cyanide ligands, providing gold complexes with the possibility of undergoing associative ligand exchange with proteins and cysteine-rich peptides. The ability of gold thiols to undergo this exchange, with biological ligands may contribute to their pharmacological activity. The unexpected N-coordination of the enzyme cyclophilin to gold(I) *via* the nitrogen atom of an active His residue, despite the presence of four Cys thiol groups, have implications for the understanding of the biochemical mechanisms of gold compounds.[14]

In two coordinate linear gold(I) phosphine complexes, the anti-tumour activity and cytotoxicity are not only modulated by the phosphine substituents but also by the nature of the *trans* ligand. Complexes which contain good leaving groups as *trans* ligand display reduced anti-tumour activity. This arises from the reactivity of these compounds towards thiols. The -SH functional groups present in biomolecules can readily replace labile *trans* ligands to form strong protein–Au(PR_3) bonds, and subsequently prevent gold(I) phosphines from reaching their intracellular targets.[15] This effect must thus be taken into account when choosing a ligand which will be coordinated to the $AuPPh_3$-unit.

Shimizu and co-workers[16] recently patented a 2-aminobenzimidazole derivative for potential medical use. This derivative is effective for treatment of a disease which is caused by abnormal serum acid level.

A comprehensive literature search of gold(I) complexes containing multiple nitrogen coordination sites delivered very few examples. Gold(I) complexes with N-donor ligands have not been studied extensively, probably due to their supposed limited stability arising from the incompatibility of the soft gold(I) centre and the hard to borderline hard nitrogen donors. The majority of the literature of gold(I) complexes describes ligands containing

[14] J. Zou, P. Taylor, J. Dorman, S.P. Robinson, M.D. Walkinshaw, P.J. Sadler, *Angew. Chem,. Int. Ed*., **2000**, *39*, 2931.
[15] S. Berners-Price, P.J. Sadler in: *Bioinorganic Chemistry* (Eds. M.J. Clarke, J.B. Goodenough, J.A. Ibers, C.K. Jørgenen, D.M.P. Mingos, J.B. Neilands, G.A. Palmer, D. Reinen, P.J. Sadler, R. Weiss, R.J.P. Williams), Springer-Verlag, Germany, **1988**, p. 38.
[16] K. Shimizu, T. Miyagai, N. Kikuchi, *PCT Int. Appl*.,**2006**, 57.

sulfur atoms. The lack of gold(I) complexes coordinated directly to an imine donor, initiated the first part of this study. This chapter was aimed at expanding the number of imine coordinated gold(I) complexes and once again emphasizing the importance of the valued gold(I) precursor complexes, $Au(C_6F_5)(tht)$ and $Au(PPh_3)NO_3$.

In Chapter 2 the following results are reported:

1) The preparation and full characterisation of the unexpected homoleptically rearranged products consisting of the bis(pentafluorophenyl)gold(I) anion and its respective ligand cation.
2) Preparation and full characterisation of a series of imine coordinated gold(I)complexes with the implementation of the gold(I) precursor, $Au(PPh_3)NO_3$.
3) The determination and discussion of structural changes found in N-containing ligands upon coordination of the free ligand to $AuPPh_3$.
4) The overall study of the observed preference of gold(I) for certain coordination sites in ligands, which contain multiple coordination sites, which in this instance consisted of a soft endocyclic sulphur donor ligand, hard- to borderline hard endocyclic nitrogen donor (imine) or a hard excocyclic nitrogen donor (amine).

2.2 Results and discussion

2.2.1 The coordination of the neutral amino-azole ligands to gold(I).

Amine, imine and thioether containing functionalised N-heterocyclic ligands were coordinated to the gold(I) starting materials i.e. $Au(C_6F_5)(tht)$ and $Au(PPh_3)NO_3$ to yield unexpected homoleptically rearranged[17] bis(pentafluorophenyl)gold(I) complexes and the respective (triphenylphosphine)gold(I) complexes. In sections 2.2.1.1 and 2.2.1.2 the synthetic value of the gold(I) precursor compounds, $Au(PPh_3)(NO_3)$ and $Au(C_6F_5)(tht)$, is once again emphasized by the utilisation thereof in the preparation of these novel complexes. The single crystal X-ray diffraction structural determinations of complexes **1**, **3** and **4** revealed an unforeseen homoleptic rearrangement, which resulted from the reaction of the 2-aminoazole compounds with $Au(C_6F_5)(tht)$, to yield $Au(C_6F_5)_2^-$ and various aminoazolium or lithium cations. Note that trace amounts of lithium chloride

[17] A.L. Hormann-Arendt, C.F. Shaw, *Inorg. Chem.* **1990**, *28*, 4683.

(from the synthesis of $Au(C_6F_5)$(tht) afford the various lithium cations). The single crystal X-ray diffraction structural determinations of complex **5** showed that this was the only complex that coordinated *via* the imine nitrogen to $Au(C_6F_5)$-unit. The conclusive characterisation by single crystal X-ray structure analyses, IR and NMR spectroscopy revealed information on a molecular level and other unexpected phenomena, such as ring opening (**9**) and delocalisation within the heterocyclic rings, which will be discussed in the various sections within this chapter. The crystal and molecular structures of the free ligands have been determined before and these results were used to investigate the structural changes upon coordination. Unfortunately, the characterisation of $Au(C_6F_5)L$ complexes was impossible in solution as a result of homoleptic rearrangement.

2.2.1.1 ***The preparation of bis(pentafluorophenyl)gold(I) complexes, 1-5.***

The most general route for the preparation of imine-functionalised heterocyclic bis(pentafluorophenyl)gold(I) involves the substitution of the labile tht ligand in $Au(C_6F_5)$(tht) by an imine ligand, yielding $Au(C_6F_5)(L)$. This coordination was only observed for **5** and possibly **2** (Scheme 2.1), while a number of products that contain $Au(C_6F_5)_2^-$ and various 2-aminoazolium or the lithium cations were observed for the other reaction mixtures. Various attempts to crystallise compound **2** from the reaction mixture, were unsuccessful and the compound obtained cannot be identified with absolute certainty. No conclusive evidence was found that the target compounds were present in solution for **1**-**4**.

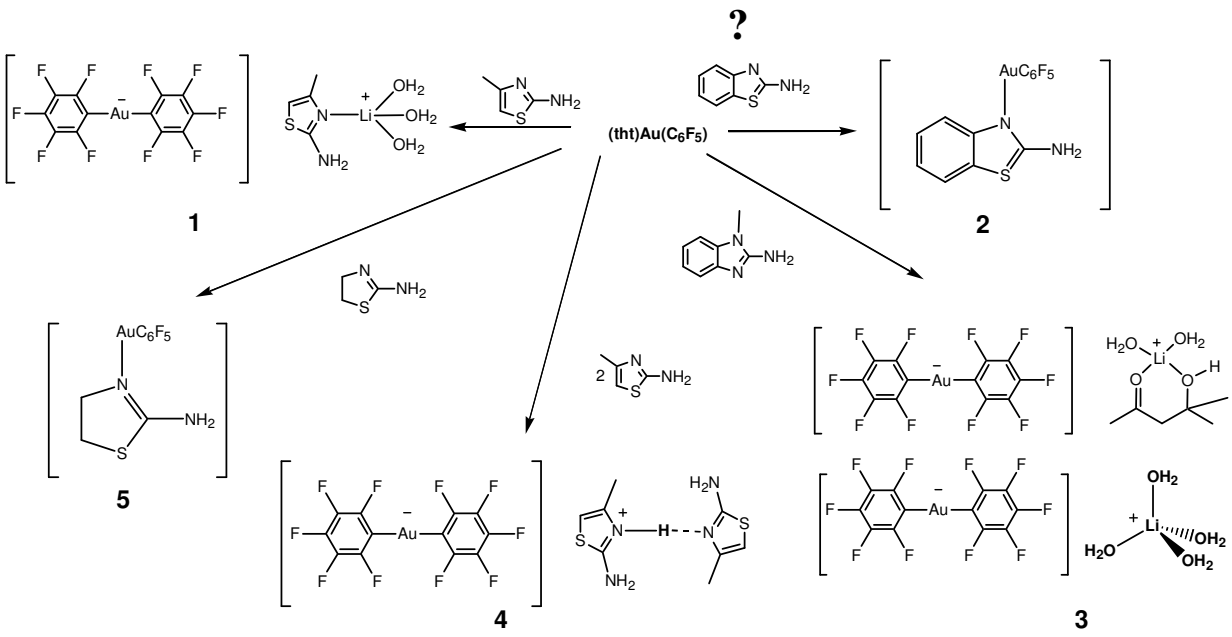

Scheme 2.2: The reaction of AuC_6F_5(tht) with 2-aminoazole compounds.

Compounds **1**, **2**, **3**, **4** and **5** were prepared by treating a solution of 2-amino-4-methylthiazole, 2-aminobenzothiazole, 2-amino-1-methylbenzimidazole or 2-aminothiazoline in diethyl ether with equimolar amounts of $Au(C_6F_5)$(tht), dissolved in diethyl ether, at room temperature under inert conditions. In our group [18] we have observed many examples of the rearrangement observed for **1**, **3** and **4** e.g. the fragment of $\{[Li(diglyme)_{2.5}(ebtz)]\}_\infty^+$ and the non-interacting $Au(C_6F_5)^-$ which were obtained from the attempted synthesis of [1,2-di(tetrazol-2-yl)ethane]-bis(pentafluorophenyl)gold(I) by addition of 1,2-di(tetrazol-2-yl)ethane to 2 molar equivalents of $Au(C_6F_5)$(tht). In another example, the 2-dimethylamino(ethylene)trimethylammonium ($TMRDAMe^+$) cation and the non-interacting $Au(C_6F_5)^-$ was formed from attempted synthesis of (1-benzyl-4-methyltetrazol-5-ylidene)(pentafluorophenyl)gold(I).

Raubenheimer and co-workers[19] have also observed a homoleptic rearrangement for the (pentafluorophenyl)(isothiazol-5-yl)gold(I) while the complex (triphenylphosphine)(isothiazol-5-yl)gold(I) can be isolated. In the instance when isothiazole is used as N-heterocyclic ligand in the neutral complex (pentafluorophenyl)(isothiazol-5-ylidene)gold(I), this rearrangement occurs slowly and

[18] W. F. Gabrielli, *PhD Dissertation* **2005**, University of Stellenbosch.

[19] H.G. Raubenheimer, M.Desmet, G.J. Kruger, *J. Chem. Soc., Dalton Trans*., **1995**, 2067.

can be followed by ^{1}H NMR measurements. Trace amounts of the rearranged product formed within days and the reaction reaches equilibrium after 18 days. The reaction occurs more rapidly for (pentafluorophenyl)(isothiazol-5-yl)gold(I), is the precursor complex and can *in situ* be converted to the carbene complex by immediate alkylation. In contrast, (triphenylphosphine)(isothiazol-5-yl)gold(I) is stable in solution and can readily be isolated in pure form. Subsequent alkylation of this product again affords a mixture that includes an ionic homoleptic rearrangement by-product.

The present products are soluble in polar organic solvents such as acetone, dichloromethane and diethyl ether and insoluble in water and alkanes such as pentane and hexane. Crystals suitable for X-ray diffraction, were obtained by vapour diffusion of pentane into a solution of the compounds in acetone (**3**) and deuterated dichloromethane (**1**, **5**, **4**) in an NMR tube stored under argon at -22ºC. Physical and analytical data for complexes **1**, **2**, **3**, **4** and **5** are summarised in Tables 2.1-2.2.

Table 2.1: Analytical data for **1**, **2** and **3**.

Complex	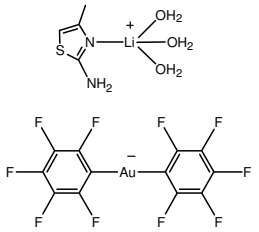 **1**	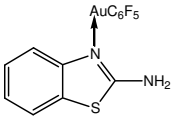 **2**	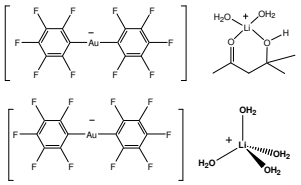 **3**
m.p. (ºC)	66	84-86	134-137
Colour	yellow	colourless	beige
Crude yield (g)	0.307 g	0.09 g	0.560 g
M_r	706.24	514.22	1286.26
M_f	$C_{16}H_{12}AuF_{10}N_2SO_3$	$C_{13}H_6AuF_5N_2S$	$C_{29}H_{22}Au_2F_{20}Li_2O_8$

Table 2.2: Analytical data for **4** and **5**.

Complex	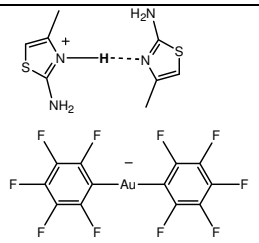 **4**	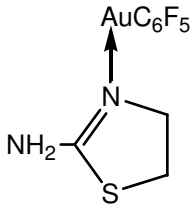 **5**
m.p. (ºC)	155 (decomp.)	97-105 (142 decomp.)
Colour	colourless	colourless
CrudeYield (g)	0.23 g	0.19 g (85 %)
M_r	760.01	466.18
M_f	$C_{20}H_{13}AuF_{10}N_4S_2$	$C_9H_6AuF_5N_2S$

2.2.1.2 The preparation of cationic imine coordinated (triphenylphosphine)gold(I) complexes, 6, 7, 9, 10A and 10B.

The novel gold(I) compounds **6**, **7**, **9** and **10** were successfully prepared, following a similar substitution approach as mentioned above, by the addition of 2-amino-4-methylthiazole, 2-aminobenzothiazole, 2-aminobenzimidazole or 2-aminothiazoline in diethyl ether to solutions of (triphenylphoshine)gold(I) nitrate, $[Au(NO_3)(PPh_3)]$, in diethyl ether at room temperature under inert conditions (Scheme 2.3).

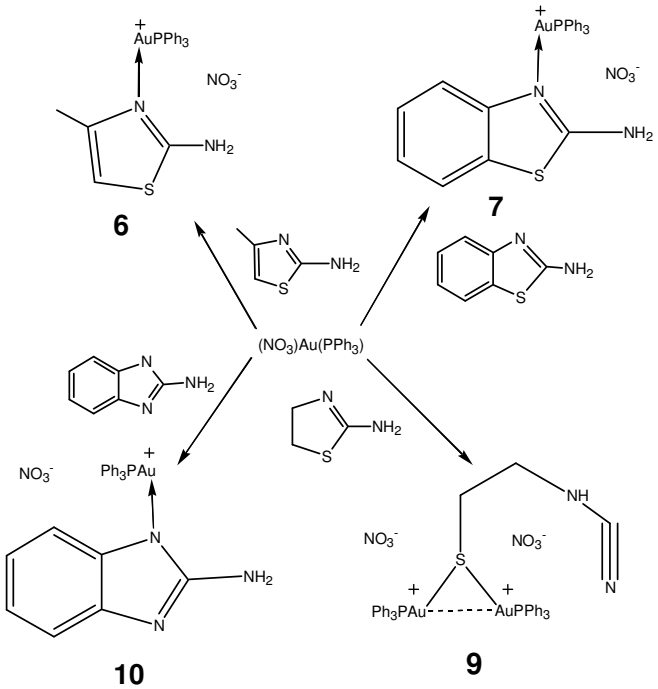

Scheme 2.3: Reactions of 2-aminoazole ligands with $Au(NO_3)PPh_3$.

The resulting white snowflake-like suspension was stirred for 5 days at room temperature. The suspension was then evaporated *in vacuo* to yield a white solid. The white solid was extracted with diethyl ether and the filtrate, containing the desired gold(I) complex, was filtered through $MgSO_4$. The resulting clear solution was concentrated *in vacuo* to yield a white solid for all the complexes except **7** which was yellow. All the complexes are soluble in polar organic solvents such as dichloromethane, acetone or methanol, slightly soluble in diethyl ether and insoluble in alkanes such as hexane and pentane. Colourless crystals were obtained by vapour diffusion of pentane into a solution of the compound in methanol (**10B**), or a concentrated solution of the complex in a NMR tube with dichloromethane as solvent (**6**, **7**) or acetone as solvent (**8**, **9**, **10A**) under argon at -22ºC. The single crystal X-ray analyses of complex **10A** reveals that its unit cell consist of a 2-aminobenzimidazole(triphenylphosphine)gold(I) nitrate only, while the unit cell of complex **10B** consists of a 2-aminobenzimidazole(triphenylphosphine)gold(I) nitrate and a solvent molecule, methanol.

The single crystal X-ray determination of a crystal obtained from a solution of complex **7** concentrated in a concentrated acetone solution revealed a formation of an unexpected two-coordinated Ag complex (**8**), bis(2-aminobenzothiazole)silver(I). The silver contaminant was obtained when $Au(PPh_3)Cl$ was treated with an excess of $AgNO_3$ to afford starting material $Au(PPh_3)NO_3$.

The single crystal X-ray of complex **9** showed the formation of μ_2-(2-mercapto-ethyl-cyanamide κ,S)bis(triphenylphosphine)gold(I) nitrate which reveals an interesting ring opening and sulphur coordination of the ligand, 2-aminothiazoline, upon reaction with $Au(PPh_3)NO_3$. The unexpected ring opening of the 2-aminothiazoline gave a new ligand, 2-mercapto-ethyl-cyanamide, which then bonded to two gold fragments, yielding $[(AuPPh_3)_2(\mu_2\text{-}SCH_2CH_2NH\text{-}CN)]$.

The 2-mercapto-ethyl-cyanamide ligand was formed by ring cleavage of the S-C bond, followed by rearrangement to give 2-mercapto-ethyl-cyanamide as the bonding ligand. Laguna and co-workers [20] reported a related structure also resulting from a ring opening, in the same substrate but coordinated differently to gold(I) producing a different

[20] M. Baradji, A. Laguna, M.R. Prezez, P.G. Jones, *Organometallics.*, **2002**, *21*, 1877.

gold(I)complex (Scheme 2.4). They employed the 'acac method' [21] which affords deprotonation readily.

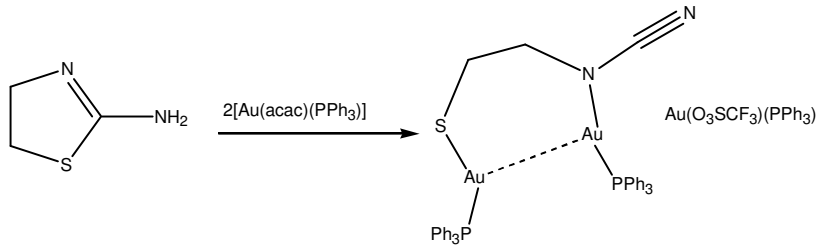

Scheme 2.4: Laguna and co-workers complex.

Laguna and co-workers[20] proposed a mechanism for the formation of their complex which involves two deprotonation steps to yield a dianionic ligand (Scheme 2.5).

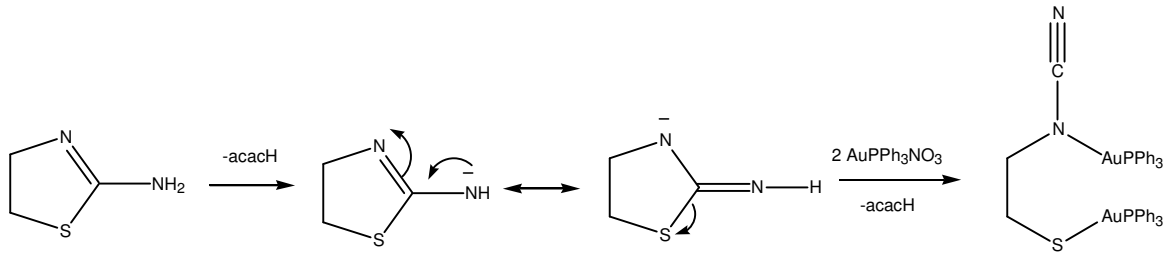

Scheme 2.5: Reaction mechanism suggested by Laguna and co-workers.

Our results differ from Laguna and co-workers since only one hydrogen atom was removed as a proton while the other migrates to the original imine nitrogen. It is not possible to say at what stage exactly S-coordination occurs (Scheme 2.6). The result is a cationic complex, μ_2-(2-mercapto-ethyl-cyanamide-κ,S)bis(triphenylphosphine) gold(I) which is neutralised by nitrate anion to produce complex **9**, μ_2-(2-mercapto-ethyl-cyanamide-κ,S)bis(triphenylphosphine)gold(I) nitate.

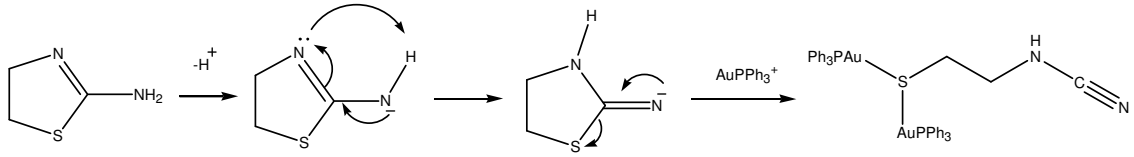

Scheme 2.6: The reaction mechanism for the formation of the 2-mercapto-ethyl-cyanamide ligand.

[21] J. Vincente, S. Luo, B.L. Scott, R. Butcher, C.J. Unkerer, C.J. Burns, G.J. Kiebas, A. Liedos, F. Maseras, J. Tomas, *Organometallics*, **2003**, *22*, 4327

Physical and analytical data for the complexes **6**, **7**, **9** and **10** are summarised in Tables 2.3-2.4.

Table 2.3: Analytical data for **6** and **7**.

Complex	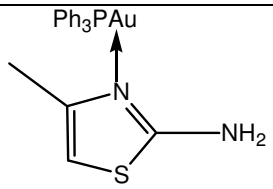 **6**	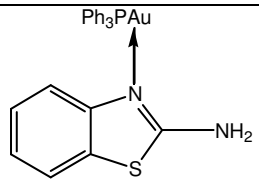 **7**
m.p. (ºC)	94-97 (130 decomp.)	97-105 (142 decomp.)
Colour	white	yellow
Yield (%)	94	82
M_r	573.08	609.45
M_f	$C_{22}H_{21}AuN_2PS$	$C_{25}H_{21}AuN_2PS$

Table 2.4: Analytical data for **9** and **10**.

Complex	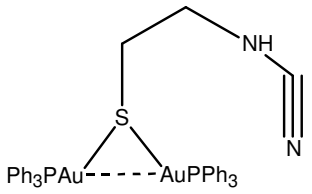 **9**	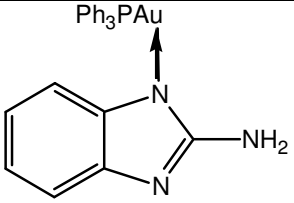 **10**
m.p. (ºC)	83-87	114-116 (179 decomp.)
Colour	colourless	colourless
Yield (%)	70	98
M_r	561.41	592.40
M_f	$C_{21}H_{21}AuN_2PS$	$C_{25}H_{22}AuN_3P$

2.2.2 Spectroscopic characterisation of compounds 1-10

2.2.2.1 Nuclear magnetic resonance spectroscopy of 1-10.

The spectra of complexes **1**-**4** could not be obtained before they decomposed and Laguna and co-workers[20], have reported the spectrum of complex **5**.

In all the other ^{1}H NMR spectra, the presence of the Au(PPh_3) moiety was confirmed by

the detection of phenyl resonances in the form of an unresolved multiplet in the region δ 7.58 - 7.68. Although the aromatic proton resonances of complexes **7** (2-aminobenzothiazole compound) and **10** (2-aminobenzimidazole compound) all appear at chemical shifts significantly downfield from those of the free ligands, in compound **10**, the protons H^5 and $H^{5'}$ as well as H^6 and $H^{6'}$ are rendered equivalent by their chemical environment and give rise to two individual singlets at δ 7.40 and δ 7.11 respectively. Unlike for compound **10**, all the aromatic protons in compound **7** are inequivalent resulting in four sets of resonances in the aromatic region of the ^{1}H NMR spectrum. In contrast, the spectrum of 2-aminobenzothiazole, the ligand of complex **7**, shows the aromatic resonances of $H^{5'}$ and $H^{5'}$ each as a doublet at δ 7.51 and δ 7.41 (^3J = 7.9 Hz) while $H^{6'}$ and H^6 resonate as a triplet each at δ 7.30 and δ 7.12 (^3J = 7.3 Hz) respectively. It is noteworthy that long-range coupling of the aromatic protons is less pronounced in the coordinated compound than in the free ligand and the aromatic protons in **7** are not distinguishable and resonate as a multiplet at δ 7.35. In the ^{1}H NMR spectrum of compound **10**, the presence of the proton signal of the NH-group is observed at δ 3.26 while in the spectrum of the free ligand, 2-aminobenzimidazole, the signal associated with NH_2-groups appears at δ 6.21. In all the other complexes, these resonances were not observed.

In the ^{31}P NMR spectra of the new compounds (**6**, **9**, **10**) only one intense singlet (δ 30.6, 37.1, 33.9) is observed. These resonances display a downfield change in chemical shift relative to the signal for the precursor compound [$Au(NO_3)(PPh_3)$] (at δ 27.2).

From the ^{13}C NMR spectra of compounds **6-10**, it is evident that coordination to gold(I) does alter the chemical shifts of the respective carbon atoms. The spectra of the complexes reveal additional sets of doublets, when compared to those of the free ligands. These signals can be allocated to the phenyl ring carbons of the $Au(PPh_3)^+$ moiety and are detected in the region δ 130-136. The low intensity doublet at c.a δ 130 can be assigned to the C–P coupled *ipso*-carbon atom, whilst the medium- to high intensity doublet at c.a δ 131 is attributable to the C–P coupled *meta*-carbon atom. The resonances of the *ortho*-carbon atoms are observed as doublets most downfield region of phenyl ring carbons of the $Au(PPh_3)^+$ moiety. The *para*-carbons resonate as a singlet at δ 133-134 in complexes **6** and **7** as a result of no detectable C-P coupling while in complexes **9** and **10**, the carbons resonate as a doublet at the same δ value, indicating the presence of C-P coupling.

The weak signal of the highly deshielded carbon (C^2), central to the heteroatoms, for **6** and **7** resonates at δ 189 and δ 168 respectively indicating a significant downfield change in chemical shift of Δδ 19 and Δδ 6 respectively when compared to the same signal of the free ligand. In the instance of the benzo compounds, an unexpected but noteworthy upfield shift of the C^2 signal in **7** and **10** of Δδ 25 and Δδ 17 respectively is observed. This phenomenon can be explained by the total chemical shift (σ). The total chemical shift ($\sigma = \sigma_{p+} \sigma_d$) is composed of a paramagnetic contribution (σ_p) and diamagnetic contribution (σ_d).[22] The chemical shifts of the signals in the ^{13}C NMR spectra do not only reflect shielding and deshielding[22] as in the ^1H NMR spectra and both the paramagnetic and diamagnetic components play a role. The diamagnetic component (σ_d) is negligible in the total chemical shift in the ^1H NMR spectra which thus reflects shielding and deshielding.

The ^1H and ^{13}C NMR spectroscopic data for 2-amino-4-methylthiazole and the complex **6** were acquired in acetone–d_6 and are summarised in Table 2.4.

The resonances for the C^5, C^4 and C^7 carbons show a downfield shift (Δδ 5.6 for C^5 Δδ 1.6 for C^4) as would be expected in an electron withdrawing metal coordination. The H^7 resonances also display a downfield shift of Δδ 0.3 when compared to uncoordinated ligand.

[22] R.F. Fenske in: *Organometallic Compounds, Synthesis, Structure and Theory* (Ed. B.L. Shapiro), Texas A & M University Press, Texas, **1983**, p. 305.

Table 2.4: ^{1}H, ^{13}C and ^{31} P NMR spectroscopic data obtained for **2-amino-4-methylthiazole** and **6**.

		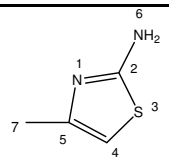 **2-amino-4-methylthiazole**	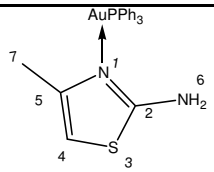 **6**
Solvent Temperature (°C)		acetone-d_6 25	acetone-d_6 25
Assignment		**Chemical shift**	
^{1}H NMR (300/400 MHz)	PPh_3	-	7.48 (m, 15H)
	H^5	6.70 (bs, H)	6.24 (s,1H)
	H^7	2.10 (s, 3H)	2.40 (s, 3H)
^{13}C NMR (75/100 MHz)	C^2	170.5 (s)	189.0 (s)
	C^5	149.9 (s)	155.5 (s)
	C^{ortho}	-	136.4 (d, ^{2}J =17 Hz)
	C^{para}	-	134.4 (s)
	C^{meta}	-	131.5 (d, ^{3}J =12 Hz)
	C^{ipso}	-	130.0 (d, ^{4}J =68 Hz)
	C^4	102.6 (s)	104.2 (s)
	C^7	18.31 (s)	18.8 (s)
^{31}P NMR (121 MHz)	PPh_3	-	30.6 (s)

The ^{1}H and ^{13}C NMR spectroscopic data for 2-aminobenzothiazole and complex **7** were acquired in acetone–d_6 are summarised in Table 2.5.

The ^{13}C NMR spectrum reveals a downfield shift of the signals for the phenyl ring atoms C^4, C^5 and $C^{6'}$ (Table 2.5). The resonance of the $C^{6'}$ carbon is shifted slightly downfield ($\Delta\delta$ 0.7) to δ 126.9 with the same observation for signals of the C^5 ($\Delta\delta$ 1.5) and C^4 ($\Delta\delta$ 0.8) carbon. The coordination of a ligand to the metal normally causes a downfield change in shift of the signals but an upfield change in chemical shift is observed for $C^{4'}$, $C^{5'}$ and C^6. This phenomenon can be explained in terms of the total chemical shift σ.

Table 2.5: ^{1}H and ^{13}C NMR spectroscopic data obtained for **2-aminobenzothiazole** and **7.**

		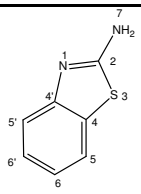 **2-aminobenzothiazole**	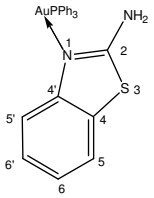 **7**
Solvent		acetone-d_6	acetone-d_6
Temperature (°C)		25	25
Assignment		**Chemical shift (ppm)**	
^{1}H NMR (300/400 MHz)	PPh_3	-	7.58 (bs, 25H)
	$H^{5'}$	7.51 (d, 1H, ^{3}J = 7.9 Hz)	
	H^{5}	7.41 (d, 1H, ^{3}J = 7.9 Hz)	7.21-7.55 (m, 4H)
	$H^{6'}$	7.30 (t, 1H, ^{3}J = 7.3 Hz)	
	H^{6}	7.12 (t, 1H, ^{3}J = 7.3Hz)	
^{13}C NMR (75/100 MHz)	C^{2}	166.9 (s)	142.5 (s)
	C^{ortho}	-	134.6 (d, ^{2}J=13.3 Hz)
	C^{para}	-	132.8 (s)
	C^{meta}	-	129.6 (d, ^{3}J=11.0Hz)
	$C^{4'}$	152.5 (s)	133.2 (s)
	C^{6}	131.9 (s)	129.8 (s)
	$C^{6'}$	126.2 (s)	126.9 (s)
	C^{5}	122.4 (s)	123.9 (s)
	C^{4}	121.4 (s)	122.2 (s)
	$C^{5'}$	119.1 (s)	116.5 (s)

The ^{1}H, ^{13}C and ^{31}P NMR spectroscopic data for 2-aminothiazoline and the complex, **9**, were acquired in acetone–d_6 and are summarised in Table 2.6.

Table 2.6: ^{1}H, ^{13}C and ^{31}P NMR spectroscopic data obtained for **2-aminothiazoline** and **9**.

		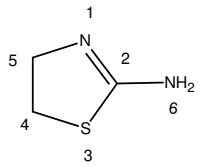 **2-aminothiazoline**	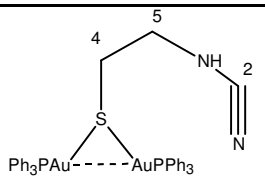 **9**
Solvent Temperature (°C)		acetone-d_6 25	acetone-d_6 25
Assignment		**Chemical shift**	
^{1}H NMR (300/400 MHz)	PPh_3	_	7.62 (m, 15H)
	H^4	3.84 (t, 2H, ^{3}J = 7.3Hz)	4.03 (t, 2H, ^{3}J = 7.5 Hz)
	H^5	3.27 (t, 2H, ^{3}J = 7.5Hz)	3.55 (t, 2H, ^{3}J = 7.5 Hz)
^{13}C NMR (75/100 MHz)	C^2	162.5 (s)	168.8 (s)
	C^{ortho}	-	135.8 (d, ^{2}J = 13.3 Hz)
	C^{para}	-	133.9 (s, ^{4}J = 1.72Hz)
	C^{meta}	-	131.3 (d, ^{3}J = 12.0 Hz)
	C^{ipso}	-	130.2 (d, ^{1}J = 60.1 Hz)
	C^5	62.1 (s)	40.5 (s)
	C^4	37.1 (s)	35.0 (s)
^{31}P NMR (121 MHz)	PPh_3	-	37.1 (s)

The ^{13}C NMR spectrum shows that the less shielded carbon, C^5, resonates in the spectrum of the ligand at δ 40.5, appearing more downfield when compared to the shielded C^4 carbon. Coordination to the metal and ring opening changes the chemical shift of the C^5 carbon upfield by Δδ 21.6 and the more shielded C^4 carbon resonates at δ 35.0 with a change in chemical shift of Δδ 2.1 upfield.

The ^{1}H, ^{13}C and ^{31}P NMR spectroscopic data of 2-aminobenzoimidazole and complex **10** were obtained in acetone–d_6 and are summarised in Table 2.7.

Table 2.7: ^{1}H, ^{13}C and ^{31}P NMR spectroscopic data obtained for **2-aminobenzimidazole** and 10 at 25ºC in acetone-d_6.

		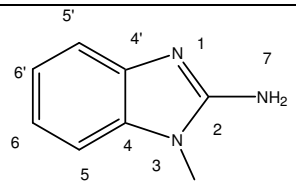 **2-aminobenzimidazole**	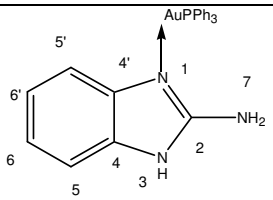 **10**
Solvent Temperature (°C)		acetone-d_6 25	acetone-d_6 25
Assignment		**Chemical shifts**	
^{1}H NMR (300/400 MHz)	PPh_3	.	7.68 (m, 15H)
	$H^{5,5'}$	6.90 (m , 2H)	7.40 (m, 2H)
	$H^{6,6'}$	7.18 m, 2H)	7.11 (m, 2H)
	H^{7}	6.21 (bs, 2H)	-
	H^{3}	-	3.26 (bs, 1H)
^{13}C NMR (75/100 MHz)	C^{2}	157.4 (s)	140.7 (s)
	$C^{4, 4'}$	140.6 (s)	133.7 (s)
	C^{ortho}	-	136.3 (d, ^{2}J = 13.2 Hz)
	C^{para}	-	134.3(d ,^{4}J = 2.9 Hz))
	C^{meta}	-	131.5 (d, ^{3}J = 13.2 Hz)
	C^{ipso}	.	130.2 (d, ^{1}J = 64.6 Hz)
	$C^{6, 6'}$	121.4 (s)	123.8 (s)
	$C^{5, 5'}$	113.7 (s)	113.9 (s)
^{31}P NMR (121 MHz)	PPh_3	-	33.9

The ^{1}H NMR spectrum of the ligand shows the NH_2 proton resonance as a broad singlet, which integrates for 2 protons, at δ 6.21 while the NH proton, which integrates for only 1 proton, is observed in the spectrum of the complex at δ 3.26.

The signals for the C^6 and $C^{6'}$ carbons indicate the same chemical environment for these atoms and they resonate as a singlet at δ 123.8 with a change in chemical shift of Δδ 2.4 downfield when compared to the same signal in the spectrum of the 2-aminobenzimidazole. The resonances of the C^5 and $C^{5'}$ carbons are observed as a singlet with a small downfield change in shift of Δδ 0.2 when compared to the free ligand's signal, thus almost unaltered by metal coordination. The $C^{4'}$ and C^2 carbons resonate upfield.

2.2.2.2 Mass spectrometry

The FAB-MS spectrometric data for complexes **6-10** are summarised in Table 2.8. The FAB-MS spectra of **1-4** do not reveal any diagnostic peaks, possibly due to decomposition, and are not reported or discussed. Compound **5** has been fully characterised by Laguna and co-workers.[31] The FAB-MS spectrum of compound **7** reveals that very little measurable fragmentation takes place with this mild ionization technique while a higher degree of fragmentation is evident from the EI-MS spectra of **6**, **9** and **10**.

Table 2.8: Mass spectrometric data for **6**, **7**, **9** and **10.**

Fragment	***m/z* (*I* in %)**			
	6	**7**	**9**	**10**
$\{[M]\text{-}NO_3 + 2H\}^+$	570 (40)	-	560 (32)	592 (49)
$3\{Au(PPh_3)\}+2H^+$	1408 (4)	-	-	-
$\{Au(PPh_3)_2\}^+$	720 (28)	-	720(65)	720 (3)
$\{Au(PPh_3)\}^+$	458 (45)	-	458 (85)	458 (44)
$\{PPh_3\}^+$	263 (6)	-	-	-
$\{C_4H_6N_2\}^+$	113 (7)	-	-	-
$\{C_3H_6N_2S\text{-}NH_2+Au\}^+$	-	-	280 (15)	-
Ph^+	-	77 (82)	-	-
$\{C_7H_7N_3\}^+$	-	-	-	134 (52)

In greater detail the positive-ion FAB spectrum of the colourless product of **6** shows a peak corresponding to the cation of the molecular ion at m/z 570, while the colourless

products of **9** and **10** also reveal the peaks of the cation of molecular ion at m/z 560 and m/z 592 respectively.

The fragment corresponding to the ligand of **6** is observed at 113 m/z as a very weak peak. The peak at 280 m/z can be assigned to a fragment consisting of the ligand of **9** which is coordinated to an Au^+ center after the loss of the exocyclic NH_2. A peak corresponding to the ligand of **10**, 2-aminobenzothiazole, at m/z 134 was observed. No diagnostic peaks except for the intense peak at m/z 77, representing a phenyl fragment, could be obtained from complex **7** spectrum.

The expected fragmentation peaks of the $AuPPh_3$-moiety are observed, $3\{Au(PPh_3)\}+2H^+$ (*m/z* 1408.7; only seen in **6**), $\{Au(PPh_3)_2\}^+$(*m/z* 720), $\{Au(PPh_3)\}^+$(*m/z* 458) and $\{PPh_3\}^+$(*m/z* 263; seen only in **6**), in the spectra of **6**, **7**, **9** and **10**.

2.2.2.3 Infrared spectroscopy

Solid state ATR (attenuated total reflectance) FT-IR spectra were recorded for ligands and complexes on a Thermo Nicolet Avatar 330 FT-IR with a Smart OMNI ATR accessory. All spectra show very broad bands of weak intensity in the ranges of 3054-3404 cm^{-1}, assignable to the stretching vibration of the N-H group. The primary amine N-H stretches appear as 2 bands in the 3500-3300 cm^{-1} region while secondary amine N-H stretches are observed as only 1 band in the region of 3432 cm^{-1}. The secondary N-H bands fall in the same region as primary N-H bands. The bands of the primary N-H vibration thus mostly obscure the secondary N-H vibration bands. The C=N vibrations are observed in the same range as the C=C vibrations. The C-N vibrations of the amines are observed in the region of 1350-1000 cm^{-1}, while C=N vibrations of imines are observed at a higher frequency in the region of 1690-1640 cm^{-1}. The C≡N vibrations of nitriles are observed at the highest frequency, in the range of 2260-2240 cm^{-1}.

The spectroscopic data and detailed discussion of **2-amino-4-methylthiazole, 2-aminobenzothiazole**, **2-amino-1-methylbenzimidazole** and **2-aminothiazoline** and the complexes **1**-**4** and **6-8**, **10** are summarised in Tables 2.24-2.30. These tables appear in the experimental section except for complex **9** (Table 2.9), where the unusual ring opening is observed, which is discussed in this section

The FT-IR spectrum of ligand **2-aminothiazoline** (Table 2.9) exhibits weak broad bands at 3401 cm^{-1} and 3059 cm^{-1} which can be attributed to the stretching of the N-H groups. The N-H bending vibration is observed as a broad weak band at 1638 cm^{-1}. The C=N stretching vibration was assigned to a weak band at 1518 cm^{-1} while the weak band at 1435 cm^{-1} can be attributed to the vibration of the single C-N bond.

Table 2.9: Infrared spectroscopic data for ligand **2-aminothiazoline** and complex **9**.

Type of vibration	**Wavenumber (cm^{-1})**	
	2-aminothiazoline	**9**
$\nu(N–H)_{strech}$	3401 (w,b), 3059 (w,b)	3295 (w,b)
$\nu(C\equiv N)$	-	2250 (w,b)
$\nu(N–H)_{bend}$	1638 (w)	1644 (w,b)
$\nu(C=N)$	1518 (w)	-
$\nu(C-N)$	1435 (w)	1435 (w)

The characteristic absorption bands in the FT-IR spectrum of **9** (Table 2.9), attributable to stretching vibration of the primary ν(N–H) moiety, are predominant at 3295 cm^{-1} with the weak N-H bending vibration band at 1644 cm^{-1}. The presence of an additional band at 2250 cm^{-1} can be assigned to the ν(C≡N) vibration while C-N vibration appears at 1435 cm^{-1}.

2.2.3 The molecular structures of the new compounds.

*Compounds **1-5***

The structure determinations of **1**, **3** and **4** reveal the formation of the bis(pentafluorophenyl)gold anion *via* a homoleptic rearrangement in each instance with various cations. All the pfp ligands have C–C bond lengths of 1.35–1.39 Å and C–F bond lengths of 1.34–1.37 Å. These values also compare favourably to pfp bond lengths and angles reported for related compounds and will therefore not be discussed in detail.[23,24,25] The geometry around the gold centre deviates from linearity in **1** [175.5(1)º] while in **3** [178.3(3) for Au(1) and 177.6(4)º for Au(2)] and **4** [179.9(3)°] it is virtually linear. The

[23] R. Uson, A. Laguna, J. Vicente, J. Garcia, P.G. Jones, G.M. Sheldrick, *J. Chem. Soc*., **1998**, 655.
[24] P.G. Jones , *Z. Kristalogr*.,**1993**, 208, 655.
[25]J. Coetzee, W.F. Gabrielli, K. Coetzee, O. Schuster, S.D. Nogai, S. Cronje, H.G. Raubenheimer *Angew. Chem. Int. Ed*., **2007**, 46, 2497.

Au-C distances for **1** [2.039(3) Å and 2.043(3) Å], **3** [2.049(4) Å, 2.053(4) Å and 2.046(4) Å, 2.049(4) Å] and **4** [2.044(6) Å] are typical. Both these structural parameters are in agreement with bond lengths and angles in related compounds.[23-25] The angle between the planes of the pfp substituents approaches planarity for **1** [torsion angles C(41)-Au(1)-C(51)-C(56) and C(41)-C46-Au(1)-C(51) at 6.39º] and **3** has an angle of 4.33º [C(41)-Au(2)-C(31)-C(36) and C(31)-Au(2)-C(41)-C(46)], which are all larger than the same angle in the homoleptically rearranged products bis(*o*-phenylene-bis(dimethylarsine)gold(I), bis(pentafluorophenyl)gold (~0º).[23] The same angle in **4** deviates completely from planarity at 66.59(0.05)º. Intermolecular aurophilic interactions are observed in complex **1** and in complex **3** intermolecular aurophilic interactions between the unique molecules in the asymmetric unit are observed. The only compound that did not show a rearrangement in solution, homoleptic or other, is **5** which instead produced the expected imine coordinated (2-aminothiazoline)pentafluorophenylgold(I) complex.

*Compounds **6-10***

The single crystal X-ray diffraction of the (triphenylphosphine)gold(I) complexes **6**, **7**, **9**, **10A** and **10B** reveal that the N-Au-P angle for **6** [175.58(8)º], **7** [178.3(8) º], **10A** [176.5(4)º] and **10B** [176.9(2)º] approaches linearity. Substitution of the weakly coordinated nitrate ligand in $[Au(NO_3)(PPh_3)]$ [26] by 2-aminoazole ligands results in a significant elongation of the Au–P bond length from 2.208(3) Å to 2.246(1) Å in **6** , to 2.233(2) Å in **7**, to 2.240(4) Å in **10A** and to 2.377(2) Å in **10B**; implying a *trans* influence by the 2-aminoazole ligand. All the complexes display the expected configuration with the characteristic propeller like phenyl rings. The Au-P bond length of 2.246(1) Å for **6**, 2.233(2) Å for **7**, 2.240(4) Å for **10A**, 2.252(3)Å for **9** and 2.238(2) Å for **10B** are all in agreement with one another and with literature values.[23] The Au-N bond lengths are 2.073(3) Å in **6**, 2.044(6) Å in **7**, 2.04(4) Å in **10A** and 2.035(6) Å in **10B** and are also typical.[23] The structures **10A** and **10B** differ only with respect to the orientation of the counterion and the inclusion of a solvent molecule in unit cell of complex **10B**. The interplanar angle between the counterion and the ligand in **10B** is 1.76º, while it is 40.85º in **10A.** The structural analyses of **9** revealed the unprecedented ring opening of the 2-aminothiazoline to give a new ligand, 2-mercapto-ethyl-cyanamide, which is coordinated through the sulphur atom to the gold atoms.

[26] J. C. Wang, M. N. I. Khan, J. P. Fackler Jr., *Acta Crystallogr.,* **1989**, C*45*, 1008-1010.

A second crystallisation of **7** from acetone instead of dichloromethane yielded an unexpected compound **8** which contains a silver atom coordinated to two 2-aminobenzothiazole ligands *via* the imine nitrogen with an N-Ag-N angle of 172.2(2)º.

The various structural aspects of each individual complexes will be discussed in detail in the following sections.

2.2.3.1 Molecular structure of 1

Colourless needles of **1** crystallised from CD_2Cl_2 (a decomposing NMR sample) in the triclinic space group $P\bar{1}$ with Z = 2 molecules in the unit cell. The asymmetric unit contains a Li^+-cation and a $Au(C_6F_5)_2^-$ anion. Note that lithium chloride (from the synthesis of $Au(C_6F_5)(tht)$) effected the formation of the Li^+-cation. The molecular structure and numbering scheme are shown in Figure 2.1 while selected bond lengths and angles are summarised in Table 2.10.

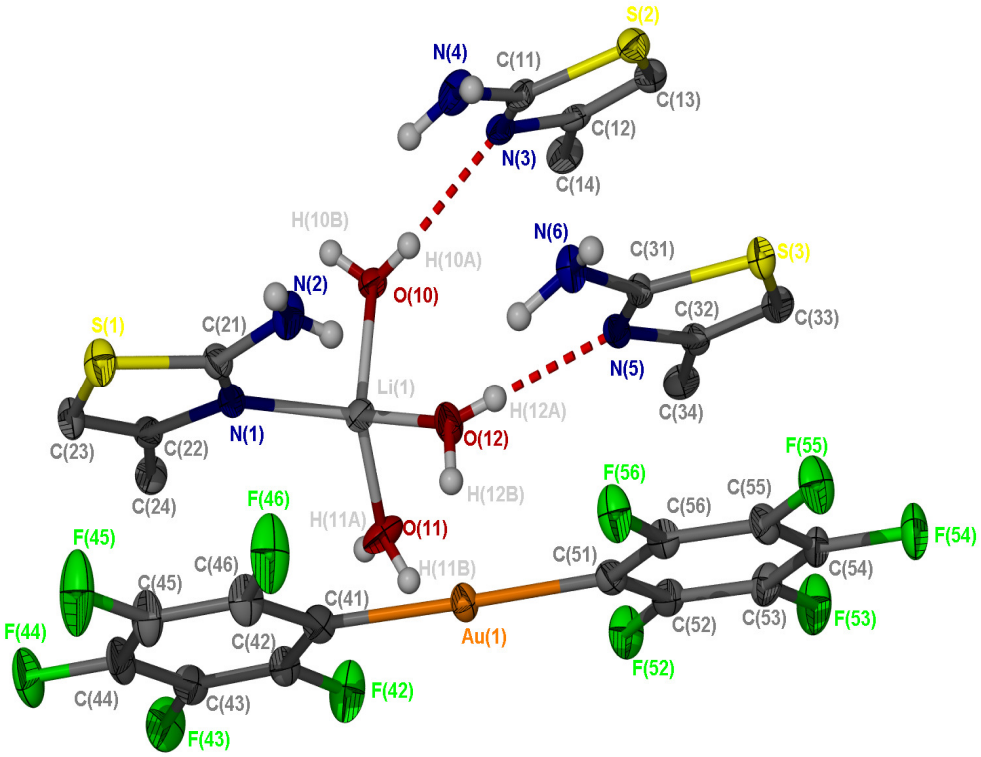

Figure 2.1: The molecular structure of **1**. The methyl hydrogen atoms were omitted for clarity.

The single C-N bonds C(22)-N(1), C(32)-N(5) and C(12)-N(3) [1.394(4), 1.393(4) and 1.396 (4) Å], and the double C=N bonds of C(21)-N(1), C(31)-N(5) and C(11)-N(3) [1.306(4), 1.304(4) and 1.317(4) Å], do not differ significantly from each other and are in close agreement with single and double C-N bond values respectively for the free 2-amino-4-methylthiazole.[27] These C-N bonds in complex **1** concur with reported standard values for double and single C-N bonds respectively [1.27 and 1.41 Å].[28] The C-S bond lengths [S(3)-C(33) of 1.733(3) Å, S(2)-C(11) of 1.722(3) Å, S(2)-C(13) of 1.729(4) Å, S(1)-C(21) of 1.731(3) Å and S(1)-C(23) of 1.732(3) Å] do not differ significantly from each other and remain, as do the C-N bond lengths, virtually unchanged by the coordination of the lithium metal or the presence of hydrogen bonding when compared to the same bond lengths in the uncoordinated ligand. The two free ligands are aligned approximately parallel to each other with an interplanar angle of 11°.

There is an increase in the bond angle of the C-C-N angle from the value in the uncoordinated ligand at 110.77º to the lithium coordinated ligand [C(13)-C(12)-N(3) 114.7(3) º] and to the hydrogen bonded free ligands, C(23)-C(22)-N(4) [115.3(3)º] and C(33)-C(32)-N(5) [114.8(3)º]. An increase is also observed for all the N-C-S angles, in the hydrogen bonded ligand [N(3)-C(11)-S(2) and N(5)-C(31)-S(2) with 114.7(3)º and 114.5(2)º] and in the cation [N(1)-C(21)-S(1) with 115.0(2)º], when compared to the same angle in the free ligand [111.2(2)º]. The C-S-C angles for the hydrogen bonded free ligands, [C(31)-S(3)-C(33) and C(11)-S(2)-C(13) of 89.2(1)º and 89.2(1)º)], do not differ appreciably and are in agreement with the same angle in the lithium coordinated ligand [89.9(1)º] which concur with the same angle in the free ligand [90.1(1)º].

[27] F. Fernandez, J.C. Daodrio, S. Garcia-Granda, P. Pertierra, *Acta. Crystallogr. Cryst. Struct. Commun*., **1996**, *C52*, 1412.
[28] A. Marchi, L. Marvelli, M. Cattabriga, R. Rossi, M. Neves, V. Bertolasi, V. Ferretti, *J. Chem. Soc., Dalton Trans.,* **1999**, 1937.

Table 2.10: Selected bond lengths (Å) and angles (°) of **1** with standard uncertainty in parenthesis.

Bond lenghts (Å)			
Au(1)-C(51)	2.039(3)		
Au(1)-C(41)	2.043(3)	C(11)-N(3)	1.317(4)
S(3)-C(31)	1.732(3)	N(1)-C(21)	1.306(4)
S(3)-C(33)	1.733(3)	N(1)-C(22)	1.394(4)
S(2)-C(11)	1.722(3)	C(22)-C(23)	1.347(5)
S(2)-C(13)	1.729(4)	C(12)-C(14)	1.496(4)
S(1)-C(21)	1.731(3)	C(21)-N(2)	1.369(4)
S(1)-C(23)	1.732(3)	C(24)-C(22)	1.494(4)
N(5)-C(31)	1.304(4)	N(4)-C(11)	1.376(5)
N(5)-C(32)	1.393(4)	N(1)-Li(1)	2.063(6)
C(32)-C(33)	1.352(4)	O(12)-Li(1)	1.915(6)
C(32)-C(34)	1.492(4)	Li(1)-O(10)	1.954(6)
Bond angles (º)			
C(51)-Au(1)-C(41)	175.5(1)	C(32)-C(33)-S(3)	110.3(2)
C(31)-S(3)-C(33)	89.2 (2)	N(1)-C(21)-S(1)	115.0(2)
C(11)-S(2)-C(13)	89.2(2)	C(23)-C(22)-N(1)	115.3(3)
C(21)-S(1)-C(23)	88.9(2)	C(22)-C(23)-S(1)	110.4(2)
C(31)-N(5)-C(32)	111.2(3)	C(32)-C(33)-S(3)	110.3(2)
C(33)-C(32)-N(5)	114.8(3)	C(21)-N(1)-C(22)	110.4(3)
C(33)-C(32)-C(34)	126.7(3)	C(22)-N(1)-Li(1)	126.4(3)
N(5)-C(32)-C(34)	118.5(3)	C(21)-N(1)-Li(1)	123.2(3)
N(5)-C(31)-S(3)	114.5(2)	O(11)-Li(1)-O(12)	106.1(3)
N(3)-C(11)-S(2)	114.7(3)	O(11)-Li(1)-O(10)	111.4(3)
C(11)-N(3)-C(12)	110.6(3)	O(11)-Li(1)-N(1)	119.0(3)
C(13)-C(12)-N(3)	114.7(3)	O(12)-Li(1)-N(1)	105.5(3)

The Li(1)-O(10), Li(1)-O(11) and Li(1)-O(12) distances [1.954(6), 1.893(6), 1.915(6) Å] differ significantly from each other but are in agreement with the reported values in the literature for bis(μ-pyrazine-2.3-diselen)hexaaquacopper(III) dilithuim bis(pyrazine-2,3-diselen)copper [1.90(1), 1.96(1), 1.96(1) Å].[29] The Li-N distance [2.063(6) Å] is in close agreement with the same bond in similar reported compounds e.g. bis(μ-pyrazine-2.3-diselen)hexaaquacopper(III) dilithuim bis(pyrazine-2,3-diselen)copper [2.13(1) Å].[29] The

[29] X. Ribas, J. C. Dias, J. Morgado, K. Wurst, E. Mollins, E. Ruiz, M. Almeida , J. Veriara, C. Rovira, *Chem. Eur. J*., **2004**, *10*, 1691

angles O(12)-Li(1)-N(1) [105.5(3)º], O(11)-Li(1)-N(1) [119.0(3)º], O(12)-Li(1)-O(11) [106.1º] and O(12)-Li(1)-O(10) [111.3º] confirm the approximate tetrahedral configuration of the central lithium atom and do not differ significantly from literature values observed for bis(μ-pyrazine-2.3-diselen)hexaaquacopper(III) dilithuim bis(pyrazine-2,3-diselen)copper [103.1(4)º, 115.5(5)º, 103.5(5),112.1(5)º].[29]

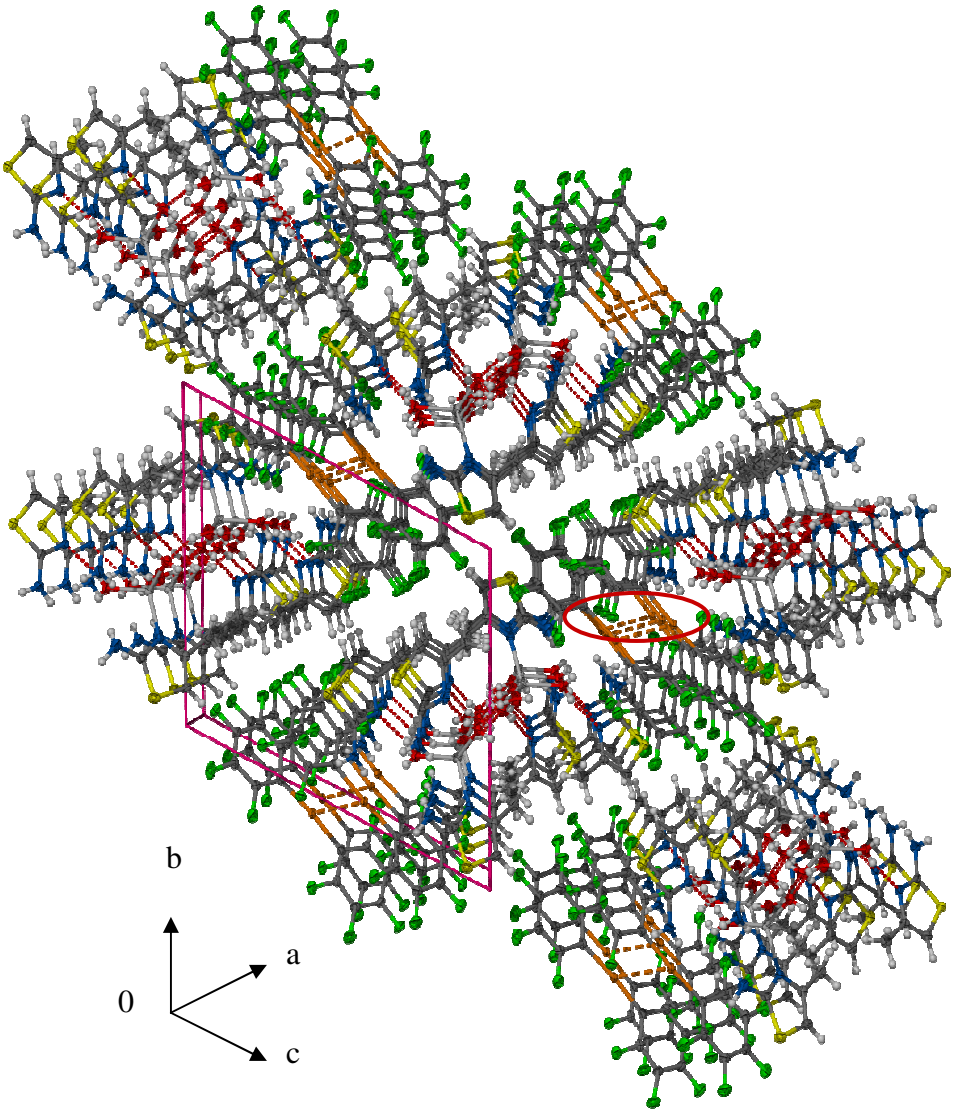

Figure 2.2: A view of the solid state structure of **1** along the a-axis.

The repetition of anion and cation-units along the b-axis is noted. The stacking of cation–cation pairs along the a-axis is observed (Figure 2.2). There is a weak aurophilic interaction (indicated by circle in Figure 2.2) of 3.45(3) Å between neighbouring gold centers. There is hydrogen bonding between the lithium coordinated water hydrogens and the imine nitrogen of the uncoordinated ligand, O(12)-H(12A)···N(5) [1.93(5) Å] and

O(10)-H(10A)···N(3) [2.04(3) Å]. The presence of π-stacking along 2 2 2 plane is shown (Figure 2.3).

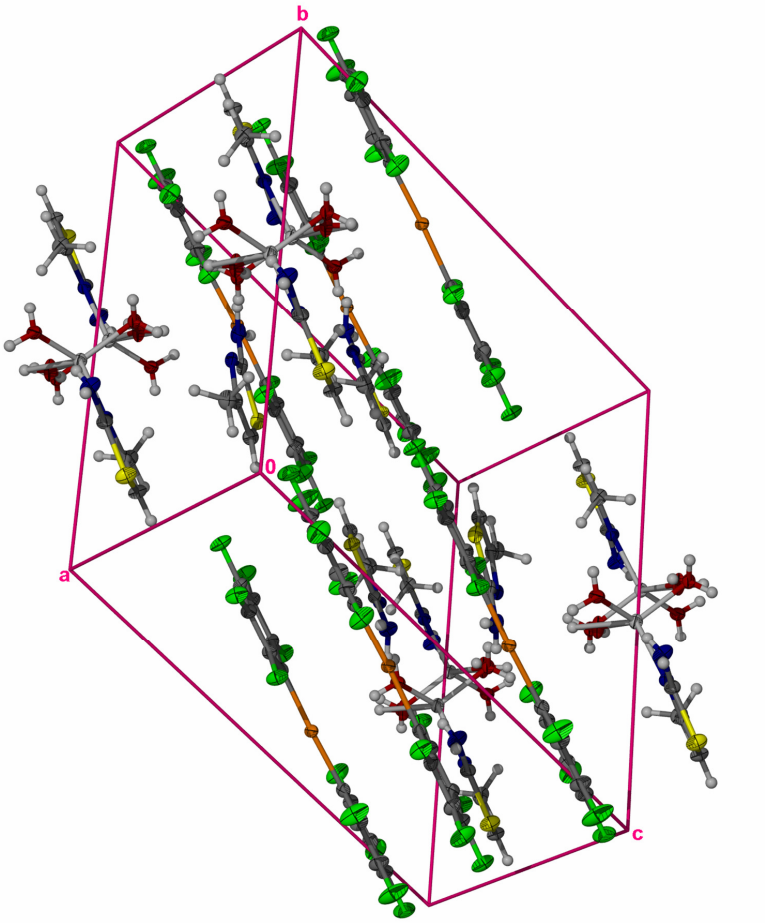

Figure 2.3: The π-stacking viewed perpendicular to the (2 2 2) plane.

In the (2 2 2) plane anions are interdispersed by the cations resulting in π-interaction between the pfp and the 5-membered rings of the 2-amino-4-methylthiazole [3.541-3.640 Å] and π-interaction between the 5-membered rings and 6-membered ring of the pfp [3.777-4.580 Å]. The π-stacking which results from the co-planarity of the pentafluorophenyl substituents, governs the crystal lattice packing in the (2 2 2) plane.

The solid state structure is thus governed by three intermolecular interactions: Au···Au interaction, π-stacking and hydrogen bonding.

2.2.3.2 Molecular structure of 3

Colourless blocks of **3** crystallised from an acetone solution in the triclinic space group *P*$\bar{1}$ with Z = 2 molecules in the unit cell. The solution of the collected single crystal X-ray diffraction data revealed that the complex is composed of two interacting $Au(C_6F_5)_2^-$ anions and two different lithium cations. Four water molecules are coordinated to one lithium cation and a 4-hydroxy-4-methylpentan-2-one molecule and two water molecules to the other. Lithium chloride, that remained from the synthesis of $Au(C_6F_5)(tht)$, afforded the formation of the Li^+-cations. The molecular structure and numbering scheme are shown in Figure 2.4 with selected bond lengths and angles summarised in Table 2.11.

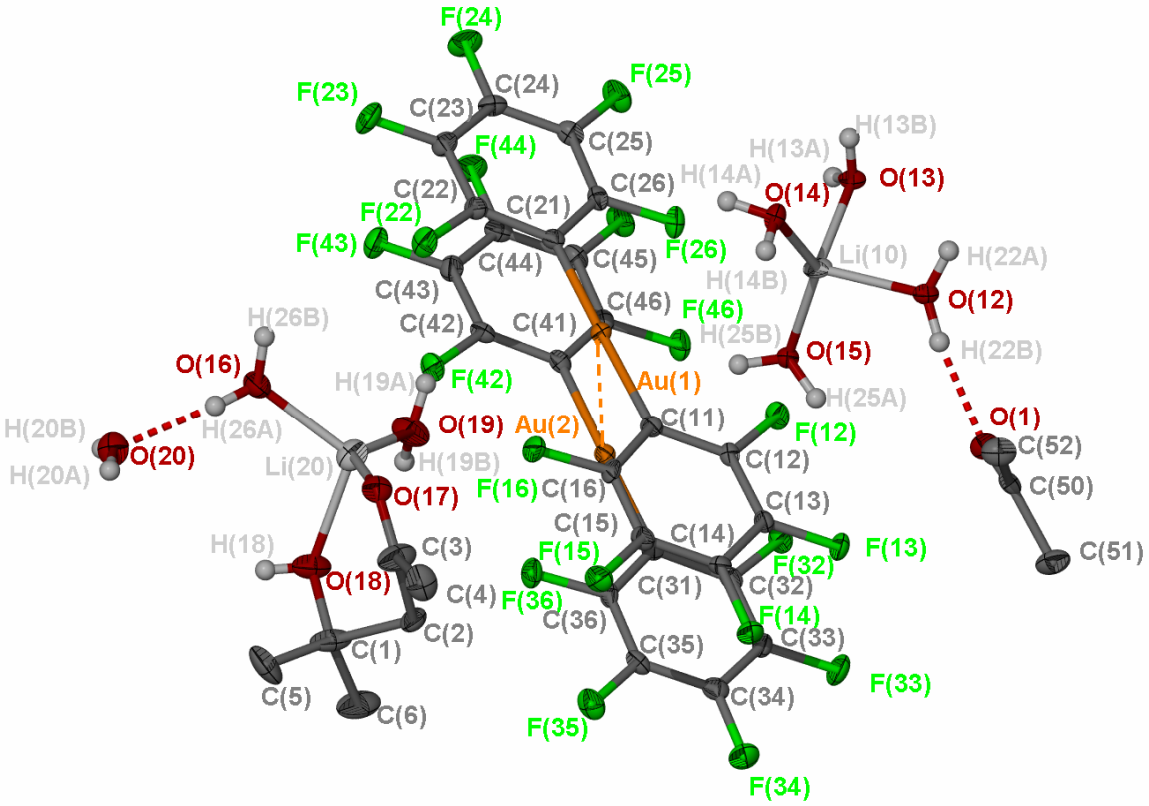

Figure 2.4: The molecular structure of **3** in the asymmetric unit, shown without the symmetry generated hydrogen bonding. The hydrogen atoms of the acetone and 4-hydroxy-4-methylpentan-2-one are omitted for clarity.

The formation of 4-hydroxy-4-methylpentan-2-one is explained in the reaction schemes in Scheme 2.7. An aldol condensation of acetone that yielded 4-hydroxy-4-methylpentan-2-

one has been described by Nicol [30] and we propose that a similar reaction occurred in our instance.

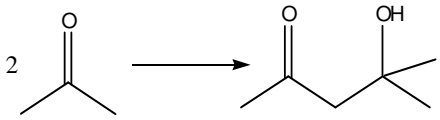

Scheme 2.7: The formation of 4-hydroxy-4-methylpentan-2-one.

The coordination of lithium to 4-hydroxy-4-methylpentan-2-one as observed in the crystal structure complex **3** is illustrated in Scheme 2.8. All the hydrogens were located for these lithium cations in the unit cell of complex **3**.

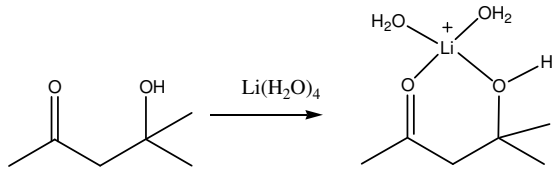

A

Scheme 2.8: The coordination of lithium to 4-hydroxy-4-methylpentan-2-one.

The other lithium cation, $Li(H_2O)_4^+$, has a four-coordinate distorted tetrahedral geometry around the central Li-atom. There is a weak intramolecular Au···Au interaction between the gold centres [3.566(4) Å]. Non-specific hydrogen bonding, between the water molecule and the fluorine atom on the pfp ring, O(20)-H(20B)···F(36)$^{£}$ [2.804(3) Å] [where $^{£}$ =1-x, -y, -z] is observed. This spatial separation of the hydrogen bearing O(20) and F(36) is 2.802(3) Å, approximately the sum of the van der Waals radii, thus this extremely weak hydrogen bonding only contributes slightly to stabilisation of the crystal.

[30] W. Nicol, *Chemical Engineering Research and Design*, 2003, *81(A8)*, 1026.

Table 2.11: Selected bond lengths (Å) and angles (°) of **3** with standard uncertainty in parenthesis.

Bond lenghts (Å)			
Au(1)-C(21)	2.049(4)		
Au(1)-C(11)	2.053(4)	O(17)-C(3)	1.203(4)
Au(1)-Au(2)	3.566(4)	Li(20)-O(16)	1.948(7)
Au(2)-C(41)	2.046(4)	O(12)-Li(10)	2.003(7)
Au(2)-C(31)	2.049(4)	O(15)-Li(10)	1.975(6)
C(1)-C(5)	1.416(7)	Li(10)-O(14)	1.946(6)
C(1)-C(6)	1.546(7)	Li(10)-O(13)	1.976(7)
C(1)-C(2)	1.594(6)	O(17)-Li(20)	2.012(7)
C(4)-C(3)	1.465(5)	O(19)-Li(20)	1.924(7)
C(3)-C(2)	1.529(6)	O(18)-Li(20)	2.000(7)
Bond angles (º)			
C(21)-Au(1)-C(11)	178.3 (3)	O(19)-Li(20)-O(16)	108.8(4)
C(41)-Au(2)-C(31)	177.6(4)	O(19)-Li(20)-O(18)	100.7(3)
O(1)-C(50)-C(52)	121.5(3)	O(19)-Li(20)-O(17)	138.1(4)
O(1)-C(50)-C(51)	121.2(3)	O(16)-Li(20)-O(17)	106.7(3)
C(52)-C(50)-C(51)	117.3(3)	O(14)-Li(10)-O(15)	136.5(4)
O(13)-Li(10)-O(12)	98.1(3)	O(15)-Li(10)-O(13)	105.8(3)
O(15)-Li(10)-O(12)	107.8(3)	O(14)-Li(10)-O(12)	95.0(3)

The hydrogen bonds observed are shown and discussed in two parts, firstly for $Li(H_2O)_4^+$ (Figure 2.12) and then for the lithium complex containing 4-hydroxy-4-methylpentan-2-one (Figure 2.13).

There is an intricate network of hydrogen bonding occurring between the solvent molecule, the lithium cation [Li(10)] and water coordinated to the second lithium in the unit cell. The hydrogen bonds are tabulated in Table 2.5 and the symmetry codes are provided.

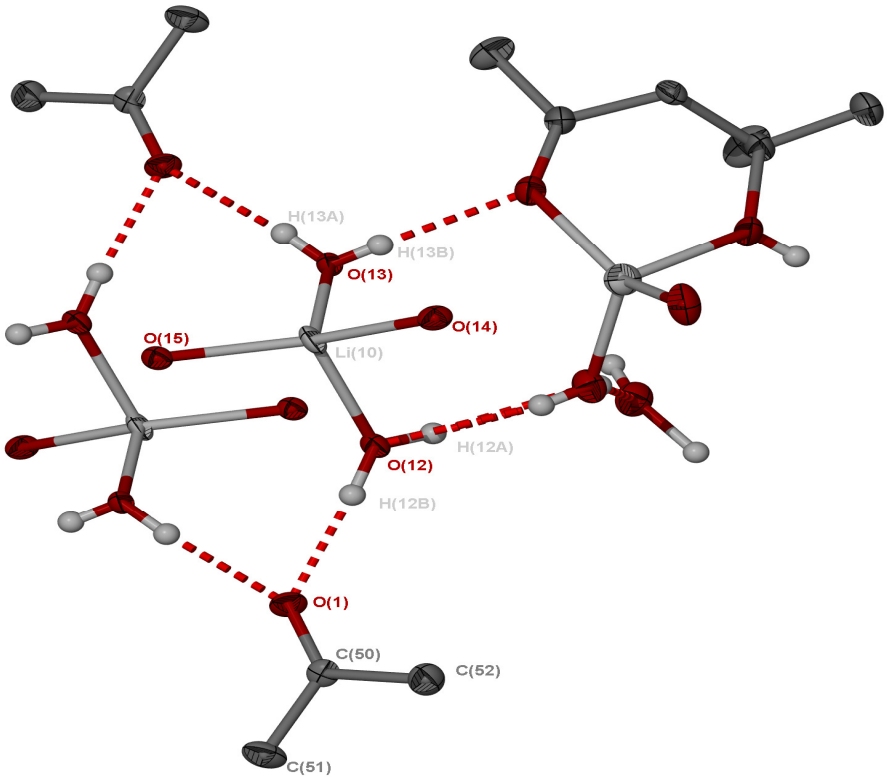

Figure 2.12: The hydrogen bonding observed for acetone and $Li(H_2O)_4^+$. The non-essential hydrogens are omitted for clarity.

Table 2.5: The hydrogen bonding between $Li(H_2O)_4^+$ and the solvent molecule (acetone) with symmetry generated units shown.

Hydrogen bonds of Li(10)	
O(12)-H(12B)-O(1)	1.91(4)
O(12)-H(12A)-O(16) *	2.09(4)
O(13)-H(13B)-O(17) $	2.11(4)
O(13)-H(13A)-O(1) *	2.04(4)

Where the symmetry code*: -x-1, 1-y, -z and $= x, 1-y, -z

The $Li(H_2O)_4^+$ ion has Li-O distances between 1.946(6) and 2.003(7) Å which do not deviate notably from reported literature values from lithium 1-pyrrolidinecarbodithioate tetrahydrate [1.906(3)-2.000(3) Å].[31] Hydrogen bonding may be responsible for the decrease in the O(13)-Li(10)-O(12) [98.1(3)º] and the O(14)-Li(10)-O(12) [95.0(5)º] angles and the increase in the O(15)-Li(10)-O(14) [136.5(4)º] angles from the normal

[31] I. Ymen, *Acta. Crystallogr.*, **1983**, *C39*, 570.

tetrahedral geometry of 109.5º for a four-coordinated metal and reported literature values of [103.4(1)º and 110.1(1)º].[31] The other lithium's O-Li-O angles O(13)-Li(10)-O(15) [105.8(3)º] and O(13)-Li(10)-(O14) [107.1º] are similar to the reported values in $Li(H_2O)_4^+$ in the lithium 1-pyrrolidinecarbodithioate tetrahydrate complex [108.8(1)º] and [108.5(1)º].[31]

The hydrogen bonding observed around the second Li(20) complex is shown in Figure 2.13 and summarised in Table 2.6 again we see a multifarious network of hydrogen bonds.

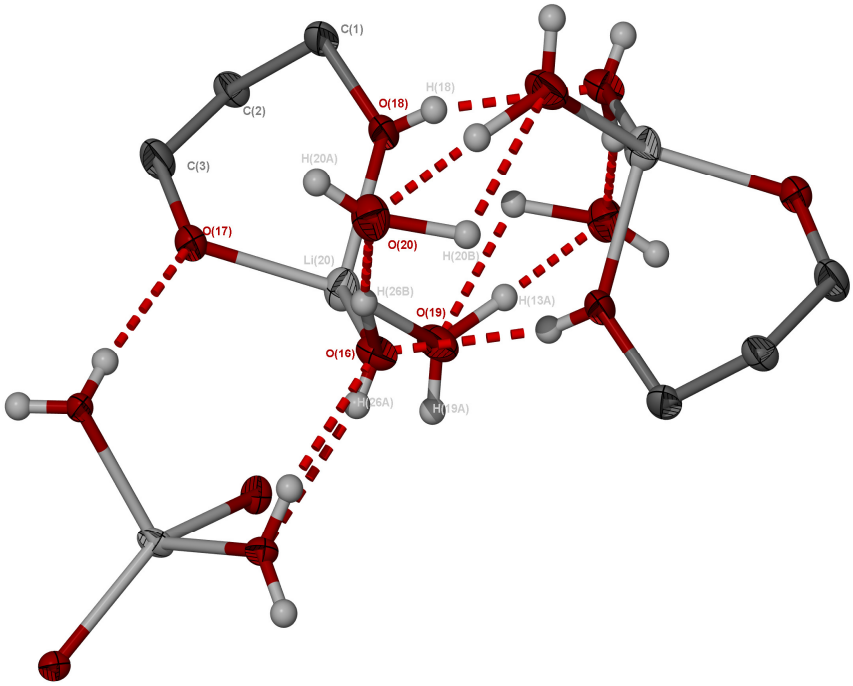

Figure 2.13: Hydrogen bonding observed for the second lithium [Li(20)] and symmetry-generated molecules.

The bond distances Li(20)-O(19) [1.924(7) Å] and Li(20)-O(16) [1.948(7) Å] do not differ significantly and are slightly smaller than the literature values observed for $Li_2(C_6H_{12}O_2)_2$(TMPP) [2.24(9) and 2.40(1)].[32] The lithium [Li(20)] coordinated to the 4-hydroxy-4-methylpentan-2-one also deviates from tetrahedral geometry. The distances, Li(20)-O(17) [2.012(7) Å] and Li(20)-O(18) [2.000(7) Å] are in agreement with reported literature values for $Li_2(C_6H_{12}O_2)_2$(TMPP) [1.943(9) and 2.059(9)].[32] The increase

[32] J. Arnold, D. Y. Dawson, C. G. Hoffman, *J. Am. Chem. Soc*., **1993**, *115*, 2707.

observed in the angle of O(19)-Li(20)-O(17) [138.1(4)º] is accompanied by a decrease in the angle of O(17)-Li(20)-O(18) [89.4(3)º]. These observations can be attributed to the constraint caused by the bidentate coordination of the 4-hydroxy-4-methylpentan-2-one, resulting in the formation of a 6-membered ring [O(17)-C(3)-C(2)-C(1)-O(18)-Li(20)]. The hydrogen bonds are tabulated in Table 2.6 and symmetry codes are provided.

Table 2.6: The hydrogen bonding between the second lithium cation [Li(20)] and its symmetry generated units.

Hydrogen bonds lithium (20)	
O(16)-H(26B)···O(20)	1.67(4)
O(18)-H(18)···O(16)$^{\&}$	2.23(5)
O(16)- H(26A)···O(12)$^{\&}$	2.16(4)
O(19)- H(19B)···O(20)$^{\&}$	1.65(4)
O(20)-H(20B)···O(19)$^{\&}$	2.770(4)

Where $^{\&}$= -x, 1-y, -z.

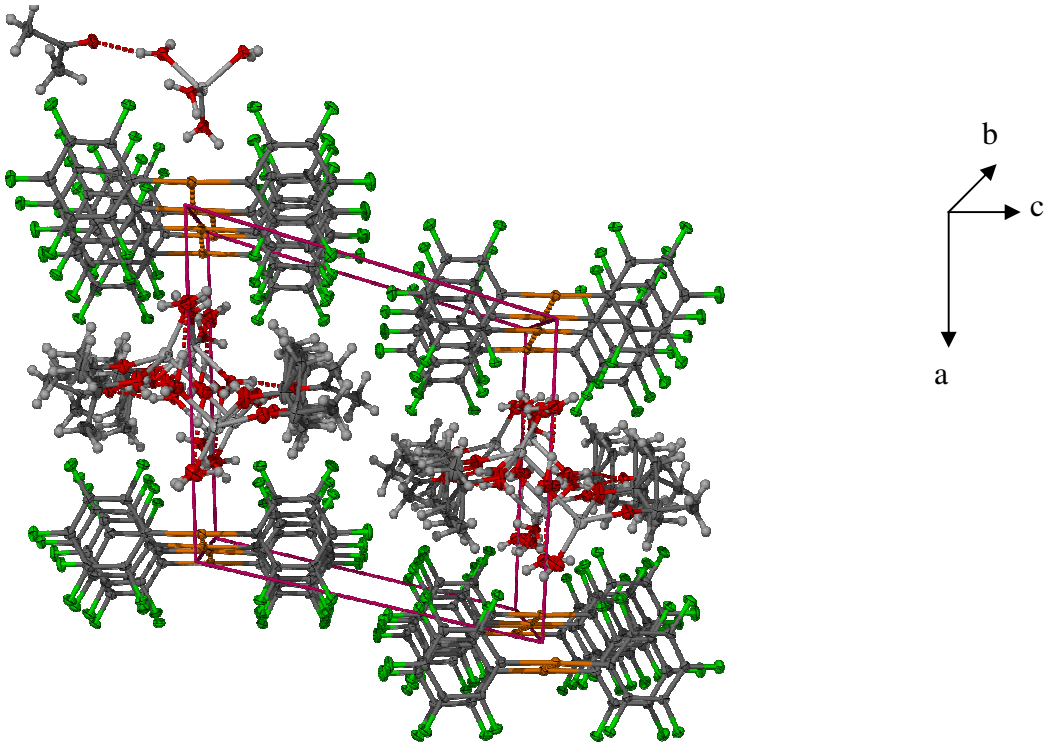

Figure 2.14: Solid-state packing of **3** viewed along the b-axis.

The anions are associated in pairs along the b-axis. Elongation of cation (hydrogen bonding) and anion (aurophilic interactions and π-stacking) layers are observed along the

b-axis and a layer of cations are observed along the c-axis. Along the a-axis cation-pairs are alternated by the anion-pairs.

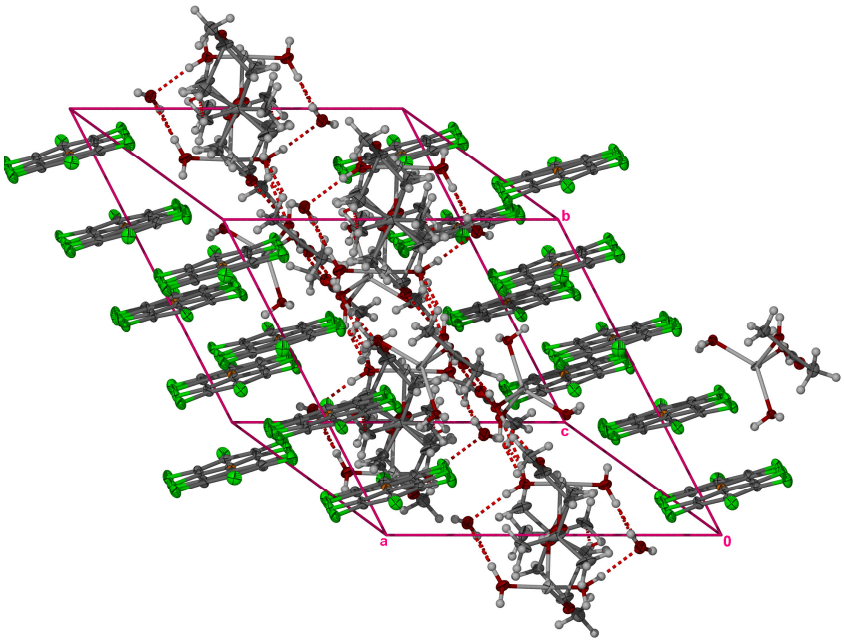

Figure 2.15: The crystal lattice organization along the ac-plane of **3**.

The anions are linked in layers along the b-axis with neighbouring layers separated by a layer of cations. Anions assemble in pairs along the b-axis with molecules in pairs linked *via* an Au···Au interaction [3.566(4)Å] and π-stacking [3.595 Å] between the pfp ligands of the aurophilic-linked anions. The presence of a non-specific hydrogen bonding involving O(20)-H(20B)···F(36) [2.1(3) Å] provides a small amount of stability to the solid state arrangement. The crystal lattice seems to be governed by hydrogen bonding, Au···Au interaction and π-stacking. The latter two are maximised by the co-planarity of the pfp rings, thus allowing a close metal-metal separation and also π-stacking.

2.2.3.3 Molecular structure of 4

The complex, **4**, crystallised from CD_2Cl_2 (a decomposing NMR sample) as colourless needles in the monoclinic space group C2/*c* with Z= 4 molecules in the unit cell. The gold centre and the centre of gravity of the hydrogen bond are positioned on the C_2 rotational axis thus Z = 4 and not Z = 8 as is the typical for the C2/*c* symmetry space group. The asymmetric unit consists of a non-interacting $Au(C_6F_5)_2^-$ anion and a 2-amino-4-methylthiazole cation co-crystallised with a 2-amino-4-methylthiazole molecule. The

molecular structure and numbering scheme are shown in Figure 2.7 with the selected bond lengths and angles summarised in Table 2.16.

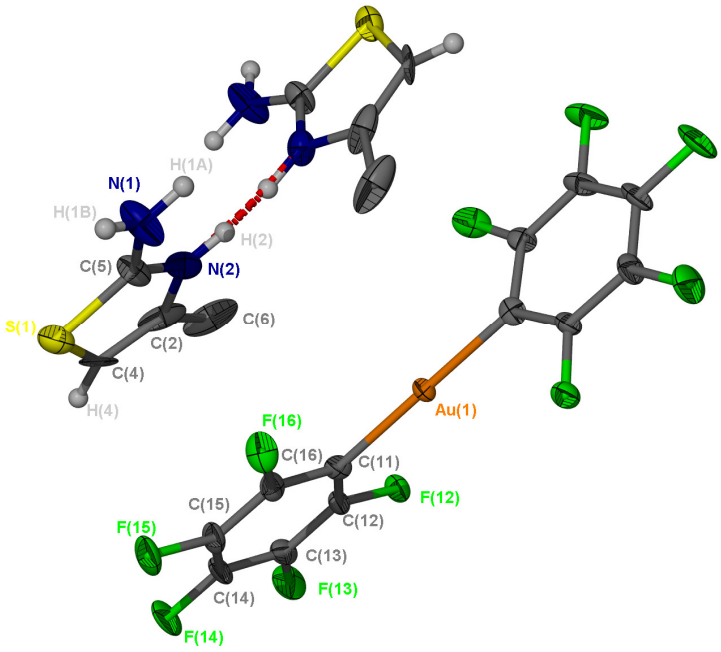

Figure 2.7: The molecular structure and numbering of **4**.

The hydrogen on N(2) is shared with a symmetry related N-atom with a hydrogen bond distance of N(2)···H(2)··N(2)$^{\$}$= 2.79(1) Å [$=1-x, y, 1/2-z]. This requires that one of the 2-amino-4-methylthiazole molecules is a cation and other one is neutral which implies that there are two molecules, in the unit cell, a free 2-amino-4-methylthiazole and a 2-amino-4-methylthiazolium cation and $Au(C_6F_5)_2^-$ anion. The formally single C(sp^2)-N(sp^2) bond, C(2)-N(2), has a bond length of 1.380(9) Å and the double C=N bond, N(2)-C(5) bond, has bond length of 1.320(8) Å, both of these values correspond to the respective values in the uncoordinated 2-amino-4-methylthiazole[27] (1.388(4) Å and 1.329(3) Å). The C(4)-C(2) bond [1.32(1) Å] is typical of a double bond in the free ligand (1.331(4) Å).[27] The single and double bond character is maintained, indicating little or no electron delocalization over these bonds. The S(1)-C(5) bond [1.711(6)Å] and S(1)-C(4) bond [1.835(9)Å] are similar to these in the free ligand [1.742(3) Å].[27] No significant difference in bond angles are observed when compared to the free ligand.[27]

Table 2.16: Selected bond lengths (Å) and angles (°) of **4** with standard uncertainty in parenthesis.

Bond lengths (Å)			
Au(1)-C(11)	2.044(6)	S(1)-C(5)	1.711(6)
N(2)-C(5)	1.320(8)	C(2)-C(4)	1.32(1)
N(2)-C(2)	1.380(9)	S(1)-C(4)	1.835(9)
Bond angles (º)			
C(11)-Au(1)-C(11)	179.9(3)	N(2)-C(2)-C(6)	117.6(7)
C(5)-N(2)-C(2)	111.5(6)	C(2)-C(4)-S(1)	107.8(5)
C(5)-S(1)-C(4)	88.3(3)		

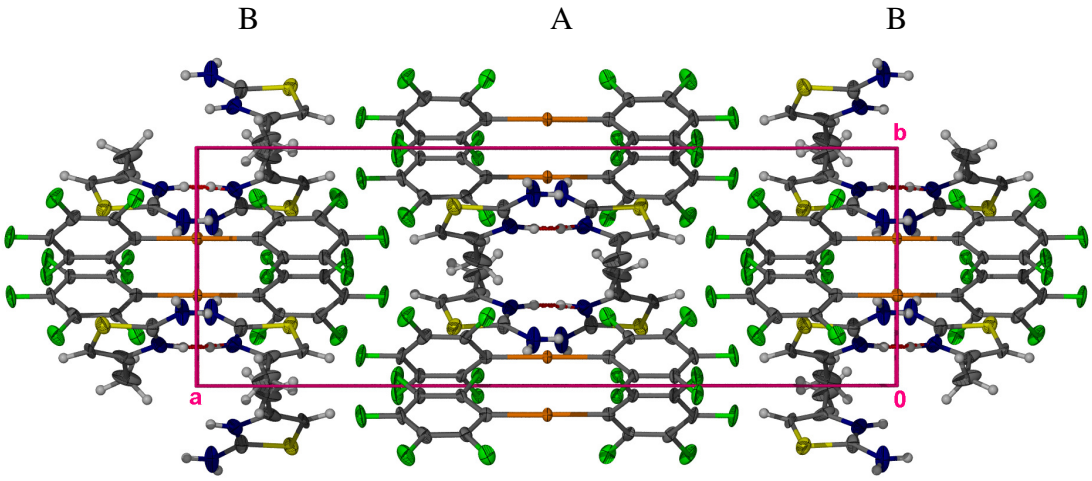

Figure 2.8: The solid-state packing of **4** viewed along the c-axis.

Two distinct layers (A and B) which alternate along the a-axis are observerable. Weak π-stacking [4.442 Å] between the pfp rings and the 5-membered rings which are parallel occurs.

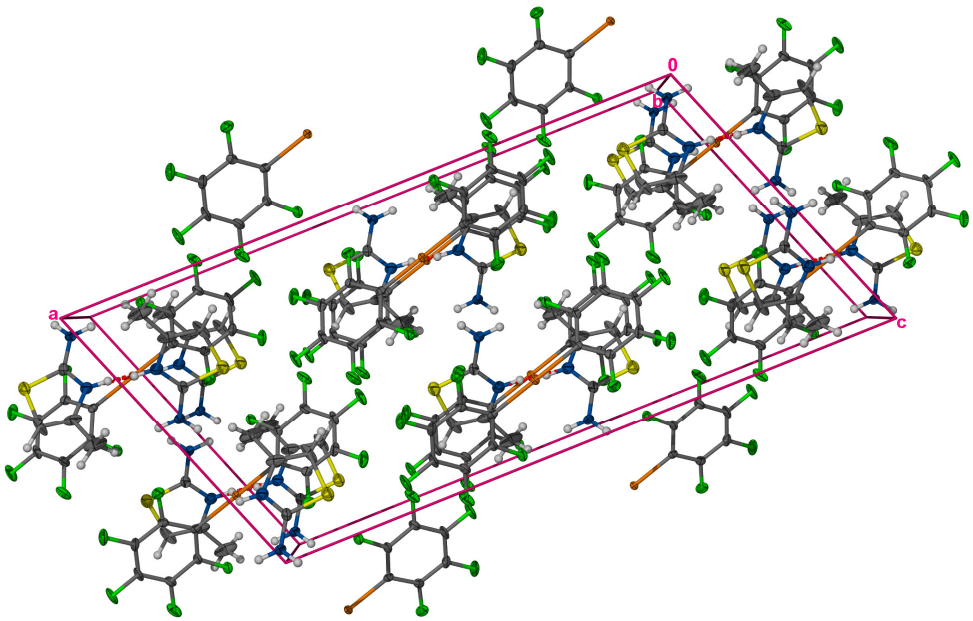

Figure 2.9: The molecular organization of **4** viewed along the ac-plane.

There is evidence of π-π stacking in layers between the pfp of the gold atoms and the thiazole rings [4.657 Å] and [3.705 Å]. Intermolecular aurophilic interactions are absent, the pfp rings of the anion are not planar resulting in a large metal-metal separation [6.580 Å]. The alignment of the thiazole molecules in between the anions also prevents metal-metal contacts. The hydrogen on N(2) is shared between the symmetry generated and symmetric thiazole which only holds the thiazoles together and has no impact on crystal packing thus crystal lattice organisation is ruled by π-stacking only.

2.2.3.4 Molecular structure of 2-aminothiazoline(pentafluorophenyl)gold(I), 5

Colourless blocks of **5** crystallised from CD_2Cl_2 (a decomposing NMR sample) in the monoclinic space group $P2_1/c$ with Z=4 molecules in the unit cell. The asymmetric unit consists of an independent molecule. The molecular structure and numbering scheme are shown in Figure 2.10 with the selected bond lengths and angles summarised in Table 2.17.

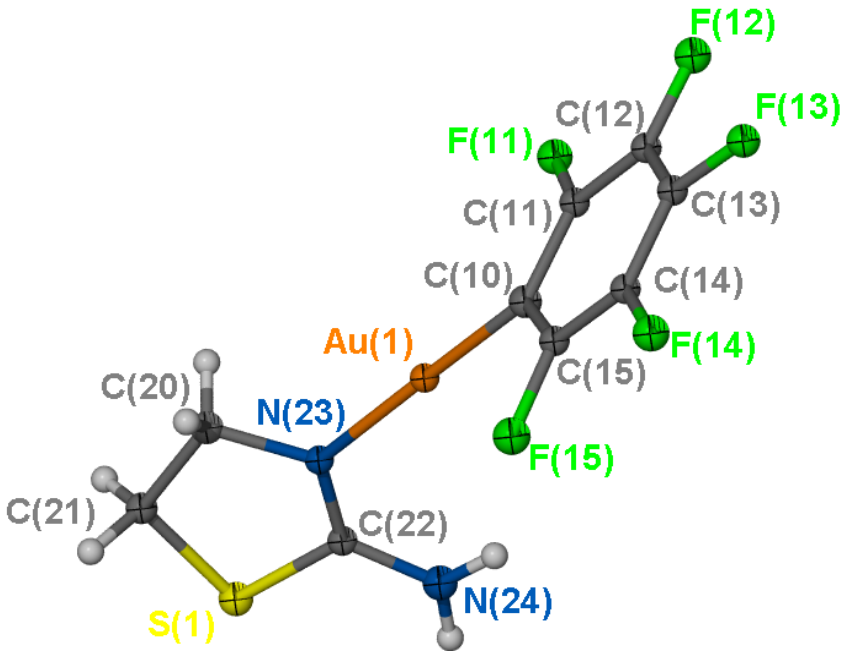

Figure 2.10: The molecular structure of **5**.

Laguna and co-workers[22] have previously affected the displacement of the labile tht ligand in the gold(I)precursor, $Au(C_6F_5)$tht, in order to obtain the coordination of 2-aminothiazoline ligand to the AuC_6F_5-moiety. The product was characterised by FAB-MS spectrometry, IR- and NMR spectroscopy but no crystal structure was determined.

The molecular structure of complex **5** can be described as a discrete monomer consisting of the $AuC_6F_5^-$ unit, coordinated to a neutral 2-aminothiazoline. The coordination about the metal centre is linear [177.4(2)º]. The Au-C separation of the imine coordinated complex, Au(1)-C(10) [1.985(7) Å] and the Au-N bond therein, Au(1)-N(23) [2.022(5) Å], are consistent with those reported for imine (pentafluorophenyl)gold(I) analogues.[14,22] The planes of the pfp and 2-aminothiazoline ligand are almost perpendicular at 82.5º. The C-N and C=N bond distances [C(20)-N(23) and C(22)-N(23) at 1.455(8) Å and 1.291(8) Å, respectively] are consistent with those in the uncoordinated ligand [1.465(2) Å and 1.302(2) Å].[22] These C-N double bonds and C-N single bonds do not differ substantially from standard values reported for such bonds [1.27 Å and 1.41 Å respectively].[28] The S-C bond distances of C(22)-S(1) and C(21)-S(1) at 1.754(6) Å and 1.808(6) Å, respectively, are in agreement with those in the ligand [1.746(2) Å and 1.823(2) Å].[35] The C-C bond distance [C(20)-C(21) at 1.536(9)Å] is similar in length to the same bond in the free 2-aminothiazoline [1.523(3) Å]. The angles in the 2-aminothiazoline ligand do not differ

significantly from those in the free ligand and the 2-aminothiazoline remains mostly unaltered by coordination.

Table 2.17: Selected bond lengths (Å) and angles (°) of **5** with standard uncertainty in parenthesis.

Bond lengths (Å)			
Au(1)-C(10)	1.985(7)	C(22)-N(24)	1.335(8)
Au(1)-N(23)	2.052(5)	C(22)-S(1)	1.754(6)
N(23)-C(22)	1.291(8)	C(20)-C(21)	1.536(9)
N(23)-C(20)	1.455(8)	S(1)-C(21)	1.808(6)
Bond angles (º)			
C(10)-Au(1)-N(23)	177.4(2)	N(23)-C(20)-C(21)	110.1(5)
C(22)-N(23)-C(20)	114.8(5)	C(22)-S(1)-C(21)	91.1(3)
N(23)-C(22)-S(1)	116.4(5)	C(20)-C(21)-S(1)	107.1(4)

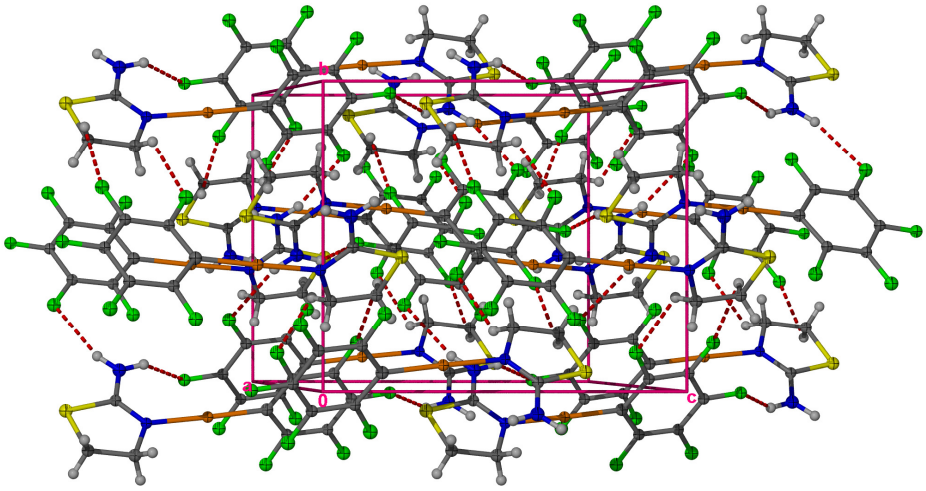

Figure 2.11: The molecular packing of **5** viewed along the bc-plane.

A view along the bc-plane reveals a head-to-tail packing along the c-axis of the molecules. It is interesting that no intermolecular aurophilic interaction occurs in this simple gold(I) complex which consists of ligands with no large steric demands. It appears that the absence of co-planarity of the two ligands prohibits metal contacts shorter than 10.164 Å along the a-axis and 7.703Å along the b-axis. The molecules are paired in the crystal lattice by weak interaction involving the hydrogen bearing CH_2 and NH_2 groups of the aminoazole ligand and the pfp ligand of a neighbouring molecule [C(20)-H(20B)···F(15), C(21)-H(21A)···F(14), C(24)-H(24A)···F(13) and C(24)-H(24B)···F(12) of 2.662 Å ,

2.579(4) Å, 2.493 Å and 2.627 Å]. These distances are close to the sum of the van der Waals radii of the fluorine atom and a carbon atom.

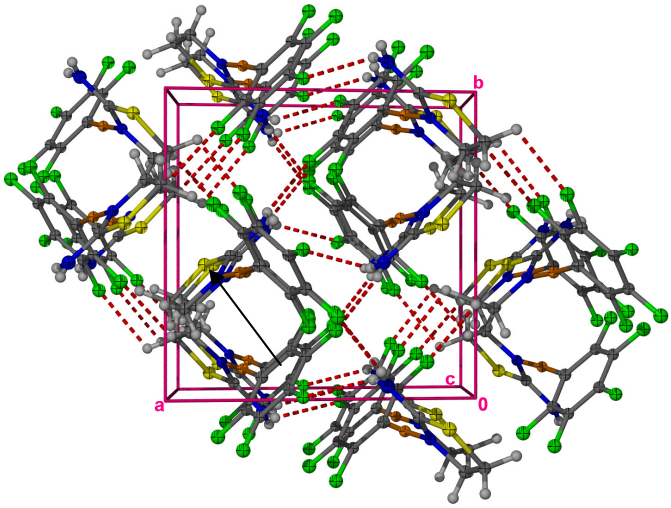

Figure 2.12: The solid-state packing of **5** viewed along the c-axis showing channels.

A view along the c-axis of the crystal lattice reveals the presence of open channels. The open channels are not large enough to host a solvent molecule. The presence of weak π-stacking [3.985 Å] between the 5-membered rings of the 2-aminothiazoline ligand was also noted. The crystal lattice organisation appears to be directed by the presence of weak H···F interactions and weak π-stacking.

2.2.3.5 Crystal structure of 2-amino-4-methylthiazole(triphenylphosphine)gold(I) nitrate, 6

Colourless needles of **6** were crystallised from CD_2Cl_2 (an NMR sample) in the triclinic space group *P*ī with Z=2 molecules in the unit cell. The asymmetric unit consists of a neutral imine ligand coordinated to a $[AuPPh_3]^+$ unit, affording a charged complex neutralised by a nitrate anion, which in turn is involved in hydrogen bonding to the cation of a neighbouring cation-anion pair. The molecular structure and numbering scheme are shown in Figure 2.13 with the selected bond lengths and angles summarised in Table 2.18.

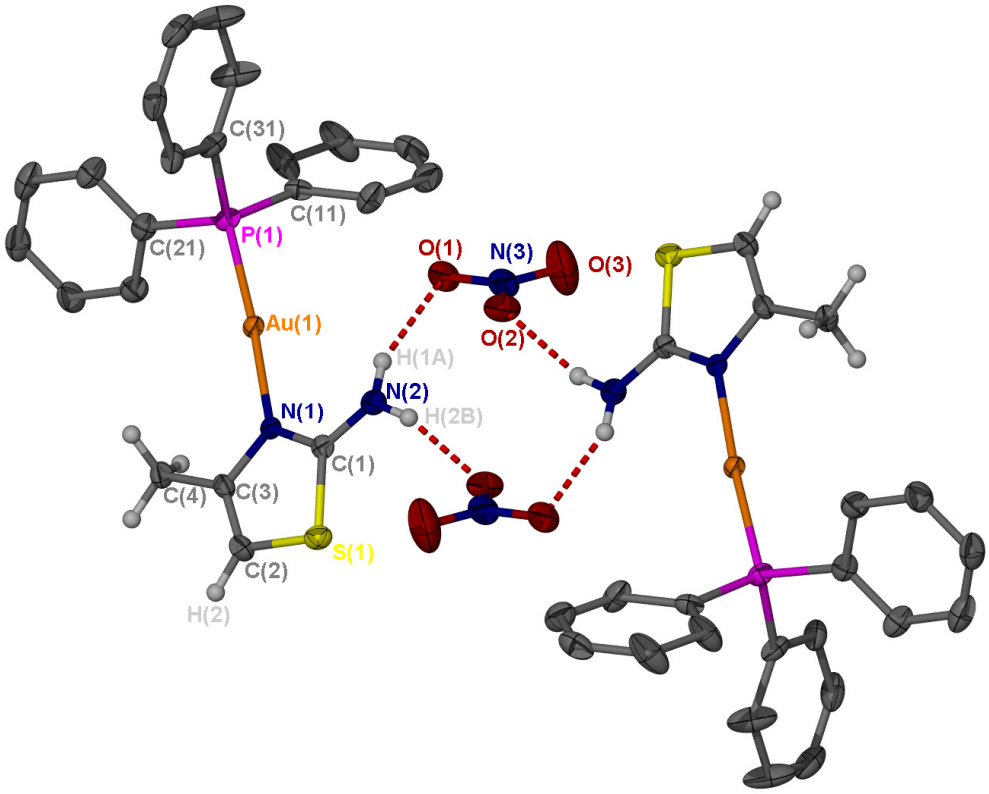

Figure 2.13: The molecular structure of **6** with a symmetry generated (unlabeled) neighbouring molecule to show hydrogen bonding.

As mentioned in the beginning of this section the Au-N and Au-P bond lengths are normal as is the N-Au-P angle. The C-N double bond length [1.317(5) Å] and the C-N single bond length [1.405(4) Å] are normal and indicate double and single bond character, respectively. These C-N double and single bonds are in agreement with reported standard values for the respective bonds [1.27 Å and 1.41 Å][28] and do not differ significantly from values for these bonds in the free ligand [1.329(3) and 1.388(4)Å].[27] The S-C bond distance [1.737(4) Å] and C(2)-S(1)-C(1) bond angle [89.2(8)º] are identical to those in the uncoordinated ligand [1.712(3) Å, 1.742(3) Å, 90.2(1)º].[27] The angle between the planes of the NO_3^- [O(1)-N(1)-O(2)-O(3)] and the aminoazole ligand [N(1)-C(1)-C(2)-C(3)-C(4)-N(2)] is 56.78(0.03)º. The bond angles of the nitrate counterion at O(3)-N(3)-O(2) [120.0(4)º], O(3)-N(3)-O(1) [121.2(3)º] and O(2)-N(3)-O(1) [118.9(4)º] are nearly 120º indicating ideal triangular geometry for the central nitrogen, these angles concur with those reported in literature. [33] The N-O lengths do not differ significantly from each other [O(1)-N(3) at 1.264(5) Å, O(2)-N(3) at 1.250(5) Å and O(3)-N(3) at 1.233(6) Å] and

[33] C.H. Wei, K.B. Jacobson, *Inorg. Chem.*, **1981**, *20*, 356.

concur with the reported literature values of [1.243, 1.244 and 1.221 Å].[33]

Table 2.18: Selected bond lengths (Å) and angles (°) of **6** with standard uncertainty in parenthesis.

Bond lengths (Å)			
Au(1)-N(1)	2.073(3)	O(1)-N(3)	1.264(5)
Au(1)-P(1)	2.246(1)	O(2)-N(3)	1.250(5)
S(1)-C(2)	1.737(4)	O(3)-N(3)	1.233(6)
S(1)-C(1)	1.737(4)	N(2)-C(1)	1.338(5)
P(1)-C(31)	1.816(2)	N(1)-C(1)	1.317(5)
P(1)-C(21)	1.826(2)	N(1)-C(3)	1.405(4)
P(1)-C(11)	1.832(2)	C(2)-C(3)	1.334(5)
Bond angles (º)			
N(1)-Au(1)-P(1)	175.58(8)	C(3)-N(2)-Au(1)	121.0(2)
C(2)-S(1)-C(1)	89.2(8)	O(3)-N(3)-O(2)	120.0(4)
C(31)-P(1)-Au(1)	114.71(9)	O(3)-N(3)-O(1)	121.2(4)
C(21)-P(1)-Au(1)	110.23(9)	O(2)-N(3)-O(1)	118.9(4)
C(11)-P(1)-Au(1)	112.60(9)	N(1)-C(1)-S(1)	113.2(3)
C(1)-N(1)-C(3)	112.2(3)	C(3)-C(2)-S(1)	111.7(3)
C(1)-N(1)-Au(1)	126.7(2)	C(2)-C(3)-N(1)	113.6(3)

A view of the crystal lattice along the a-axis indicates a head to tail arrangement of the complex along the b-axis (Figure 2.14). The π-stacking of the thiazole rings [3.932 Å] seems to order the head-to-tail fashion of packing. The gold atoms are located along the b-axis with a metal-metal separation of 6.836 Å and thus no aurophilic interaction is observed. The sterically bulky phenyl rings of the PPh_3 ligand seem to prevent a smaller metal-metal separation than 9.510 Å along the a-axis. Hydrogen bonding is observed between the amine hydrogen and the oxygen of the nitrate ion, N(2)-H(1A)···O(1) at 2.11(5) Å and N(2)-H(1B)···O(2) [1-x,1-y,-z] at 2.07(5) Å. The π-stacking and hydrogen bonding interactions seem to dictate the ordering of the crystal lattice.

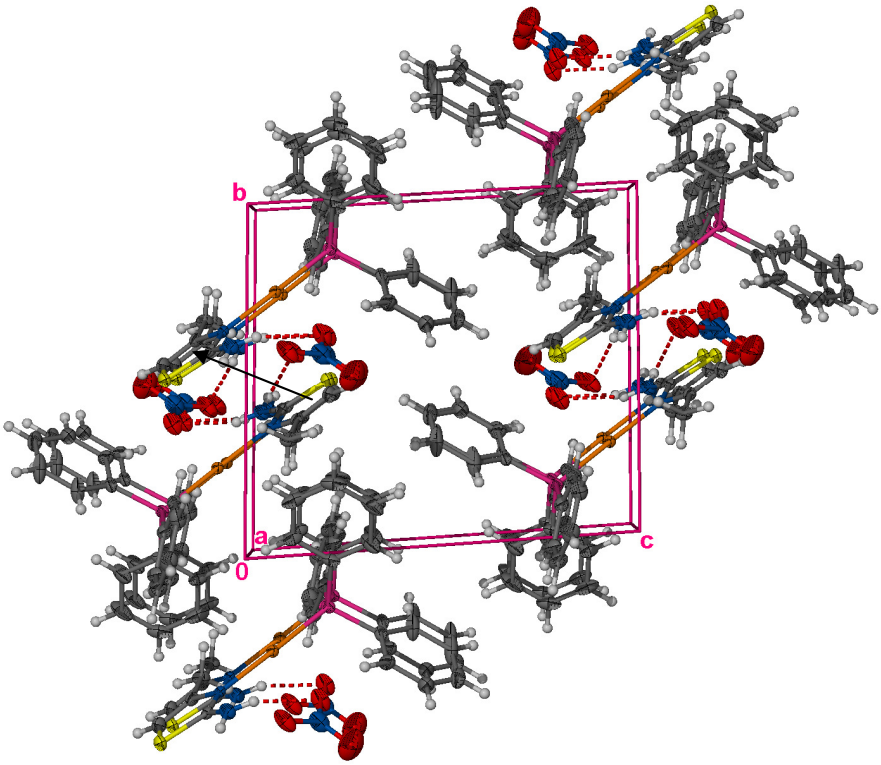

Figure 2.14: Solid-state packing of **6** viewed along the a-axis. Hydrogen bonds are indicated by a dashed line.

2.2.3.6 Crystal structure of 2-aminobenzothiazole(triphenylphosphine)gold(I) nitrate, 7

Complex **7** co-crystallised with one molecule of dichloromethane in the triclinic space group *P*$\bar{1}$ with Z = 2 molecules in the unit cell. The asymmetric unit contains one unique ionic part consisting of a gold(I) complex cation and a NO_3^- counterion interacting with a dichloromethane solvent molecule. A hydrogen bond between the amine proton of the 2-aminobenzothiazole ligand and the oxygen of the nitrate counter ion is also observed. The molecular structure and numbering scheme are shown in Figure 2.15 with the selected bond lengths and angles summarised in Table 2.19.

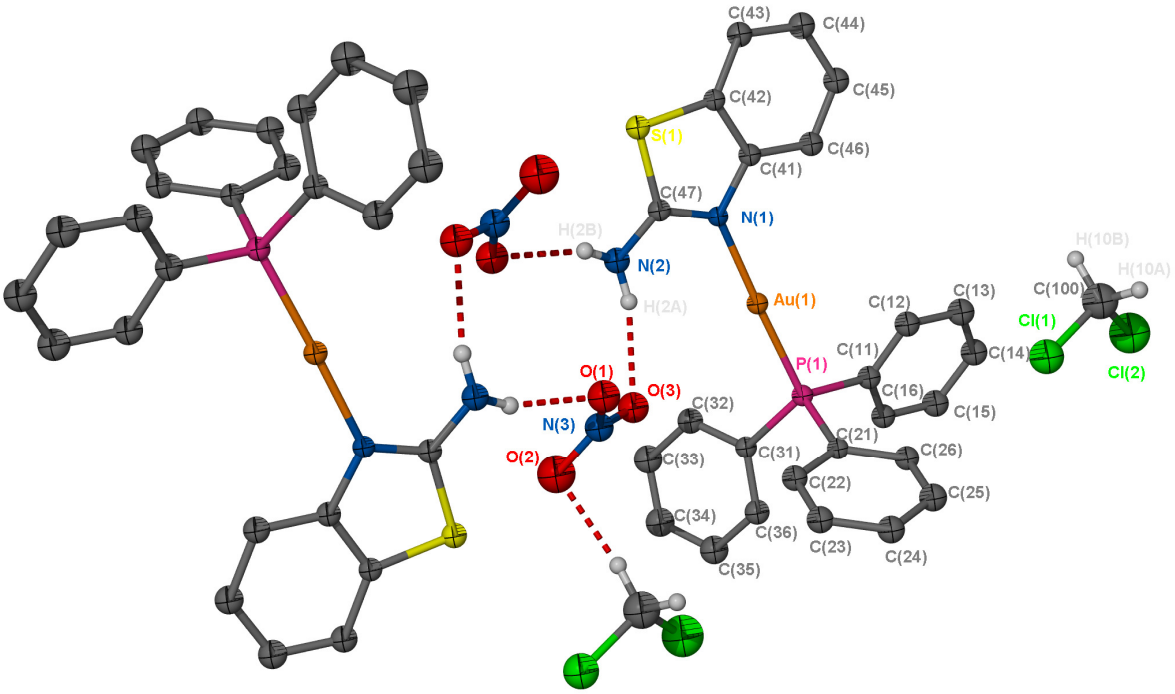

Figure 2.15: The molecular structure of **7** showing the hydrogen bonding involving the symmetry-generated atoms. Non-essential hydrogen atoms were omitted for clarity

The Au-N and Au-P bond distances and N-Au-P bond angle are normal as mentioned at the beginning of this section (section 2.3). The C-N single bonds of N(1)-C(41) [1.40(1) Å] and C(47)-N(2) [1.33(1) Å] agree with literature values [1.397(7) Å and 1.315(8) Å] while the C-N double bond, C(47)-N(1) [1.32(1) Å] also agrees with the literature value [1.340(7) Å].[34] The only true C-N single bond is N(1)-C(41) [1.40(1) Å] while the bond lengths for C(47)-N(2) [1.33(1) Å] and the C-N double bond, C(47)-N(1) [1.32(1) Å], indicate delocalisation over the N(2)-C(47)-N(1) bonds. The N(2)-C(47)-N(1) angle of 111.4(7)º is smaller than in the protonated ligand [122.4(6)º][34] in $(HL)_2CuCl_4$, where HL = 2-aminobenzothiazolium. The C-S distances [1.753(8) Å and 1.749(8) Å] and C(47)-S(1)-C(42) angle [89.4(4)º] agree with the corresponding distances and angle in the free ligand [1.726(6) Å, 1.762(6) Å and 90.7(3)º] in $(HL)_2CuCl_4$.[34] All the other bond lengths and bond angles in the coordinated 2-aminobenzothiazole agree with those in the free ligand.

The angle between the plane of the NO_3^- [O(1)-N(1)-O(2)-O(3)] and the imine ligand [N(1)-C(47)-N(2)-C(41)-C(42)-C(43)-C(44)-C(45)-C(46)] is 48.47º. The N-O distances

[34] L.Antolini, A. Benedetti, A.C. Fabretti, A. Giusti, *Inorg. Chem.,* **1988**, *27,* 2192.

1.25(1)-1.26(2) Å are similar to those reported in literature with values of 1.221-1.244 Å.[33] The bond angles around the nitrogen atom of the nitrate anion show no noteworthy differences.[33]

Table 2.19: Selected bond lengths (Å) and angles (°) of **7** with standard uncertainty in parenthesis.

Bond lengths (Å)			
Au(1)-N(1)	2.044(6)	N(1)-C(47)	1.32(1)
Au(1)-P(1)	2.233(2)	N(2)-C(47)	1.33(1)
C(41)-N(1)	1.40(1)	O(3)-N(3)	1.26(1)
C(42)-S(1)	1.753(8)	O(1)-N(3)	1.25(1)
S(1)-C(47)	1.749(8)	N(3)-O(2)	1.26(2)
Bond angles (º)			
N(1)-Au(1)-P(1)	178.3(8)	N(1)-C(47)-S(1)	114.9(6)
C(31)-P(1)-C(11)	108.9(4)	N(2)-C(47)-S(1)	120.5(7)
C(31)-P(1)-C(21)	104.0(4)	O(1)-N(3)-O(2)	119.3(8)
C(11)-P(1)-C(21)	104.9(4)	O(1)-N(3)-O(3)	120.1(8)
C(41)-C(42)-S(1)	109.8(6)	O(2)-N(3)-O(3)	120.4(9)
C(47)-N(1)-C(41)	111.4(7)	C(47)-N(1)-C(41)	111.4(7)º
N(1)-C(47)-N(2)	124.6(8)	C(47)-S(1)-C(42)	89.4(4)º

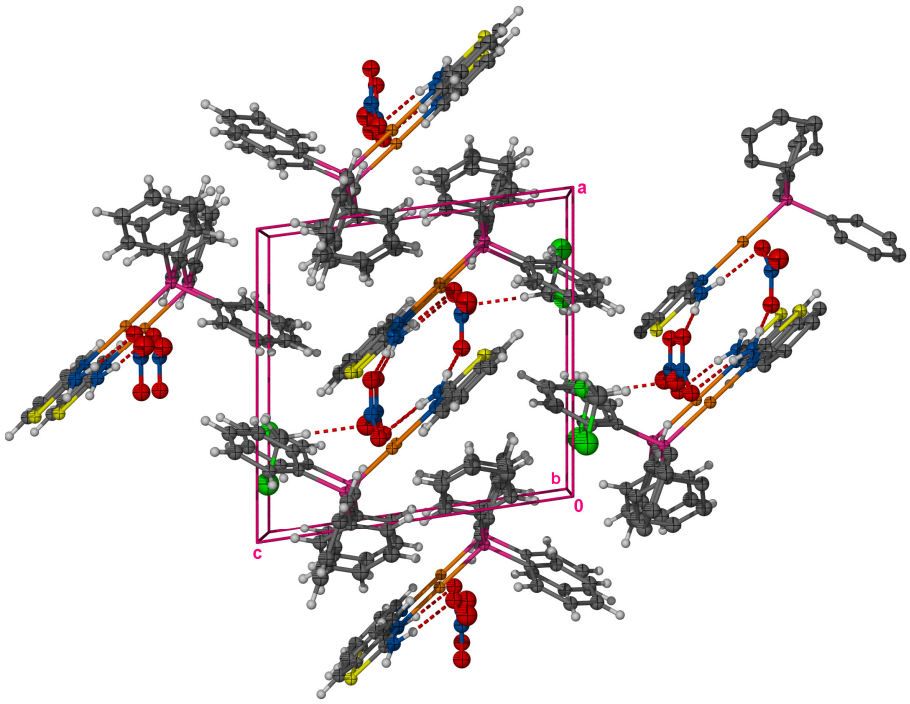

Figure 2.16: The solid-state packing of **7** viewed along the b-axis.

The crystal lattice of **7** displays a molecular arrangement similar to that of complex **6**. A head-to-tail arrangement is observed along the a-axis. While a face-to-face arrangement of the molecules (on top of each other) is observed along the b-axis. These "dimers" are linked *via* hydrogen bonds, N(2)-H(2A)···O(3) and N(2)-H(2B)···O(1) [1-x, -y, -z-1] at 2.1(3) Å and 2.0(1) Å respectively. The dichloromethane is hydrogen bonded to the symmetry generated oxygen of the nitrate C(100)-H(10B)···O(2) at 3.18(7)Å [1-x, -y, -z-1]. The solid state packing of **7** is largely governed by hydrogen bonding and weak π-stacking [3.710 Å].

The presence of the sterically bulky phenyl rings prevents the formation of closer gold-gold contacts and the aurophilic interaction is absent. The absence of aurophilic interactions can also be attributed to the steric demands of the 2-aminobenzothiazole preventing a molecular separation smaller than 4.047 Å. The favouring of hydrogen bond formation over aurophilic association may be an enthalpy effect. Through NMR experiments the energy of aurophilic interactions [29-30 $kJ.mol^{-1}$] and hydrogen bonding [20-30 $kJ.mol^{-1}$] were estimated to be of the same magnitude.[35] Hydrogen bonding in the unit cell occurs in a ratio of 5:2 (interaction:molecules) while the aurophilic interaction ratio would have been 1:2 if one could predict it. The formation of hydrogen bonds brings about a higher energy gain, compared to association *via* aurophilic interactions.[35] This observation is in agreement with those of Laguna and co-workers who stated that hydrogen bonding can compete with aurophilic interaction.[36]

2.2.3.7 Molecular structure of bis(2-aminobenzothiazole)silver(I), 8

The unexpected discovery of **8** is attributed to the crystallisation of the compound from a concentrated solution of crude **7** in an acetone solution. Amounts of silver nitrate left during the synthesis of PPh_3AuNO_3 afforded **8**. The compound crystallises in the monoclinic space group $P2_1/n$ with Z= 4 molecules in the unit cell. The asymmetric unit contains a single molecule, which co-crystallised with a molecule of dichloromethane. The molecular structure is shown in Figure 2.17 and the molecular data are displayed in

[35] H. Schmidbaur, W. Graf, W. Müller, G. Müller, *Angew. Chem. Int., Ed. Eng.* **1988**, *27*, 417.
[36] A. Codina, E.J. Fernández, P.G. Jones, A. Laguna, J.M. López-de-Luzuriaga, M. Monge, M.E. Olmos, J. Pérez, M.A. Rodriguez, *J. Am. Chem. Soc*. **2002**, *124*, 6781.

Table 2.20.

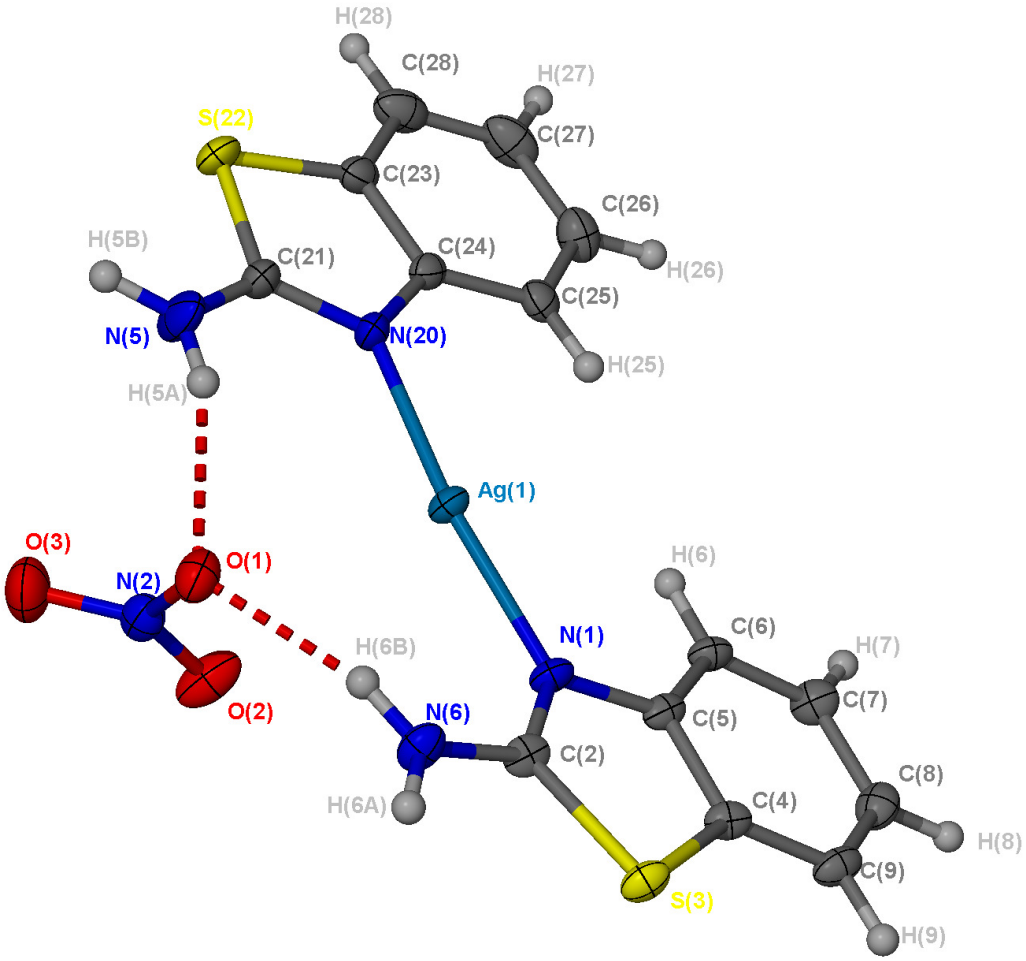

Figure 2.17: The molecular structure and atom numbering of **8**.

The N-Ag distances [2.127(5) Å and 2.142(5) Å] are similar to the reported values for $\{[AgL][CF_3SO_3]\}_\infty$ where L=*N,N*'-bis(3-pyridinecarboxamide)-1,2-ethane [2.076 Å and 2.085 Å].[37] The N-Ag-N angle [172.2(2)º] agrees with the angle in $\{[AgL][CF_3SO_3]\}_\infty$ at 173.44(6).[40] The S-C distances of S(22)-C(23) [1.736(8) Å] and S(3)-C(4) [1.739(7) Å] are in agreement with each other and reported values of the free 2-aminobenzothiazole [1.762(6) Å].[37] The other S-C distances S(22)-C(21) [1.747(7)Å] and S(3)-C(2) [1.749(7) Å] concur with each other and with the same bond distances in the uncoordinated ligand [1.726(6)Å].[37] The C-N double bond distances, C(21)-N(20) [1.316(9) Å] and C(2)-N(10) [1.295(9) Å], are similar and and do not differ from those in the free ligand [1.340(7) Å]. The C-N single bonds [1.410(9) Å and 1.404 Å] are normal [28] and in agreement with those

[37] S. Muthu, J.H.K. Yip, J.J. Vittal, *J. Chem. Soc, Dalton Trans.,* **2001**, *3577.*

in the free ligand [1.398(8) Å].[37] There are no noteworthy differences between the bond lengths and bond angles of the uncoordinated ligand and those of the coordinated ligand. The plane defined by the coordinated 2-aminobenzothiazole, N(6)-C(2)-S(3)-C(4)-N(1)-C(5)-C(6)-C(7)-C(8)-C(9), and the plane of a second coordinated ligand N(25)-C(21)-N(20)-S(22)-C(23)-C(24)-C(25)-C(26)-C(27)-C(28)-C(29), have an interplanar angle of 5.47(0.24)º. The NO_3^- [O(1)-N(1)-O(2)-O(3)] has an interplanar angle of 74.11(0.20)º with the silver cation.

Table 2.20: Selected bond lengths (Å) and angles (°) of **8** with standard uncertainty in parenthesis.

Bond lengths (Å)			
Ag(1)-N(20)	2.127(5)	S(3)-C(4)	1.739(7)
Ag(1)-N(1)	2.142(5)	S(3)-C(2)	1.749(7)
N(20)-C(21)	1.316(9)	C(23)-C(24)	1.399(9)
N(20)-C(24)	1.401(9)	N(1)-C(2)	1.295(9)
S(22)-C(23)	1.736(8)	N(1)-C(5)	1.410(9)
S(22)-C(21)	1.747(7)	C(4)-C(5)	1.404(9)
N(25)-C(21)	1.34(1)	N(6)-C(2)	1.326(9)
Bond angles (º)			
N(20)-Ag(1)-N(1)	172.2(2)	C(4)-S(3)-C(2)	89.9(3)
C(21)-N(20)-C(24)	110.3(6)	C(2)-N(1)-C(5)	111.7(6)
C(23)-S(22)-C(21)	89.0(3)	N(1)-C(2)-S(3)	114.9(5)
N(20)-C(21)-S(22)	115.9(5)		

Along the b-axis the molecules have a π-π distance of 5.817 Å which is too large for π-π stacking. The solvent molecule, dichloromethane is interdispersed between the monomeric cation-anion units. There are repeating layers of the momomeric units along the a-axis. The presence of hydrogen bonds is observed between the amine groups on the 2-aminobenzothiazole ligand and the nitrate ion. The hydrogen bonds, N(6)-H(6A)···O(2)* [2.07(8) Å] (where*= x, y-1, z), N(6)-H(6B)···O(1) [1.98(7) Å], N(25)-H(25A)···O(1) [2.14(8) Å] and N(25)-H(25B)···O(1)$ [2.09(8) Å] (where $= 3/2-x, 1/2+y, 1/2-z) govern the crystal lattice organization.

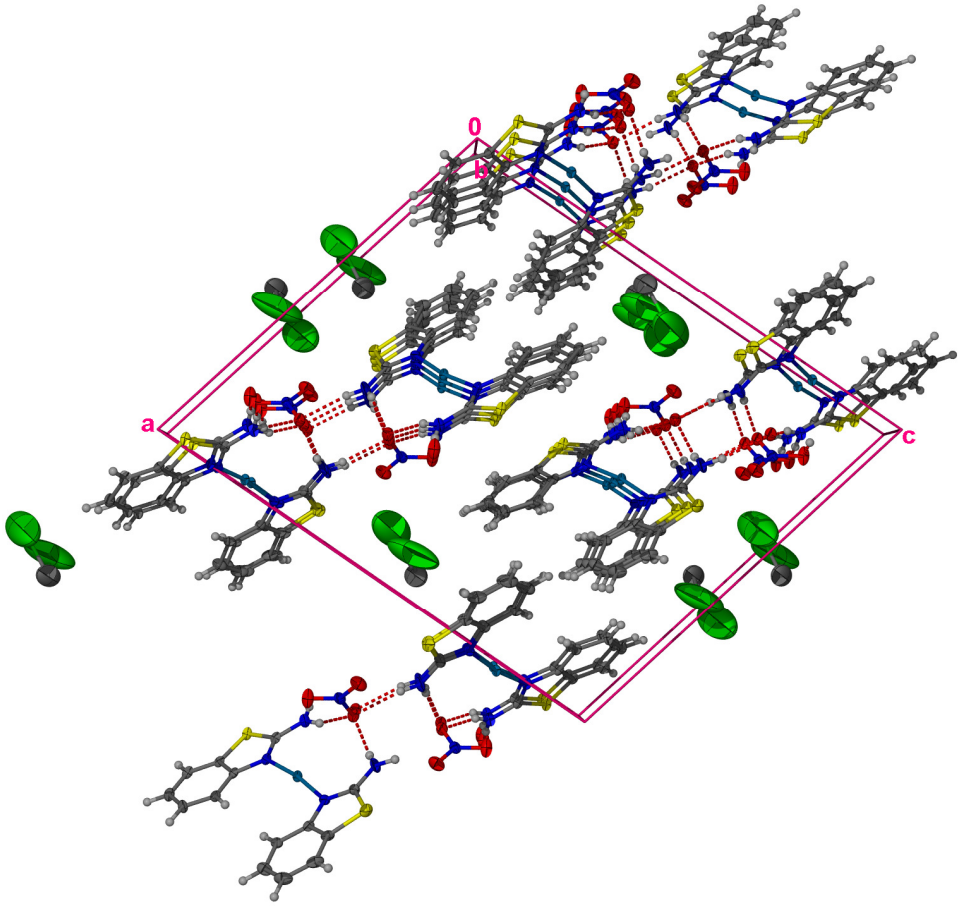

Figure 2.18: The solid-state packing of **8** viewed along the ac-plane with a highly disordered dichloromethane molecule.

2.2.3.8 Molecular structure of μ$_2$-(2-mercapto-ethyl-cyanamide-κ,S)bis(triphenylphosphine)gold(I) nitrate,9

The unusual dinuclear mercapto complex, **9**, crystallised as colourless blocks from an acetone solution in the monoclinic space group $P2_1$ with only two unique molecules within the unit cell. The molecular structure is shown in Figure 2.26 and the numbering of the atoms are shown in Figure 2.19 with the selected bond lengths and angles summarised in Table 2.21.

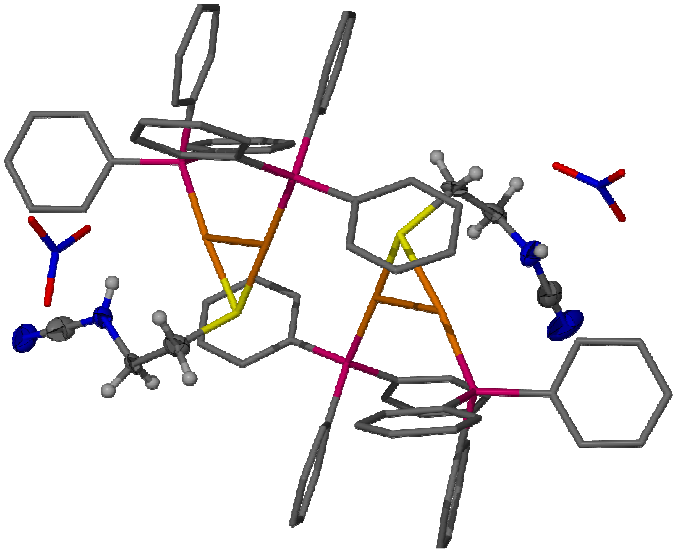

Figure 2.19: The content of the unit cell of **9**.

The unexpected ring opening of the 2-aminothiazoline gave a new ligand, 2-mercapto-ethyl-cyanamide, which then coordinated *via* the sulphur atom to each of the gold fragments, yielding μ_2-(2-mercapto-ethyl-cyanamide-κ,S)bis(triphenylphosphine)gold(I) nitrate, complex **9**.

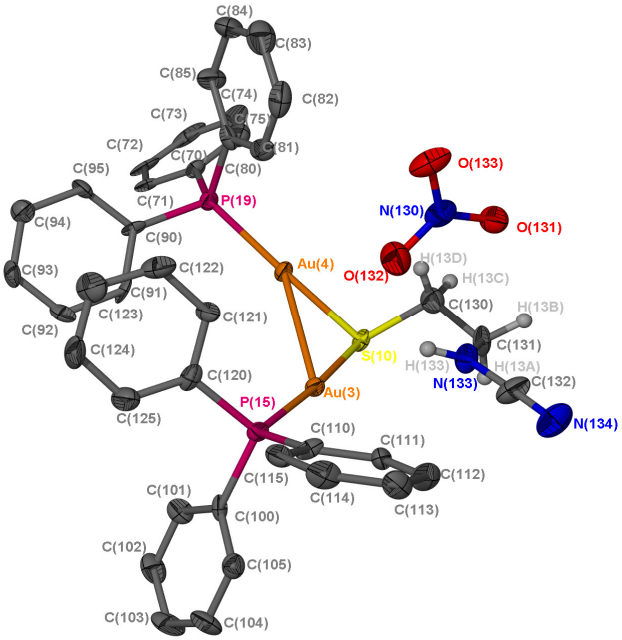

Figure 2.20: A molecule of **9** in the unit cell. The phenyl hydrogen atoms were omitted for clarity.

The two molecules in the asymmetric unit do not show noteworthy discrepancies when compared to each other. The intramolecular aurophillic interaction with Au(4)···Au(3) bond distances of 3.0901(6) Å and Au(1)···Au(2) of 3.1142(6) Å are noted. The Au-P

bond distances, Au(3)-P(15) [2.259(3) Å] and Au(4)-P(19) [2.270(3)Å], agree and are similar to the reported literature values of [S(Au_2dppf)] (dppf= 1,1–bis(diphenylphosphine)ferrocene) [2.247(2) Å].[38] The Au-S distances [Au(3)-S(10) and Au(4)-S(10) of 2.325(3) Å and 2.324(3) Å] agree with the Au-S bond distance in the complex [S(Au_2dppf)] [2.300(2) Å].[38]

The P-Au-S angles are all larger than the reported values for the related complex, [S(Au_2dppf)] [173.78(6)º],[38] with the P(19)-Au(4)-S(10) angle at 175.2º(1) and the P(15)-Au(3)-S(10) angle at 178.2º(1). The rest of the angles do not show any noteworthy discrepancies.

The molecules in the asymmetric unit of **9**, assemble in a head-to-head fashion in pairs along the c-axis and each unique molecule is stacked on top of another along the a-axis. There is no π-staking [10.40 Å] between phenyl rings of neighbouring rings. No hydrogen bonding is observed. The head-to-head stacking of each molecule in the asymmetric unit is governed by intermolecular aurophilic interactions, Au(2)···Au(4) at 3.934(7) Å.

[38] F. Canales, M.C. Gimeo, A. Laguna, P.G. Jones, *J. Am. Chem. Soc*., **1996**, *118*, 4839.

Table 2.21: Selected bond lengths (Å) and angles (°) of **9** with standard uncertainty in parenthesis.

Bond lengths (Å)			
Au(1)-P(2)	2.252(3)	O(2)-N(6)	1.14(2)
Au(1)-S(1)	2.318(3)	O(3)-N(6)	1.24 (2)
Au(1)-Au(2)	3.1142(6)	Au(4)-P(19)	2.270(3)
S(1)-C(1)	1.84(1)	Au(4)-S(10)	2.324(3)
S(1)-Au(2)	2.315(3)	N(6)-O(17)	1.12(2)
P(1)-Au(2)	2.259(3)	O(133)-N(130)	1.26(1)
O(131)-N(130)	1.25(1)	N(133)-C(132)	1.31(2)
C(1)-C(2)	1.49 (2)	N(133)-C(131)	1.45(1)
Au(3)-P(15)	2.259(3)	S(10)-C(130)	1.86(1)
Au(3)-S(10)	2.325(3)	N(9)-C(11)	1.36(2)
Au(3)-Au(4)	3.0901(6)	C(11)-N(10)	1.12(2)
C(2)-N(9)	1.48(2)	N(134)-C(132)	1.16(2)
Bond angles(º)			
P(2)-Au(1)-S(1)	174.7(2)	P(19)-Au(4)-Au(3)	132.74(8)
P(2)-Au(1)-Au(2)	128.92(8)	S(10)-Au(4)-Au(3)	48.34(7)
S(1)-Au(1)-Au(2)	47.72(7)	O(17)-N(6)-O(2)	114.0(1)
C(1)-S(1)-Au(2)	111.0(4)	O(17)-N(6)-O(3)	122.5(1)
C(1)-S(1)-Au(1)	108.8(4)	O(2)-N(6)-O(3)	123.5(1)
Au(2)-S(1)-Au(1)	84.47(9)	C(132)-N(133)-C(131)	116.5(1)
C(2)-C(1)-S(1)	117.0(8)	Au(4)-S(10)-Au(3)	83.32(8)
P(1)-Au(2)-S(1)	173.4 (1)	O(131)-N(130)-O(133)	120.5(1)
P(1)-Au(2)-Au(1)	128.79(7)	O(131)-N(130)-O(132)	119.9(1)
S(1)-Au(2)-Au(1)	47.81(7)	O(133)-N(130)-O(132)	119.5(1)
P(15)-Au(3)-S(10)	175.2 (1)	N(133)-C(131)-C(130)	111.0(1)
P(15)-Au(3)-Au(4)	127.15(7)	N(134)-C(132)-N(133)	178.3(7)
S(10)-Au(3)-Au(4)	48.34(7)	C(11)-N(9)-C(2)	115.9(2)
N(9)-C(2)-C(1)	111.8(1)	N(10)-C(11)-N(9)	177(2)
P(19)-Au(4)-S(10)	178.5(1)	C(131)-C(130)-S(10)	112.3(9)

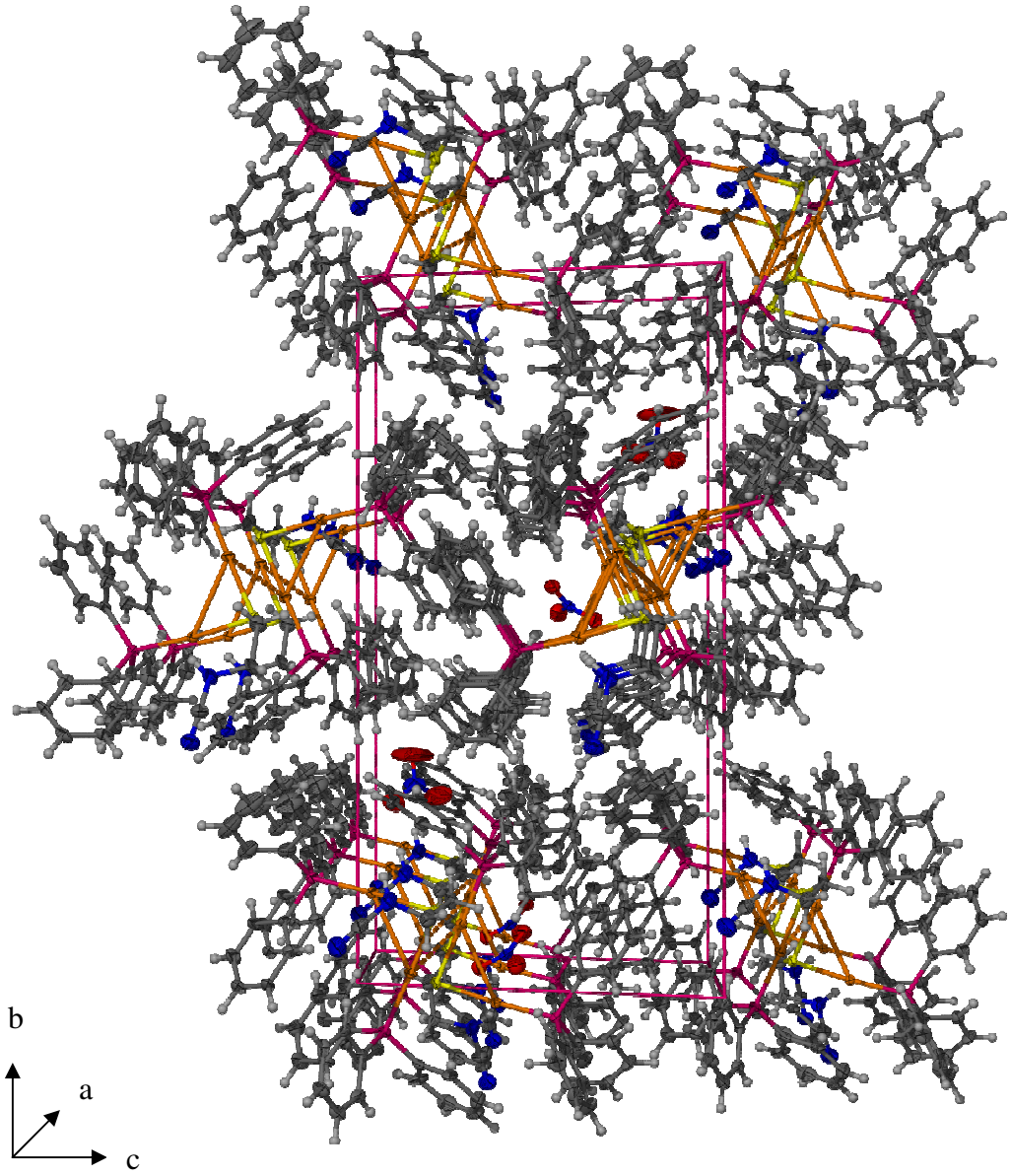

Figure 2.21: The solid-state structure of **9** viewed along the a-axis.

2.2.3.9 Crystal structure of 2-aminobenzimidazole(triphenylphosphine)gold(I) nitrate, 10A and 10B

Colourless needles of **10A** crystallised from an acetone solution while **10B** crystallised from a methanol solution in the space groups $P2_1/c$, **10A**, and $P2_1$, **10B**, and are both monoclinic. The unit cells consist of Z = 4 for both **10A** and **10B**. The compound **10B** has the same molecules in unit cell as **10A** but an extra solvent molecule, methanol thus **10A** and **10B** are not polymorphs of each other. The molecular structures and atom numbering of **10A** and **10B** are shown in Figure 2.22, while the molecular data are summarised in Table 2.22 (**10A**) and Table 2.23 (**10B**).

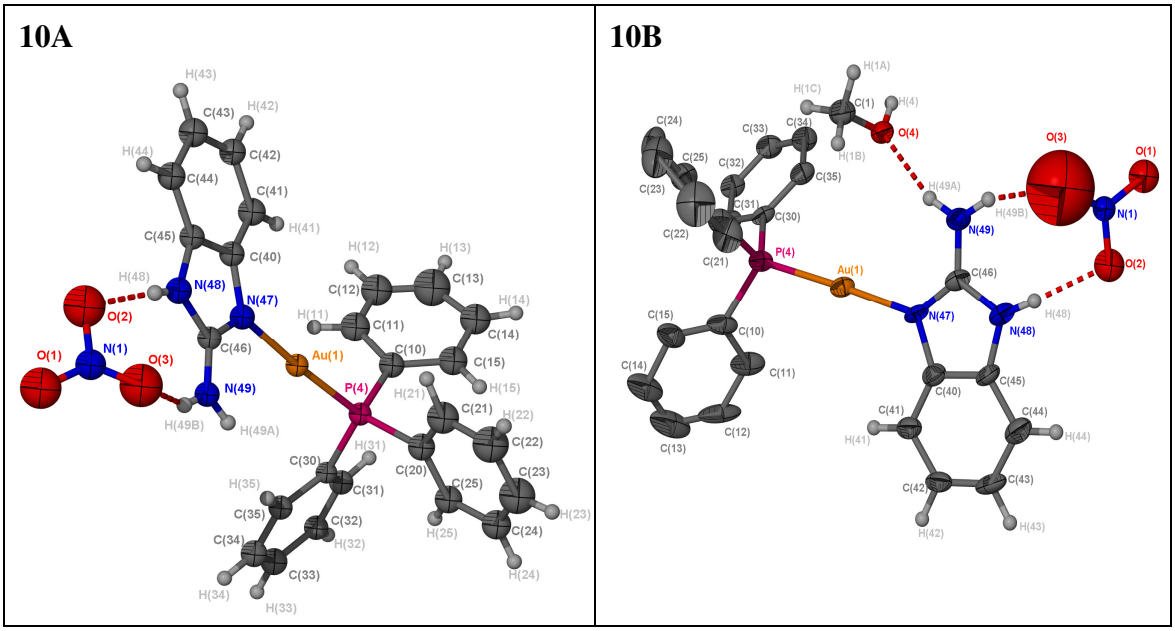

Figure 2.22: Molecular structures of compounds **10A** (left) and **10B** (right). Thermal ellipsoids are set at 50%. The O(3) atom of complex **10B** is highly disordered.

Table 2.22: Selected bond lengths (Å) and angles (°) of **10A** with standard uncertainty in parenthesis.

Bond lengths (Å)			
Au(1)-N(47)	2.04(4)	C(46)-N(48)	1.38(2)
Au(1)-P(4)	2.240(4)	N(48)-C(45)	1.42(2)
P(4)-C(30)	1.80(6)	N(1)-O(3)	1.14(2)
N(49)-C(46)	1.27(2)	N(1)-O(1)	1.24(3)
N(47)-C(46)	1.37(2)	N(1)-O(2)	1.34(3)
N(47)-C(40)	1.39(2)	C(40)-C(45)	1.37(2)
Bond angle (º)			
N(47)-Au(1)-P(4)	176.5(4)	C(46)-N(48)-C(45)	105(4)
C(46)-N(47)-C(40)	106(4)	C(40)-C(45)-N(48)	108(5)
N(47)-C(46)-N(48)	110(5)		

The C-N double bond, N(47)-C(46) at 1.37(2) Å, resembles a single bond upon coordination and is in agreement with the standard value reported for a single bond [1.41 Å] rather than that of a double bond [1.27 Å]. The C-NH_2 bond distance [1.27(2) Å]

differs significantly from the same bond in the free ligand [1.349(2) Å][39] indicating significant double bond character and thus the importance of resonance structure ***B*** for complex **10A** is reflected (Scheme 2.9).

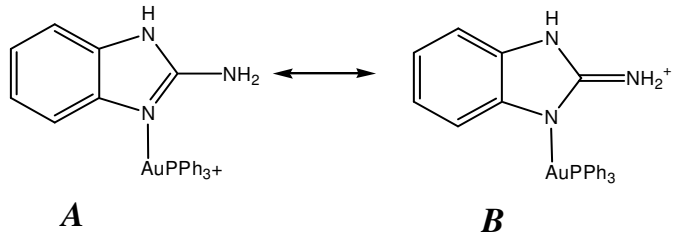

A ***B***

Scheme 2.9: Resonance structures of **10A**.

The other C-N separations in the 2-aminobenzimidazole ligand [C(40)-N(47), C(46)-N(48) and C(45)-N(48)of 1.39(2) Å,1.38(2) Å and 1.42(2) Å] are in agreement with standard literature values for single C-N bonds [1.41 Å].[28] All the angles remain virtually unchanged upon coordination indicating very little change in the hybridisation of the ring atoms. The interplanar angle between the plane in **10A** of the counterion [O(1)-N(1)-O(2)-O(3)] and the plane of the aminoazole ligand [N(49)-C(46)-N(47)-C(45)-N(48)-C(40)-C(41)-C(42)-C(43)-C(44)-C(45)] is 40.83(0.05)º.

Table 2.23: Selected bond lengths (Å) and angles (°) of **10B** with standard uncertainty in parenthesis.

Bond lengths (Å)			
Au(1)-N(47A)	2.035(6)	C(46A)-N(48A)	1.356(9)
Au(1)-P(4A)	2.238(2)	N(48A)-C(45A)	1.377(9)
P(4A)-C(10A)	1.824(6)	N(1A)-O(3A)	1.140(9)
N(49A)-C(46A)	1.323(9)	N(1A)-O(1A)	1.149(9)
N(47A)-C(46A)	1.329(9)	N(1A)-O(2A)	1.142(9)
N(47A)-C(40A)	1.409(8)	C(40A)-C(45A)	1.409(9)
Bond angle (º)			
N(47A)-Au(1A)-P(4A)	176.9(2)	C(46A)-N(48A)-C(45A)	107.4(6)
C(46A)-N(47A)-C(40A)	106.5(6)	C(40A)-C(45A)-N(48A)	107.0(6)
N(47A)-C(46A)-N(48A)	111.7(6)		

[39] J.W. Bats, *Acta. Crystallogr.*, **1999**, *C55*, 1352.

The bond distances of Au-N and Au-P are not unusual and are discussed in the beginning of section 2.3. The N-Au-P angle [176.9(2) Å] agrees with the same angle in **10A** [176.5(4) Å]. The bond distances and angles in the 2-aminobenzothiazole ligand are similar to those in **10A** and in the free ligand.[39] The C-N single bond, C(46A)-N(48A) at 1.356(9) Å and the C-N double bond, N(47A)-C(46A) at 1.329(9) Å, deviate somewhat from standard values reported for single and double bonds respectively [1.41 Å and 1.28 Å],[28] indicating delocalisation along the N(48A)-C(46A)-N(47A) thus differing to a small extent from **10A**. The only true single bond C-N distances, C(40A)-N(47A) and C(45A)-N(48A) [1.409(8) Å and 1.377(9) Å], are in agreement with reported standard values [1.41 Å].[28] The interplanar angle in **10B** between the plane of the counterion [O(1)-N(1)-O(2)-O(3)] and the plane of the aminoazole ligand [N(49)-C(46)-N(47)-C(45)-N(48)-C(40)-C(41)-C(42)-C(43)-C(44)-C(45)] is 1.76(1.04)º while in **10A** it is 40.83(0.05)º.

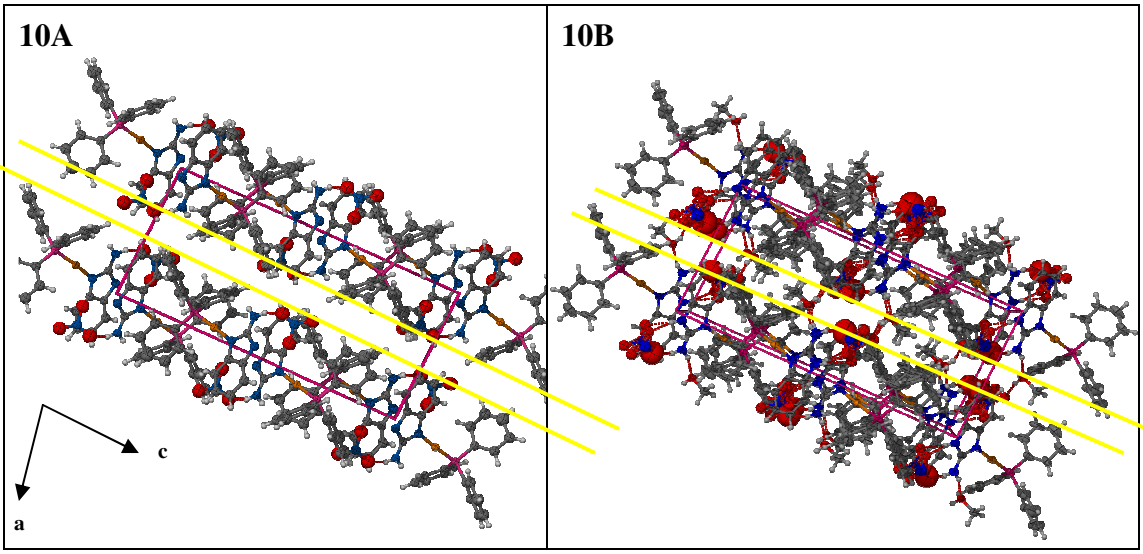

Figure 2.23: The solid-state packing of **10A** and **10B** viewed the along ac-plane.

The compound **10B** has the same packing as **10A** when viewed along the ac-plane. Packing viewed along the ac-plane shows a distinct layer which is repeated along the a-axis. In the layer the molecules are orientated in a head-to-head manner towards each other (Figure 2.23). The molecules pack in a head-to-head manner along the c–axis. The neighbouring molecules are stacked on top of each other, as a result of π-stacking between the 5-membered and 6-membered rings in the 2-aminobenzothiazole ligands of neighbouring molecules, along the b-axis at a distance of 4.060 Å for **10A** and 4.045 Å for **10B**. The counterion is dispersed arbitrarily in the packing of both **10A** and **10B**.

The hydrogen bonds in complex **10A** are observed between the nitrate anion and the NH groups of the 2-aminobenzimidazole, N(48) and N(49), at N(49)-H(49B)···O(3) [2.07(3) Å] and N(48)-H(48)···O(2) [1.84(3) Å]. The presence of hydrogen bonding in **10B** is observed between the counterion and the NH-group of the 2-aminobenzimidazole at N(49A)-H(49B)···O(3) [1.92(2) Å] and N(48A)-H(48A)···O(2) [1.9(1) Å] and these values agree with the hydrogen bonding distances observed in **10A**. There is additional hydrogen bonding between the solvent and the amine hydrogen of N(49)-H(49A)···O(4) [1.99(7)Å] which affects the crystal packing because the solvent molecules of **10B** are situated in-between the layers along the a-axis (indicted by yellow lines in Figure 2.23).

π-Stacking and hydrogen bonding govern the crystal lattice organisation in **10A** and **10B**.

2.3 Conclusion

The reaction of 2-amino-4-methylthiazole, 2-aminobenzothiazole, 1-methyl-2-aminobenzimidazole with $Au(C_6F_5)$tht yielded products which, owing to homoleptic rearrangement are labile in solution and could only be characterised by single crystal X-ray diffraction.

Structural analyses of the homoleptically rearranged products revealed that the Au-C bond lengths and C-Au-C bond angles in the anions concur with literature values. The torsion angles between the pfp substituents approach 0º for **1** and **3** but in **4** an angle of 66.59 (0.05)º was found. The organization of the crystal lattice is governed by Au···Au interaction, hydrogen bonding and π-π stacking in **1** and **3** while in **4** and **5** only π-π stacking was observed.

Reactions with 2-aminothiazoline and the two gold(I) starting materials used in this study yielded products that were the exception. It was the only ligand that coordinated to the AuC_6F_5-moiety (to produce complex **5**) without experiencing a homoleptic rearrangement. Even though Laguna and co-workers had previously isolated the complex we were now able to unambiguously determine the crystal structure. The molecular structure determinations revealed that coordination *via* the endocyclic imine nitrogen is preferred to the soft endocyclic sulphur atom or the exocyclic amine nitrogen.

Upon reaction with the stronger Lewis acid $Au(PPh_3)(NO_3)$, an unexpected ring opening of the 2-aminothiazoline ligand occurred to yield a new ligand, 2-mercapto-ethyl-cyanamide, which coordinated to two $AuPPh_3^+$ groups, to produce $[(AuPPh_3)_2(\mu_2\text{-}SCH_2CH_2NH\text{-}CN)]NO_3$, complex **9**. This complex contains intramolecular aurophillic interaction. Intermolecular Au···Au interaction directs the packing of the cation assemblies. A similar reaction using $PPh_3Au(acac)$ has been previously carried out by Laguna and co-workers but affords a different product. We have determined a **new** molecular structure indicating coordination *via* the sulphur atom only.

The successful synthesis and complete characterisation of a series of novel cationic (phosphine)gold(I) complexes derived from 2-amino-4-methylthiazole, 2-aminobenzothiazole, 2-aminobenzimidazole and 2-amino-1-methylbenzimidazole, each one containing a possibility of 3 coordination sites *i.e.* the exocyclic nitrogen atom of the amine, an endocyclic nitrogen atom of the imine and the endocyclic thioether sulfur atom of the heterocyclic , were described. Despite the fact that the soft sulphur atoms were available for the coordination, the present work showed again that, coordination preferentially occurs through the imine-nitrogen of the ligand, which is regarded as a hard to borderline hard coordination site.

NMR studies showed that only small changes in chemical shifts of the resonances occur upon coordination. The unexpected upfield shift in resonances in the ^{13}C NMR spectra can be explained by the total chemical shift σ ($\sigma = \sigma_p + \sigma_d$) as the ^{13}C NMR spectra not only reflect shielding and deshielding as in the ^1H NMR spectra.

From the FT-IR spectroscopic measurements it was concluded that the υ(C=N) absorption bands shift significantly towards higher frequencies upon coordination of ligands to the gold(I) centre. This trend is also applicable to the $\upsilon(N\text{-}H)_{stretch}$ of the absorption bands.

The FAB mass spectra of the (2-aminoazole)(phosphine)gold(I) nitrate complexes all gave *m/z* values representing the complex cation and fragments of the $AuPPh_3^+$ moiety.

X-ray crystallographic investigation, of the (2-aminoazole)(phosphine)gold(I) complexes, revealed that the geometry about the gold(I) centre in all complexes is essentially linear with Au–N and Au-P separations in good agreement with literature values reported for

related compounds. Coordination of the free ligands to the metal centre did not alter the ligand bond lengths and angles substantially. Two crystallisations of the (2-aminobenzimidazole)(triphenylphosphine)gold(I) yielded two crystal types, **10A** and **10B**, with **10A** crystallising from an acetone solution while **10B** crystallised from a methanol solution. Both have similar unit cells, except for the inclusion of a solvent molecule in **10B**. An unexpected two-coordinated silver imine complex, **8**, was also isolated and structurally analysed.

Finally, crystal structure determinations of the (2-aminoazole)(phosphine)gold(I) complexes revealed that hydrogen bonding and π-π interactions play fundamental roles in the solid state packing of **6**, **7** and **10**.

Aurophilic interactions and the factors that determine aurophilic interactions e.g the electronic effect of the ligand on the gold(I) centre, steric effects and packing forces are still actively analysed and have propelled Au···Au interactions into the domain of supramolecular chemistry. The presence of intermolecular aurophilic interactions is observed in complexes **1**, **3** and **9** with the latter revealing intramolecular Au···Au as well.

2.4 Experimental

2.4.1 General procedures and instruments

Reactions were carried out under argon using standard Schlenk and vacuum-line techniques. Tetrahydrofuran (THF), *n*-hexane, *n*-pentane and diethyl ether were distilled under N_2 from sodium benzophenone ketyl, acetone from 3 Å molecular sieves, and dichloromethane from CaH_2. The 2-amino-4-methylthiazole, 2-aminobenzothiazole and 2-aminothiazoline were purchased from Aldrich. 2-Aminobenzimidazole and KOH were purchased from Fluka and tetrahydrothiophene (tht) from Acros. Literature methods were used to prepare pentafluorophenyl(tetrahydrothiophene)gold(I)[40] from chloro(tetrahydro-thiophene)gold(I) [41] and nitrato(triphenylphosphine)gold(I) [42] from chloro(triphenyl-phoshine)gold(I).[43]

[40] R. Usón, A. Laguna, M. Laguna, *Inorg. Synth.* **1989**, *26*, 85.
[41] R. Usòn, A. Laguna in: *Organometallic Synthesis, Vol. 3* (Eds. R.B. Lang, J.J. Eisch), Elsevier, Amsterdam, **1986**, p. 325.
[42] L. Malatesta, L. Naldini, G. Simonetta, F. Cariati, *Coord. Chem . Rev*., **1966**, *1*, 255.
[43] M.I. Bruce, B.K. Nicholson, O. Bin Shawkataly, *Inorg. Synth.* **1989**, 324.

Melting points were determined on a Stuart SMP3 apparatus and are uncorrected. Mass spectra were recorded on an AMD 604 (EI, 70 eV), VG Quattro (ESI, 70 eV methanol, acetonitrile) or VG 70 SEQ (FAB, 70 eV) instrument. In the instance of EI-MS and FAB-MS the isotopic distribution patterns were checked against the theoretical distribution. NMR spectra were recorded on a Varian 300/400 FT or INOVA 600 MHz spectrometer (^{1}H NMR at 300/400/600 MHz, ^{13}C NMR at 75/100/150 MHz, and ^{31}P NMR at 121/161 MHz) with the chemical shifts reported relative to solvent resonance or an external reference of 85 % H_3PO_4 (^{31}P). Infrared spectra were recorded on a Thermo Nicolet Avatar 330FT-IR instrument equipped with a Smart OMNI ATR (attenuated total reflectance) sampler. Elemental analysis was carried out at the Soil Science Department, University of the Stellenbosch. Prior to elemental analysis, the products were evacuated under high vacuum for 10 h.

2.4.2 Preparations and procedures

2.4.2.1 Preparation of 2-amino-1-methylbenzimidazole, I

Powdered KOH (0.37 g, 6.50 mmol) was added to a solution of 2-amino-1-methylbenzimidazole (0.43 g, 3.25 mmol) in acetone (20 ml). A thick colourless precipitate was visible after 10 min. After the addition of CH_3I (0.20 ml, 0.46 g, 2.25 mmol) the reaction mixture was stirred briskly for 20 min, after which the brown solution was transferred to a separating funnel containing benzene (90 ml). The organic layer was washed with water (1 × 20 ml), a saturated NaCl solution (20 ml) and subsequently dried over anhydrous $MgSO_4$ for 2h. The solvent was removed *in vacuo* to obtain the (0.45 g, 3.1 mmol) off-white solid in a high yield of 90%.

2.4.2.2 Preparation of 1

The ligand, 2-amino-4-methylthiazole (1.6 mmol, 0.199 g), was added to a solution of the gold(I) starting complex, $Au(C_6F_5)$(tht), (1.6 mmol, 0.468 g) in diethyl ether (50ml). The resulting yellow suspension was stirred for 2 h where upon evaporation to dryness *in vacuo* yielded a colourless solid. The resulting solid was redissolved in diethyl ether (60ml) and filtered through $MgSO_4$, to remove any solid contaminants and water that might promote decomposition of the gold(I)complex. With subsequent drying of the

filtrate *in vacuo* a colourless product (0.307 g, 50 %) was obtained. Colourless needles suitable for X-ray diffraction were obtained from a concentrated solution of deuterated dichloromethane in an NMR tube maintained at -22ºC for 2 days.

2.4.2.3.1 *IR spectra of 2-amino-4-methylthiazole and **1***

The FT-IR spectrum of the **2-amino-4-methylthiazole** (Table 2.24) exhibits broad intense absorption bands at 3450 and 3250 cm^{-1}, attributable to the stretching vibrations of the primary NH_2 group. Other bands observed in this region (3500-2800 cm^{-1}) include the aliphatic sp^3 C–H bonds. Strong bands observed in the region of 1608 cm^{-1} can be assigned to the C=N stretching vibrations while the weak band detected at 1350 cm^{-1} belongs to vibrations of the C–N single bonds. Furthermore, the weak band observed in the region of 1499 cm^{-1} corresponds to the C=C stretching group's vibrations while the out of plane bending vibrations (δ^b_{oop}) of the aromatic C=C bonds are obscured by the nujol peak.

Table 2.24: Infrared spectroscopic data of ligand, 2-amino-4-methylthiazole and **1**.

	Wavenumber (cm^{-1})	
Type of vibration	**2-amino-4-methylthiazole**	**1**
$\nu(N–H)_{stretch}$	3450 (wb), 3250 (w)	3500 (wb), 3361 (w)
$\nu(C_6F_5)$ and $\delta^b(C_6F_5)$	-	1503 (w)
	-	1047 (m)
	-	948 (m)
	-	784 (m)
$\nu(N\text{-}H)_{bend}$	1600 (m)	1605 (m)
$\nu(C=N)$	1499 (w)	1551 (w)
$\nu(C–N)$	1350 (w)	1377 (w)
Ar $\nu(C=C)$	1100 (w)	1100 (w)

In the FT-IR spectrum of **1** (Table 2.24) the diagnostic, intense broad absorption bands of the $\nu(N–H)$ vibration, appear at 3500 cm^{-1} and 3361 cm^{-1} and is shifted to a slightly higher wavenumber with respect to the corresponding band observed in the spectrum of the free ligand. The absorption band, $\nu(N–H)$, generated by the bending vibrations of the N-H bonds, emerges at the slightly higher wavenumber of 1605 cm^{-1}, when compared to the

observed band of the free ligand at 1600 cm^{-1}. The absorption band ν(C=N) vibration occurs at 1551 cm^{-1}, whereas the ν(C–N) vibration results in a band of medium intensity at 1377 cm^{-1}, both these bands are observed at a higher wavenumber when correlated to the values of the free ligand. In addition, bands attributed to aromatic δ^{b}_{oop}(C=C) vibrations are identified at 1100 cm^{-1} and appear at the identical wavenumber as in the free ligand. The presence of four new intense absorption bands in the spectrum, in the regions 1503cm^{-1}, 1047 cm^{-1}, 948cm^{-1} and 784 cm^{-1}, of the complex was observed and are attributable to the $Au(C_6F_5)_2$ anion.

2.4.2.3 Preparation of 2

The same protocol as described in section 2.4.2.2 was used with 2-aminobenzothiazole (0.110 g, 0.49 mmol) and $Au(C_6F_5)$(tht) (0.223 g, 0.49 mmol), yielding a colourless solid (0.09 g, 75 %).

*2.4.2.3.1 IR spectrum of 2-aminobenzothiazole and **2**.*

Characteristic absorption bands in the FT-IR spectrum of the **2-aminobenzothiazole** (Table 2.25), attributable to the stretching vibrations of the N–H, C=N and C-N moieties, are prominent at 3394 cm^{-1} and 3272 cm^{-1}, 1529 cm^{-1} and 1340 cm^{-1}. Additionally, characteristic aromatic ν(C=C) bands are observed at 1106 cm^{-1}.

Table 2.25: Infrared spectroscopic data of the ligand, **2-aminobenzothiazole** and **2**.

Type of vibration	**Wavenumber (cm^{-1})**	
	2-aminobenzothiazole	**2**
$\nu(N–H)_{stretch}$	3394 (w), 3272 (w)	3400 (wb), 3368 (wb)
$\nu(C_6F_5)$ and $\delta^{b}(C_6F_5)$	-	1528 (w)
	-	1046 (m)
	-	951 (m)
	-	784 (m)
$\nu(N-H)_{bend}$	1644 (m)	1619 (m)
ν(C=N)	1529 (w)	1501 (w)
ν(C–N)	1340 (w)	1304 (w)
ν(C=C)	1106 (w)	1100 (w)

The four new intense absorption bands in the spectrum of the complex **2** (Table 2.25) are attributable to the $Au(C_6F_5)_2$ anion, at 1528cm^{-1}, 1046 cm^{-1}, 951cm^{-1} and 784 cm^{-1}. The N-H stretch vibrations at 3400 cm^{-1} and 3368 cm^{-1} are at a higher wavenumber in the free ligand while the rest of the complex's vibrations are observed at lower wavenumbers when compared to the vibrations in the spectrum of the free ligand. The most dramatic shift is observed for the C-N band from 1340 cm^{-1} to 1304 cm^{-1}.

2.4.2.4 Preparation of 3

The same protocol as described in section 2.4.2.2 was used with 2-amino-1-methylbenzimidazole (0.137 g, 0.93 mmol) and $Au(C_6F_5)$(tht) (0.422 g, 0.93 mmol). After evaporation, a beige oily residue was obtained. The oily residue was rinsed with pentane to yield a beige solid (0.56 g, 44%). Colourless blocks were obtained by the slow diffusion of *n*-pentane into a concentrated solution of **3** in acetone maintained at -22ºC for a week.

*2.4.2.4.1 IR spectrum of 2-amino-1-methylbenzimidazole and **3**.*

The FT-IR spectrum of the free ligand, **2-amino-1-methylbenzimidazole** (Table 2.26), shows a very weak broad absorption bands at 3446 cm^{-1} and 3300 cm^{-1} with a weak band at 1650 cm^{-1} which is attributable to the stretching- and bending vibrations of the N–H group respectively. The weak bands at 1538 cm^{-1} and 1376 cm^{-1} can be assigned to the C=N and C-N vibration bands respectively. Other diagnostic bands in the spectrum of 2-amino-1-methylbenzimidazole are observed in the region 1106 cm^{-1}, attributable to the stretching vibrations of the aromatic C=C bonds, while the out of plane δ^{b}_{oop}(C=C) bending is obscured by nujol peak at 728.83 cm^{-1}.

Table 2.26: Infrared spectroscopic data of ligand, **2-amino-1-methylbenzimidazole** and **3**.

Type of vibration	Wavenumber (cm^{-1})	
	2-amino-1-methyl-benzimidazole	**3**
$\nu(N–H)_{stretch}$	3446(w), 3300 (w)	3610 (wb), 3413 (wb)
$\nu(C_6F_5)$ and $\delta^b(C_6F_5)$	-	1503 (w)
	-	1057 (m)
	-	952 (m)
	-	782 (m)
$\nu(N\text{-}H)_{bend}$	1650 (w)	1671 (m)
$\nu(C=N)$	1538 (w)	1542 (w)
$\nu(C–N)$	1376 (w)	1362 (w)
$\nu(C=C)$	1106 (w)	1058 (m)

In the FT-IR spectrum of **3** (Table 2.26) the absorption bands characteristic of the N–H stretching occur at 3610 $cm^{-1}$and 3413 cm^{-1}, at a higher wavenumber than in the free ligand while the bending vibration at 1671 cm^{-1} is also located at a higher wavenumber than in the free ligand. Additional diagnostic bands in the spectrum of **3** are those of the ν(C-N) and ν(C=N) vibrations which are observed at 1542 cm^{-1} and 1362 cm^{-1}. The C=N vibration is at a lower wavenumber than in the free ligand. The C=C vibration is also at lower wavenumber than in the free ligand.

Intense absorption bands in the regions 1503cm^{-1}, 1057cm^{-1}, 952cm^{-1} and 782 $cm^{-1}$are observed, attributable to $Au(C_6F_5)_2^-$ entities.

2.4.2.5 Preparation of 4

The same protocol as described in section 2.4.2.2 was used with 2-amino-4-methylthiazole (0.063 g, 0.5 mmol) and $Au(C_6F_5)$(tht) (0.249 g, 0.5 mmol). The resulting mixture was then stirred for 1.5 h and evaporated to dryness *in vacuo*. The oily residue was washed with three 10 ml portions of pentane and dried *in vacuo* to yield a colourless solid. The product was redissolved in diethyl ether (100 ml). After the addition of a second mol equivalent of C_6F_5Au(tht) (0.249 g, 0.5 mmol) to the above solution it was again stirred for 1.5 h and dried *in vacuo*. The colourless product was then redissolved in diethyl ether (50ml) and filtered through $MgSO_4$. The resulting solution was then evaporated to

dryness yielding a colourless solid in high yield (0.23 g, 61 %). Crystals suitable for X-ray diffraction was obtained from a concentrated solution of the product in deuterated dichloromethane at -22ºC within 4 days.

*2.4.2.5.1 IR spectrum of 2-amino-4-methylthiazole and **4**.*

Characteristic absorption bands in the FT-IR spectrum of **2-amino-4-methylthiazole** (Table 2.26), attributable to the stretching vibrations of the N–H, C=N and C-N groups, are prominent at 3450 cm^{-1} and 3250cm^{-1}, 1499 cm^{-1} and 1350 cm^{-1} respectively. The N-H bending vibration is observed at 1600 cm^{-1}. Additionally, characteristic aromatic ν(C=C) bands are observed at 1100 cm^{-1}.

Table 2.27: Infrared spectroscopic data of **2-amino-4-methylthiazole** and **4**.

	Wavenumber (cm^{-1})	
Type of vibration	**2-amino-4-methylthiazole**	**4**
ν(N–H)	3450 (wb),3250 (w)	3474 (w), 3366 (w)
ν(C_6F_5) and δ^b(C_6F_5)	-	1503 (w)
	-	1060 (m)
	-	948 (m)
	-	784 (m)
ν(N-H)bend	1600 (m)	1626 (m)
ν(C=N)	1499 (w)	1574 (w)
ν(C–N)	1350 (w)	1383 (w)
Ar ν(C=C)	1100 (w)	1098 (w)

The presence of four new intense absorption bands, at 1503cm^{-1}, 1060 cm^{-1}, 948cm^{-1} and 784 cm^{-1}, in the spectrum of **4** (Table 2.27) result from the $Au(C_6F_5)_2^-$ anion. The N-H stretch vibrations at 3474 cm^{-1} and 3366 cm^{-1} are at a higher wavenumber than in the free ligand. The rest of the complex's vibrations were all observed at higher wavenumbers when compared to the free ligand, except for the C=C vibration at 1098 cm^{-1}.

2.4.2.6 Preparation of 2-aminothiazoline(pentafluorphenyl)gold(I), 5

The ligand, 2-aminothiazoline (0.056 g, 0.55 mmol), was added to solution of $Au(C_6F_5)$(tht) (0.25 g, 0.55 mmol) in diethyl ether (70 ml) and stirred for 2.5 h. The

colourless suspension was then evaporated to dryness *in vacuo*. The colourless residue was extracted with diethyl ether (40 ml) and filtered through $MgSO_4$. The filtrate was reduced in *vacuo* to yield an oily product. The oily product was washed with pentane (10 ml) and dried *in vacuo*. The desired white product was obtained in high yield (0.19 g, 85 %). The crystals of **5** were obtained as colourless blocks from a concentrated solution of the product in deuterated dichloromethane at -22ºC.

2.4.2.7 Preparation of 2-amino-4-methylthiazole(triphenylphosphine)gold(I) nitrate, 6

The ligand, 2-amino-4-methylthiazole (0.06 g, 0.55 mmol), was added to an equal molar amount (0.29 g, 0.55 mmol) of $Au(PPh_3)NO_3$ in a diethyl ether suspension (60 ml). The resulting white snowflake-like suspension was stirred for 5 days at room temperature. During this stirring period, the formation of the imine coordination complex was accompanied by the formation of a new suspension with a notably different texture and off-white colour. The mixture was then evaporated to complete dryness *in vacuo* to yield a white solid. The white solid was extracted with diethyl ether (50 ml). The solution containing the desired gold(I)complex was filtered through $MgSO_4$ to remove solid contaminants and any water that might contribute to decomposition of the gold(I)complexes and the filtrate stripped of solvent *in vacuo*. The solid oily yellow residue was sequentially washed with *n*-pentane (30 ml) to yield the yellow solid (0.30 g, 94%). Crystals of the yellow solid were obtained from a concentrated solution of the product in deuterated dichloromethane in an NMR tube, producing colourless needles at -22ºC.

2.4.2.7.1 *IR spectrum of **6***.

In the FT-IR spectrum of **6** (Table 2.28), the diagnostic and weak bands of the ν(N–H) vibrations appear at 3309 cm^{-1} and 3119 cm^{-1}, at a slightly lower wavenumber with respect to the corresponding band observed in spectrum of **2-amino-4-methylthiazole** This might be due to coordination to the metal. The ν(N–H)bending vibration appears at 1627cm^{-1} which is at a slightly higher wavenumber than the corresponding band in the free ligand, **2-amino-4-methylthiazole**. The C=N vibration (1531 cm^{-1}) and the C-N band appears at a slightly higher frequency of 1435cm^{-1} when compared to the same wavenumber in the

free ligand.

Table 2.28: Infrared spectroscopic data of **2-amino-4-methylthiazole** and **6.**

Type of vibration	**Wavenumber (cm^{-1})**	
	2-amino-4-methylthiazole	**6**
$\nu(N–H)_{stretch}$	3450 (w,b), 3250(w,b)	3309 (w,b),3119 (w,b)
$\nu(N–H)_{bend}$	1600 (w)	1627 (w)
ν(C=N)	1499 (w)	1531 (w)
ν(C-N)	1350 (w)	1435 (w)
ν(C=C)	1100 (m)	1100 (m)
$sp^2\ \delta^b_{oop}$ (C=C)	690 (s)	690 (s)

2.4.2.8 Preparation of 2-aminobenzothiazole(triphenylphosphine)gold(I) nitrate, 7

Complex **7** was prepared using the same protocol as described in section 2.4.2.7 with the ligand, 2-aminobenzothiazole (0.057 g, 0.38 mmol) and $Au(PPh_3)NO_3$ (0.20 g, 0.38 mmol) in diethyl ether (60 ml), yielding a colourless solid (0.19 g, 82 %). Colourless crystals of **7** were obtained from a concentrated solution of the product in dichloromethane at -22ºC. The unexpected complex, bis(2-aminobenzothiazole)silver(I), **8** was obtained from a concentrated solution of acetone at -22ºC. The silver contaminants were obtained when $Au(PPh_3)Cl$ was treated with an excess of $AgNO_3$ to afford starting material $Au(PPh_3)NO_3$.

2.4.2.8.1 *IR spectrum of 7*

In the FT-IR spectrum of **7** (Table 2.29) the diagnostic and weak bands of the ν(N–H) vibration appear at 3304 cm^{-1} and 3054 cm^{-1}. The band at 3045 cm^{-1} is observed as a shoulder of the ν(N–H) vibration, at 3304 cm^{-1}. This is an indication of the overtone of the N-H bending vibration at 1627 cm^{-1}; this shoulder is normally absent but is enhanced because of Fermi resonance interaction with the symmetric N-H group. These bands are at a slightly lower wavenumber with respect to the corresponding bands in the free ligand. The C=N band at 1542 cm^{-1} and C-N band at 1480 cm^{-1} have a higher wavenumber when compared to the free ligand's bands. This tendency is also observed for the band of the C=C vibration ($sp^2\ \delta b_{oop}$) at 691 cm^{-1} when compared to the ligand vibration band at 684

cm^{-1}. The medium intensity C=C band at 1100 cm^{-1} and the rest of the vibration bands are unaltered by coordination.

Table 2.29: Infrared spectroscopic data for ligand **2-aminobenzothiazole** and complex **7.**

Type of vibration	Wavenumber (cm^{-1})	
	2-aminobenzothiazole	**7**
$\nu(N–H)_{stretch}$	3394 (w,b),3272(w,b)	3304 (w,b), 3054 (w,b)
$\nu(N–H)_{bend}$	1644 (w)	1640 (w)
ν(C=N)	1529 (w,b)	1542 (w,b)
ν(C-N)	1340 (w)	1480 (w)
ν(C=C)	1106 (m)	1100 (m)
$sp^2\ \delta^b_{oop}$ (C=C)	684 (s)	691 (s)

2.4.2.9 Preparation of μ_2-(2-mercapto-ethyl-cyanamide-κ;S)bis(triphenylphosphine)gold(I) nitrate, 9

Compound **9** was obtained using the experimental procedures described in 2.4.2.7 implementing $Au(PPh_3)NO_3$ (0.14 g, 0.26 mmol) and 2-aminothiazoline (0.03 g, 0.26 mmol), yielding a colourless solid as a product (0.100 g, 70 %). Crystals suitable for an X-ray structure determination were obtained from a concentrated perdeuterated acetone solution of the product in an NMR tube maintained at -22ºC.

2.4.2.10 Preparation of 2-aminobenzimidazole(triphenylphosphine)gold(I) nitrate, 10

The same protocol as in section 2.4.2.7 was followed with $Au(PPh_3)NO_3$ (0.09 g, 0.18 mmol) and 2-aminobenzimidazole (0.08 g, 0.18 mmol) to yield a pure colourless solid (0.103 g, 98 %). Single crystals in the form of colourless needles of **10** were obtained from slow diffusion of *n*-pentane into an acetone solution of the compound at -22ºC. The other structure of **10A**, **10B**, was obtained from a concentrated solution of **10A** in methanol in an NMR tube.

*2.4.2.10.1 IR spectrum of 2-aminobenzimidazole and **10***

In the FT-IR spectrum of the ligand **2-aminobenzimidazole**, apart from the weak stretching vibration bands of the N-H functional group at 3404 cm^{-1} and 3069 cm^{-1}, a weak C=N stretching vibration is observed at 1542 cm^{-1} while the medium intensity vibration band at 1436 cm^{-1} can be attributed to the vibration of the C-N single bond. Furthermore, the absorption frequencies of the C=C stretching vibration at 1100 cm^{-1} and bending vibration at 665 cm^{-1} confirms the presence of the aromatic C=C bonds of the phenyl ring.

Table 2.30: Infrared spectroscopic data of **2-aminobenzimidazole** and **10**.

Type of vibration	Wavenumber (cm^{-1})	
	2-aminobenzimidazole	**10**
$\nu(N–H)_{strech}$	3404 (w,b), 3069 (w,b)	3344 (w,b), 3070 (w,b)
$\nu(N–H)_{bend}$	1638 (w,b)	1638 (w)
ν(C=N)	1542 (w,b)	1595 (w,b)
ν(C-N)	1436 (m)	1438 (m)
ν(C=C)	1100 (w)	1100 (m)
$sp^2\ \delta^b_{oop}$ (C=C)	665 (w,b)	688 (s)

The characteristic absorption bands of **10** (Table 2.30) i.e. the stretching vibration of the moiety ν(N–H), are predominant at a lower wavenumber (3340 cm^{-1}) than in spectrum of the free ligand, while the second band at 3070 cm^{-1} is unaltered by coordination. The C=N and C-N bands are at higher frequencies of 1595 cm^{-1} and 1438 cm^{-1} respectively. The weak N-H bending vibration at 1638cm^{-1} remains unchanged by ligand coordination. The strong vibration band of C=C ($sp^2\ \delta^b_{oop}$) at 688 cm^{-1} is at a higher wavenumber when compared to the identical band in the spectrum of the ligand at 665 cm^{-1}, while the C=C vibrations (1100cm^{-1}) are observed as a medium intensity peak which is unaltered by coordination.

2.4.3 X-ray structure determinations

The crystal data collection and refinement details for complexes **1**, **3**, **4**, **5**, **6, 7, 8, 9, 10A** and **10B** are summarised in Tables 2.30-2.34. Data sets were collected on a

Bruker SMART Apex CCD diffractometer with graphite monochromated Mo-K_α radiation (k_α = 0.71073 Å).[44] Data reduction was carried out with standard methods using the software package Bruker SAINT.[45] All data sets were corrected for absorption using SADABS.[46,47] The structures were solved by direct methods which yielded the position of the metal atoms, and conventional difference Fourier methods. All non-hydrogen atoms were refined anisotropically by full-matrix least squares calculations on F^2 using SHELXL-97[48] within the X-seed environment.[49,50] The hydrogen atoms were fixed in calculated positions unless otherwise mentioned. Figures were generated with POV-Ray for Windows, with the displacement ellipsoids at the 50% probability level. Further information is available from Dr. S. Cronje at the Department of Chemistry and Polymer Science, Stellenbosch University.

[44] SMART Data Collection Software (version 5.629), Bruker AXS Inc., Madison, WI, **2002**.
[45] SAINT, Data Reduction Software (version 6.45), Bruker AXS Inc., Madison, WI, **2003**.
[46] R.H. Blessing, *Acta Crystallogr.,* **1995**, *A51*, 33.
[47] SADABS (version 2.05), Bruker AXS Inc., Madison, WI, **2002**.
[48] G.M. Shelrick, SHELX-97. Program for Crystal Structure Analysis, University of Göttingen (Germany), **1997**.
[49] L.J. Barbour, *J. Supramol. Chem.* **2001**, *1*, 189.
[50] J.L. Atwood, L.J. Barbour, *Cryst. Growth Des.* **2003**, *3*, 3.

Table 2.30: Crystallographic data of compounds **1** and **3**

Compound	**1**	**3**
Molecular formula	$C_{24}H_{24}AuF_{10}LiN_6O_3S_3$	$C_{33}H_{23.75}Au_2F_{20}Li_2O_{10}$
Molecular weight	934.58	1368.08
Crystal system	triclinic	triclinic
Crystal dimensions (mm^3)	0.22 x 0.20 x 0.02	0.27 x 0.20x 0.09
Crystal shape and colour	Colourless blocks	Colourless blocks
Space group	$P\bar{1}$ (No. 2)	$P\bar{1}$ (No. 2)
a (Å)	8.2753(8)	12.917(2)
b (Å)	13.894(1)	13.720(2)
c (Å)	15.617(2)	15.2178(2)
α (°)	115.099(1)	64.202(2)
β (°)	90.244(2)	66.747(2)
γ(°)	96.227(2)	62.689(2)
Volume ($Å^3$)	1614.0(3)	2092.1(4)
Z	2	2
d_{calcd} (g/cm^3)	1.923	2.172
μ (Mo-Ka) (mm^{-1})	4.848	7.146
Absorption correction	Semi-empirical from equivalents (SADABS)	Semi-empirical from equivalents (SADABS)
$F_{(000)}$	908	1292
θ-range for data collection (°)	2.48 to 26.47	1.53 to 26.46
Index range	-10 < h < 10, -17 < k < 17, -19 < l < 19	-16 < h < 16, -17 < k < 17, -19 < l < 19
No. of reflections collected	17559	22723
No. of unique reflections	6643 (R_{int} = 0.0280)	8547 (R_{int} = 0.0269)
Max. and min. transmission	0.4152 and 0.9093	0.2485 and 0.5656
Refinement parameters / restraints	484 parameters, 16 restraints	648 parameters, 0 restraints
Goodness of fit on F^2	1.047	1.028
Final R-indices [I>2σ >(I)]	R_1=0.0257	R_1=0.0239
	wR_2=0.0568	wR_2=0.0574
R indices (all data)	R_1=0.0292	R_1=0.0287
	wR_2=0.0582	wR_2=0.0599
Largest diff. peak and hole ($e.A^{-3}$)	-0.979 and 1.660	1.215and -0.691
Weighting scheme [a]	a=0.0321	a =0.0278/ b=1.7453

[a] $wR_2 = \{\Sigma[w(F_o^2-F_c^2)^2]/\Sigma[w(F_o^2)^2]\}^{1/2}$; $w = 1/[\sigma^2(F_o^2)+(aP)^2+bP+d+\text{esin}\theta]$; $P = [f(\text{Max}(0 \text{ or } F_o^2)] + (1\text{-}f)\ F_c^2$

Table 2.31: Crystallographic data of compounds **4** and **5**.

Compound	**4**	**5**
Molecular formula	$C_{20}H_{13}AuF_{10}N_4S_2$,	$C_9H_6AuF_5N_2S$
Molecular weight	760.43	466.18
Crystal system	monoclinic	monoclinic
Crystal dimensions (mm^3)	0.24 x 0.11x 0.03	0.09 x 0.06x 0.04
Crystal shape and colour	Colourless needle	Colourless block
Space group	C2/c (No. 15)	$P2_1/c$ (No. 14)
a (Å)	24.896(6)	10.164(3)
b (Å)	7.864(2)	9.783(3)
c (Å)	12.598(3)	11.455(3)
α (°)	90	90
β (°)	110.801(4)	105.455(4)
γ (°)	90°	90
Volume ($Å^3$)	2305.7(9)	1097.9(5)
Z	4	4
d_{calcd} (g/cm^3)	2.191	2.820
μ (Mo-Ka) (mm^{-1})	6.661	13.639
Absorption correction	Semi-empirical from equivalents (SADABS)	Semi-empirical from equivalents (SADABS)
$F_{(000)}$	1448	856
θ-range for data collection (°)	1.75 to 26.43	2.08 to 26.43
Index range	-16 < h < 30, -9 < k <9, -15 <l < 15	-12< h < 10, -12 < k < 8, -14< l < 8
No. of reflections collected	6524	6207
No. of unique reflections	2372 (R_{int} = 0.0326)	2253 (R_{int} = 0.0309)
Max. and min. transmission	0.2978 and 0.8252	0.3833 and 0.5981
Refinement parameters / restraints	169 parameters, 0 restraints	89 parameters, 0 restraints.
Goodness of fit on F^2	1.051	1.059
Final R-indices [I>2σ>(I)]	R_1 = 0.0323 wR_2 = 0.0768	R_1 = 0.0307 wR_2 = 0.0744
R indices (all data)	R_1 = 0.0359 wR_2 = 0.0784	R_1 = 0.0329 wR_2 = 0.0758
Largest diff. peak and hole ($e.A^{-3}$)	0.162 and -2.013	-1.331 and 2.414
Weighting scheme [a]	a = 0.0427/ b =11.6028	a = 0.0316/ b = 9.0086

[a] $wR_2 = \{\Sigma[w(F_o^2-F_c^2)^2]/\Sigma[w(F_o^2)^2]\}^{1/2}$; $w = 1/[\sigma^2(F_o^2)+(aP)^2+bP+d+\text{esin}\theta]$; $P = [f(\text{Max}(0 \text{ or } F_o^2)] + (1\text{-f}) F_c^2$

Table 3.32: Crystallographic data of compounds **6** and **7**.

Compound	**6**	**7**
Molecular formula	$C_{22}H_{21}AuN_3O_3PS$	$C_{25}H_{21}AuClN_2OPS$
Molecular weight	635.41	660.88
Crystal system	triclinic	triclinic
Crystal dimensions (mm^3)	0.089 x 0.064 x 0.042	0.154 x 0.077 x 0.042
Crystal shape and colour	Yellow needles	Yellow needles
Space group	$P\bar{1}$ (No. 2)	$P\bar{1}$ (No. 2)
a (Å)	9.510(3)	11.052(3)
b (Å)	11.684(4)	11.107(3)
c (Å)	12.802(4)	11.719(3)
α (°)	82.913(5)	105.692(4)
β (°)	76.729(5)	97.679(4)
γ (°)	73.875(5)	90.049(4)
Volume ($Å^3$)	1327.3(8)	1371.5(5)
Z	2	2
d_{calcd} (g/cm^3)	1.590	1.600
μ (Mo-Ka) (mm^{-1})	5.705	5.613
Absorption correction	Semi-empirical from equivalents (SADABS)	Semi-empirical from equivalents (SADABS)
$F_{(000)}$	616	640
θ-range for data collection (°)	1.64 to 26.67	1.82 to 26.44
Index range	-12< h < 11, -14 < k < 14, -16 < l < 16	-13 < h < 13, -13 < k < 13, -14 < l < 14
No. of reflections collected	14043	14753
No. of unique reflections	5508 (R_{int} = 0.0236)	5577 (R_{int} = 0.0335).
Max. and min. transmission	0.1979 and 0.7116	0.4725 and 0.7950
Refinement parameters / restraints	253 parameters, 0 restraints	157 parameters, 0 restraints
Goodness of fit on F^2	1.092	1.104
Final R-indices [I>2σ >(I)]	R_1 = 0.0261	R_1 = 0.0566
	wR_2 = 0.0680	wR_2 = 0.1404
R indices (all data)	R_1 = 0.0282	R_1 = 0.0606
	wR_2 = 0.0690	wR_2 = 0.1434
Largest diff. peak and hole ($e.A^{-3}$)	-1.233 and 2.626	-6.620 and 6.019
Weighting scheme [a]	a = 0.0464	a = 0.0805/ b = 10.3926

[a] $wR_2 = \{\Sigma[w(F_o^2-F_c^2)^2]/\Sigma[w(F_o^2)^2]\}^{1/2}$; $w = 1/[\sigma^2(F_o^2)+(aP)^2+bP+d+\text{esin}\theta]$; $P = [f(\text{Max}(0 \text{ or } F_o^2)] + (1\text{-}f)\ F_c^2$

Table 2.34: Crystallographic data of compounds **8** and **9**.

Compound	**8**	**9**
Molecular formula	$C_{15}H_{12}AgN_5O_3Cl_2S$	$C_{39}H_{35}Au_2N_3O_3P_2S$
Molecular weight	553.19	1081.63
Crystal system	monoclinic	monoclinic
Crystal dimensions (mm^3)	0.200 x 0.080 x 0.050	0.154 x 0.077 x 0.042
Crystal shape and colour	Colourless blocks	Colourless blocks
Space group	$P2_1/n$ (No. 14)	$P2_1$ (No. 4)
a (Å)	17.096(4)	10.400 (1)
b (Å)	5.817(1)	26.355(3)
c (Å)	20.421(4)	14.132(2)
α (°)	90	90
β (°)	102.867(3)	106.677(2)
γ (°)	90	90
Volume ($Å^3$)	1979.8(7)	3710.6(7)
Z	4	4
d_{calcd} (g/cm^3)	1.856	1.936
μ (Mo-Ka) (mm^{-1})	1.527	8.083
Absorption correction	Semi-empirical from	Semi-empirical from equivalents
$F_{(000)}$	1096	2072
θ-range for data collection (°)	1.41 to 26.24	1.50 to 26.47
Index range	-16 < h < 21, -7 < k < 7, -22 < l < 25	-11 < h < 12, -33 < k < 19, -17 < l < 16
No. of reflections collected	10936	21883
No. of unique reflections	4047 (R_{int} = 0.0285)	13103 (R_{int} = 0.0357)
Max. and min. transmission	0.7500 and 0.9276	0.5750 and 0.8856
Refinement parameters / restraints	253 parameters, 0 restraint	903 parameters, 1 restraint
Goodness of fit on F^2	1.056	1.046
Final R-indices [I>2σ >(I)]	R_1 = 0.0710	R_1 = 0.0410
	wR_2 = 0.1752	wR_2 = 0.0805
R indices (all data)	R_1 = 0.0790	R_1 = 0.0498
	wR_2 = 0.1808	wR_2 = 0.0892
Largest diff. peak and hole ($e.A^{-3}$)	-1.975 and 2.824	-1.356 and 1.709
Weighting scheme [a]	a = 0.08699/ b= 24.2649	a = 0.0390

[a] $wR_2 = \{\Sigma[w(F_o^2-F_c^2)^2]/\Sigma[w(F_o^2)^2]\}^{1/2}$; $w = 1/[\sigma^2(F_o^2)+(aP)^2+bP+d+\text{esin}\theta]$; $P = [f(\text{Max}(0 \text{ or } F_o^2)] + (1\text{-f}) F_c^2$

Table 2.35: Crystallographic data of compounds **10A** and **10B**

Compound	**10A**	**10B**
Molecular formula	$C_{25}H_{21}AuN_4O_3P$	$C_{26}H_{26}AuN_4O_4P_2$
Molecular weight	653.39	686.44
Crystal system	monoclinic	monoclinic
Crystal dimensions (mm^3)	0.19 x 0.06 x 0.06	0.154 x 0.077 x 0.042
Crystal shape and colour	Colourless needles	Colourless blocks
Space group	$P2_1/c$ (No. 14)	$P2_1$ (No. 4)
a (Å)	9.7420(9)	9.7420(9)
b (Å)	13.677 (1)	13.677(2)
c (Å)	21.083(2)	21.083(2)
α (°)	90	90
β (°)	93.197(2)	93.197(2)
γ (°)	90	90
Volume ($Å^3$)	2804.8(4)	2804.8(4)
Z	4	4
d_{calcd} (g/cm^3)	1.547	1.626
μ (Mo-Ka) (mm^{-1})	5.332	5.338
Absorption correction	Semi-empirical from	Semi-empirical from
$F_{(000)}$	1268	1344
θ-range for data collection (°)	1.78 to 26.42	1.78 to 26.42
Index range	-10 < h < 12, -17 < k < 17, -26 < l < 16	-10 < h < 12, -17< k < 17, -17 < l < 26
No. of reflections collected	16245	16245
No. of unique reflections	5748 (R_{int} = 0.0445)	5748(R_{int} = 0.04)
Max. and min. transmission	0.403 and 0.4229	0.5750 and 0.8856
Refinement parameters / restraints	137 parameters, 0 restraints	324 parameters, 23 restraint
Goodness of fit on F^2	1.492	1.058
Final R-indices [I>2σ >(I)]	R_1 = 0.1242	R_1 = 0.0461
	wR_2 = 0.3485	wR_2 = 0.1120
R indices (all data)	R_1 = 0.1444	R_1 = 0.0637
	wR_2 = 0.3696	wR_2 = 0.1193
Largest diff. peak and hole ($e.A^{-3}$)	-6.093 and 13.155	-1.356 and 0.997
Weighting scheme [a]	a = 0.20000	a = 0.0640

[a] $wR_2 = \{\Sigma[w(F_o^2-F_c^2)^2]/\Sigma[w(F_o^2)^2]\}^{1/2}$; $w = 1/[\sigma^2(F_o^2)+(aP)^2+bP+d+\sin\theta]$; $P = [f(\text{Max}(0 \text{ or } F_o^2)] + (1\text{-}f)\ F_c^2$

Chapter 3

Novel 2-aminoazole complexes of Chromium(0) and Tungsten(0)

3.1 Introduction

The stable, colourless, crystalline hexacarbonyls $M(CO)_6$ are octahedral, low-spin and diamagnetic as anticipated from the 18-electron rule. The replacement of the carbonyl groups by σ- or π- donor ligands is possible, giving rise to variety of complexes of the form $[M(CO)_{6-x}L_x]$ or $[M(CO)_{6-2x}(L\text{-}L)_x]$ with L= NO, NH_3, CN, PF_3 and L-L=bipy, butadiene.

Pentacarbonyl(pyridine)metal(0) complexes of group 6 metals have been known for a long time[1] and have been thoroughly characterised. A search of the Scifinder Scholar database for $Cr(CO)_5$ compounds with coordinated cyclic nitrogen ligands revealed only the amine coordinated pyridine-type complex, (2,6-diaminopyridine)(pentacarbonyl)chromium(0), while for $W(CO)_5$ a number of entries were found.[2] It has been shown that a non-bulky substituent on position 2 of the pyridine does not hinder the coordination of the ligand to the transition metal.[3] Pyridine derivatives with donor atoms at position 2 or 6 are expected to show more than one bonding mode, thus 2,6-diaminopyridine (dap) can bond through the hard sp^3 hybridsed nitrogen of the amines or the borderline hard sp^2 hybridised nitrogen in the aromatic ring. The former being a stronger σ-donor, but a much weaker π-acceptor than the latter. Markan and co-workers[3] investigated bonding modes for 2,6-diaminopyridine and their results revealed coordination to soft chromium through one of the hard amine groups with monodentate coordination. The single crystal X-ray structure determinations of the 2,6-diaminopyridine complex revealed a slightly distorted octahedral geometry around the chromium with the equatorial CO groups bent away from the N-donor ligands.

[1] R.B. Martin in: *Metal ions in Biological Systems* (Eds. A Sigel, H. Sigel), **1996**, Marcel Dekker, New York, *vol. 32*, p. 521.
[2] I.A. Morkan, K. Güven, S. Özkar, *J. Organomet. Chem*., **2004**, *689*, 2319.
[3] S. Swachittanout, H. Holmann, R. van Eldrik, J. Reedijk, *Inorg. Chem*., **1993**, *32*, 4544.

$W(CO)_5L$ complexes are of interest as they display unpredicted chemical behaviour as far as their "soft" or "hard Lewis" acid characteristics are concerned.[4] The species $W(CO)_5L$, with L as a carbene ligand, agrees with a soft metal description for the $W(CO)_5$[5] fragment but preference for the sp^3 exocyclic amines compared to the softer sp^2 aromatic imines, suggest a hard metal description of the character of $W(CO)_5$ units.[6]

$W(CO)_5$ units have been shown to exhibit a potentially useful coordination chemistry as heavy atom labels of the purine bases, adenosine (A) and guanosine (G) (Scheme 3.1), with coordination distributed among the N_7, N_1 and N_3 sites similar to the Ru coordination center where N_3 and N_1 sites predominate over bonding to the N_7 site.[7]

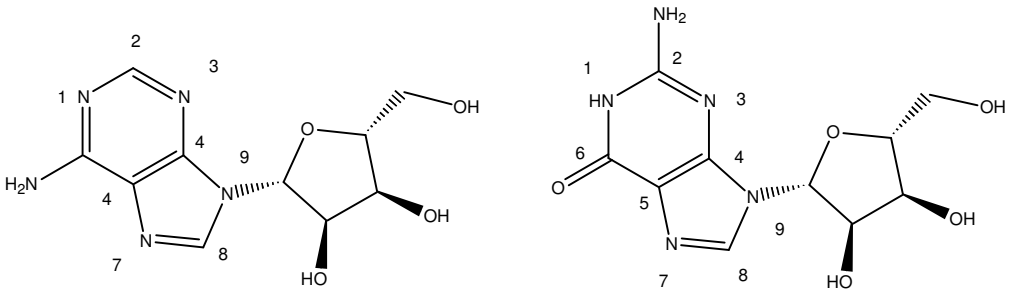

Scheme 3.1: The purine DNA bases, adenosine and guanosine.

Although the $W(CO)_5$ unit coordinates on the pyrimidine base, cytidine, *via* N_3 there is no evidence of coordination *via* the exocyclic amine. No coordination was observed with the nucleobases thymidine (T) and uracil (U) (Scheme 3.2).(4)

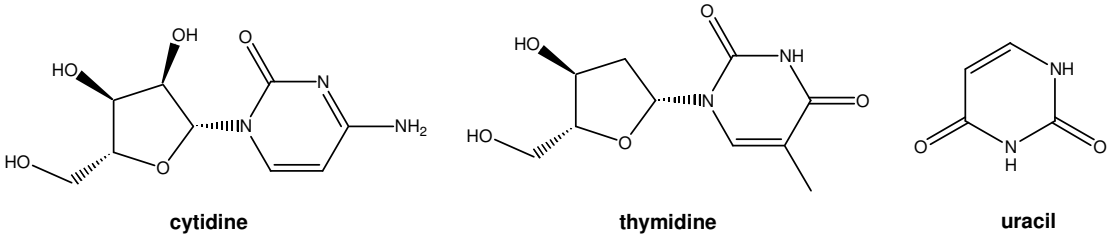

Scheme 3.2: The pyrimidine DNA bases, cytidine, thymidine and uracil.

[4] T.W. Stringfield, R.E. Sheperd, *Inorg. Chem. Commum.*, **2001**, *4*, 760.
[5] E.O. Fisher, A. Maasböl, *Angew. Chem., Int. Ed*, **1964**, *3*, 580.
[6] L. Tutt, J.I. Zinc, *J. Am. Chem. Soc*., **1986**, *108*, 5830.
[7] D. Chatterjee, M.S. Ward, R.E. Sheperd, *Inorg. Chim. Acta.,* **1999**, *285*, 170.

The DNA bases cytidine, adenosine and guanosine have structural motifs that appear in the similar structures of 2-aminopyrimidine (2-ampym), 4-aminopyrimidine (4-ampym), 2-aminopyridine (2-ampy) and 4-aminopyridine (4-ampy).[5]

Recent studies by Stringfield and co-workers[5] on the coordination modes of $W(CO)_5$ units to purines and pyrimidines revealed that the soft $W(CO)_5$ unit bonds exclusively to the hard exocyclic amine of 2-ampym and 4-ampym. While metal coordination *via* the endocyclic nitrogens are observed for Cu(II),[8] Pt(II) and Ag(I).[9]

Darensbourg and co-workers[10] were the first to report the synthesis and characterisation of $W(CO)_5$(2-ampy) in which the $W(CO)_5$ unit is bonded to the borderline hard endocylic N_1. It was observed that the change from 2-ampy to 2-ampym (Scheme 3.3.) results in a nearly complete reversal of bonding site preference of the $W(CO)_5$ unit. A sensitive balance exists between the coordination of the $W(CO)_5$ unit to the hard excocyclic amino group or to the borderline hard endocyclic donors in pyridines, pyrimidines and purines.

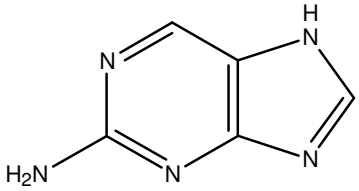

2-amino-purine

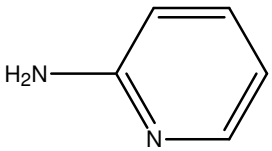

2-amino-pyridine

2-ampy

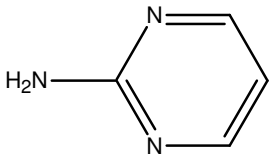

2-amino-pyrimidine

2-ampym

Scheme 3.3: Structures of purine, pyridine and pyrimidine.

Stringfield and Sheperd[11] have investigated the preferential excocyclic amino coordination of $W(CO)_5$ units with 4-ampy, 4-(dimethylamino)pyridine (4-Me_2ampy), 2-ampym and 2-(dimethylamino)pyridine (2-Me_2ampy) illustrating the anticipated altered variation of $W(CO)_5$L isomers with variation of basicity of exocyclic amino lone pair.

Their results indicate that both the position and extent of exocyclic amine methylation affects the distribution and preferential bonding of $W(CO)_5$ units to aminopyridines. 2-

[8] P.O. Lomme, H. Knuittila, E. Lindel, *Acta. Crystallogr.,* **1996**, C*52*, 51.
[9] G. Smith, B.A. Clout, D.E. Lynch, K.A. Byriel, C.H.L. Kennard, *Inorg. Chem.,* **1998**, *37*, 3236.
[10] D.J. Darensbourg, B.F. Frost, D.L. Larkin, *Inorg. Chem.*, **1993**, *40*, 2001.
[11] T.W. Stringfield, R.E. Sheperd, *Inorg. Chim. Acta.*, **2003**, *343*, 156.

Ampy coordinates almost exclusively *via* the endocyclic N_1 donor, while changing to 4-ampy produces a kinetic split between the endocyclic N^1 and the exocyclic amine in a ratio of 42:58. Placement of two methyl groups on the exocyclic amine enhances basicity and, even against the influnce of steric effects, effords more than 95% in coordination of the excocyclic dimethylamino group.

The placement of a methyl group on the amine of 2-ampy is sufficient to tamper with the coordination balance between the N_1 donor and the exocyclic amine. A complete shift from the 2-ampy preference of N_1 coordination to exocyclic amine coordination for 2-Me_2ampy was observed, thus the dimethylamino group enforces exocylic coordination for both 2-Me_2ampy and 4-Me_2ampy.

The interesting results, like ring opening and delocalisation, obtained in **Chapter 2** motivated us to consider coordination of the same series of ligands to the soft metal centres of group 6, chromium(0) and tungsten(0). In this chapter we examine the results obtained from of our series of ligands , which contain multiple bonding sites, by analysing the preference of coordination for the series of ligands towards chromium(0) and tungsten(0). **Chapter 3**, thus provides an overview of a series of new 2-aminoazole complexes of chromium(0) and tungsten(0) complexes by:

1) The description of the preparation of a series of 2-aminoazole complexes, prepared with the ligands used in **Chapter 2**, containing pentacarbonyl tungsten and -chromium units and the full characterisation of the novel complexes obtained.
2) The evaluation, through a comprehensive study, with the implementation of various analytical techniques, of the influence of the ligand on structural parameters of the $M(CO)_5$-unit (M = Cr or W) and of the $M(CO)_5$-unit on the ligand upon coordination.

3.2 Results and discussion

3.2.1 Chromium(0) and tungsten(0) compounds of 2-aminoazoles.

Sections 3.2.1.1 and 3.2.1.2 describe the preparation and isolation of the various pentacarbonylchromium(0) and pentacarbonyltungsten(0) compounds, while section 3.2.2 is devoted to the spectroscopic characterisation of these complexes *via* IR and NMR spectroscopy and FAB-MS spectrometry. In section 3.2.3 the crystal structures of the new

chromium- and tungsten containing complexes are analysed. In addition, this section includes the molecular structure of complexes (**14** and **19)** that contain the imine coordinated 2-aminothiazoline ligand, now without any ring opening as was observed in Chapter 2 (complex **9**).

3.2.1.1 Preparation of chromium complexes 11-15.

The substitution of THF in $(CO)_5Cr(THF)$, produced octahedral complexes with coordination through the imine nitrogen (Scheme 3.4).

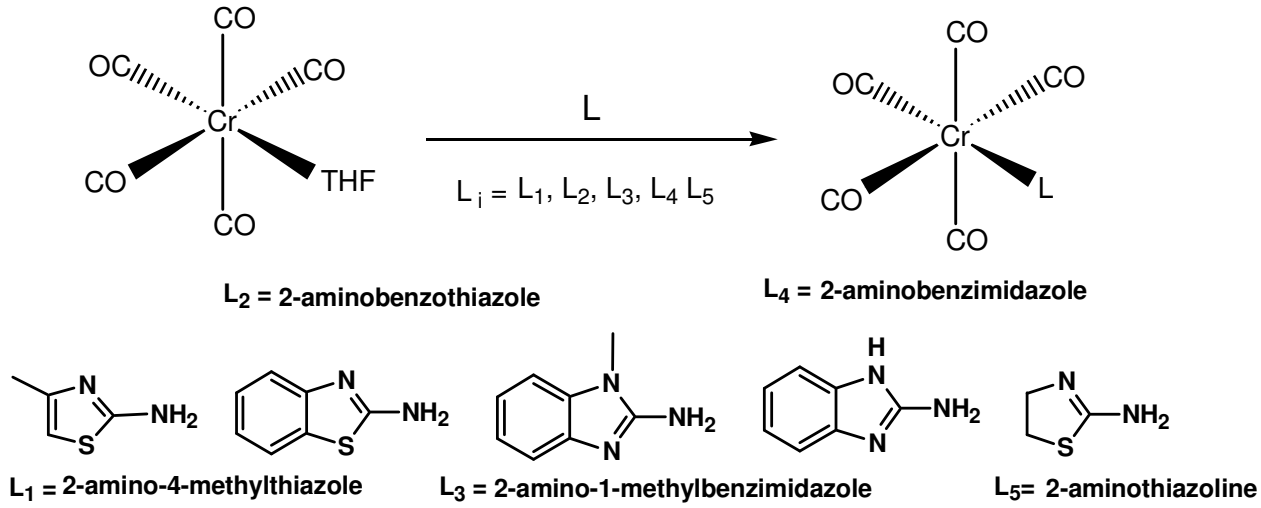

Scheme 3.4: Preparation of 2-aminoazole complexes of chromium(0).

The synthetic procedure involved the UV-irradiation of $Cr(CO)_6$ in THF for 2 h under nitrogen in a quartz reaction vessel while stirring continuously.[12] The solution was then transferred to a Schlenk tube and the appropriate ligand (L_i) was added while stirring was continued for another 2 h. After stripping of solvent, the resulting solid was redissolved in diethyl ether, filtered through SiO_2 and dried *in vacuo* to yield yellow, microcrystalline material. The products were soluble in organic solvents such as acetone, dichloromethane, THF, diethyl ether or DMSO and in hexane and pentane as well. Crystals suitable for X-ray crystal structure determinations were obtained by vapour diffusion of pentane into concentrated solutions of the compounds in acetone (**12, 13**) or diethyl ether (**14**) under

[12] J.A. Costamagna, J. Granifo, *Inorg. Synth., 23,* **1985**, 1.

argon atmosphere at -22 ºC. The physical and analytical data of compounds **11-15** are summarised in Tables 3.2-3.3.

Table 3.2: Physical data of complexes **11** and **12**.

Complex	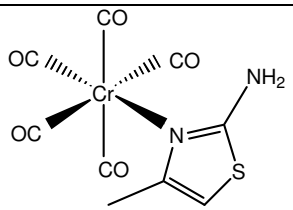 **11**	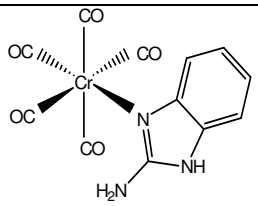 **12**
m.p. (ºC)	86-88 (decomp.)	148-150
Colour	yellow	yellow
Crude yield (%)	52	97
M_r	306.22	325.20
M_f	$C_9H_6CrN_2O_5S$	$C_{12}H_7CrN_3O_5$

Tabel 3.3: Physical data of complexes **13-15.**

Complex	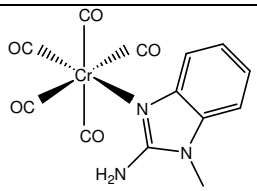 **13**	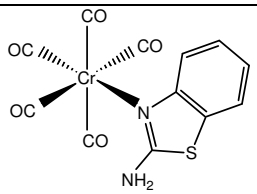 **14**	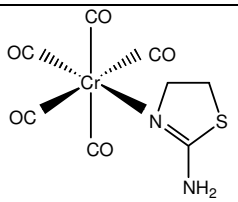 **15**
m.p. (ºC)	147-149 (decomp.)	149-150 (decomp.)	81-87 (114 decomp.)
Colour	yellow	yellow	yellow
Crude yield (%)	42	47	45
M_r	339.22	342.25	294.21
M_f	$C_{13}H_9CrN_3O_5$	$C_{12}H_6CrN_2O_5S$	$C_8H_6CrN_2O_5S$

3.2.1.2 Preparation of tungsten complexes 16-19

The experimental procedures again involved the substitution of THF. The octahedral complexes (Scheme 3.5) were all imine coordinationed.

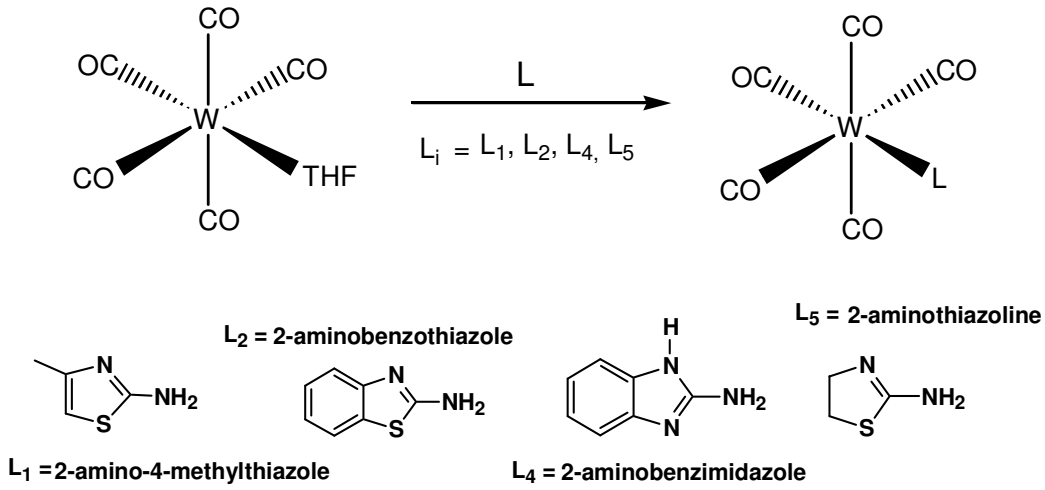

Scheme 3.5: Preparation of **16-19.**

The same experimental procedure as described in section 3.2.1.1 for the chromium complexes was used, yielding a microcrystalline product which was used in analyses.

The products are soluble in organic solvents such as acetone, dichloromethane, THF, diethyl ether or DMSO and hexane and pentane. Crystals suitable for X-ray crystal structure determinations were obtained by vapour diffusion of pentane into solutions of the compounds in acetone (**17**, **19**) or diethyl ether (**18**) under argon at -22 ºC. The physical and analytical data of compounds **16–19** are summarised in Tables 3.4 and 3.5.

Table 3.4: Physical data and chemical data of complexes **16** and **17**.

Complex	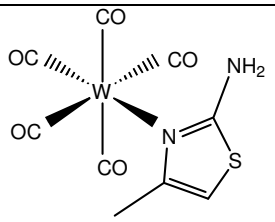 **16**	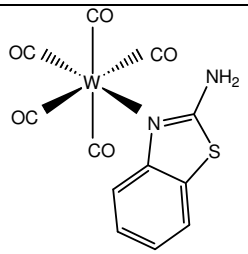 **17**
m.p. (ºC)	106-108 (decomp.)	146-147 (decomp.)
Colour	yellow	yellow
Crude yield (%)	50	51
M_r	438.06	474.09
M_f	$C_9H_6N_2O_5SW$	$C_{12}H_6N_2O_5SW$

Table 3.5: Physical data and chemical data of complexes **18** and **19**.

Complex	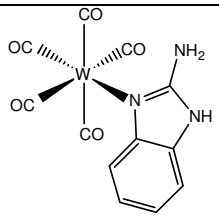 **18**	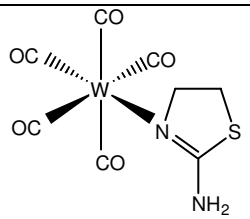 **19**
m.p. (ºC)	165-167 (decomp.)	109-110 (153 decomp.)
Colour	yellow	colourless
Crude yield (%)	27	35
M_r	457.04	501.07
M_f	$C_{12}H_7N_3O_5W$	$C_{13}H_{21}N_2O_5SW$

3.2.2 Spectroscopic characterisation of compounds 11-18

3.2.2.1 Nuclear magnetic resonance spectroscopy

The ^{1}H NMR spectra show that all the proton resonances experience a significant downfield shift upon coordination of the ligand to the $Cr(CO)_5$ and $W(CO)_5$ fragments. The resonances in the ^{13}C NMR spectra generally also experience a downfield shift upon coordination of the ligands; exceptions are discussed in the following sections for the individual complexes.

The ^{13}C NMR spectra of all the complexes show resonances for the CO ligands, the more intense signal can be assigned to the *cis* CO ligands and the other signal to the *trans CO* ligands. The *cis* CO ligands resonate at ~δ 210 for chromium complexes and at ~δ 195 for the tungsten complexes compared to the chemical shifts for the *trans CO* ligands at ~δ 220 in chromium complexes and at ~δ 205 for the tungsten complexes. The much larger electron density on the tungsten metal when compared to the chromium metal is responsible for the CO signals of the tungsten complex appearing upfield from those of the chromium complexes.

The ^{15}N NMR spectra reveal that the NH_2 signal appears downfield to that of the imine nitrogen. Upon coordination the NH_2 resonance becomes more shielded, and appears upfield from the NH_2 in the free ligand, while the imine nitrogen becomes more deshielded and resonates downfield when compared to the signal of the free ligand. When the imine nitrogen of 2-amino-4-methylthiazole and 2-aminothiazoline is bonded to

$W(CO)_5$-unit (**16** and **19**) the shielding is reflected in the change in chemical shift observed for the signal from δ -122.5 and δ -164.0 in the uncoordinated ligand to δ -198.5 and δ -233.0 upon coordination. The NH_2 resonates downfield at δ -282.7 (**19**) and δ -293.6 (**16**). All attempts to detect the nitrogen atoms in the other complexes failed, despite the use of both indirect and direct detection methods.

^{1}H , ^{13}C , ^{15}N NMR spectroscopic data, utilising acetone–d_6 as solvent were obtained for all the ligands and complexes. The data are summarised in Tables 3.6.-3.10. Unfortunately, the N^{15} NMR spectrum of **15** could not be obtained owing to the decomposition of the complex during the longer data collection time needed.

Table 3.6: ^{1}H, ^{13}C and ^{31}P NMR spectroscopic data obtained for **2-aminothiazoline**, **15** and **19**

	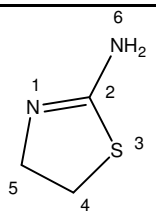 **2-aminothiazoline**		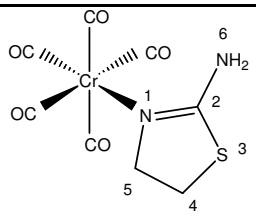 **15**	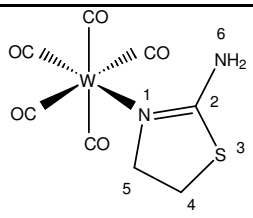 **19**
Solvent Temperature (ºC)	acetone-d_6 25		acetone-d_6 25	acetone-d_6 25
Assignment	**Chemical shift (ppm)**			
^{1}H NMR (300/400 MHz)	H^6	n.o	6.54 (bs, 2H)	6.80 (bs, 2H)
	H^4	3.84 (t, 2H, ^{1}J = 7.3Hz))	3.96 (t, 2H, ^{1}J = 7.3Hz)	4.12 (t, 2H, ^{1}J = 7.3Hz)
	H^5	3.27 (t, 2H, ^{1}J = 7.3Hz)	3.39 (t, 2H, ^{1}J = 7.3Hz)	3.42 (t, 2H, ^{1}J = 7.3Hz)
^{13}C NMR (75/100 MHz)	*trans* CO	–	222.6 (s)	207.2 (s)
	C^2	162.5 (s)	216.6 (s)	193.3 (s)
	cis CO	–	213.7(s)	199.7 (s)
	C^5	62.1 (s)	69.7 (s)	71.4 (s)
	C^4	37.1 (s)	33.9 (s)	34.7 (s)
^{15}N NMR (61 MHz)	N^4	-305.9	n.o	-282.7
	N^1	-163.98	n.o	-233

The ^{1}H NMR spectrum indicates that all the proton resonances experience a significant downfield shift upon coordination of ligand to $Cr(CO)_5$ and $W(CO)_5$ units. The signal of the proton, H^4, shows a downfield shift upon coordination of the ligand to chromium ($\Delta\delta$ 0.12) and tungsten ($\Delta\delta$ 0.28). The resonance of the proton H^5, again shows a downfield shift of $\Delta\delta$ 0.12 for chromium and $\Delta\delta$ 0.15 for tungsten upon coordination of ligand. The NH_2 protons show a characteristic broad peak at δ 6.54 for the chromium and δ 6.80 for the tungsten complex. The NH_2 signal is not observed in the spectrum of the free ligand.

The ^{13}C NMR spectrum reveals that all resonances, except for the resonance of C^4, also experience a significant downfield shift upon coordination of the ligand to the $Cr(CO)_5$ and $W(CO)_5$ units. The low intensity signal observed at δ 222.6 and δ 207.2 can be attributed to the *trans* CO ligands of the chromium and tungsten complexes respectively, while the more upfield medium intensity signals at δ 213.7 and δ 199.7 can be allocated to the *cis* CO ligands. The low intensity signal at δ 162.5 for **15** and δ 193.3 for **19** can be attributed to the highly deshielded carbon, C^2. The C^2 carbon resonance reflects a significant downfield shift when coordination to the $Cr(CO)_5$ ($\Delta\delta$ 54.1) and $W(CO)_5$ ($\Delta\delta$ 30.8) metal units takes place. The signal of the C^5 carbon experiences a downfield shift upon coordination to the chromium- ($\Delta\delta$ 7.6) or tungsten units ($\Delta\delta$ 9.3) when compared to the resonance for the free ligand. The C^4 carbon, contrary to the expectation, experiences a small upfield change in chemical shift when compared to the free ligand, with a change of $\Delta\delta$ 3.2 for the chromium and $\Delta\delta$ 2.4 for the tungsten complex. This observation is not unusual as the total chemical shift σ ($\sigma = \sigma_p + \sigma_d$) in the ^{13}C NMR does not only reflect shielding and deshielding.[13] The total chemical shift (σ) consists of two parts, namely the paramagnetic contribution (σ_p) and diamagnetic contribution (σ_d), in the equation $\sigma = \sigma_p + \sigma_d$. The diamagnetic component is ignored in ^{1}H NMR where chemical shifts only reflect shielding and deshielding but the diamagnetic contribution plays a more significant role in ^{13}C NMR and cannot be ignored. As interpreted the ^{13}C NMR chemical shifts do not simply reflect shielding and deshielding as in ^{1}H NMR.

The data collected for the ^{15}N NMR spectrum revealed as expected that the N^4 nuclei at δ -305.9, appear at a higher field in the ^{15}N NMR spectrum when compared to the resonance for the imine nitrogen, N^1, δ -164.0. All attempts to detect the nitrogen atoms of **15** failed.

[13] R.F. Fenske in: *Organometallic Compounds, Synthesis, Structure and Theory* (Ed. B.L. Shapiro), Texas A & M University Press, Texas, **1983**, p. 305.

Upon coordination of $W(CO)_5$ to the N^1 atom, it is shielded, resonating more upfield from the observed signal in the ligand (δ -163.98 to δ -233), while the deshielding of N^4 causes a downfield shift from δ -305.9 to δ -285.7.

^1H and ^{13}C NMR spectroscopic data for the ligand and the complexes **12**, **18** are summarised in Table 3.7. Despite the use of indirect and direct methods, no ^{15}N NMR spectrum of **18** or **12** could be obtained before the onset of decomposition of the complex.

Table 3.7: ^1H and ^{13}C spectroscopic data obtained for **2-aminobenzimidazole**, **12** and **18**.

		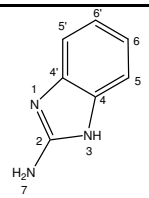 **2-aminobenzimidazole**	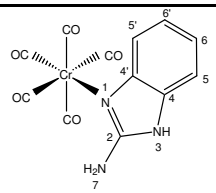 **12**	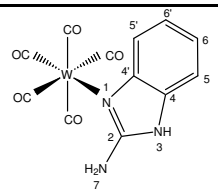 **18**
Solvent		methanol-d_4	methanol-d_4	methanol-d_4
Temperature (°C)		25	25	25
Assignment		**Chemical shift (ppm)**		
^1H NMR (300/400 MHz)	$H^{5,5'}$	7.18 (m , 2H)	6.90-7.19 (m, 4H)	7.05-7.20 (m, 4H)
	$H^{6,6'}$	6.96 (m, 2H)		
	H^3	4.95 (bs ,2H)	n.o.	n.o.
^{13}C NMR (75/100 MHz)	*trans* CO		221.5 (s)	202.7 (s)
	cis CO		216.1(s)	199.2 (s)
	C^2	156.7 (s)	157.3 (s)	144.6 (s)
	$C^{4'}$	139.5 (s)	144.3 (s)	133.9 (s)
	C^4		134.0 (s)	
	$C^{6'}$	121.4(s)	121.9 (s)	122.6 (s)
	C^6		121.5 (s)	122.4 (s)
	$C^{5'}$	112.8(s)	116.8 (s)	118.1(s)
	C^5		110.2 (s)	110.8 (s)

The ^1H NMR spectra of **12** and **18** do not provide conclusive evidence that the complexes have formed. The phenyl protons of the 2-aminobenzimidazole ligand are typically

detected as multiplets at δ 6.90-7.19 for the chromium and δ 7.05-7.20 for the tungsten complexes. The signal for the NH protons appears as a characteristic broad peak at δ= 4.95 for the free ligand, but are not observed for the complexes.

The ^{13}C NMR spectrum provides us with evidence that the expected compound has formed by the detection of the signals for both the *cis* and *trans* CO ligands (discussed at the beginning of this section). This evidence is also supported by the IR data (*vide infra*) and conclusive evidence is provided by mass spectra (*vide infra*). The tungsten unit's resonances for the *cis* and *trans* CO ligands are located at δ 221.5 and δ 216.1 respectively. The W-C coupling in the *cis* and *trans* CO signals is not observed as a result of the low intensity of the signals. The signal of very low intensity at δ 157.3 for chromium complex and δ 144.6 for the tungsten complex is characteristic for the highly deshielded carbon, C^2. The C^4 and $C^{4'}$ carbons are rendered equivalent by their chemical environment in the spectrum of the free ligand [δ 139.5] and in the tungsten complex resonating at δ 133.9 while in the chromium complex they are inequivalent and their resonances are observed at δ 134.0 and δ 144.4. Although the carbons C^6 and $C^{6'}$ are chemically inequivalent in the spectrum of the free ligand they are similar in the chromium and tungsten complexes. The resonances for these carbons show only a very small change in chemical shift upon coordination (Δδ ~1 for the tungsten complex and Δδ ~0.5 for the chromium complex). The same is true for the $C^5$and $C^{5'}$carbons. One would expect the resonances to show a downfield change in chemical shift upon coordination but some signals display an upfield change in chemical shift e.g. those for C^2, C^4, $C^{4'}$ and C^5. This can be explained by the composition of the total chemical shift σ.[13]

^{1}H, ^{13}C and ^{15}N NMR spectroscopic data of **16** are summised in Table 3.8. The NMR spectrum of **11** could not be obtained due to immediate decomposition of the complex.

Table 3.8: ^{1}H, ^{13}C and ^{15}N NMR spectroscopic data obtained for **2-amino-4-methylthiazole** and **16**.

Complex		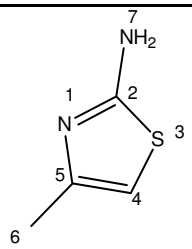 **2-amino-4-methylthiazole**	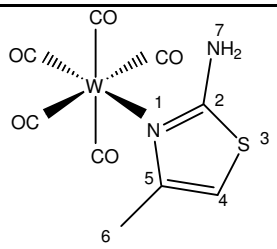 **16**
Solvent Temperature (°C)		acetone-d_6 25	acetone-d_6 25
Assignment		**Chemical shift (ppm)**	
^{1}H NMR (300/400 MHz)	H^7	6.70 (bs, 2H)	7.17 (bs, 2H)
	H^4	6.06 (s, 1H)	6.56 (s, 1H)
	H^6	2.10 (s, 3H)	2.43 (s, 3H)
^{13}C NMR (75/100 MHz)	*trans CO*	_	203.2 (s)
	cis CO	_	199.9 (s)
	C^2	170.5 (s)	174.0 (s)
	C^5	149.9 (s)	150.7 (s)
	C^4	102.6 (s)	104.5 (s)
	C^6	18.31 (s)	22.6 (s)
^{15}N NMR (61 MHz)	N^7	-313.7	- 293.6
	N^1	-122.5	-198.5

The ^{1}H NMR spectrum of **16** indicates that all the proton resonances experience a downfield shift upon coordination of the ligand to the $W(CO)_5$ unit.

The signal for the proton H^4 is observed at δ 6.56 indicating a downfield change in chemical shift of Δδ 0.5 upon coordination to the tungsten complex. The resonance for the methyl proton, H^6, is detected at δ 2.43 with a downfield change in chemical shift of Δδ 0.33 when compared to the free ligand. The signal for the NH_2 protons appears as a characteristic broad signal at δ 6.70 for the free ligand and at δ 7.17 for the tungsten complex.

The ^{13}C NMR spectrum indicates that the signals experience a downfield shift upon coordination of the ligand to the $W(CO)_5$ unit. The signal of low intensity at δ 222.6 can be attributed to the *trans* CO ligand while the more upfield single resonance of medium intensity at δ 199.9 can be allocated to the *cis* CO ligands. Another signal of low intensity at δ 174.0 is assigned to the highly deshielded carbon, C^2, which appears downfield when compared to the free ligand. The signals for C^5 (δ 150.7) and C^4 (δ 104.5) appear downfield (Δδ 0.8 and Δδ 1.9 respectively) when compared to the same signals in the free ligand. The signal for the methyl carbon, C^6, at δ 22.6 displays a change in chemical shift of Δδ 4.29 upfield when compared to the same signal in the free ligand at δ 18.31 again not reflecting electronic changes in the free ligand upon coordination.

^{15}N NMR spectrum revealed the following:

i) As expected, the N^7resonance appears at higher field than the resonance for the N^1nuclei.

ii) The coordination of the tungsten complex to the imine nitrogen, N^1, shifts the signal upfield from δ -122.5 to δ -198.5.

iii) The N^7 nitrogen signal shifts from δ -313.7 in the free ligand to δ -293.6, downfield thus indicating that $N^7$is less shielded.

^1H and ^{13}C NMR spectroscopic data for **14** and **17** are summarised in Table 3.9. Unfortunately, the N^{15} NMR data could not be obtained for **14** and **17** due to the decomposition of the complexes.

Table 3.9: The spectroscopic data obtained for **2-aminobenzothiazole**, **14** and **17**.

		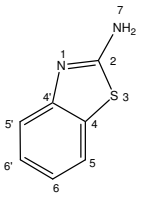 **2-aminobenzothiazole**	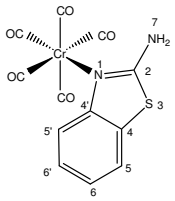 **14**	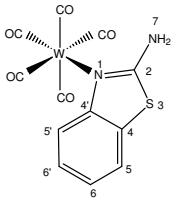 **17**
Solvent Temperature (°C)		acetone-d_6 25	acetone-d_6 25	acetone-d_6 25
Assignment		**Chemical shift (ppm)**		
^{1}H NMR (300/400 MHz)	$H^{5'}$	7.63 (d, 1H, ^3J = 7.8 Hz, , ^{1}J = 0.98 Hz)		
	H^5	7.41 (d, 1H, ^3J = 7.3 Hz)		
	$H^{6'}$	7.24 (t, 1H, ^3J = 7.3 Hz , ^1J = 1.5 Hz)	7.05-8.01 (bm, 4H)	7.10-8.05 (bm, 4H)
	H^6	7.05 (t, 1H, ^3J = 7.3Hz, ^1J = 1.5 Hz)		
	H^7	7.00 (bs, 2H)	n.o.	n.o.
^{13}C NMR (75/100 MHz)	*Trans CO*	-	222.9 (s)	203.4 (s)
	Cis CO	-	216.3 (s)	193.3 (s)
	C^2	168.4 (s)	168.2 (s)	172.6 (s)
	$C^{4'}$	154.9 (s)	155.1 (s)	153.4 (s)
	C^6	133.5 (s)	133.7 (s)	128.4 (s)
	$C^{6'}$	127.3 (s)	127.3 (s)	127.3 (s)
	C^5	123.1 (s)	123.4 (s)	123.6 (s)
	C^4	122.5 (s)	122.5 (s)	122.9 (s)
	$C^{5'}$	120.2(s)	120.4(s)	120.2 (s)

The ^{1}H NMR spectra of **14** and **17** are inadequate in determining the changes in the chemical shifts of the proton resonances upon coordination of the ligand because all the signals for the aromatic protons are observed as a broad multiplet at δ 7.05-8.01 for the chromium- and δ 7.05-8.05 for the tungsten compound.

The ^{13}C NMR resonances show only small changes in chemical shifts of the resonances upon coordination of ligand to the $Cr(CO)_5$ and $W(CO)_5$ units but confirm the formation of the compounds. The low intensity signals of the *trans* CO ligands of the chromium and tungsten complexes are observed at δ 222.9 and δ 203.4 respectively while the *cis* CO ligands are located at δ 216.3 and δ 193.3 respectively. The presence of the chromium hexcarbonyl CO signal (δ 213.7) and a tungsten hexcarbonyl CO (δ 199.6) indicate that decomposition had occurred during the measurements. Another low intensity signal at δ 168.2 for **14** and δ 172.6 for **17** can be attributed to the highly deshielded C^2 carbon. The C^2 carbon resonance experienced a small upfield shift upon coordination to the chromium metal (Δδ 0.2) and a downfield shift in the instance of tungsten (Δδ 4.2). The carbon $C^{4'}$, is less shielded because it is located in close proximity to the nitrogen atom, χ_N (3) > χ_S (2.5), and thus located downfield from the resonance of the C^4 carbon which is in close proximity to the sulphur atom. The $C^{4'}$ signal will also display a larger change in chemical shift when compared to the signal for C^4, upon coordination to the metal. A small or no change in chemical shift is observed for these carbons upon coordination (C^4 Δδ 0.2 and $C^{4'}$Δδ 1.5) for the chromium complexes and the C^4 carbon is unaltered by coordination while a change for $C^{4'}$of Δδ 0.4 is observed in the tungsten complexes. The coordination of 2-aminobenzothiazole to the $Cr(CO)_5$ or $W(CO)_5$ unit results in minute chemical changes for the signals of C^5 and $C^{5'}$, which appear at less than Δδ 0.6 downfield when compared to the free ligand. The signal for the more shielded C^6 carbon in the complex **17** is observed upfield at δ 128.4 (Δδ 5.4) when compared to the free ligand (δ 133.5) while the same signal for the same atom in **14** is observed downfield at δ 133.7. The signal for $C^{6'}$, in both complexes, is observed at a chemical shift identical to that of $C^{6'}$ in the free ligand at δ 127.3.

In general the signals for the ligands are expected to shift downfield upon coordination, but some small upfield changes in chemical shift were observed for $C^{4'}$ and C^6 in the tungsten complexes. The changes can be explained taking the total chemical shift (σ) into account.[13]

3.2.2.2 Mass spectrometry

The spectra of the chromium containing complexes, **11**-**12**, did not yield useful characteristic peaks for these complexes even though they were determined using the less harsh, softer FAB-MS technique. Some information was obtained from the spectra of **14** and **15.** The peak observed at *m/z* 305.6 can be assigned to the structure **(A)** in Scheme 3.7.

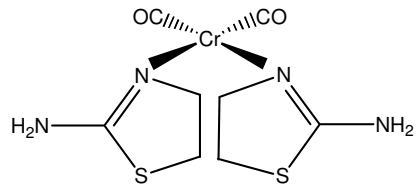

(A)

Scheme 3.7: The structure corresponding to a peak at *m/z* 305.6.

This peak at *m/z* 305.6 reveals that a fragment consisting of a $Cr(CO)_2$ unit complexed to two 2-aminothiazoline ligands is formed in the spectrometer during the analyses of **15**. The same peak in the spectrum of **14** reveals the loss of the 6-membered ring from the ligand, rendering the 2-aminobenzothiazole, a 2-aminothiazoline after coordination of the two to $Cr(CO)_2$ followed.

The spectral data of the tungsten complexes **16-19** were acquired by using the softer, less invasive positive ion FAB-MS technique and are summarised in Table 3.10. The complexes exhibit fragmentation patterns in which the molecular ions are observed as the fragment with the highest molecular mass. Peaks representing the loss of CO ligands follow each other while the loss of as many as four CO-units are observed. The only peak representing a fragment of the ligand i.e. 2-amino-4-methylthiazole at *m/z* 114 is present in the spectrum of **16**.

Table 3.10: Mass spectrometric data for **16-19**.

Fragment	*m/z* (***I*** **in %**)			
	16	**17**	**18**	**19**
$[M]^+$	437 (27)	474 (22)	456 (13)	424 (18)
$\{[M]\text{-}CO\}^+$	407 (35)	446 (5)	429 (3)	397 (12)
$\{[M]\text{-}2CO\}^+$	381 (20)	418 (8)	399 (13)	371 (10)
$\{[M]\text{-}3CO\}^+$	353 (11)	390 (12)	-	342 (2)
$\{[M]\text{-}4CO\}^+$	325 (4)	362 (3)	-	-
$\{L\}^+$	114 (45)	-	-	-
$\{L\text{-}NH_2\text{-}CH_3\}^+$	81 (20)	-	-	-
$\{[M]\text{-}2CO\text{-}NH_2\text{-}Ph\}^+$	-	-	306 (22)	-
$3\{L\}^+$	-	-	-	306 (21)

The molecular ions were observed as weak peaks for **16** (*m/z* 437), **17** (*m/z* 474), **18** (*m/z* 456) and **19** (*m/z* 424). The 2-amino-4-methylthiazole ligand undergoes a NH_2 -and methyl fragment loss producing a fragment at *m/z* 81. The identical fragment peak of *m/z* 306 is observed for **18** and **19**. The peak can be assigned to a fragment consisting of 3 molecules of the free ligand for **19** while for **18** the peak at *m/z* 306 ($\{[M]\text{-}2CO\text{-}NH_2\text{-}Ph\}^+$) represents the loss of a 6-membered ring, a carbonyl group and NH_2 fragment from the molecular ion.

3.2.2.3 Infrared spectroscopy

The IR spectroscopic data were collected on a Thermo Nicolet Avatar 330 FT-IR machine by means ATR. The ν(CO) vibrations are observed in the typical explained pattern and intensity associated with pentacarbonyl compounds. The presence of pentacarbonyl was indicated by characteristic A^1 vibration (located at high frequency) followed by the intense E_1 band with one or two weaker bands, which are located to the left (B_1) and the right of this band (A_1^2) (see Scheme 3.8). The E-band is so intense because it is twice degenerated and thus the strongest band. The fundamental vibrations are observed because of a small change in local symmetry.

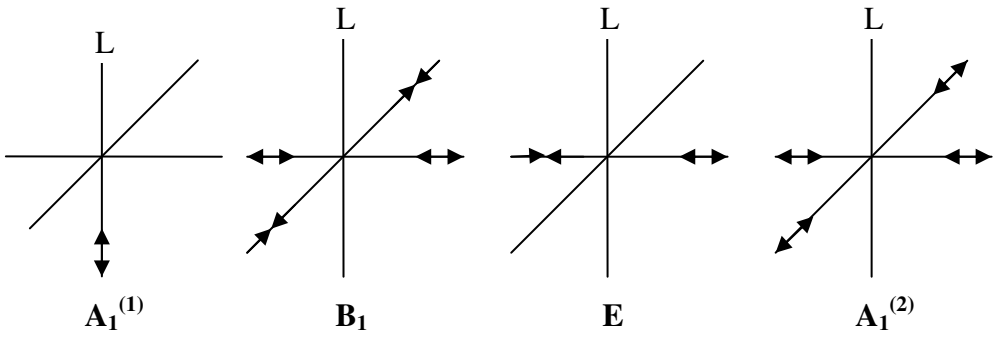

Scheme 3.8: Fundamental vibrations of pentacarbonyl.

All the complexes display four bands; $A_1^{(1)}$, B_1, E and $A_1^{(2)}$. The normally Raman active but IR inactive band, B_1, is also present indicating a somewhat distorted C_{4v}-symmetry. The spectroscopic data of the ν(CO)-absorption vibrations in the Cr-complexes are summarised in Table 3.11.

Table 3.11: IR-data of the chromium complexes **11, 14, 15** in hexane.

	cm^{-1}		
Symmetry vibration	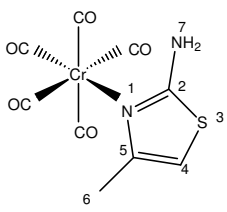 **11**	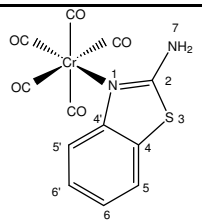 **14**	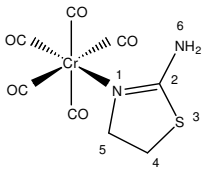 **15**
$A_1^{(1)}$	2067.0 (w)	2067.0 (w)	2066.3 (w)
B_1	2025.6 (w)	2022.4 (w)	2028.2 (w)
E	1938.0 (s)	1936.3 (m)	1934.3 (s)
$A_1^{(2)}$	1918.3 (sh)	1916.2 (sh)	1916.8(sh)

The spectra of complexes **12** and **13** are not analysed since the presence of $Cr(CO)_6$, formed as a decomposition product, obscures the E-symmetry and $A_1^{(2)}$ symmetry band. The $A_1^{(1)}$ band in all the complexes, is an indication of the $\nu(CO)_{trans}$, and is observed as a wide band in 2067.0 cm^{-1} region. The $A_1^{(2)}$ symmetry band at 1916-1918 cm^{-1} is observed as shoulder peaks of the E-symmetry band.

The spectra of the tungsten-complexes were also obtained in a liquid cell with the complexes dissolved in a hexane solution. The spectroscopic data of the ν(CO)-absorption bands for the W-complexes are tabulated in Table 3.12.

Table 3.12: IR-data of the tungsten complexes **17** and **19**.

	cm^{-1}	
Symmetry vibration	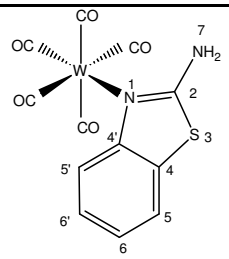 **17**	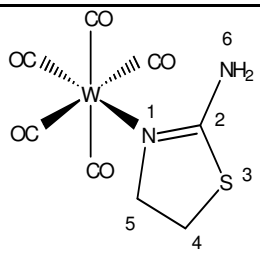 **19**
$A_1^{(1)}$	2069.5 (w)	2069.3 (w)
B_1	2024.5 (w)	2025.5 (w)
E	1932.3 (m)	1929.2 (s)
$A_1^{(2)}$	1918.0 (sh)	1916.8 (sh)

The presence of the hexacarbonyl vibrations are observed as a strong band at ~1983.5 cm^{-1} in all the IR spectra of the tungsten complexes, **16** and **18,** obscuring the E-symmetry and $A_1^{(2)}$ rendering them worthless for analyses of the IR spectra. The $A_1^{(1)}$ symmetry, with the highest frequency of all the bands, of complexes **17** and **19** are located at ~2069 cm^{-1}. The B_1 symmetry band is observed at ~2025 cm^{-1}, E symmetry band at ~1930 cm^{-1} and the $A_1^{(2)}$ symmetry band as a shoulder at ~1917 cm^{-1}.

The comparison of the symmetry bands of the ligand, 2-aminothiazoline, in the chromium complex (**15**) and the tungsten complex (**19**) reveals only small differences (3-4 cm^{-1}).

3.3 Structure determinations of compounds 12-14 and 17-19

The crystal and molecular structures of compounds **12-14** and **17-19** were determined by single crystal X-ray diffraction and are, to the best of our knowledge, now reported for the first time. The discussion of the structures of the free ligands serve as references for the discussion of their coordination complexes.

The X-ray structure determinations revealed that the Cr-N distance for **12** [2.137(2) Å], **13** [2.143(5) Å and 2.136(5) Å] and **14** [2.160Å and 2.164 Å] are normal.[14] The Cr-C distances of **12** ranges from 1.840(3)-1.936(3)Å while for **13** they are in range of 1.829(7)-1.916(5) Å and in **14** the distances range from 1.834(4)-1.922(4) Å. We observe that for complex **12** the *cis* Cr-C distance [1.889(3)-1.936(3)Å] is longer than the *trans* Cr-C distance [1.840(3)Å]. The same tendency is observed for **13** and **14** and in literature.[14] The complexes are essentially octahedral with some deviation from ideal symmetry owing to the fact that the CO groups are bent away. The C-Cr-C angles of **12** [C(3)-Cr(1)-C(4) 87.6(1)°and C(3)-Cr(1)-C(1) 89.0(1)º] and **13** [O(13)-Cr(1)-O(14) 87.2(9)º and O(33)-Cr(2)-O(34) 87.6(2)º] indicate that the *cis* CO groups are bent away from the N-containing ligands with the same trend also observed in complex **14.** The C-Cr-N angles for **12** [C(3)-Cr(1)-N(17) at 177.3(1)º] and **13** [C(33)-Cr(2)-N(21)of 176.7(3)º and C(13)-Cr(1)-N(1) at 176.5(2)º] and for **14** [174.96(4)º and 177.2(6)º] are close to 180°.

The W-N distances for **18** [2.248(3) Å] and **19** [2.249(6) Å] are similar to the literature values of pentacarbonyl-*s*(*t*-butylpyrozol)tungsten [2.235(2)Å],[15] while in **17** the distance [2.274(4)Å] is longer than normal. The W-C distances in **17** range from 1.960(5) to 2.054(5) Å, in **18** from 1.967(4) to 2.055(4) Å and in **19** from 1.968(5) to 2.049(6) Å, which are all in are in good agreement with similar compounds [1.959-2.049Å].[15] For complex **17** the *cis* W-C distance [2.026(6)-2.054(5)Å] is longer than the *trans* W-C distance [1.960(5)Å]. The same observation concerning *cis* and *trans* W-C distances are observed in **18** and **19**. The complexes are essentially octahedral with some deviation from ideal symmetry owing to the fact that the CO groups are bent away from the 2-aminoazole ligand. The C-W-C angles of the *cis* CO groups for **17** [C(6)-W(1)-C(7) 89.1(2)º and C(6)-W(1)-C(4) 87.4(2)º], in **18** [C(30)-W(2)-C(32) 86.6(7)º and C(30)-W(2)-C(33) 87.8(6)º] and in **19** [C(6)-W(1)-C(5) 86.2(2)º and C(6)-W(2)-C(5) 87.6(2)º] all deviate from 90º indicating that the *cis CO* groups are bent away from the ligand. The C-W-N angle for **17** [177.2(4)º] and **19** [178.4(8) º] deviates slightly from 180º while in **18** [173.0(4)º] it deviates notably from 180º. Particular observations for the various complexes are now discussed in the following sections.

[14] R. Aumann., H. Heinen, C. Kruger, *Chem. Ber.,* **1987**, *120*, 1287.
[15] W. L. Jia, L. F. Jang, J. F. Chai, J. T. Wang, *Transition Met. Chem*., **2001**, *26*, 400.

3.2.3.1 Crystal and molecular structure of 2-aminobenzimidazole)pentacarbonyl chromium, 12

The complex **12** crystallised from acetone as yellow needles in the monoclinic space group $P2_1/c$ with Z = 4 molecules in the unit cell. The asymmetric unit contains a single molecule co-crystallised with a solvent molecule of water. The asymmetric unit is shown in Figure 3.1 and relevant angles and distances are tabulated in Table 3.13.

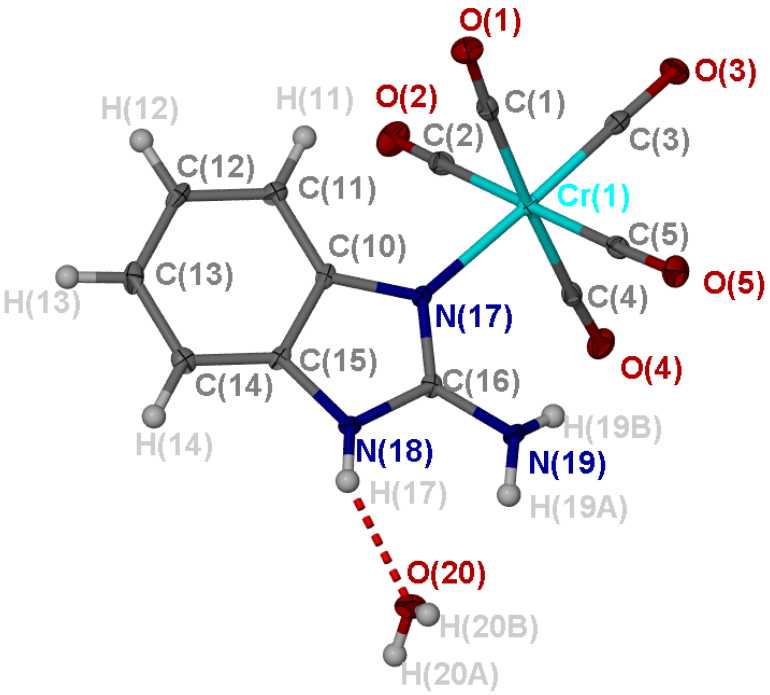

Figure 3.1: The asymmetric unit of **12**. A red dashed line indicates hydrogen bonds.

The double bond distance N(17)-C(16) [1.324(3) Å] is significantly longer than the standard reported values for C=N [1.27 Å][16] while the C-N bond distance of N(18)-C(16) [1.350(7) Å] is shorter than standard C-N [1.41 Å],[16] indicating a degree of delocalisation. The C-N and C=N values concur with the same values in the uncoordinated 2-aminobenzimidazole ligand [1.312(2) Å and 1.35(2) Å]. [17] The other C-N distances [N(18)-C(15), N(17)-C(10) of 1.386(3) Å and 1.406(3) Å] agree with the same values in the free ligand and reported values for a single C-N bond [1.41 Å].[16] The angles and bond lengths stay virtually unchanged upon coordination of free 2-aminobenzimidazole to the metal.

[16] A. Marchi, L. Marvelli, M. Cattabriga, R. Rossi, M. Neves, V. Bertolasi, V. Ferretti, *J. Chem. Soc., Dalton Trans,*. **1999**, 1937.
[17] J.W. Bats, *Acta. Crystallogr.*, **1999**, *C55*, 1352.

Table 3.13: Selected bond lengths (Å) and angles (°) of **12** with standard uncertainty in parenthesis.

Bond lengths (Å)			
Cr(1)-C(3)	1.840(3)	N(17)-C(16)	1.324(3)
Cr(1)-C(4)	1.889(3)	N(17)-C(10)	1.406(3)
Cr(1)-C(5)	1.901(3)	N(18)-C(16)	1.350(3)
Cr(1)-C(2)	1.911(3)	N(18)-C(15)	1.386(3)
Cr(1)-C(1)	1.936(3)	N(16)-C(16)	1.368(3)
Cr(1)-N(17)	2.137(2)	C(10)-C(15)	1.402(3)
Bond angles (º)			
C(3)-Cr(1)-C(4)	87.6(1)	C(16)-N(17)-C(10)	104.5 (9)
C(3)-Cr(1)-C(1)	89.0(1)	C(16)-N(18)-C(15)	107.1(2)
C(5)-Cr(1)-C(2)	177.3(1)	N(18)-C(16)-N(17)	113.6(2)

The packing along ac-plane shows a layer of 2-aminobenzimidazole units of molecules of **12** alternated by a layer of $Cr(CO)_5$-units along the a-axis. Elongation of these layers occurs along the c-axis. The solvent molecules are situated in a less polar but very crowded 2-aminobenzimidazole layer and are directed by hydrogen bonding. Hydrogen bonding is observed between the imidazole NH and the solvent molecule, N(18)-H(17)···O(20), 2.08 (3) Å.

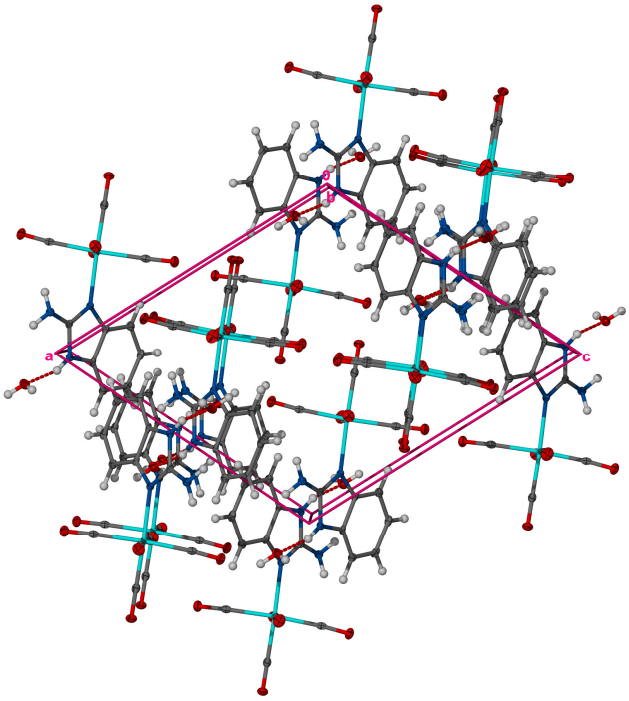

Figure 3.2: Solid state packing of **12** viewed along the ac-plane.

The presence of π-stacking [3.499 Å] is observed in the bc-plane along the c-axis between the 6-membered ring and the 5-membered ring of the neighbour indicated by the various arrows in Figure 3.3. Thus π-stacking and hydrogen bonding seem to govern crystal lattice organisation in the solid state.

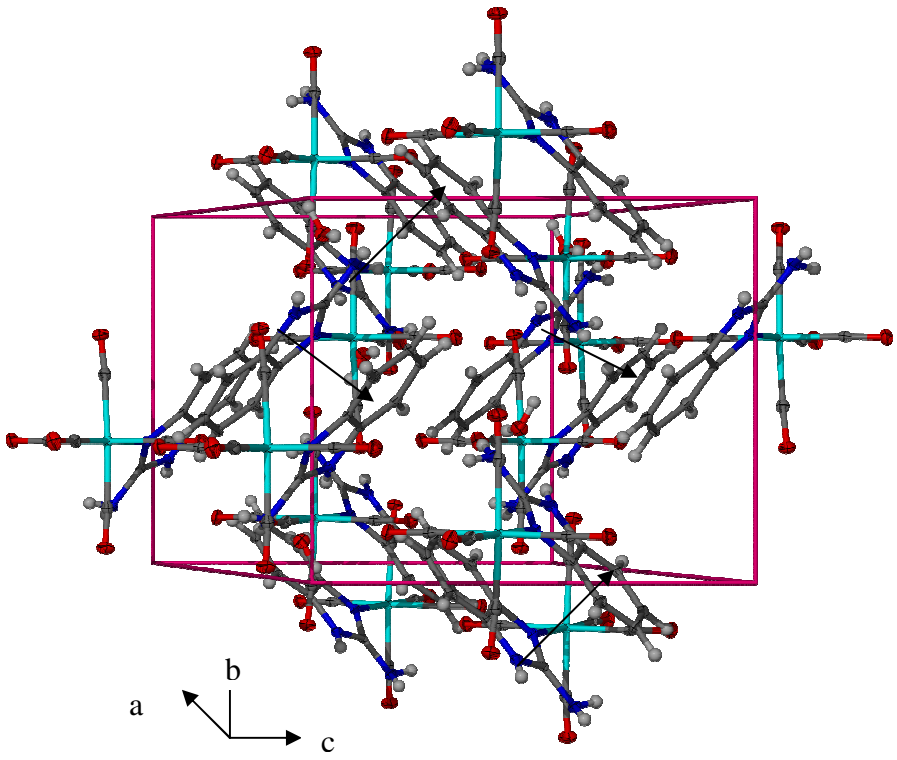

Figure 3.3: Solid state packing of **12** viewed along the c-axis in the bc-plane.

3.2.3.2 Crystal and molecular structure of 2-amino-1-methylbenimidazole)pentacarbonylchromium, 13.

Complex **13** crystallised form acetone as colourless prisms in the orthorhombic space group *Pnma* with Z= 4 molecules in the unit cell. The asymmetric unit contains two unique molecules. The asymmetric unit is shown in Figure 3.4 and relevant angles and distances are tabulated in table (Table 3.15).

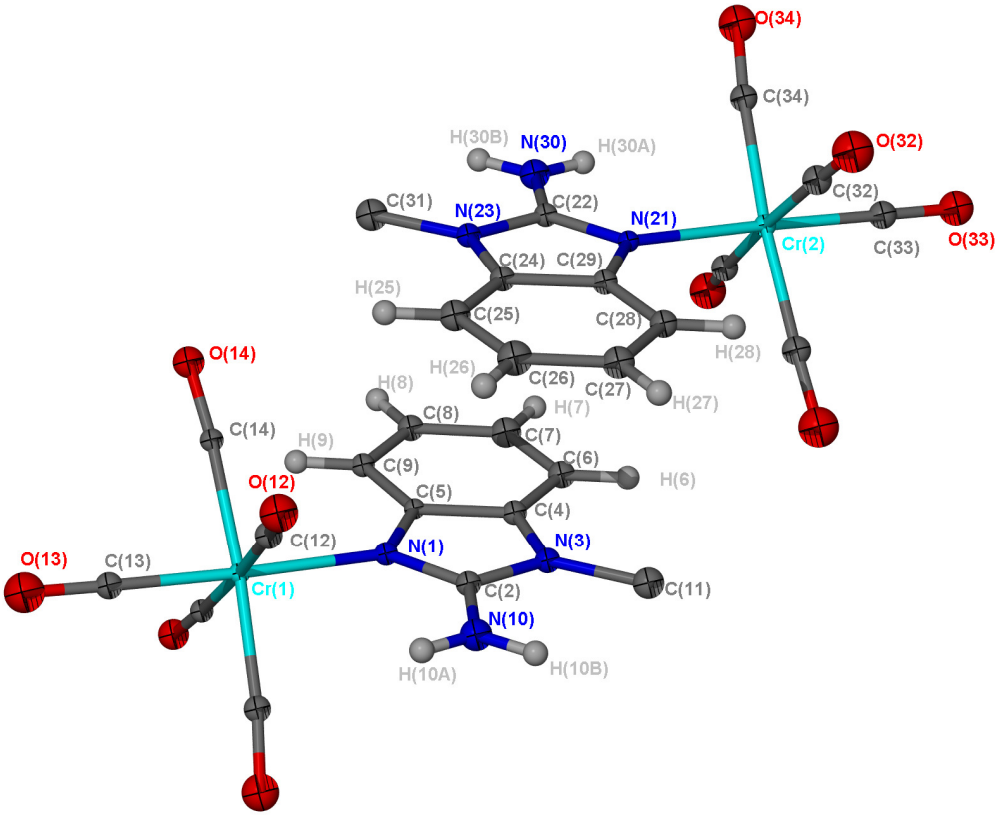

Figure 3.4: The molecular structure of **13** with the methyl hydrogen atoms omitted for clarity.

The two molecules in the unit cell do not differ significantly from each other and they are related by a pseudo-inversion centre. The double bonds N(1)-C(2) [1.321(8) Å] and N(21)-C(22) [1.331(8) Å] do not differ significantly and are longer than standard values for C=N [1.27 Å] [16] but agree with the bond distance in the free ligand of 1.347(3) Å.[18] The N-C bonds, N(3)-C(2) [1.349(9) Å] and N(23)-C(22) [1.372(8)], are longer than the same bond in the 2-amino-1-methylbenzimidazole [1.347(3) Å].[18] From the bond lengths

[18] I.G. Borodkina, A.S. Antsyshkina, G.C. Sadikov, A.E. Mistryukov, D.A. Garnovskii, A.I. Uraev, G.S. Bordkin, E.D. Garnovskaya, V.S. Sergienko, A.D. Garnoviskii, *Coord. Chem.*, **2003**, *29*, 555.

and angles along N(1)-C(2)-N(3) it is clear that the electron density is delocalised across these atoms. The C-N bond distances of N(1)-C(5) [1.390(8) Å] and N(3)-C(4) [1.381(8) Å] are in agreement with those in the uncoordinated ligand [1.388(4) Å and 1.397(4)Å]. The N-CH_3 distance, N(3)-C(11) [1.429(9) Å], does not differ significantly from those in the uncoordinated ligand value at 1.452(4)Å. The other bond angles and distances do not display noteworthy changes upon coordination to metal.

Table 3.15: Selected bond lengths (Å) and angles (°) of **13** with standard uncertainty in parenthesis

Bond lengths (Å)			
Cr(2)-C(33)	1.829(7)	Cr(1)-C(13)	1.831(7)
Cr(2)-C(32)	1.891(5)	Cr(1)-C(12)	1.896(5)
Cr(2)-C(34)	1.916(5)	Cr(1)-C(14)	1.908(5)
Cr(2)-N(21)	2.136(5)	Cr(1)-N(1)	2.143(5)
N(21)-C(22)	1.331(8)	N(1)-C(2)	1.321(8)
N(21)-C(29)	1.402(8)	N(1)-C(5)	1.390(8)
C(29)-C(24)	1.417(9)	C(4)-N(3)	1.381(8)
N(23)-C(22)	1.372(9)	C(2)-N(3)	1.349(9)
N(23)-C(24)	1.387(8)	C(2)-N(10)	1.360(8)
N(23)-C(31)	1.429(9)	C(5)-C(4)	1.410(9)
N(30)-C(22)	1.333(8)	N(3)-C(11)	1.456(9)
Bond angles (º)			
O(13)-Cr(1)-O(14)	87.2(9)	O(33)-Cr(2)-O(34)	87.6(2)
C(13)-Cr(1)-N(1)	176.5(2	C(33)-Cr(2)-C(32)	87.9(2)
C(2)-N(1)-C(5)	104.9(5)	C(33)-Cr(2)-N(21)	176.7(3)
N(1)-C(2)-N(3)	113.7(6)	C(22)-N(21)-C(29)	105.0(5)
C(2)-N(3)-C(4)	106.7(5)	C(22)-N(23)-C(24)	107.3(5)
N(1)-C(2)-N(10)	125.1(6)	N(21)-C(22)-N(30)	126.2(6)
N(3)-C(2)-N(10)	121.2(6)	N(21)-C(22)-N(23)	112.9(5)

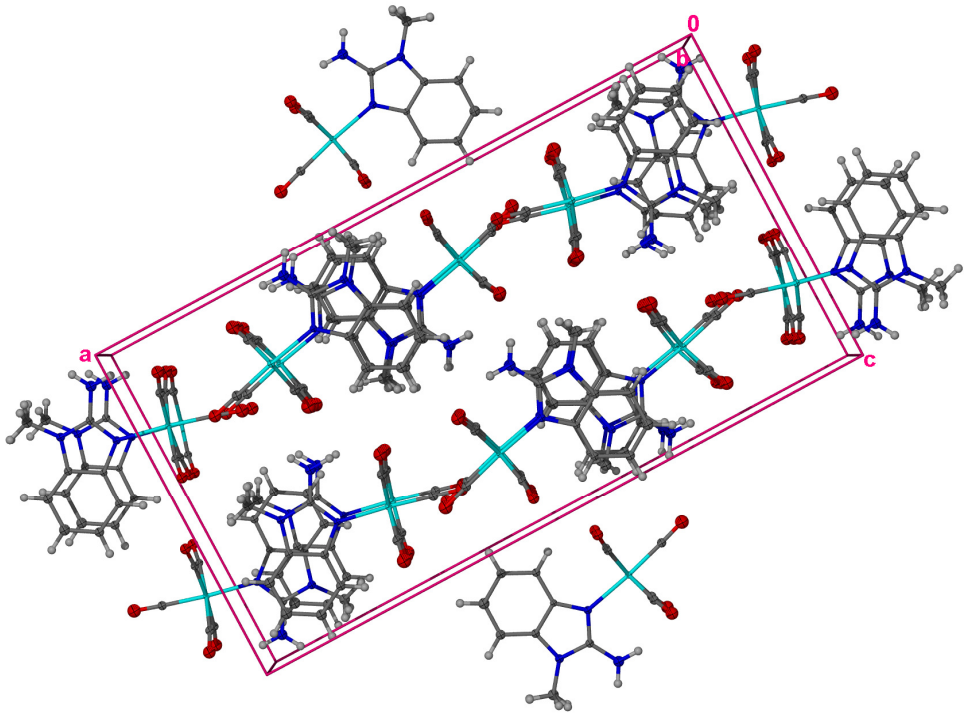

Figure 3.5: Solid-state packing of **13** along the ac-plane.

A view along the ac-plane reveals that molecules are stacked on neighbouring molecules, which alternate in orientation, along the b-axis with π-stacking at 3.770 Å between the 6-membered rings and 5-membered rings. Only π-stacking seems to determine the crystal lattice organisation in the solid-state since other interactions are absent.

3.2.3.3 Crystal and molecular structure of (2-aminobenzothiazole)penta-carbonylchromium, 14.

The complex **14** crystallised form diethyl ether as colourless prisms in triclinic space group $P\bar{1}$ with Z =4 molecules in the unit cell. The asymmetric unit contains two unique molecules. The asymmetric unit is shown in Figure 3.6 and relevant angles and distances are tabulated in Table 3.16.

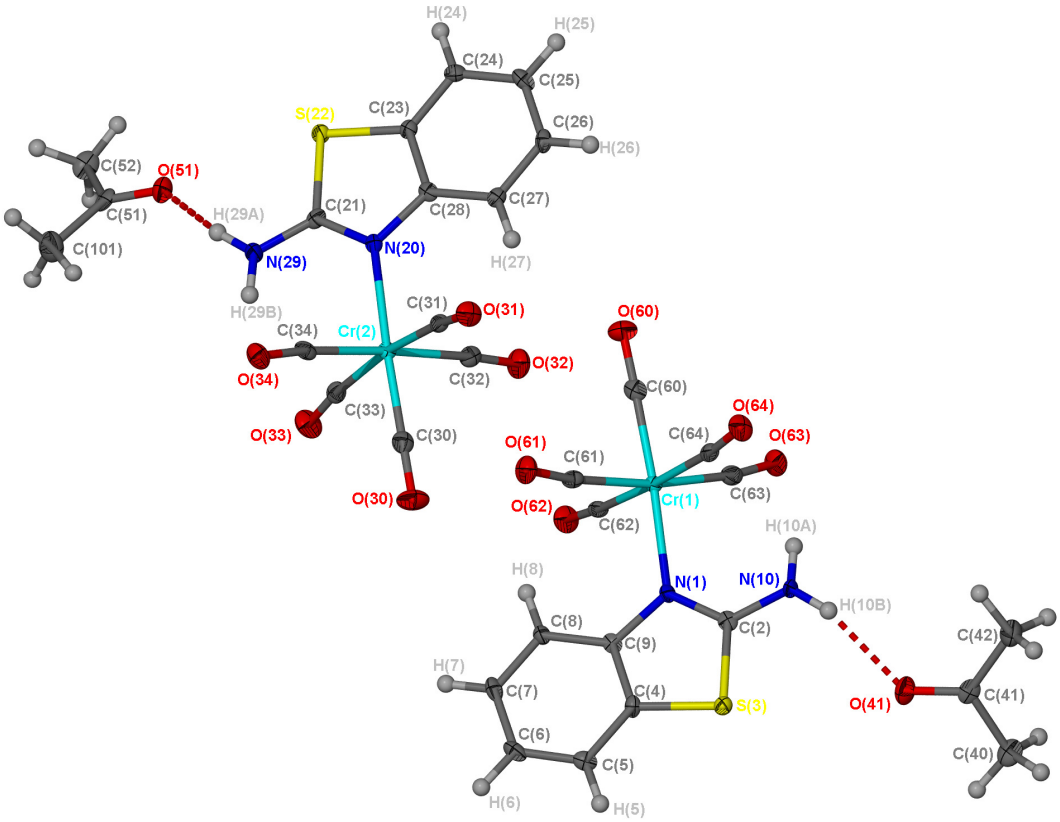

Figure 3.6: The molecular structure and numbering of **14**.

The two molecules in the asymmetric unit do not differ significantly from each other. The double bond N(1)-C(2) [1.319(5) Å] is longer than the reported standard values for a C=N bond [1.27 Å][16] but are in agreement with the same bond in the free ligand of 1.340(7) Å.[19] The N(1)-C(9) and N(20)-C(9) values of 1.423(5) Å are longer but in agreement with the free ligand [1.397(9) Å].[19] The S-C distances of S(3)-C(2) [1.742(4) Å] and S(3)-C(4) [1.738(4) Å] are in agreement with the same bonds in the free ligand [1.753(8) Å and 1.749(8) Å]. The angles do not differ significantly from the same angle in the free ligand.

[19] L.Antolini, A. Benedetti, A.C. Fabretti, A. Giusti, *Inorg. Chem.,* **1988**, *27,* 2192.

Table 3.16: Selected bond lengths (Å) and angles (°) of **14** with standard uncertainty in parenthesis.

Bond lengths (Å)			
Cr(1)-C(60)	1.834(4)	Cr(2)-C(30)	1.837(4)
Cr(1)-C(63)	1.898(4)	Cr(2)-C(34)	1.895(4)
Cr(1)-C(64)	1.907(4)	Cr(2)-C(33)	1.906(4)
Cr(1)-C(62)	1.913(4)	Cr(2)-C(31)	1.915(4)
Cr(1)-C(61)	1.922(4)	Cr(2)-C(32)	1.918(4)
Cr(1)-N(1)	2.160(3)	Cr(2)-N(20)	2.164(3)
S(3)-C(4)	1.738(4)	S(22)-C(23)	1.738(4)
S(3)-C(2)	1.742(4)	S(22)-C(21)	1.743(4)
N(1)-C(2)	1.319(5)	N(20)-C(21)	1.309(5)
N(1)-C(9)	1.423(5)	N(20)-C(28)	1.423(5)
N(10)-C(2)	1.334(5)	N(29)-C(21)	1.341(5)
C(4)-C(9)	1.393(6)	C(28)-C(23)	1.396(5)
Bond angles (º)			
C(60)-Cr(1)-C(63)	86.9 (8)	C(30)-Cr(2)-C(34)	87.6(8)
C(60)-Cr(1)-C(64)	87.2(8)	C(30)-Cr(2)-C(33)	85.7(8)
C(63)-Cr(1)-C(61)	172.3(7)	C(34)-Cr(2)-C(32)	176.7 (7)
C(60)-Cr(1)-N(1)	175.0 (5)	C(30)-Cr(2)-N(20)	177.2(6)
C(4)-S(3)-C(2)	89.1 (9)	C(23)-S(22)-C(21)	88.9(9)
C(2)-N(1)-C(9)	109.5(3)	C(21)-N(20)-C(28)	109.7(3)
N(1)-C(2)-S(3)	116.4(3)	N(29)-C(21)-S(22)	117.6(3)

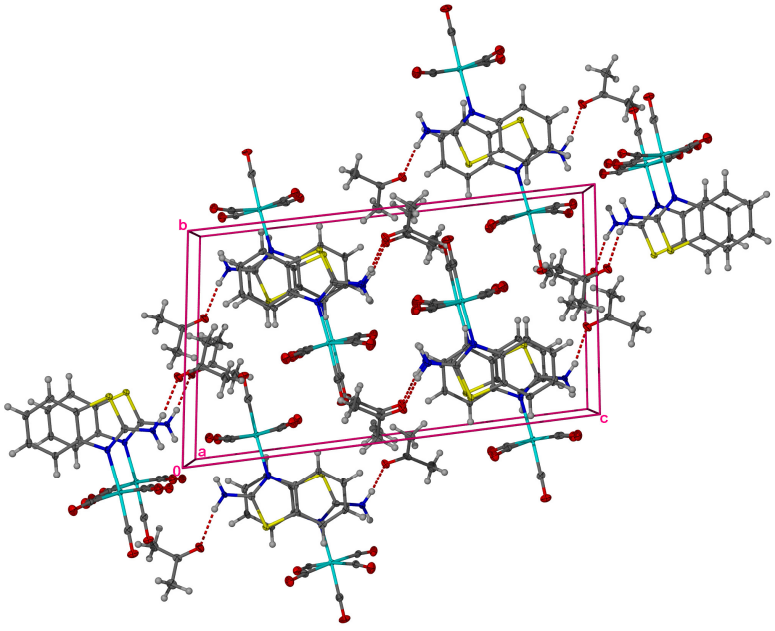

Figure 3.7: Solid-state packing of **14** viewed along the a-axis

A view along the a-axis reveals that the molecules are packed on their orientation alternated neighbouring molecule, along the a-axis, rendering a centroid (6-membered)–centroid (5-membered) distance in neighbouring molecules which indicates π-stacking [3.968 Å]. Hydrogen bonding is observed between the amine group of the 2-aminobenzothiazole and the co-crystallising acetone [N(29)-H(29A)···O(51) at 2.03(5) Å and N(10)-H(10B)···O(41) at 2.12(5) Å]. The π-stacking and hydrogen bonding seem to preside over solid state crystal lattice packing.

3.2.3.4 Crystal and molecular structure of (2-aminobenzothiazole)penta-carbonyltungsten, 17

The yellow needles of complex **17** co-crystallised with one equivalent of acetone from a concentrated solution of the compound in acetone in the triclinic space group $P\bar{1}$ with Z =2 molecules in the unit cell. The asymmetric unit is shown in Figure 3.8 and the relevant angles and distances are summarised and tabulated in Table 3.17.

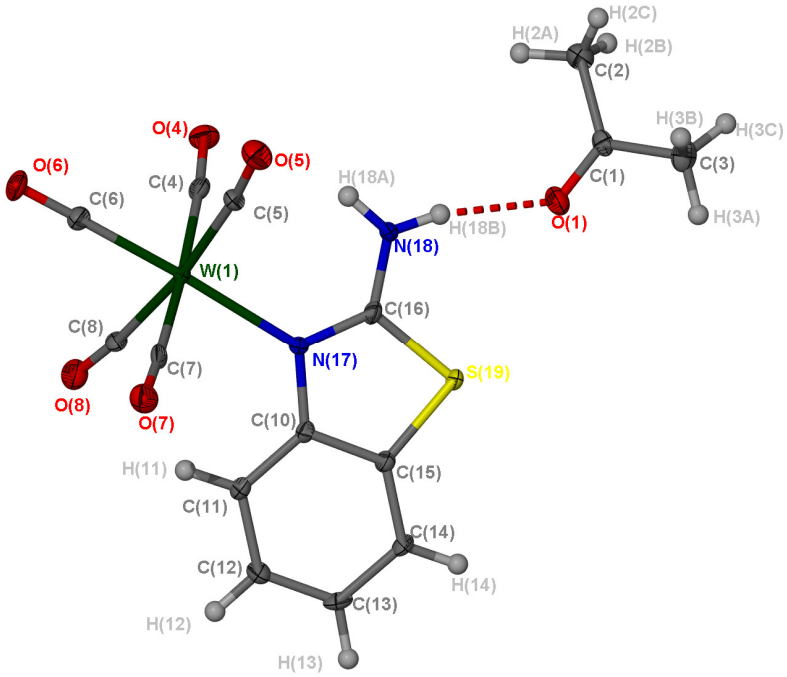

Figure 3.8: The molecular structure of **17** showing the atom numbering.

The S-C distances [C(16)-S(19) and C(15)-S(19) at 1.745(5) Å and 1.741(4) Å] and the C-S-C angle C(16)-S(19)-C(15) [89.2(2)º] agree with the same parameters in the

uncoordinated 2-aminobenzothiazole {1.762(6)/ 1.726(6)/ 90.7(3)}[19]. The C-N single bond [N(17)-C(10) 1.409(5) Å] is similar to the reported value for the uncoordinated ligand [1.397(7) Å][19] and is in agreement with reported standard values [1.41 Å].[16] The N-C double bond N(17)-C(16) [1.324(6)Å], is in agreement with the same bond in the uncoordinated ligand [1.340(7) Å] and deviates from the reported standard C=N values of 1.29 Å.[16] The C(10)-N(17)-C(16) angle is slightly smaller [109.9(3)º] than that of the free 2-aminobenzothiazole [113.5(5)º].[19]

Table 3.17: Selected bond lengths (Å) and angles (°) of **17** with standard uncertainty in parenthesis.

Bond lengths (Å)			
W(1)-C(6)	1.960(5)	S(19)-C(16)	1.741(4)
W(1)-C(4)	2.026(5)	S(19)-C(15)	1.745(5)
W(1)-C(5)	2.027(5)	N(17)-C(16)	1.324(6)
W(1)-C(8)	2.036(5)	N(17)-C(10)	1.409(5)
W(1)-C(7)	2.054(5)	C(16)- N(18)	1.334(6)
W(1)-N(17)	2.274(4)		
Bond angles (º)			
C(6)-W(1)-C(4)	87.4(2)	C(5)-W(1)-N(17)	95.4(7)
C(6)-W(1)-C(7)	89.1(2)	C(16)-N(17)-C(10)	109.8(4)
C(6)-W(1)-N(17)	177.2(4)	N(17)-C(16)-S(19)	116.1(3)
C(16)-S(19)-C(15)	89.2(2)		

The crystal structure reveals the repetition of layers along the b-axis and the propagation of the layer along the c-axis. The stacking of molecules on neighbouring molecules is observed along the a-axis. This stacking produces face-to-face, π-stacking of six membered rings to the inverted neighbour's five membered ring, with a distance of 3.980 Å. There is a hydrogen bond between the co-crystallised acetone and the amine group of the 2-aminobenzothiazole with a heteroatom-heteroatom separation of 2.03(5) Å. Thus, hydrogen bonding and π-stacking determine crystal lattice organisation.

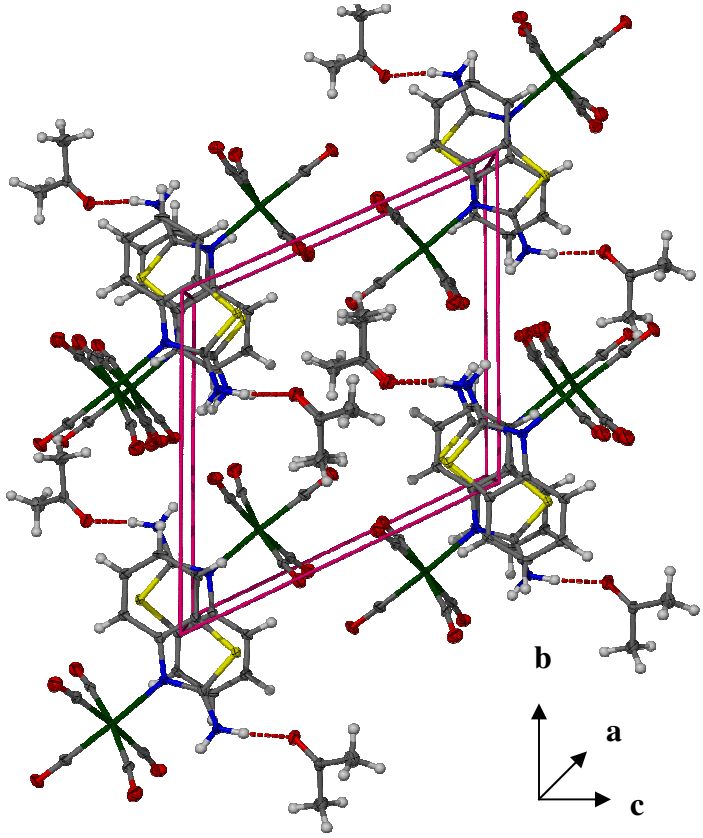

Figure 3.9: Crystal lattice organization of **17** viewed along the a-axis.

3.2.3.5 Crystal and molecular structure of (2-aminobenzimidazole)penta-carbonyltungsten, 18

The yellow complex **18** co-crystallised with one molecule of diethyl ether in the triclinic space group *P*ī with Z =2 molecules in the unit cell. The asymmetric unit is shown in Figure 3.10 and the relevant angles and distances are tabulated in Table 3.18.

The C-N bonds, N(28)-C(21) [1.404(5) Å] and N(27)-C(26) [1.390(5) Å], have true single bond character and concur with the observed in uncoordinated 2-aminobenzimidazole (1.397(3) and 1.388(4) Å)[18] and concur with standard values for C-N bonds [1.41 Å].[16] The C-N bond of N(28)-C(20) [1.334(5) Å] is similar to the reported value for a standard double bond [1.28 Å][16] and the C-N bond of N(27)-C(20) [1.352(5) Å] is similar to the reported value for a standard single bond [1.41 Å][16] thus indicating a complete delocalisation. The bonds N(28)-C(20) and N(27)-C(20) are in agreement with the same bonds in the uncoordinated ligand [1.339(3) and 1.347(3) Å]. The angles show no noteworthy deviations upon the coordination of the 2-aminobenzimidazole to the metal.

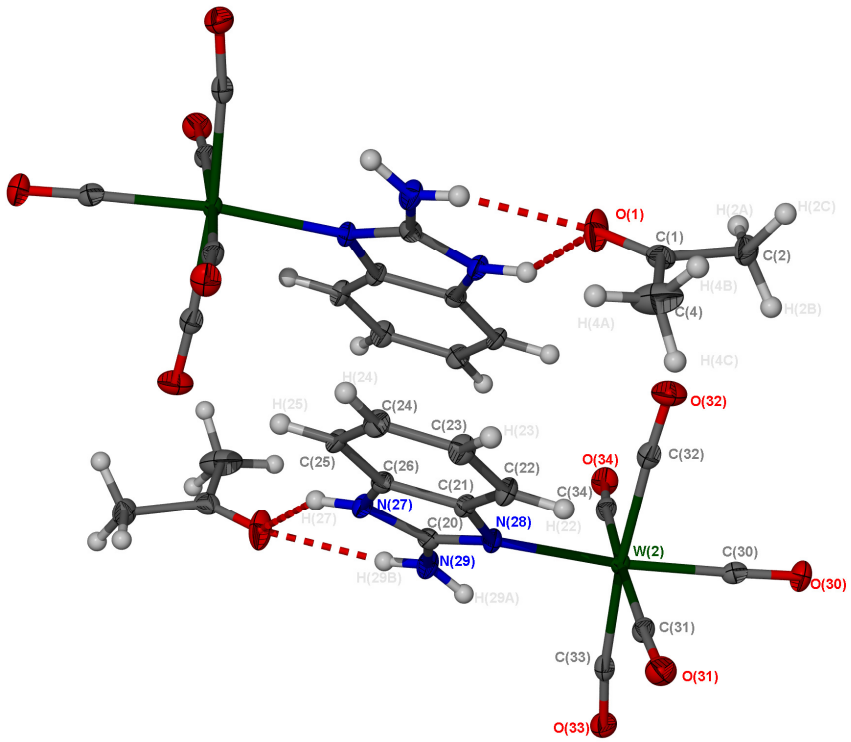

Figure 3.10: The molecular structure of **18**, showing the asymmetric unit, unlabeled atoms are symmetry generated and related to the numbered molecule by an inversion centre.

Table 3.18: Selected bond lengths (Å) and angles (°) of **18** with standard uncertainty in parenthesis.

Bond lengths (Å)			
W(2)-C(30)	1.967(4)	N(27)-C(20)	1.352(5)
W(2)-C(33)	2.028(4)	N(27)-C(26)	1.390(5)
W(2)-C(34)	2.041(4)	N(28)-C(20)	1.334(5)
W(2)-C(32)	2.053(4)	C(21)-C(26)	1.396(5)
W(2)-C(31)	2.055(4)	N(28)-C(21)	1.404(5)
W(2)-N(28)	2.248(3)	N(29)-C(20)	1.347(5)
Bond angles(º)			
C(30)-W(2)-C(33)	87.8(6)	C(30)-W(2)-N(28)	173.0(4)
C(30)-W(2)-C(34)	87.8 (6)	C(20)-N(27)-C(26)	107.3(3)
C(30)-W(2)-C(32)	86.6(7)	C(20)-N(28)-C(21)	104.6(3)
C(30)-W(2)-C(31)	88.3(6)	N(28)-C(20)-N(27)	113.0(4)

The stacking of molecules proceeds along the a-axis in a head-to-tail fashion where they are related *via* an inversion centre. This arrangement allows π-stacking [3.481Å] of the 2-

aminobenzimidazole. The molecule-units are elongated along the c-axis. Solvent molecules are located next to the polar $W(CO)_5$ unit where it is less crowded. The 2-aminobenzimidazole is involved in hydrogen bonding to the acetone molecule with N(29)-H(29B)···O(1) [2.21(6) Å] and N(27)-H(27)···O(1) [2.18(6) Å]. Hydrogen bonding and π-stacking thus govern the solid-state arrangement.

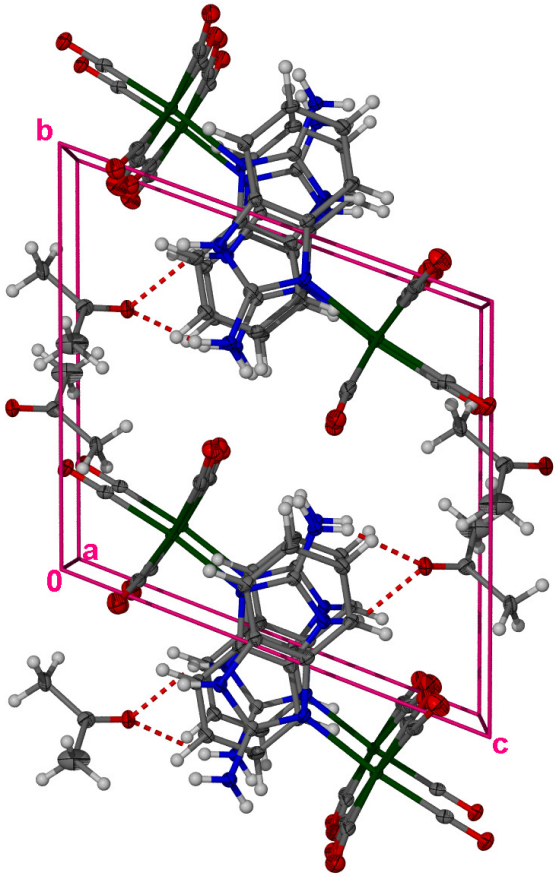

Figure 3.11: Solid-state packing of **18** viewed along a-axis.

3.2.3.6 Crystal and molecular structure of (2-aminothiazoline)penta-carbonyltungsten, 19

Yellow needles of **19** crystallised from acetone in the monoclinic space group $P2_1/c$ with Z= 4 molecules in the unit cell. The asymmetric unit contains a single molecule and is shown in Figure 3.12, relevant angles and distances are tabulated in Table 3.19.

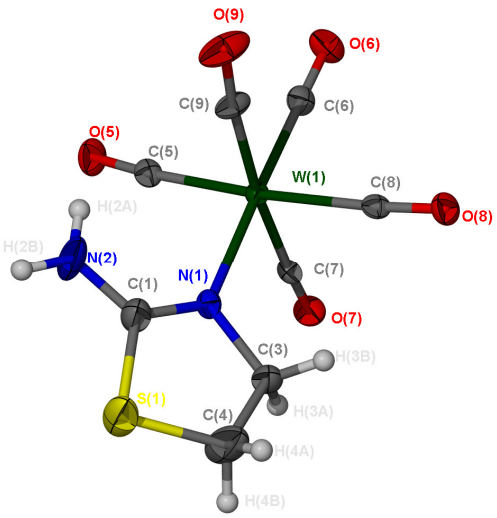

Figure 3.12: The molecular structure of the asymmetric unit of **19**.

Table 3.19: Selected bond lengths (Å) and angles (°) of **19** with standard uncertainty in parenthesis.

Bond lengths (Å)			
W(1)-C(6)	1.968(5)	W(1)-N(1)	2.249(4)
W(1)-C(9)	2.027(5)	N(1)-C(3)	1.490(7)
W(1)-C(5)	2.042(6)	C(1)-S(1)	1.762(6)
W(1)-C(7)	2.047(5)	S(1)-C(4)	1.707(8)
W(1)-C(8)	2.049(6)	N(1)-C(1)	1.274(7)
Bond angles (º)			
C(6)-W(1)-C(9)	86.3(2)	N(1)-C(1)-S(1)	116.5(4)
C(6)-W(1)-C(5)	86.2(2)	C(4)-S(1)-C(1)	90.7(3)
C(6)-W(1)-C(7)	89.8(2)	C(3)-C(4)	1.478(8)
C(6)-W(1)-C(8)	87.6(2)	C(3)-C(4)-S(1)	111.0(5)
C(6)-W(1)-N(1)	178.4(8)	C(4)-C(3)-N(1)	109.2(5)
C(1)-N(1)-C(3)	112.1(5)		

The single N-C bond, N(1)-C(3) [1.490(7) Å] agrees with the same bond in the free ligand [1.465(2) Å] while the double bond N(1)-C(1) [1.274(7) Å] concurs with the same bond in uncoordinated 2-aminothiazoline [1.324(2) Å] and are both similar to the standard values [C=N (1.28 Å) and C-N single bond (1.41 Å)].[14] The C(3)-C(4) [1.478(8) Å] bond

distance is shorter than that of the same bond in the free ligand [1.523(3) Å][20] and the C-S distance, S(1)-C(4) [1.707(8) Å], is shorter than the same distance [1.823(2) Å] in the 2-aminothiazoline ligand. The angle remains virtually unaffected by coordination.

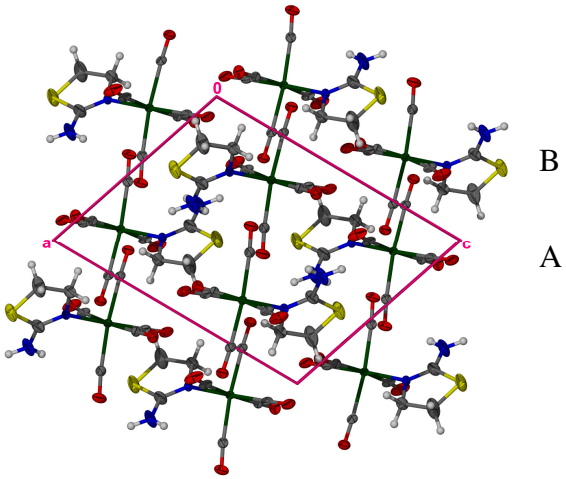

Figure 3.13: The solid state packing of **19** viewed along the ac-plane.

We observe two layers, A and B, with a head-to-tail packing arrangement, which is repeated along the b-axis with elongation, of each layer, occurring along the c-axis. No π-stacking or hydrogen bonding is observed.

3.3 Conclusions

The successful synthesis and complete characterisation of a series of new Cr(0) and W(0) complexes derived from 2-aminoazole ligands have been described. We have now extended the family of $Cr(CO)_5$ compounds with N-heterocyclic ligands tremendously. The new series of tungsten compounds serve as controls towards results obtained in the former family. The present work has shown that the borderline hard imine donor in 2-aminoazole ligand is the preferred site for coordination of soft Cr(0) and W(0) despite the presence of a soft thioether donor in the ligand. Most of these complexes are reasonably stable and have been fully characterised.

Although NMR studies have shown a downfield shift in the resonances of the ligand upon coordination to the $Cr(CO)_5$ and $W(CO)_5$ metal centres, a profound change is observed in

[20] D.E. Lynch, *Acta. Crystallogr.*, **2004,** *C60*, o699.

the chemical shift (downfield) of the imine nitrogen in the ^{15}N NMR spectrum of the complexes when compared to the free ligands with Δδ 76 (**16**) and Δδ 69 (**19**).

FT-IR spectra confirmed the coordination of the ligand in the octahedral complexes since the distinctive vibrations in the ν(CO) region of group 6 pentacarbonyl compounds are observed in all spectra of the new compounds.

Mass spectra of the tungsten complexes have revealed fragmentation patterns in which the molecular ions are observed and fragmentation indicating the sequential loss of CO groups was detected.

X-ray crystallographic investigation of the new complexes has confirmed the octahedral coordination around the central metal atom and that all ligands are imine coordinated. The 2-aminobenzimidazole and 2-aminobenzothiazole complexes of chromium and tungsten are not isostructural since a different solvent co-crystallised with each metal complex. The Cr-N and W-N separations as well as the parameters of the CO ligands are in agreement with literature values. The coordination of ligands to the metal centre does not alter the bond distances and angles in the ligand significantly when compared to the free ligand. Finally, the results have shown that hydrogen bonding and π-π interactions play fundamental roles in directing the packing of the molecular assemblies.

3.4 Experimental

3.4.1 General procedures and instruments

All reactions were carried out under argon using standard Schlenk- and vacuum-line techniques. Tetrahydrofuran (THF), diethyl ether, *n*-hexane and *n*-pentane were distilled under N_2 from sodium benzophenone ketyl and *N,N*-dimethylformamide (DMF) from CaH_2. The ligands, 2-aminothiazoline, 2-amino-4-methylthiazole, 2-aminobenziothiazole and 2-aminobenzimidazole were purchased from Aldrich and used without further purification unless otherwise noted.

Melting points were determined on a Stuart SMP3 apparatus and are uncorrected. Mass spectra were recorded on a VG 70 SEQ (FAB, 70 eV, recorded in a *m*-nitrobenzylalcohol matrix) instrument. NMR spectra were recorded on a Varian 300/400 FT or INOVA 600

MHz spectrometer (^{1}H NMR at 300/400/600 MHz, ^{13}C NMR at 75/100/150 MHz, ^{15}N NMR at 60.8 MHz) with the chemical shifts reported relative to the solvent resonance or an external reference CH_3NO_2 (^{15}N). Infrared spectra were recorded on a Thermo Nicolet Avatar 330FT-IR instrument equipped with a Smart OMNI ATR (attenuated total reflectance) sampler. Elemental analysis was carried out at the Soil Science Department, University of the Stellenbosch. Prior to elemental analysis, the products were evacuated under high vacuum for 10 h.

3.4.2 Preparations and procedures

3.4.2.1. Preparation of (2-amino-4-methylthiazole)pentacarbonylchromium(0), 11

The irradiation of hexacarbonylchromium(0) (0.44 g, 2.0 mmol) in 150 ml of THF for 2 h yielded an orange solution.[12] The solution was transferred to a Schlenk tube *via* a cannula whereupon the ligand, 2-amino-4-methylthiazole (0.23 g, 2.0 mmol), was added. The mixture was stirred at room temperature for 2h.

The resulting yellow solution was evaporated *in vacuo.* The yellow residue was then extracted with diethyl ether (60 ml) and filtered through SiO_2, to remove solid impurities. After the removal of solvent from the yellow solution, a yellow product was obtained (0.10 g, 52 %). TLC analysis with a 1:1 ratio of hexane/diethyl ether was used to determine that only one product was present.

3.4.2.2 Preparation of (2-aminobenzimidazole)pentacarbonylchromium, 12

Complex **12** was prepared implementing the procedures mentioned above using equimolar amounts of hexacarbonylchromium(0) (0.44 g, 2.0 mmol) and 2-aminobenzimidazole ligand (0.27 g, 2.0 mmol). TLC analysis in 1:1 hexane/diethyl ether indicated the presence of a single pure product (0.64 g, 97%). Yellow single crystals were obtained by slow diffusion of *n*-pentane into a concentrated solution of **12** in acetone maintained at -22ºC for a few weeks.

3.4.2.3 Preparation of (2-amino-1-methylbenzimidazole) pentacarbonyl-chromium, 13

Complex **13** was prepared as described above using hexacarbonylchromium(0) (0.28 g, 1.3 mmol) and 2-amino-1-methylbenzimidazole (0.19 g, 1.3 mmol), yielding a yellow solid (0.18 g, 42 %). TLC analysis in 1:1 hexane/diethyl ether indicated the presence of a single pure product. Colourless prisms were obtained by slow diffusion of *n*-pentane into an acetone solution.

3.4.2.4 Preparation of (2-aminobenzothiazole)pentacarbonylchromium, 14

Complex **14** was prepared using the same method as above employing hexacarbonylchromium(0) (0.44 g, 2.0 mmol) and 2-aminobenzothiazole (0.19 g, 1.3 mmol), yielding a yellow solid (0.32 g, 47 %). TLC analysis in 1:1 hexane/diethyl ether indicated the presence of a single pure product. Crystals of **14** were obtained by the slow diffusion of *n*-pentane into a concentrated diethyl ether solution.

3.4.2.5 Preparation of (2-aminothiazoline)pentacarbonylchromium, 15

Complex **15** was prepared using the same method as for the preparation of **11** employing hexacarbonylchromium(0) (0.46 g, 2.0 mmol) and 2-aminothiazoline (0.21 g, 2.0 mmol), yielding a yellow solid (0.26 g,45 %). TLC analysis in 1:1 hexane/diethyl ether indicated the presence of a single pure product.

3.4.2.6 Preparation of (2-amino-4-methylthiazole)pentacarbonyltungsten, 16

The irradiation for 2 h of hexacarbonyltungsten(0) (0.45 g, 1.3 mmol), in a vessel, containing 150 ml of THF yielded an yellow solution. The solution was transferred *via* a cannula to a Schlenk tube whereupon 2-amino-4-methylthiazole (0.29 g, 2.0 mmol) was added followed by stirring at room temperature for another 2 h. The resulting light-yellow solution was dried *in vacuo* to a yield yellow solid. The yellow solid was then redissolved in diethyl ether (60 ml) and filtered through SiO_2, to remove solid contaminants and decomposed products. The filtrate was stripped of solvent to produce a pure yellow product **16** (0.44 g, 50 %).

3.4.2.7 Preparation of (2-aminobenziothiazole)pentacarbonyltungsten, 17

The same experimental procedure as described above was used to prepare **17** with hexacarbonyltungsten(0) (0.45 g, 1.28 mmol) and 2-aminobenziothiazole (0.3 g, 2 mmol). The solution was stirred for an hour and after work up a luminescent yellow product in a moderate yield (0.476 g, 51 %) was isolated. Yellow crystals of complex **17** were obtained *via* slow diffusion of *n*-pentane into a acetone solution at -22ºC.

3.4.2.8 Preparation of (2-aminobenzimidazole)pentacarbonyltungsten, 18

The method described above using hexacarbonyltungsten(0) (0.45g, 1.3 mmol) and an excess of 2-aminobenzimidazole (0.27g, 2 mmol) producing a yellow solid after work-up, with low yield (0.16 g, 27 %). Slow diffusion of *n*-pentane into a solution containing **18** in diethyl ether at -22ºC produced yellow needle-like crystals.

3.4.2.9 Preparation of (2-aminothiazoline)pentacarbonyltungsten, 19

The same method as above was used, utilizing hexacarbonyltungsten(0) (1.40 g, 4.0 mmol) and 2-aminothiazoline (0.4 g, 4.0 mmol) producing a yellow product **19** in low yield (0.60 g, 35%). Yellow needles were obtained by the slow diffusion of *n*-pentane into a concentrated acetone solution.

3.4.2 X-ray structure determinations

Crystal data collection and refinement details of compounds **12**, **13**, **14**, **17**, **l8** and **19** are summarised in Tables 3.20-3.22. Data sets were collected on a Bruker SMART Apex CCD diffractometer with graphite monochromated MoK_α radiation (λ = 0.71073 Å).[21] Data reduction was carried out with standard methods using the software package Bruker SAINT absorpstion correction was applied using SADABS.[22,23,24] All the structures were solved using direct methods, which yielded the position of the metal atoms, and conventional difference Fourier methods. All non-hydrogen atoms were refined anisotropically by full-matrix least squares calculations on F^2 using SHELX-97[25] within

[21] SMART Data Collection Software (version 5.629), Bruker (2002)AXS Inc. (Madison), WI, **2002**.
[22] SAINT, Data Reduction Software (version 6.45), Bruker (2003) AXS Inc. (Madison), WI, **2003**.
[23] R.H. Blessing, *Acta Crystallogr.,* **1995**, A*51*, 33.
[24] SADABS (Version 2.05), Bruker, AXS Inc., Madison, Wisconsin, USA, **2002**.
[25] G.M. Shelrick, SHELX-97. Program for Crystal Structure Analysis, University of Göttingen (Germany), **1997**.

an the X-seed environment.[26,27] The hydrogen atoms were fixed in calculated positions unless otherwise stated. Figures were generated with POV Ray for Windows, with the displacement ellipsoids at 50% probability level unless stated otherwise. Further information is available from Dr. S. Cronje at the Department of Chemistry and Polymer Science, Stellenbosch University.

[26] L.J. Barbour, *J. Supramol. Chem.* **2003**, *1*, 189.
[27] J.L. Atwood, L.J. Barbour, *Cryst. Growth Des.* **2003**, *3*, 3.

Table 3.20: Crystallographic data of compounds **12** and **13**.

Compounds	**12**	**13**
Molecular formula	$C_{12}H_9CrN_3O_6$	$C_{13}H_9CrN_3O_5$
Molecular weight	343.22	339.23
Crystal system	monoclinic	orthorhombic
Crystal dimensions	0.30 × 0.10 × 0.05	0.09 x 0.06 x 0.04
Crystal shape and colour	Yellow needles	Colourless prisms
Space group	$P2_1/c$ (No. 14)	*Pnma* (No. 62)
a (Å)	12.345(2)	26.652(8)
b (Å)	10.248(1)	7.268(2)
c (Å)	11.787(1) Å	14.306(5) Å
α (°)	90	90
β (°)	114.061(2)°	90
γ (°)	90	90
Volume ($Å^3$)	1361.7(3)	2771(2)
Z	4	4
d_{calcd} (g/cm^3)	1.674	0.813
μ(Mo-Ka) (mm^{-1})	0.875	0.427
Absorption correction	Semi-empirical from equivalents (SADABS)	Semi-empirical from equivalents (SADABS)
$F_{(000)}$	696	688
θ -range for data	*1.81 to 28.27*	*1.53 to 26.42*
Index range	-12< h < 16, -12< k <13, -15 < l < 13	-33< h < 27, -6< k < 9, -17< l < 17
No. of reflections	8563	15695
No. of unique reflections	3230 unique (R_{int} = 0.0400)	3055 unique (R_{int} = 0.0552)
Max. and min.	0.980 and 0.884	0.3833 and 0.5981
Refinement parameters	219 parameters, 0 restraints	122 parameters, 0 restraints
Goodness of fit on F^2	1.046	7.189
Final R-indices [I>2s >(I)]	R_1 = 0.0454 wR_2 = 0.1005	R_1 = 0.1046 wR_2 = 0.2265
R indices (all data)	R_1 = 0.0626 wR_2 = 0.1010	R_1 = 0.0845 wR_2 = 0.2106
Largest diff. peak and	-0.345 and 0.501	-0.632 and 3.432
Weighing Scheme [a]	a = 0.0518/ b= 013339	a = 1.228 / b= 12.6569

[a] $wR_2 = \{\Sigma[w(F_o^2-F_c^2)^2]/\Sigma[w(F_o^2)^2]\}^{1/2}$; $w = 1/[\sigma^2(F_o^2)+(aP)^2+bP+d+\text{esin}\theta]$; $P = [f(\text{Max}(0 \text{ or } F_o^2)] + (1\text{-f}) F_c^2$

Table 3.21: Crystallographic data of compounds **14** and **17**.

Compounds	**14**	**17**
Molecular formula	$C_{15}H_{12}N_2O_6SCr$	$C_{15}H_{12}N_2O_6SW$
Molecular weight	400.33	532.18
Crystal system	triclinic	triclinic
Crystal dimensions (mm)	0.14 × 0.09 × 0.05	0.22 x 0.20 x 0.02
Crystal shape and colour	Colourless prism	Yellow needles
Space group	*P*ī (No. 2)	*P*ī (No. 2)
a (Å)	7.6 (2)	7.666(3)
b (Å)	11.734(2)	11.253(4)
c (Å)	20.313(3)	11.792(5)
α (°)	81.059(3)	64.333(5)
β (°)	74.738(6)	74.571(6)
γ (°)	90	85.210(6)°
Volume ($Å^3$)	1714.2(4)	883.2(6)
Z	4	2
d_{calcd} (g/cm^3)	1.551	2.001
μ (Mo-Ka) (mm^{-1})	0.823	6.690
Absorption correction	Semi-empirical from equivalents (SADABS)	Semi-empirical from equivalents (SADABS)
$F_{(000)}$	816	508
θ-range for data collection	1.81 to 26.44	1.98 to 26.42
Index range	-9< h < 9, -14 < k < 12, -25 < l < 28	-9< h < 9, -14 < k < 14, -14 < l < 14
No. of reflections collected	9980	9267
No. of unique reflections	5180 (R_{int}= 0.0295)	3601 (R_{int}= 0.0465)
Max. and min. transmission	0.7611 and 0.4986	0.4152 and 0.9093
Refinement parameters /restraints	228 parameters,0 restraints	228 parameters, 0 restraints
Goodness of fit on F^2	0.823	1.111
Final R-indices [I>2s >(I)]	R_1 = 0.0861 wR_2 = 0.1483	R_1 = 0.0297 wR_2 = 0.0815
R indices (all data)	R_1 = 0.061 wR_2 = 0.1355	R_1 = 0.0304 wR_2 = 0.0821
Largest diff. peak and hole	-0.374 and 0.905	-1.071 and 1.770
Weighting Scheme [a]	a = 0.0669/ b=1.6483	a = 0.0446

[a] $wR_2 = \{\Sigma[w(F_o^2-F_c^2)^2]/\Sigma[w(F_o^2)^2]\}^{1/2}$; $w = 1/[\sigma^2(F_o^2)+(aP)^2+bP+d+\text{esin}\theta]$; $P = [f(\text{Max}(0 \text{ or } F_o^2)] + (1\text{-f}) F_c^2$

Table 3.22: Crystallographic data of compounds **18** and **19**

	18	**19**
Molecular formula	$C_{15}H_{13}N_3O_6W$	$C_8H_6N_2O_5SW$
Molecular weight	515.13	426.06
Crystal system	triclinic	monoclinic
Crystal dimensions (mm)	0.12 × 0.12 × 0.09	0.21 × 0.05 × 0.03
Crystal shape and colour	Yellow blocks	Yellow needles
Space group	$P\bar{1}$ (No. 2)	$P2_1/c$ (No. 14)
a (Å)	7.6522(9)	9.1731(17)
b (Å)	10.5764(13)	11.286(2)
c (Å)	11.5663(14) Å	11.945(2)
α (°)	108.844(2)	90
β (°)	103.092(2)	108.203(3)
γ (°)	94.503(2)°	90
Volume (Å^3)	851.13(18)	1174.7(4)
Z	2	4
d_{calcd} (g/cm^3)	2.010	2.409
μ (Mo-Ka) (mm^{-1})	6.823	10.021
Absorption correction	Semi-empirical from equivalents (SADABS)	Semi-empirical from equivalents (SADABS)
$F_{(000)}$	492	792
θ-range for data collection (°)	1.93 to 28.27	2.34 to 26.37
Index range	-10< h < 10, -14 < k < -14 < l < 15	-9 < h < 11, -9 < k < 14, -14 < l < 14
No. of reflections collected	9595	6730
No. of unique reflections	3933 (R_{int} =0.0290)	2388 (R_{int} = 0.0344)
Max. and min. transmission	0.4788 and 0.3645	0.765 and 0.593
Refinement parameters	236 parameters, 0	154 parameters, 0
Goodness of fit on F^2	1.050	1.069
Final R-indices [I>2s >(I)]	R_1 = 0.0263 wR_2 = 0.0580	R_1 = 0.0282 wR_2 = 0.0677
R indices (all data)	R_1 = 0.0314 wR_2 = 0.0595	R_1 = 0.0312 wR_2 = 0.0693
Largest diff. peak and hole	-1.180 and 1.744	-0.971 and 1.626
Weighting Scheme [a]	a = 0.0315	a = 0.0330 / b= 1.7364

[a] $wR_2 = \{\Sigma[w(F_o^2-F_c^2)^2]/\Sigma[w(F_o^2)^2]\}^{1/2}$; $w = 1/[\sigma^2(F_o^2)+(aP)^2+bP+d+\text{esin}\theta]$; $P = [f(\text{Max}(0 \text{ or } F_o^2)] + (1\text{-f}) F_c^2$

Chapter 4

Preparation and characterisation of novel gold(I) and gold(III) complexes containing *N*-(2-methylphenyl)imidodicarbonimidic diamide

4.1 Introduction

Biguanides, and their N-substituted dervatives, are bidentate ligands that contain nitrogen donor atoms. The most widely studied guanidines are those which have at least one N-H capable of ionisation, i.e. tetrasubstituted guanidines (Scheme 4.1). The possible ionisation may have very important consequences for the metal-ligand interactions of initially neutral systems.

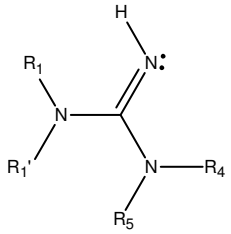

Scheme 4.1: Typical backbone of a guanidine molecule.

When for example, 1,2,3-triphenylguanidine, PhHNC{NPh}{NHPh} (**A**) (Scheme 4.2), coordinates to form bis-ligand adducts of Co, Ag and Pd species with imine coordination in all the cases,[1,2] the availability of NH-groups in the system enables additional hydrogen bonding in the form of intra- and intermolecular NH···X bonds in the interaction in the solid state. The presence of intramolecular hydrogen bonding to the chlorine ligand is observed in the Co and Pt complexes while intermolecular hydrogen bonding to a triflate counter-ion is observed in the silver species (**B**) (Scheme 4.2).

[1] P.J. Bailey, K.J. Grant, S. Pace, L.J. Stewart, *J. Chem. Soc., Dalton Trans*., **1997**, 4263.
[2] N. Mincheva, T. Todorov, O. Angleeova, P.J. Bailey, M. Mitewa, *J. Coord. Chem*., **2000**, *50*, 169.

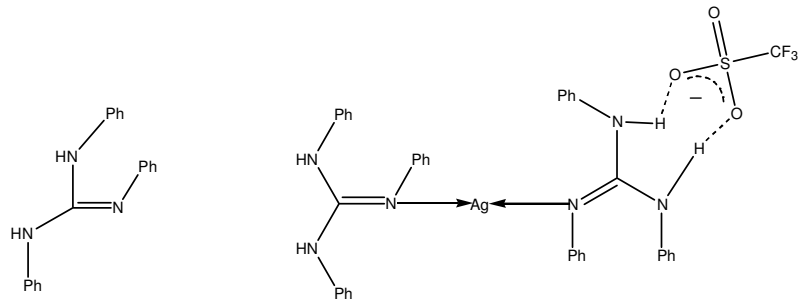

A **B**

Scheme 4.2: The ligand, 1,2,3-triphenylguanidine, and it's silver complex.

Compared to their aminidine relatives, the simple coordination of guanidines to metal centres remains rather underdeveloped.[3] There has been a renewed interest in the application of neutral guanidines in coordination chemistry by Schmidbaur[4] at cationic gold centres producing both mixed (**C**) and the homoleptic species (**D**), with the latter showing Au···Au interaction (Figure 4.3).

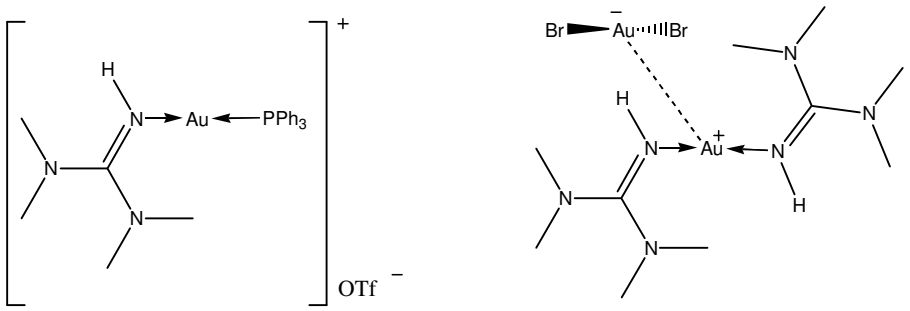

C **D**

Figure 4.3: Complexation of acyclic biguanindes to yield the cationic phosphine complex (**C**) and the homoleptic complex (**D**).

When comparing biuret **(E)** and biguandines **(F)**, from a chemical and structural point of view, guanidines may be considered to be a derivative of biuret obtained by the substitution of both oxygen atoms of biuret with isoelectronic NH groups (Scheme 4.4).

E **F**

Scheme 4.4: Biuret **(E)** and biguandine **(F)**.

[3] P.J. Bailey and S. Pace, *Coord. Chem. Rev*., **2001**, *214*, 91.
[4] W. Schneider, A. Bauer, A. Schier, H. Schmidbaur, *Chem. Ber*., **1997**, *130*, 1417.

The biuret derivative are considered to be strong σ- and π- donating ligands forming stable complexes with transtion metals in high or unusual oxidation states by utilizing the availability of vacant d-orbitals of the metal which overlap with filled π -orbitals of the chosen ligand.

Marchi and co-workers[5] studied the synthesis and characteristics of rhenium(V) and technetium(V) complexes of biguanidine derivatives, HL^n (Scheme 4.5), and were the first to structurally characterise oxo- and nitride- complexes of technetium. The active proton occurs on the central nitrogen atom.

HL^n ligands

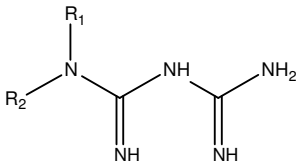

n =1 $R_1 = R_2 = Me$

n = 2 $R_1 = H$, $R_2 = C_2H_4$-Ph

n = 3 R_1=H, R_2=Ph

Scheme 4.5: Different biguanidine ligands.

The complexes reported were synthesized by a facile exchange reaction between the ligand and the appropriate technetium or rhenium complex. The authors have confirmed that it is possible to promote deprotonation of the coordinated ligand and thus change the charge on the final complex. The active proton occurs on the central nitrogen atom (Scheme 4.6).

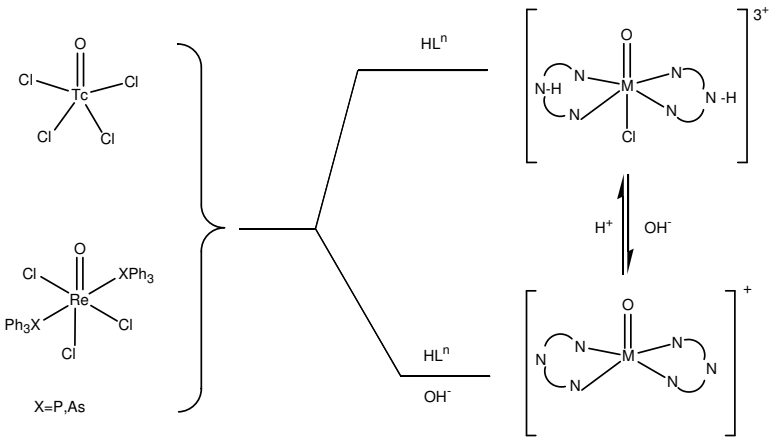

Scheme 4.6: Reaction scheme showing the protonated and deprotonted complexes.

[5] A. Marchi, L. Marvelli, M. Cattabriga, R. Rossi, M. Nerves, V. Bertolosi, V. Ferretti, *J. Chem. Soc., Dalton Trans.*, **1999**, 1937.

Since the synthesis of amido complexes of gold have been described,[6] a variety of neutral and ionic complexes of gold(I) with 1,1-dimethylbiguanide and related ligands possibly also involved in homoleptic rearrangements and aurophilic interactions can be envisaged.

Biguanides have attracted considerable attention for their hypoglycemic activity,[7] especially metformin which has been used for over 30 years as an antidiabetic medication. Metformin (1,1-dimethylbiguanide) is very successful in treatment of type II diabetes. Metformin inhibits hepatic glucose products and increases sensitivity of peripheral tissues to insulin. There is also a link between insulin abnormalities like insulin resistance and rheumatoid arthritis [8,9,10] for which gold drugs are being used as mentioned previously (Chapter 1).

Metformin, and derivative of it, are well acclaimed for their medicinal value and display versatility in their biological activity from the therapeutic treatment of pain, anxiety, memory disorder[11] and malaria[12] to fungicidal and microbial properties.[13] The ligand, *N*-(2-methylphenyl)imidodicarbonimidic diamide (**H**) a derivative of metformin (**G**) and is thus a useful model for the preparation of complexes (Scheme 4.7).

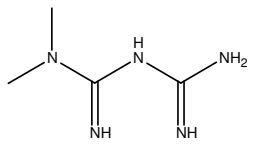

G

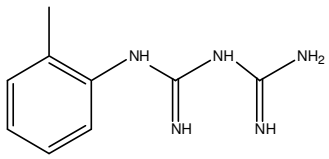

H

Scheme 4.7: Metformin (**G**) and *N*-(2-methylphenyl)imidodicarbonimidic diamide (**H**).

[6] U. E. I. Horvath, S. Cronje, J. M. McKenzie, L. J. Barbour, H. G. Raubenheimer, *Z. Naturforsch.*, **2004**, *59b*, 1605
[7] C.R. Sirtori, C. Pasik, *Pharmacol. Res.,* **1994**, *30*, 187.
[8] P.H. Dessein, B.I. Joffe, A. Stanwix, A.S. Botha, Z. Moomal, *J. Rheumatol*., **2002**, *29*, 462.
[9] J. Walsmith, R. Roubenoff, *Int. J. of Cardiology.*, **2002***, 85*, 89.
[10] O. Oncul, C. Top, S. Ozkan, S. Cavuslu, M. Danaci, *J. of Int. Med. Res.*, **2002**, *30*, 386.
[11] P. Morain, C. Abraham, B. Portevin and G. De Nanteuil, *Mol. Pharmacol*., **1994**, 46, 732.
[12] W.M. Watkins, J.D. Chutlay, D.G. Sixsmith, H.C. Spencer, R.E. Howells*, J. Phar*., **1987**, *39*, 261.
[13] M. Rosin, A. Welk, O. Bernhardt, M. Ruhnau, F.A. Pitten, T. Kramer, A. Kramer, *J. Clin. Periodontol.*, **2001**, *28*, 1121.

The similarities between metformin and *N*-(2-methylphenyl)imidodicarbonimidic diamide are obvious. Both are neutral and have the same C-N-backbone with the identical available coordination sites. *N*-(2-methylphenyl)imidodicarbonimidic diamide has an extra site for deprotonation and has a bulky methyl substituted phenyl ring (2-tolyl) instead of the two methyls of the metformin ligand.

As mentioned in 2.1 the unexpected N-coordination of the enzyme cyclophilin to gold(I) *via* the nitrogen atom of an active His residue despite the presence of four Cys thiol groups, have implications for the understanding of the biochemical mechanisms of gold compounds.[14] Similar results showing a preference of gold(I) compounds for neutral nitrogen donors compared to neutral thioether donor groups, has been reported recently.[15] The complexation of gold with guanidine is also relevant to the uptake, transport and action of gold(I) drugs in biological systems where guanidines are widely distributed as natural ligands.[16] This provided the motivation for our study of gold(I) complexes of *N*-(2-methylphenyl)imidodicarbonimidic diamide with possible biological activity.

Important factors to be taken into consideration when evaluating metal complexes for potential medicinal use are:

1) Their solubility and stability in biological media.
2) The compounds must contain an active species or convert into an active species upon introduction of the drug into the biological system.
3) The ability to selectively target unhealthy propagating cells, i.e cancerous over the healthy cells.

To achieve the last mentioned goal, fine-tuning of the hydrophilic/hydrophobic balance is required. McKeage and co-workers[17] have shown that the selectivity of complexes can be fine-tuned by adjusting the hydrophilic/hydrophobic balance of the coordinated ligands. This can be achieved through the introduction of appropriate functional groups.

[14]J. Zou, P. Taylor, J. Dorman, S. P. Robinson, M. D. Walkinshaw, P. J. Sadler, *Angew. Chem. Int. Ed*., **2000**, *39*, 2931.
[15]S. Cronje, H. G. Raubenheimer, H.S.C. Spies, C. Esterhuysen, H. Schmidbaur, A. Schier, G. J. Kruger, *Dalton Trans*., **2003**, 2859.
[16] L. Styer*, Biochemistry 3th ed*., W.H. Freeman and Co., New York, **1988**, p.988
[17] M.J. McKeage, S. Berners-Price, P. Galettis, R.J. Bowen, W. Brouwer, L. Ding, L. Zhuang, B.C. Baguley, *Cancer Chemother. Pharmacol,*. **2000**, *46*, 343.

Furthermore, Baker *et al.*[18] established that cationic compounds with intermediate lipophilicity display the greatest selectivity. Their superior selectivity arises from their ability to permeate the mitochondria of carcinoma cells, because carcinoma cells exhibit elevated plasma and membrane potentials, with respect to normal cells. This negative membrane potential allows lipophilic cationic complexes to rapidly cross the membrane barrier and accumulate in the mitochondrial plasma. The mitochondria play a fundamental role in the regulation of programmed cell death that holds the key to triggering selective cell death.[18]

The work presented in this chapter was inspired by the biological activity displayed by the metformin ligand[9-13] together with the known anti-cancer potential of (phosphine)gold(I) compounds and cationic gold(I) complexes.[18] The present study was aimed at the preparation and extensive characterisation of a series of *N*-(2-methylphenyl)imidodicarbonimidic diamide gold(I) and gold(III) complexes obtained from precursor starting materials, $AuC_6F_5(tht)$ and $dppm(AuNO_3)_2$. The ultimate future goal is to determine whether a possible synergism exists between the important metal-ligand functionalities incorporated into the complexes by assessment of their potential as anti-inflammatory and anti-cancer agents.

We were not successful in preparing gold(I) complexes containing the *N*-(2-methylphenyl)imidodicarbonimidic diamide ligand but still obtained interesting results. The synthesis and characterisation of the dinuclear bridged gold(I) compound, bis[μ_2-bis(diphenylphosphino)]methane(nitrato) digold(I) perdeuteromethanol, $(C_6F_5)_2Au^-$ with an unique imonium cation and new gold(III) complex of *N*-(2-methylphenyl)imidodicarbonimidic diamide will be reported in Chapter 4.

4.2 Results and discussion

Section 4.2.1 describes the preparation and isolation of the various gold(I) and gold(III) compounds of *N*-(2-methylphenyl)imidodicarbonimidic diamide, while section 4.2.2. is devoted to the spectroscopic characterisation of these compounds. In section 4.2.3 the crystal structures obtained are described. The molecular structure of an interesting

[18] M.V. Baker, P.J. Barnard, S. Berners-Price, S.K. Brayshaw, J.L. Hickey, B.W. Skelton, A.H. White, *Dalton. Trans.,* **2006**, 3708.

dinuclear bridged gold(I) compound, bis[μ_2-bis(diphenylphosphino)]methane(nitrato) digold(I) which co-crystallised with deuterated methanol and two interesting structures of $(C_6F_5)_2Au^-$ with an unique imonium cation and a new gold(III) complex of *N*-(2-methylphenyl)imidodicarbonimidic diamide are described for the first time.

4.2.1 Synthesis of synthetic methods

The preparation of a binuclear gold(I) complex with dppm as a ligand (Scheme 4.1) is described in section 4.2.1.1. The preparation of the various gold(I) complexes using *N*-(2-methylphenyl)imidodicarbonimidic diamide (Scheme 44.2.) are described in section 4.2.1.2 while the preparation of the gold(III) complex is summarised in Scheme 4.3 and described in section 4.2.1.3.

4.2.1.1 The preparation of a binuclear gold(I) complex containing a phosphine bridge.

A suspension of $AgNO_3$ in ethanol was added to $(dppm)AuCl_2$ in dichloromethane, whereupon the suspension was stirred and then filtered. The filtrate was evaporated to dryness *in vacuo*, yielding a microcrystalline material (Scheme 4.8).

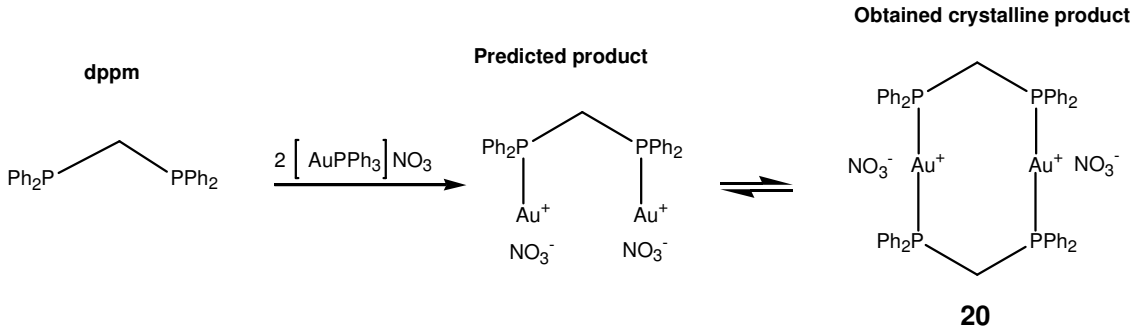

Scheme 4.8: Reaction scheme for the formation of complex **20**.

Compound **20** is somewhat unstable towards air. This complex is soluble in most organic solvents but insoluble in solvents like water and alkanes. Crystals suitable for an X-ray crystal structure determination were obtained from a concentrated solution of perdeuterated methanol in an NMR tube.

The dinuclear bridged cation, bis[μ_2-bis(diphenylphosphino)] digold(I), of the bis[μ_2-bis(diphenylphosphino)]methane(nitrato) digold(I), with various other anions was previously independently described by Schmidbaur and Bauer [19] and Usón and co-workers.[20] Our product is unique as a result of the inclusion of a nitrate anion involved in hydrogen bonding with deuterated methanol which co-crystallised with complex. The preparation of $[(dppm)_2(Au)_2]$ in literature[21] involved the reaction of the chloro-ylide gold(I) complex, $[AuCl(CH_2PPh_3)]$ with an equimolar amount of bis(diphenylphosphino)methane in an acetone solution resulting in precipitation of the yellow $[(dppm)_2(Au)_2]$ product. The crystal structure determination confirmed that the dinuclear bridged complex (Scheme 4.8) had formed, it was also characterised by NMR spectroscopy and MS spectrometry. The physical and analytical data of **20** are summarised in Table 4.1.

Table 4.1: Analytical data of complex **20**.

Complex	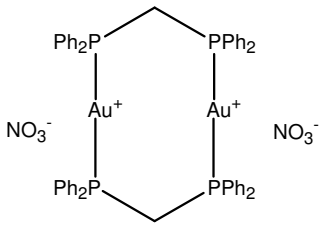 **20**
m.p. (ºC)	414.8
Colour	colourless
Crude yield (%)	88
M_r	1316.20
M_f	$C_{52}H_{50}Au_2N_2O_6P_2$

4.2.1.2 The preparation of a gold(I) complex with *N*-(2-methylphenyl)imidodicarbonimidic diamide from $Au(C_6F_5)(tht)$.

This procedure involves the substitution of the labile tht ligand in $AuC_6F_5(tht)$ by the diamide ligand yielding $AuC_6F_5(L)$, but the crystal structure determination of **21** and **21A**, however, revealed that a homoleptic rearrangement had occurred as shown in Scheme 4.9.

[19] H. Schmidbaur and A. Bauer, *J. Chem. Soc., Dalton Trans.,* **1997**, 1115.
[20] R. Usón. A. Laguna, M.Laguna, M. Concepción Gimeno, P.G. Jones, C. Fittschen, G.M. Sheldrick, *J. Chem. Soc., Chem. Commun*, **1986,** 509.

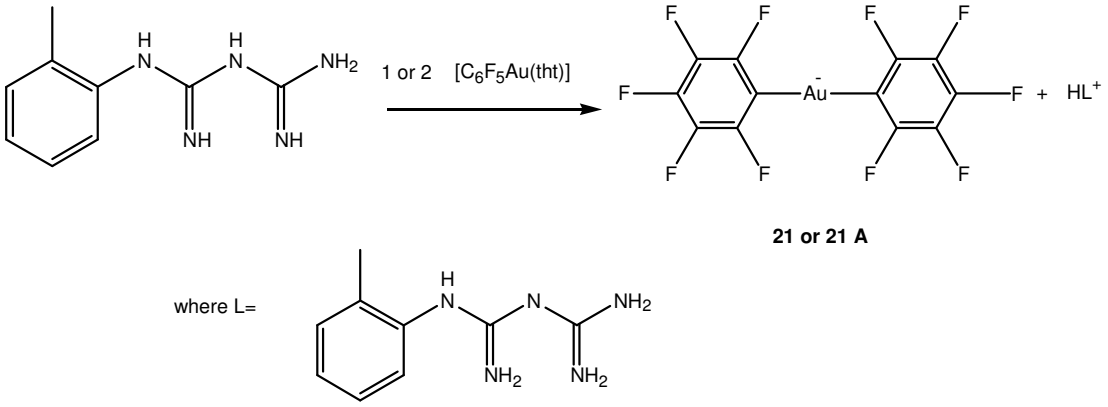

Scheme 4.9: The preparation of complex **21 or 21A.**

Compound **21** was prepared by treating a solution of $Au(C_6F_5)(tht)$ in diethyl ether, with an equimolar amount (**21**) or 0.5 molar equivalents of *N*-(2-methylphenyl)imidodicarbonimidic diamide (**21 A**) at room temperature under inert conditions. This followed a period of stirring where after the solvent was stripped off to yield **21** and **21 A** respectively. Crystal structure determinations of crystals obtained from concentrated solutions of the products of the two reactions (mentioned above), revealed the same compounds, had formed, except for the inclusion of solvent molecule in **21**. The compounds are bis(pentaflurophenyl)gold(I)anion and an *N*-(2 methylphenyl)imidodi-carbonimidic diamide cation (imonium cation). This imonium cation of *N*-(2 methylphenyl)imidodicarbonimidic diamide, that occurs in a tautomeric form (Scheme 4.10 **I** and **J**), can be represented as a cation wherein the positive charge is shared between the two nitrogen atoms as illustrated in Scheme 4.10 (**K**).

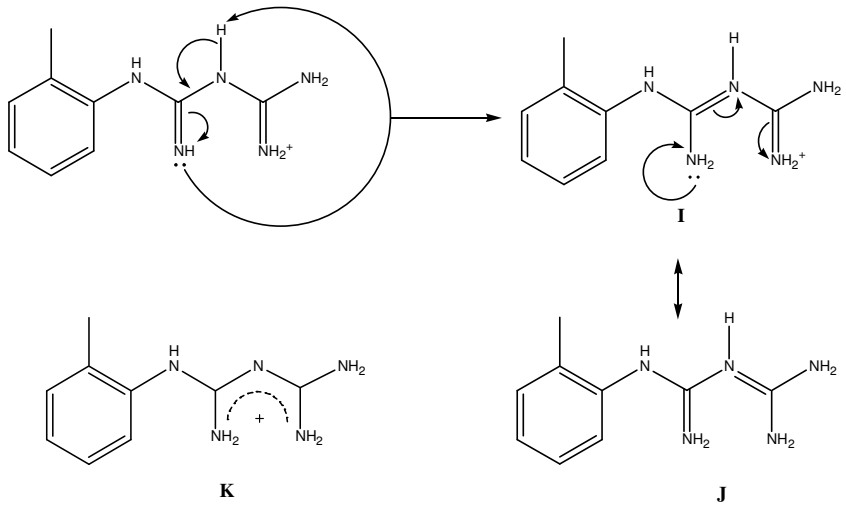

Scheme 4.10: The toutomeric forms (**I** and **J**) and imonuim cation (**K**).

Well documented ligand rearrangements of gold(I) are reported in literature and take place according to Eq. 1 (charges omitted), where L^1 and L^2 correspond to two different, normally soft, ligands.[21,22]

$$2\ AuL^1L^2 \rightleftharpoons AuL^1_2 + AuL^2_2 \qquad \text{Eq. (1)}$$

The formation of a anion in homoleptically rearranged products is a known feature in gold(I) chemistry and many examples exist in literature e.g. bis[(*o*-phenylene)bis(dimethylarsine)]gold(I) bis(pentaflurophenyl)gold(I). [23] This type of rearrangement was slow enough to be followed by ^{1}H NMR when isothiazole is used as N-heterocyclic substrate in the neutral complex (pentafluorophenyl)(isothiazol-5-ylidene)gold(I).[24] Trace amounts of the rearranged product formed within days while the reaction equilibrium was reached after 18 days. This reaction occurred more rapidly for (pentafluorophenyl)(isothiazol-5-yl)gold(I), the precursor complex, which prompted an *in situ* carbene preparation by immediate alkylation.

Compound **21** is very air and moisture stable. The complex is soluble in organic solvents such as acetone, dichloromethane, diethyl ether, or DMSO but insoluble in solvents like water and alkanes such as hexane and pentane. Crystals suitable for X-ray crystal structure determination of **21** were obtained by vapour diffusion of pentane into a solution of the compound in acetone and for **21A** by allowing slow crystallisation from a concentrated diethyl ether solution. Although it was possible to obtain the crystal structure of the compound, low solubility precluded characterisation by means of NMR and IR spectroscopy and MS spectrometry. The physical and analytical data of **21** are summarised in Table 4.2.

[21] S. Ahmad, *Coord. Chem. Rev.* **2004**, *248*, 231.
[22] S. Onaka, Y. Katsukawa, M. Shiotsuka, O. Kanegawa, M.Yamashita, *Inorg. Chim. Acta* **2001**, *312*, 100.
[23] R. Usón. A. Laguna, J. Vincente, J. Garcia, P.G. Jones, C. Fittschen and G.M. Sheldrick, *J. Chem. Soc., Dalton Trans.*, **1981,** 655.
[24] H.G. Raubenheimer, M.Desmet, G.J. Kruger, *J. Chem. Soc., Dalton Trans*., **1995**, 2067.

Table 4.2: The analytical data of **21**.

Complex	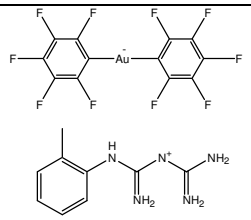 **21**
m.p. (ºC)	83-85
Colour	colourless
Crude yield (%)	83
Mr	738.35
M_f	$C_{22}H_{17}AuF_{10}N_5$

4.2.1.3 The preparation of a gold(III) complex of *N*-(2-methylphenyl)imidodicarbonimidic diamide.

The reaction of *N*-(2-methylphenyl)imidodicarbonimidic diamide with $Na[AuCl_4].2H_2O$ afforded complex **22** (Scheme 4.10).

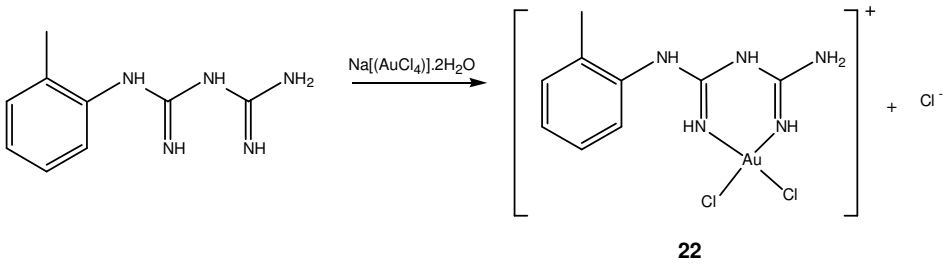

22

Scheme 4.10: The preparation of complex **22**.

A solution of $Na(AuCl_4).2H_2O$ in methanol/H_2O (3:2) was added to *N*-(2-methylphenyl)imidodicarbonimidic diamide and stirred for 18 h. The product was suspended in acetonitrile, centrifuged and the excess liquid was decanted. The orange product was obtained in high yield (0.414 g, 67 %). The compound is very air and moisture stable. The complex is soluble in organic solvents such as methanol, dichloromethane, or DMSO but insoluble in solvents like alkanes such as hexane or pentane. Crystals suitable for an X-ray crystal structure determination were obtained by allowing slow crystallisation from a concentrated methanol/H_2O solution. The physical and analytical data of complex **22** are summarised in Table 4.3.

The other example of a biguanidine coordinated to a gold(III) was reported by Lemoine and co-workers[37] and has a 1,1-dimethylbiguanide (metformin) as ligand, i.e. *cis*-dichloro(metforminuro)gold(III) dimethylacetamide solvate. In this instance, the biguanidine ligand is deprotonated while in our example, **22**, the ligand is not.

Table 4.3: Analytical data of complex **22**.

Complex	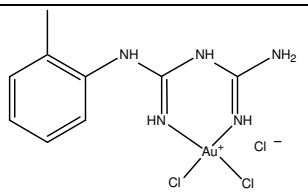 **22**
m.p. (ºC)	197 (decomp.)
Colour	colourless
Crude yield (%)	67
M_r	487.17
M_f	$C_{11}H_{19}AuN_5Cl_3$

4.2.2 Spectroscopic characterisation of compounds 20 and 22

4.2.2.1 Nuclear magnetic resonance spectroscopy

The ^{1}H NMR spectrum of complex **20** revealed that the phenyl protons all appear in their characteristic multiplet at δ 7.30-7.80 while a strong ethanol solvent peak obscures the signal for the CH_2 group of the dppm, at δ 1.2.

The ^{13}C NMR spectrum showed a multiplet at δ 134.8 and δ 130.9, these signals can be attributed to the *ortho* and the *meta* carbons of phenyl ring on the phosphine respectively. It is unusual for *ortho* and the *meta* carbons of this type of phenyl ring to be observed as multiplets and not as doublets (due to J_{pc}) but this can be attributed to magnetic inequivalence. The prerequisite for an atom to be magnetically equivalent is that nuclei must be isochronous: have the identical chemical shift and must display equal coupling (same *J* values). Thus in an AA'XX' system the conditions for magnetic equivalence, for A and X, implies that $J = J'$ and that L=0 so that a A_2X_2 spin system is obtained. The AA'XX' system where magnetic inequivalent atoms are observed is characterised by two

resonance frequencies ν and four coupling constants *J* i.e the A and X nuclei are chemically but not magnetically equivalent (Scheme 4.11).[25]

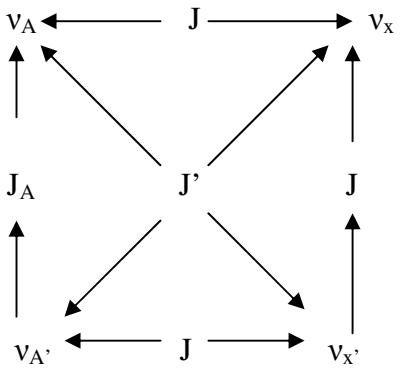

Scheme 4.11: The J-coupling observed for atoms that are magnetically equivalent but chemically equivalent.

The singlet carbon resonance at δ 134.0 and the doublet signal observed at δ 128.0 can be ascribed to the *ipso* and *para* carbons of the phenyl ring of the $AuPPh_2$-moiety. The CH_2 signal of the dppm is observed as a multiplet at δ 27.4. The presence of free $PPh_2CH_2PPh_2$ was observed in the ^{13}C NMR spectrum, possibly as a result of decomposition or unreacted reagent, the CH_2–group of the free ligand is observed as a multiplet at δ 39.6 while the phenyl carbons are observed in region of δ 128.9-129.0.

The ^{31}P NMR spectrum revealed a single broad peak at δ 37.1 that can be attributed to the coordinated phosphorus of the PPh_2-unit in complex **20**, while free dppm, formed as a result of decomposition or unreacted reagent, was observed as broad resonance at δ 27.9.

The ^{1}H, ^{13}C NMR and ^{31}P NMR spectroscopic data of **20** were obtained and summarised in Table 4.4.

[25]H. Günther, *Angew. Chem. Int. Ed.*, **1972**, 11, 861.

Table 4.4: ^{1}H ,^{13}C and ^{31} P NMR spectroscopic data of complex **20**.

		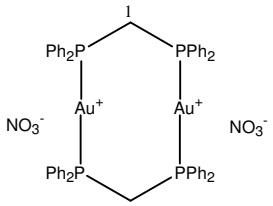 **20**
Solvent Temperature (°C)		methanol-d_4 25
Assignment		**Chemical shift**
^{1}H NMR (300/400 MHz)	CH_2	n.o.
	PPh_2	7.30-7.80 (m, 20H)
^{13}C NMR (75/100 MHz)	C^{ortho}	134.8 (m)
	C^{para}	134.0 (s)
	C^{meta}	130.9 (m)
	C^{ipso}	128.0 (d, ^{1}J = 67 Hz)
	C^{1}	27.4 (s)
^{31}P NMR (121MHz)	PPh_2	37.1 (s)

^{1}H and ^{13}C NMR spectroscopic data for the *N*-(2-methylphenyl)imidodicarbonimidic diamide ligand and complex **22** in DMSO-d_6 are summarised in Table 4.5.

The ^{1}H NMR spectrum showed that the signal of the phenyl protons appear as individual multiplets for H^{11}, H^{10}, $H^{12}$and H^{13} at δ 7,25, δ 7.07, δ 6.82, δ 6.76 in the free ligand and as a multiplet, that can not be assigned to individual protons, at δ 7.23 for the complex. The

methyl proton, H^{13}, resonates as an singlet at δ 2.08 in the free ligand and with a change in chemical shift of Δδ 0.42 downfield to δ 2.50 upon coordination to the metal.

The ^{13}C NMR spectrum displays the following downfield changes in chemical shifts of the signals of the carbons upon the coordination to the gold centre: i) The highly deshielded carbon, C^4, resonates at δ 161.1 thus reflecting a change in chemical shift of Δδ 1.3 downfield upon coordination to the metal. ii) The C^2 carbon is less shielded than C^4 and resonates as a multiplet at δ 156.9 in the complex, upfield (Δδ 0.3) from the same signal in the free ligand which is observed as a singlet at δ 157.2. Usually a downfield change in chemical shift, because of deshielding, is expected for the signals of the ligand upon coordination. This upfield change in chemical shift is not unusual as the total chemical shift σ ($\sigma = \sigma_p + \sigma_d$) in the ^{13}C NMR spectrum does not only reflect shielding and deshielding [26] as in the ^1H NMR spectra but it is constituted of a paramagnetic contribution (σ_p) and diamagnetic contribution (σ_d) which both play a significant role in determining the value of the chemical shift in the^{13}C NMR spectra. While the diamagnetic component (σ_d) is negligible in the ^1H NMR it needs to be considered in the^{13}C NMR spectrum.

The carbon, C^7, in complex **22** is observed as a multiplet signal of very low intensity at δ 154.9 representing a significant downfield shift of Δδ 5.6. The same signal is observed as a singlet in the free ligand at δ 149.3. The signals for the carbons, C^9 and C^{11}, in the ligand are observed as a high intensity singlet at δ 130.2 but in the complex, the signal for C^9 is observed as a singlet at δ 151.9 while the carbon, C^{11}, resonates as a singlet at δ 130.4. The signal for the carbon, C^8, resonates at δ 126.5 in the free ligand and experiences an upfield change in chemical shift of Δδ 0.2 to δ 126.3 upon coordination to the metal centre. The resonance the carbon C^{10} is observed at δ 126.1 in complex **22** indicating a downfield change in chemical shift of Δδ 3.6 from the same signal in the free ligand located at δ 121.5. The signal of C^{12} indicates a notable downfield change in chemical shift of Δδ 4.5 from δ 121.2 to δ 125.7 upon the coordination of ligand to the metal. The protons of the methyl signal are observed at δ 18.2 indicating a change in chemical shift of Δδ 0.4 downfield when compared to the same signal in the free ligand at δ 17.8.

[26] R.F. Fenske in: *Organometallic Compounds, Synthesis, Structure and Theory* (Ed. B.L. Shapiro), Texas A & M University Press, Texas, **1983**, p. 305.

Table 4.5: ^{1}H, ^{13}C and ^{31} P NMR spectroscopic data of complex **22.**

		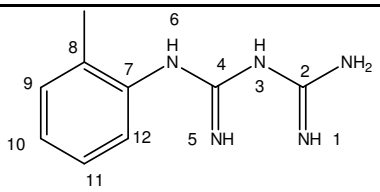 ***N*-(2 methylphenyl) imidodicarbonimidic diamide**	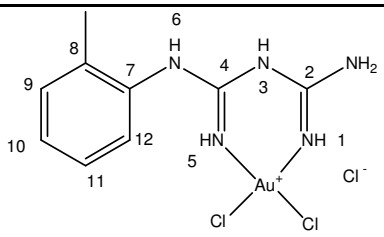 **22**
Solvent Temperature (°C)		$(CD_3)_2SO$ 25	$(CD_3)_2SO$ 25
Assignment		**Chemical shift (ppm)**	
^{1}H NMR (300/400 MHz)	H^{11}	7.25 (m, 1H)	
	H^{9}	7.07 (m, 1H)	
	H^{10}	6.82 (m, 1H)	
	H^{12}	6.76 (m, 1H)	
	H^{13}	2.08 (s, 3H)	7.23 (m, 4H) 2.50 (s, 3H)
^{13}C NMR (75/100 MHz)	C^{4}	159.8 (s)	161.1 (s)
	C^{2}	157.2 (s)	156.9 (m)
	C^{7}	149.3 (s)	154.9 (m)
	C^{9}	130.2 (s)	151.9 (s)
	C^{11}		130.4 (s)
	C^{8}	126.5 (s)	126.3 (s)
	C^{10}	121 .5 (s)	126.1 (s)
	C^{12}	121.2 (s)	125.7 (s)
	C^{13}	17.8 (s)	

4.2.2.1 Mass spectrometry

The mass spectrometric data of complexes 20 (FAB) and 22 (ES) are summarised in Table 4.6. In spite of the mild ionisation of the FAB-MS technique, no diagnostic peaks for **21** were observed.

Table 4.6: The mass spectrometric data of complexes **20** and **22**.

	***m/z* (*I* in %)**	
Fragment	**20**	**22**
$\{[M]\text{-}Cl\}^+$		458(100)
$\{[M]\text{-}2NO_3\}^+$	1161(55)	
$\{[M]\text{-}2NO_3\text{-}Au\}^+$	963(37)	
$\{[M]\text{-}2NO_3\text{-}Au\text{-}CH_2\text{-}(PPh_2)_2\}^+$	579 (43)	

The cation of the molecular ion of **20** was observed at *m/z* 1161 while the peak at *m/z* 963 corresponds to a peak representing the loss of an Au-unit from the molecular cation. This fragmentation is followed by the loss of dppm, yielding a fragment at *m/z* 579. The only peak observed for complex **22** was observed at *m/z* 458 which can be assigned to the cation of the molecular ion of this complex.

4.3 Structure determinations of 20, 21, 21A and 22

4. 3.1 Crystal and molecular structure of bis[μ2-bis(diphenylphosphino)]methane-digold(I) perdeuteromethanol nitrate, 20

Complex **20**, bis[μ_2-bis(diphenylphosphino)]methane-digold(I) perdeuteromethanol nitrate, crystallised to form colourless blocks from a deuterated methanol solution in the monclinic space group $P2_1/n$ with Z=2 molecules in the unit cell. This is the first example of bis[μ_2-bis(diphenylphosphino)]methane-digold(I) that has a deuterated molecule in the unit cell showing a hydrogen bond.[27] The asymmetric unit is shown in Figure 4.1 and relevant angles and distances are tabulated in Table 4.7

[27] L. de Jongh, C.E. Strasser, S. Cronje, H.G. Raubenheimer, *Acta. Crystallogr.*, **2007**, *E63*, m2137.

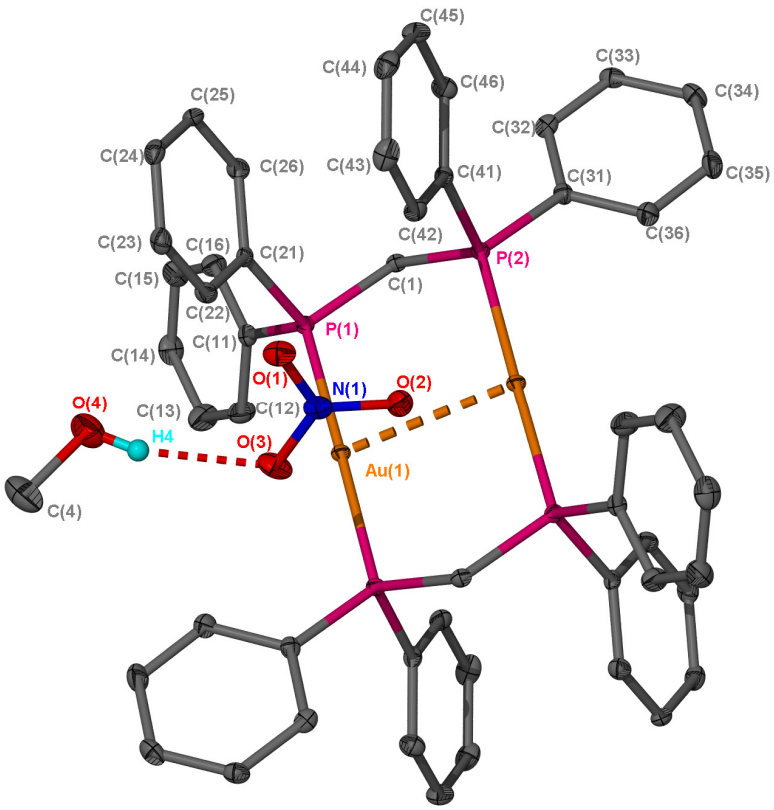

Figure 4.1: A view of the dication and one anion of **20** showing the atom-numbering scheme with the unlabelled atoms symmetry-generated.

The asymmetric unit of **20** consists of one half of the dication, $[(\mu\text{-dppm})_2Au_2]^{2+}$ and contains one nitrate anion and one deuterated methanol molecule. The rest of the molecule is related by a centre of symmetry at the mid point of the Au···Au vector. The Au···Au separation is 3.0245(3) Å and is in agreement with a strong Au···Au interaction.[28] The Au ions adopt the normal linear two-coordinated geometry that is slightly distorted by the aurophilic bonding, just like other compounds containing this type of dication.[29] The bond parameters are similar to reported values for $Au_2(dppm)$ with the novel tris(trichlorogermyl)gold(I) dianion, $[Au_2(dppm)_2][Au(GeCl_3)_3]$.[30] There is a short transannular intramolecular Au···Au interaction [3.0245(3) Å] in **20** but this is slightly longer than the same type of interaction in bis[μ-bis(diphenylphosphino)methane-digold(I) bis(perchlorate)[26] [2.9258(9) Å] and bis[μ-bis(diphenylphosphino)methane-digold(I) bis(hexafluorophosphate) dichloromethane[25] [2.98(2) Å]. The Au-P bond distances [2.3116(8) and 2.3173(8) Å] do not differ significantly from reported values (2.134(3) and

[28] H. Schmidbaur, *Chem Soc. Rev.*, **1995**, *24*, 391.
[29] M.N.I. Khan, C. King, D.D. Heinrich, J.P. Fackler (jr.), L.C. Porter, *Inorg. Chem.*, **1989**, *28*, 2150.
[30] A. Bauer, H. Schmidbaur, *J. Chem. Soc., Dalton Trans.*, **1997**, 1115.

2.179(1) Å). The P-Au-P angle [177.76º] is similar to the same angle in bis[μ-bis(diphenylphosphino)methane-digold(I) bis(hexafluorophosphate) dichloromethane disolvate[31] which has a value of 177.9(3)º. The P(1)-Au(1)-Au(1) angle [-x-1,-y-1,-z] of 89.62(2)º is in agreement with the same angle in bis[μ-bis(diphenylphosphino)methane-digold(I) bis(perchlorate) [91.02(4)º]. [32] and bis[μ-bis(diphenylphosphino)methane-digold(I) bis(hexafluorophosphate) dichloromethane disolvate [91.18º].[25]

Table 4.7: Selected bond lengths (Å) and angles (°) of **20** with estimated standard uncertainty in parenthesis (where ^{i} is -x-1,-y-1,-z).

Bond lengths (Å)	
Au(1)—P(1)	2.3116 (8)
Au(1)—P(2)^{i}	2.3175 (8)
Au(1)—Au(1)^{i}	3.0245 (3)
Bond angles (º)	
P(1)—Au(1)—P(2)^{i}	177.76 (3)
P(1)—Au(1)—Au(1)^{i}	89.62 (2)
P(2)i—Au(1)—Au(1)^{i}	91.70 (2)

The gold complex, nitrate and methanol are in layers parallel to the ac-plane. The phenyl rings of the ligand point into the methanol and nitrate layer. The nitrate anions form channels parallel to the a-axis. The nitrate anions are also aligned towards the gold atoms with distances of 3.47 Å for the Au [1-x, 1-y, -z] atom, which is symmetry generated, and 3.36 Å for the Au [x, y, z] atom. The perdeuteromethanol solvent is linked to the oxygen of the nitrate anion [O(4)–O(3) of 2.908(4)Å], *via* a hydrogen bond [O(4)-D(4)···O(3)] of 2.10(4) Å. Crystal lattice organization is governed by hydrogen bonding and aurophilic interactions.

[31] M. Wu, L. Zang, Z. Cheng, *Acta Crystallogr.*, **2003**, *E59*, m72.
[32] Q. Y. Cao, B. Yei, J. H. Liu, *Acta Crystallogr.*, **2006**, *E62*, m2730.

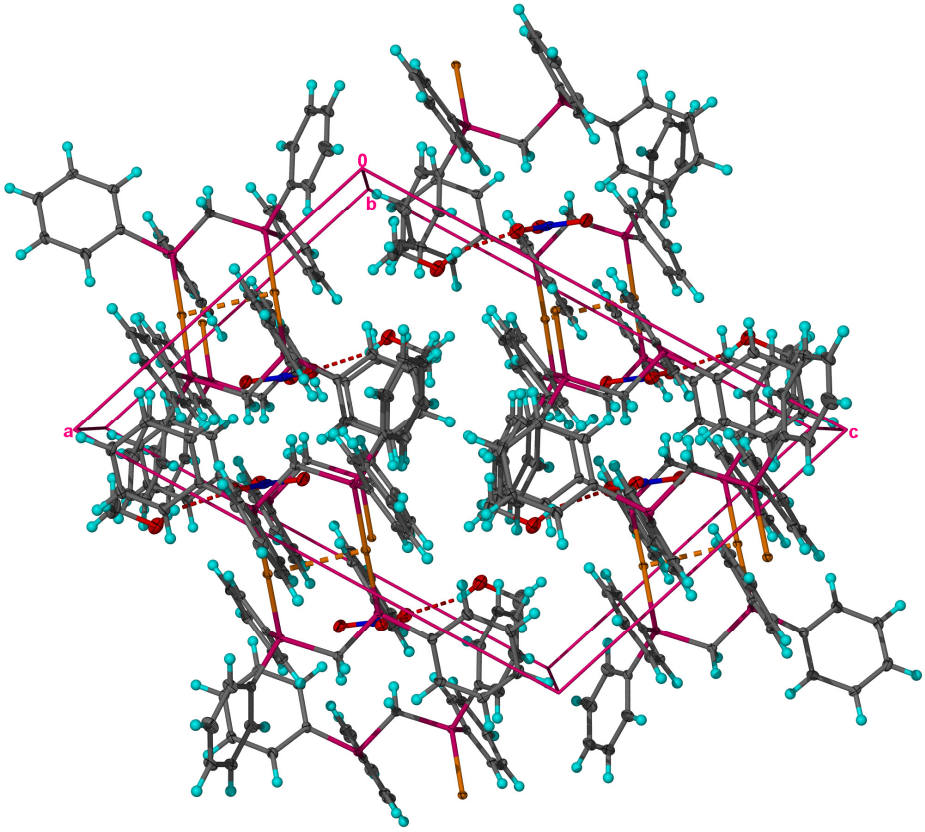

Figure 4.2: A view of the unit cell of **20** showing molecular packing along the ac-plane. Hydrogen atoms were omitted for clarity.

4.3.2 Crystal and molecular structure of N-(2-methylphenyl)imidodicarbonimidic diamide

The X-Ray structure of *N*-(2-methylphenyl)imidodicarbonimidic diamide, was determined so that the structural features of the free ligand could be compared to the coordinated ligand. The diamide, *N*-(2-methylphenyl)imidodicarbonimidic diamide, crystallised from a CH_2Cl_2 solution to form colourless blocks in the triclinic space group $P\bar{1}$ with Z = 8 molecules in the unit cell. There are 4 molecules per asymmetric unit with 2 molecules of water co-crystallised in the asymmetric unit. The asymmetric unit is shown in Figure 4.3 and the relevant angles and distances are tabulated in Table 4.8.

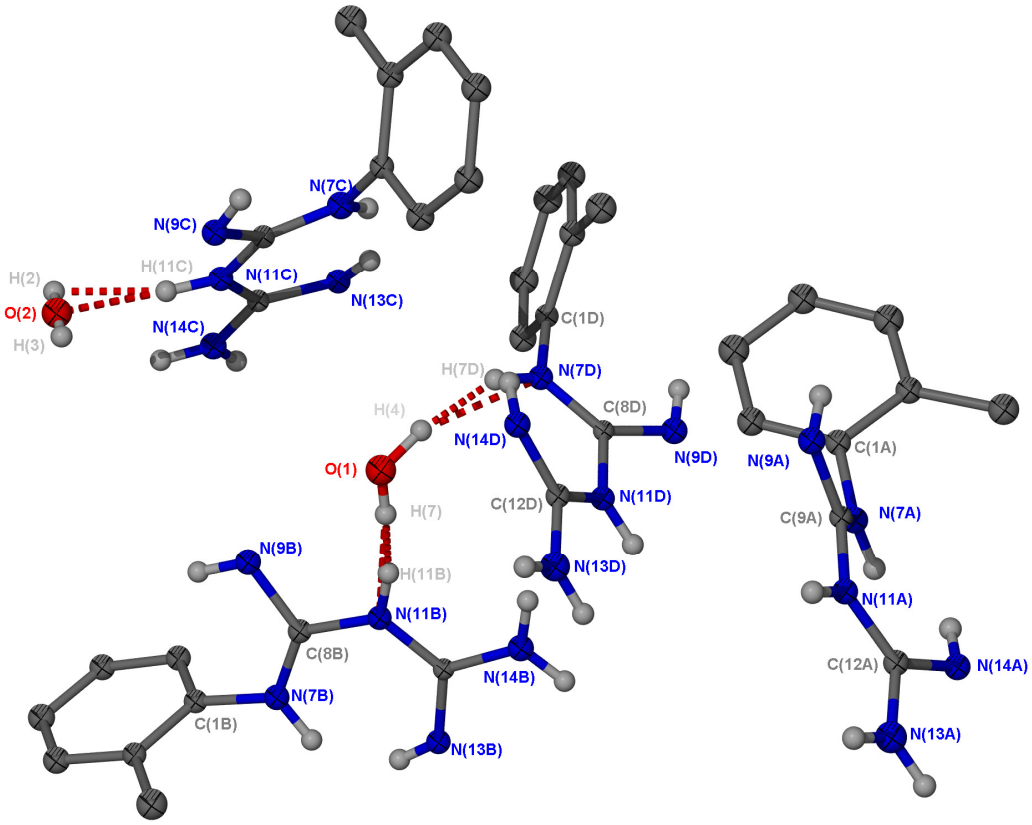

Figure 4.3: The molecular structure of *N*-(2-methylphenyl)imidodicarbonimidic diamide hydrate. Intramolecular hydrogen bonding and symmetry-generated hydrogen bonding were omitted for clarity.

The bond lengths and angles of the molecules in the asymmetric unit do not differ significantly from each other. The angles of the plane through the phenyl ring [C(1)-C(6)] and the N-backbone [N(7)-C(8)-N(9)-N(11)-C(12)-N(13)-N(14)] are 59.63 (0.16)º for molecule A , 63.36 (0.11)º for molecule B, 81.20 (0.12)º for molecule C and 65.52 (0.15)º for molecule D in the asymmetric unit (Figure 4.12). The bond C(1A)-N(7A), at 1.424(5) Å is the only true single bond and agrees with the reported standard value of 1.40Å,[33] while the length of the bond N(7A)-C(8A) [1.289(5) Å] is characteristic of a double bond and concurs with the reported standard value of 1.29 Å.[34] The other C-N bonds [C(8A)-N(9A), C(8A)-N(11A), N(11A)-C(12A) and C(12A)-N(14A) of 1.367(5), 1.376(5), 1.317(5) and 1.351(6) Å respectively] are shorter than the reported standard value for a single bond thus indicating double bond character and π-delocalation along the ligand backbone, N(7)-C(8)-N(11)-C(12)-N(13). The conclusion is supported by the N-C-N angles, N(7A)-C(9A)-N(11A) at 123.8(4)º, N(11A)-C(12A)-N(13A) at 118.8(4)º and

[33] A. Marchi, L. Marvelli, M. Cattabriga, R. Rossi, M. Neves, V. Bertolasi, V. Ferretti, *J. Chem. Soc., Dalton Trans,*. **1999**, 1937.

C(8A)-N(11A)-C(12A) [122 .7(4)º], which are all comparable to the angles around sp^2 hybridised atoms.

Table 4.8: Selected bond lengths (Å) and angles (°) of N-(2-methylphenyl)imidodicarbonimidic diamide with estimated standard uncertainty in parenthesis.

Bond lengths (Å)			
N(11B)-C(12B)	1.324(5)	N(11D)-C(12D)	1.317(5)
N(11B)-C(8B)	1.372(5)	N(11D)-C(8D)	1.375(5)
N(14B)-C(12B)	1.341(5)	N(9D)-C(8D)	1.359(6)
N(13B)-C(12B)	1.344(5)	N(7D)-C(8D)	1.297(5)
N(9B)-C(8B)	1.383(5)	N(7D)-C(1D)	1.423(5)
N(7B)-C(8B)	1.283(5)	N(14D)-C(12D)	1.349(5)
N(7B)-C(1B)	1.415(5)	N(13D)-C(12D)	1.318(5)
N(11A)-C(12A)	1.317(5)	N(11C)-C(12C)	1.321(5)
N(11A)-C(8A)	1.376(5)	N(11C)-C(8C)	1.369(5)
N(8A)-C(8A)	1.367(5)	N(14C)-C(12C)	1.345(5)
N(14A)-C(12A)	1.351(6)	N(7C)-C(8C)	1.292(5)
N(7A)-C(8A)	1.289(5)	N(7C)-C(1C)	1.407(6)
N(7A)-C(1A)	1.424(5)	N(13C)-C(12C)	1.343(6)
N(13A)-C(12A)	1.324(6)	N(9C)-C(8C)	1.381(6)
Bond angles(º)			
C(12B)-N(11B)-C(8B)	122 .7(4)	C(12D)-N(11D)-C(8D)	122 .7(4)
N(7B)-C(8B)-N(11B)	125.2(4)	N(11D)-C(12D)-N(13D)	118.6(4)
N(11B)-C(12B)-N(13B)	117.9(4)	N(7D)-C(8D)-N(9D)	123.6(4)
C(12A)-N(11A)-C(9A)	122 .7(4)	C(12C)-N(11C)-C(8C)	122 .9(4)
N(7A)-C(9A)-N(11A)	123.8(4)	N(7C)-C(8C)-N(11C)	125.2(4)
N(11A)-C(12A)-N(13A)	118.8(4)	N(11C)-C(12C)-N(13C)	118.1(4)

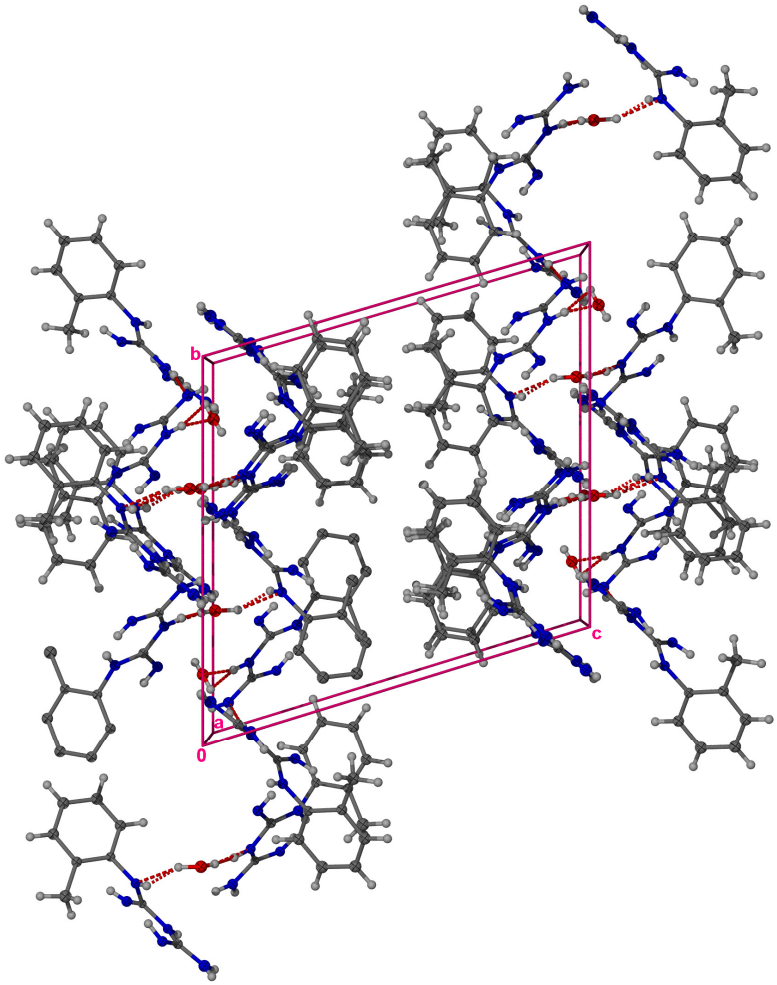

Figure 4.4: The solid-state packing of the diamide along the a-axis.

The repeating layers of the phenyl rings, with the shortest separation between layers of 9.8 Å, along the b-axis are not involved in π-stacking interaction and thus not important to crystal lattice organisation. The solvent molecule and nitrogen atoms are involved in hydrogen bonding, N(11B)-H(11B)···O(1) [1.84(5) Å] , O(1)-H(4)..N(7D) [2.29(7) Å], O(2)-H(10)···N(11C) [2.38(9) Å], N(7D)-H(7D)···O(1) [2.30(6) Å] and N(11C)-H(11C)···O(2) [1.85(5) Å]. The presence of hydrogen bonding between N(11) of each molecule and its symmetry generated neighbour's NH_2 group is also observed with N(11A)-H(11A)···N(13C) [x, 1+y, z] at 2.78(5) Å and N(11D)-H(11D)···N(13B) [-x, 1-y, -z] at 2.82(5) Å.

The presence of intramolecular hydrogen bonding is also observed between the hydrogen of N(14) and the atom N(7) and between the hydrogen of N(7) and the atom N(14) and the

distances of the interactions are tabulated in Table 4.9 for each molecule in the asymmetric unit.

Table 4.9: Intramolecular hydrogen bonds.

Hydrogen bonds lengths(Å)	
N(14A)-H(8)···N(7A)	2.19(5)
N(7A)-H(7A)···N(14A)	2.25(5)
N(14B)-H(14B)···N(7B)	2.21(4)
N(7B)-H(7B)···N(14B)	2.05(5)
N(14C)-H(14C)···N(7C)	2.21(4)
N(7C)-H(7C)···N(14C)	2.05(6)
N(14D)-H(14)···N(7D)	2.15(5)
N(7D)-H(7D)···N(14D)	2.29(6)

No other interactions are observed and the intricate network of hydrogen bonding seems to govern packing of crystal in solid state.

4.3.3.1 Crystal and molecular structures of 21 and 21A products of the homoleptic rearrangment.

Near linear geometry is observed for the central gold atom of the bis(pentafluorophenyl)gold(I) anion for **21** [177.9(3)º] and **21A** [178(6)º]. The Au-C distances are typical [Au(2)-C(10) (2.046(4) Å) and Au(2)-C(20) (2.053(3) Å) respectively] for **21** and for **21A** [Au(1)-C(30) (2.041(5)Å) and Au(1)-C(20) (2.043(5) Å) respectively]. Both these structural parameters are in agreement with bond lengths and angles in related compounds (2.041 Å and 177.90º).[34,35] The angle between the planes of pfp substituents approaches co-planarity in **21** with an interplanar angle of 9.58º [C(20)-Au(2)-C(10)-C(11) and C(10)-Au(2)-C(20)-C(25)] while in the structure of **21A** [C(20) Au(1)-C(30)-C(35) and C(30)-Au(1)-C(20)-C(21)] the pfp substituents are planar with an interplanar angle of 0.34 (0.06)º as observed for bis(*o*-phenylene)bis(dimethylarsine)-gold(I)[34] and bis(pentafluorophenyl)gold(I)[35] with the angle ~0º.

[34] R. Uson, A. Languna, J.Vicente, J. Garcia, P.G. Jones, G.M. Sheldrick, *J. Chem. Soc*., *Dalton Trans*., **1981**, 655.
[35] P.G. Jones, *Z. Kristalogr*., **1993**, *208*, 655.

4.3.3.1 Crystal and molecular structure of compound 21

Colourless needles of **21** were obtained from a concentrated solution of the compound in diethyl ether in the triclinic space group $P\bar{1}$ consisting of Z=2 in the unit cell. The asymmetric unit consists of a bis(pentaflurophenyl)gold(I)anion and an *N*-(2-methylphenyl)imidodicarbonimidic diamide cation. The cation presents itself as an imonuim compound which experiences hydrogen bonding to the neighbouring cation of next $[C_6F_5Au]^-$[imonuim cation]$^+$ ion pair. The unlabeled cation in Figure 4.15 is symmetry generated in order to portray the hydrogen bonding. The phenyl, methyl, terminal amine, and diethyl ether protons are fixed in calculated positions, while the rest of the hydrogen atoms were all located. The molecular structure and numbering scheme is shown in Figure 4.5 with the selected bond lengths and angles summarised in Table 4.10. The imonium cation is shown in Scheme 4.12.

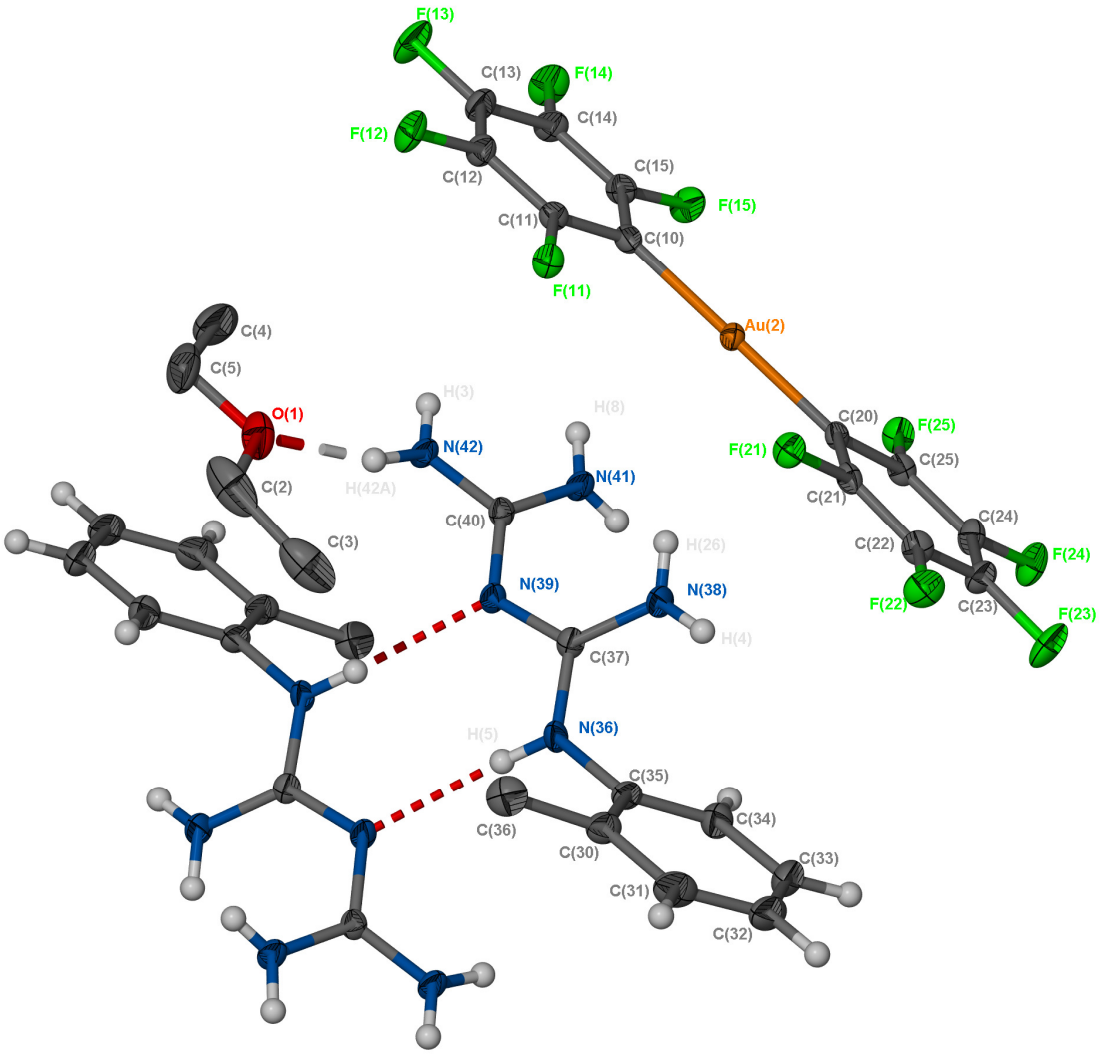

Figure 4.5: The molecular structure of **21**, hydrogen bonds are indicated by dashed lines.

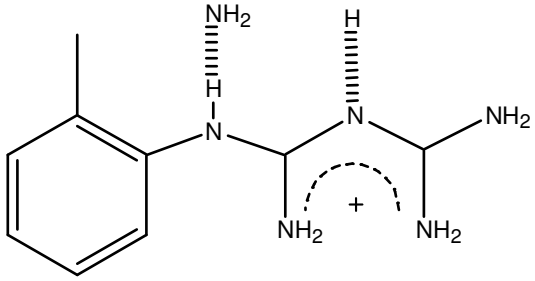

Scheme 4.12: The imonuim cation of complex **21** where hydrogen bonds are indicated by hashed line.

The C-N bonds, N(39)-C(37) [1.337(4) Å], N(39)-C(40) [1.348(4) Å], N(42)-C(40) [1.325(4) Å], N(38)-C(37) [1.334(4) Å], N(41)-C(40) [1.329(4) Å] and N(38)-C(37) [1.337(4) Å] all have intermediate bond length values between the reported values for a standard double bond C-N [1.27 Å][34] and single bond C-N [1.41 Å],[34] thus indicating delocalisation over these bonds, N(38)-C(37)-N(39)-C(40)-N(41), just as in the free ligand. The angles for the C-N backbone in **21** agree with same angles in the free *N*-(2-methylphenyl)imidodicarbonimidic diamide ligand. The angle between the planes defined by N(41)-N(37)-C(40) and N(39)-N(38)-N(36) is 46º for **21** but the same angle in the free ligand is only 8º, indicating that the C-N backbone in the free ligand is almost linear while half of C-N backbone is twisted at 46º angle in the cation of **21**. The angles between the plane defined by the phenyl ring [C(30)-C(31)-C(32)-C(33)-C(34)-C(35)-C(36)] and the N(36)-C(37)-N(39)-C(40) backbone is 56.6º and in agreement with the same angle between the same planes in the free ligand.

Table 4.10: Selected bond lengths (Å) and angles (°) of **21** with estimated standard uncertainty in parenthesis.

Bond lengths (Å)			
Au(2)-C(10)	2.046(4)	N(42)-C(40)	1.325(4)
Au(2)-C(20)	2.053(3)	N(38)-C(37)	1.334(4)
N(39)-C(37)	1.337(4)	N(41)-C(40)	1.329(4)
N(39)-C(40)	1.348(4)	N(38)-C(37)	1.337(4)
Bond angles (º)			
C(10)-Au(2)-C(20)	177.98(13)	N(41)-C(40)-N(39)	124.1(3)
C(37)-N(39)-C(40)	122.3(3)	N(39)-C(37)-N(38)	125.5(3)
N(42)-C(40)-N(41)	118.9(3)	C(37)-N(36)-C(35)	125.0(3)
N(42)-C(41)-N(39)	117.0(3)	N(39)-C(37)-N(38)	116.1(3)

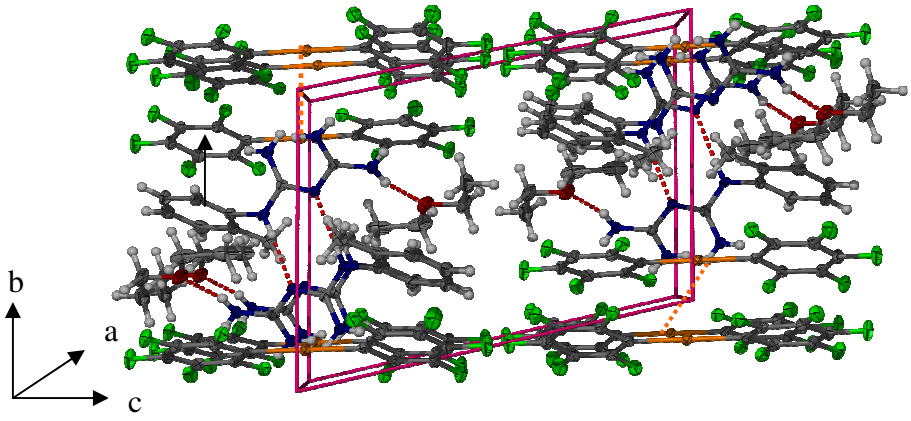

Figure 4.6: A view of the solid state structure of **21** along the a-axis.

The layers of anions along the c-axis are alternated by layers of cations along the b-axis producing 2 layers of cations along the b-axis in the ac-plane. The anions are positioned across another anion in a neighbouring layer along the a-axis. The same trend is observed for the cations along the same axis. The interdispersed double layer of cations prevents π-stacking of the pfp in the layers of anions, but π -stacking [3.869 Å] is observed in the same layer of molecules involved in Au···Au interactions [3.588 Å]. The hydrogen bonds observed are between the amine group of the imonium cation and the solvent molecule, N(42)-H(42A)···O(1) [1.97(4) Å] and the symmetry generated cation, N(36)-H(36A) [1-x;-y-1,-z] and N(39) [2.14(4)Å]. Packing in the crystal lattice seems to be governed by π-stacking, intermolecular Au···Au interactions and intricate network of hydrogen bonding.

4.3.3.2 Crystal and molecular structure of compound 21A

The compound **21A** crystallises from diethyl ether to form colourless needles in the triclinic space group $P\bar{1}$, with Z=2 molecules in the unit cell. The asymmetric unit consists of a bis(pentaflurophenyl)gold(I) anion and a *N*-(2-methylphenyl)imidodicarbonimidic diamide cation. The asymmetric unit of **21A** has the same content in the asymmetric unit of **21** but without the solvent molecule, diethyl ether. The compounds, **21** and **21 A**, were prepared under different reaction conditions but the crystal structure revealed same anion-cation pair. The complex **21A** was obtained by adding 2 molar equivalents of $Au(C_6F_5)(tht)$ and not 1 molar equivalent as in the case of **21**. The phenyl, methyl, and amine protons are fixed in calculated positions, while the rest of the hydrogens were all

located. The molecular structure and numbering scheme is shown in Figure 4.7 with selected bond lengths and angles summarised in Table 4.11.

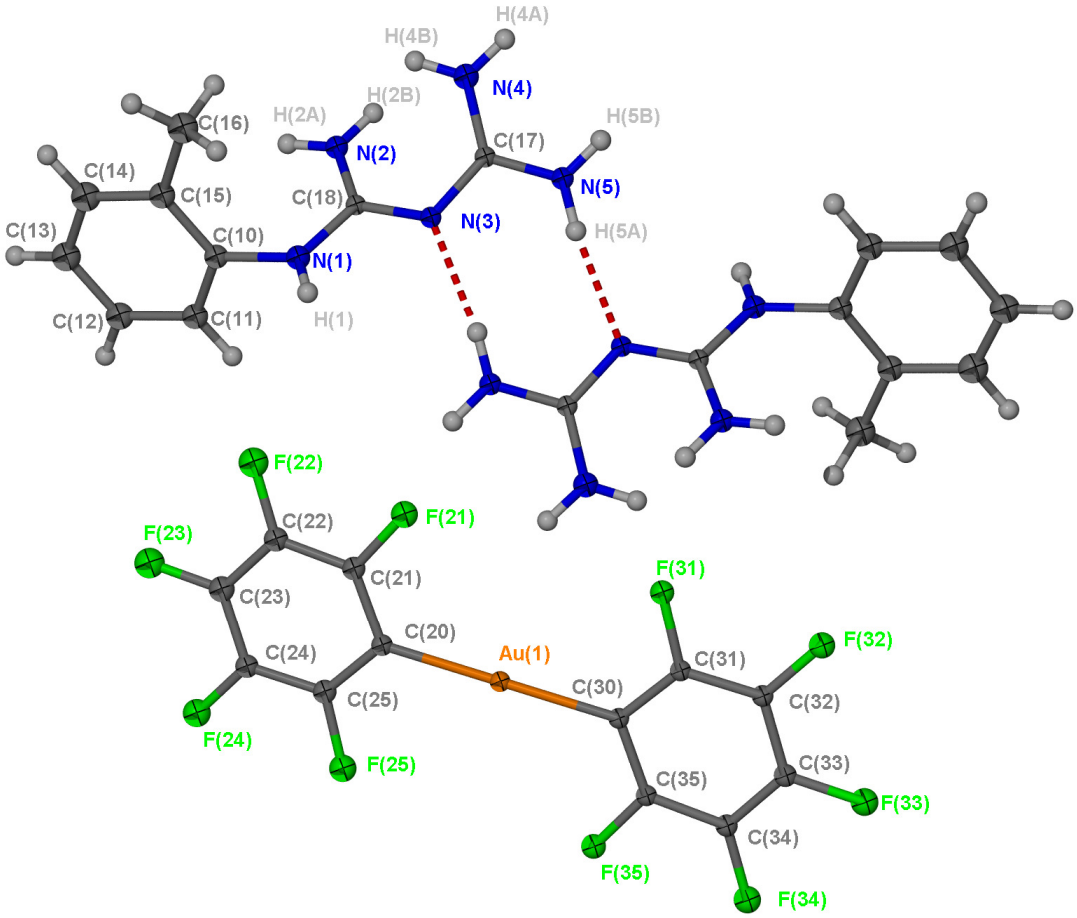

Figure 4.7: Molecular structure of **21A**.

The imonuim cation is identical to the cation of **21** and formation can be explained by Scheme 4.11. The only difference between the imonium cations of **21A** and **21** is the different hydrogen bonding (Scheme 4.13).

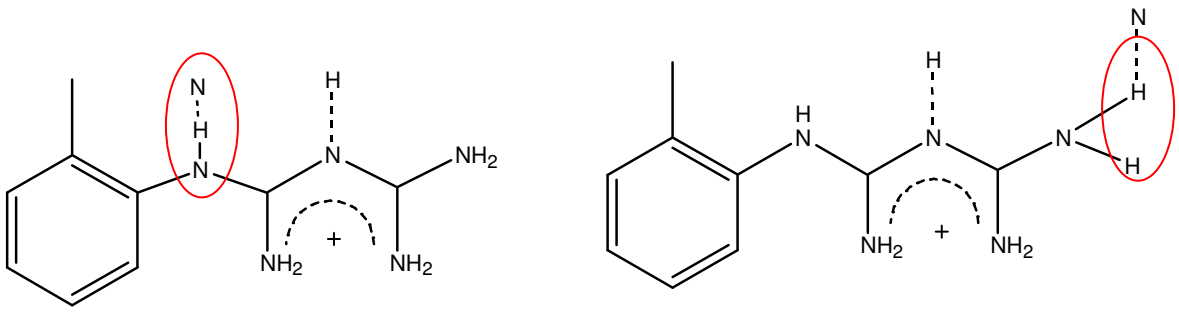

21 **21A**

Scheme 4.13: The difference between the crystal structure of **21** and **21A** is indicted by red circles.

The only true single bond C-N is C(10)-N(1) [1.446(6) Å]. The C-N bond lengths of N-backbone N(2)-C(18) [1.330(6) Å], C(18)-N(3) [1.341(6) Å], N(3)-C(17) [1.337(6)]and N(4)-C(17) [1.343(6) Å] are intermediate between a single bond C-N [1.41 Å][34] and a double bond C=N [1.27 Å],[34] suggesting charge stabilisation by extensive delocalisation of π-electrons over these bonds. The delocalisation over N(4)-C(17)- N(3)-C(18)-N(2) is again observed just as in the instance of the free ligand and **21**. The C-N bond lengths of C(17)-N(5) and C(18)-N(1) of 1.320 Å and 1.336 Å respectively also indicate some delocalisation. The bond angles of the atoms in the C-N backbone concur with those in **21**. The C(17)-N(3)-C(18) angle is 122.6(4)º cohering to the same angle in **21**.

The angle between the planes of the phenyl ring [C(10)-C(11)-C(12)-C(13)-C(14)-C(15)-C(16)] and N(1)-C(18)-N(2)-N(3) backbone is 60.3º and thus similar to the same angle in the free ligand and **21** . The N-backbone is not linear and the angle between the planes defined by N(38)-N(37)-C(36) and N(39)-N(40)-N(41) is 40.2º and which correlates to the angle of 46º in **21** but not to the angle in the free ligand (8º).

Table 4.11: Selected bond lengths (Å) and angles (°) of **21A** with estimated standard uncertainty in parenthesis

Bond lengths (Å)			
Au(1)-C(20)	2.041(5)	C(18)-N(3)	1.341(6)
Au(1)-C(30)	2.043(5)	N(3)-C(17)	1.337(6)
C(10)-N(1)	1.446(6)	N(4)-C(17)	1.343(6)
N(2)-C(18)	1.330(6)	C(17)-N(5)	1.320(6)
N(1)-C(18)	1.336(6)		
Bond angles (º)			
C(20)-Au(1)-C(30)	178.5(6)	C(17)-N(3)-C(18)	122 .6(4)
N(1)-C(18)-N(3)	116.6(4)	N(5)-C(17)-N(3)	116.9(4)
N(5)-C(17)-N(3)	116.9(4)		

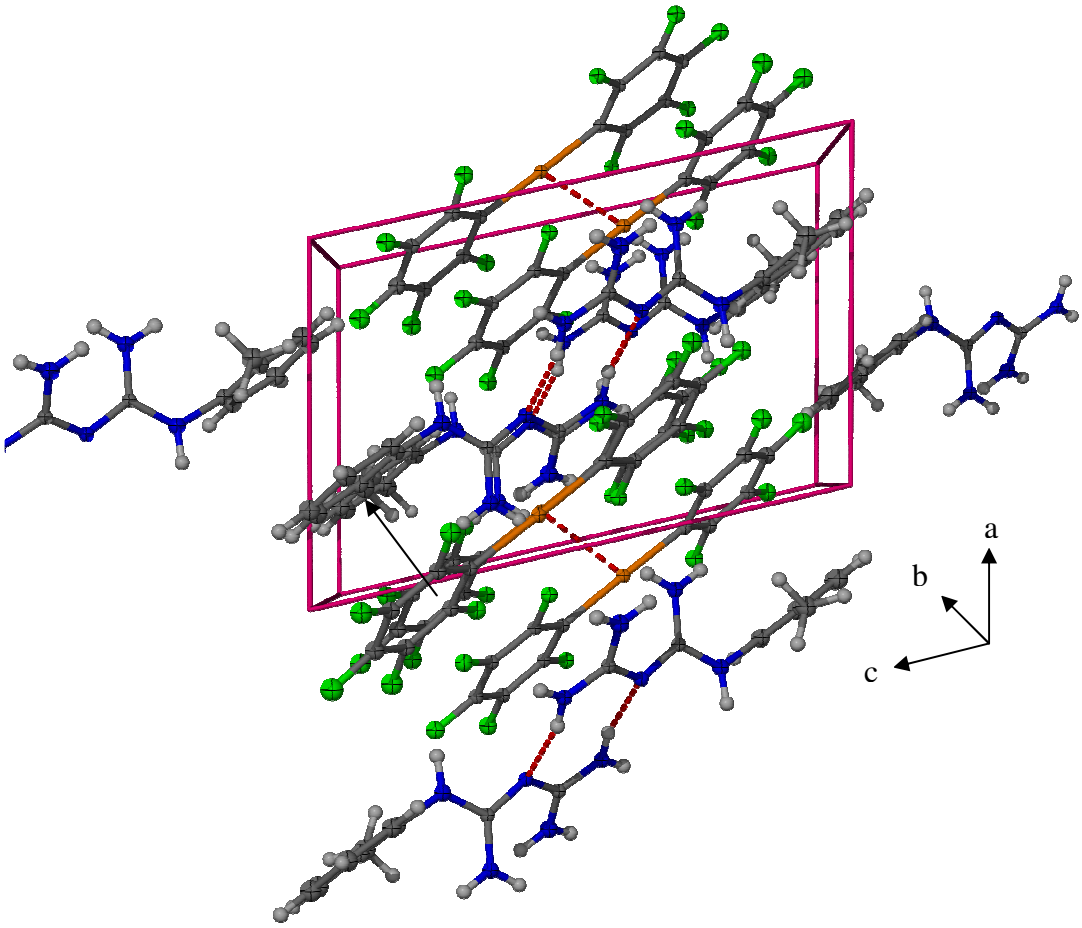

Figure 4.8: A view of the solid state structure of **21A** along the b-axis.

Two layers of anions are alternated by two layers of cations along the b-axis. The presence of a hydrogen bond between N(3) [2.09(6)Å] of the cation and the symmetry generated cation N(5)-H(5A) [-x-1,-y,1-z] is observed. The $Au(C_6F_5)^-_2$ is perfectly planar and an Au···Au [3.499 Å] interaction along the a-axis between two neighbouring anions in neighbouring layers is observed. The same unit that experiences the Au···Au interaction is also involved in π-stacking [3.559 Å]. Hydrogen bonding, aurophilic interaction and π-stacking thus govern the crystal lattice organization.

4.3.4 Crystal and molecular structure of compound 22

Complex **22** crystallised to form yellow blocks from a methanol/water solution in the monoclinic space group $P2_1/c$ with Z = 4 molecules in the unit cell. The asymmetric unit is shown in Figure 4.19 and relevant angles and distances are tabulated in Table 4.12.

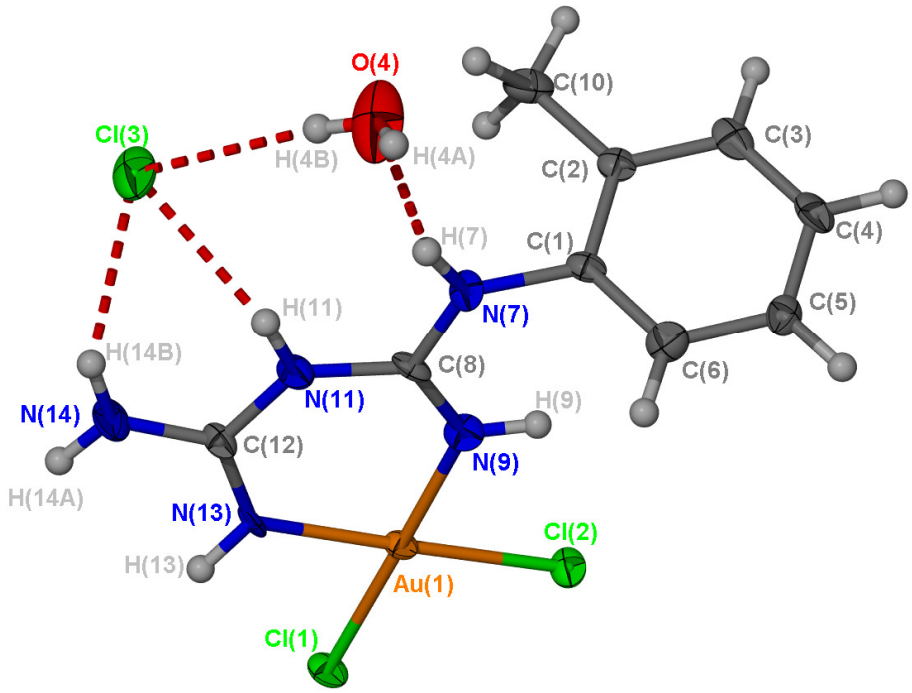

Fig. 4.9: The molecular structure of complex **22**. Hydrogen bonds are indicated with a red dashed line.

In this structure the ligand does not carry a negative charge as was observed for the reported example of the biguanidine ligand, metformin, in the complex dichloro(metforminuro)gold(III) dimethylacetamide.[36] The crystal structure determination of *cis*-dichloro(*N*-(2-methylphenyl)imidodicarbonimidic-diamide)gold(III) chloride shows clearly that the hydrogen atom is still present on the central N atom, N(11), with a chloride ion, rendering the overall complex neutral.

The crystal structure of **22** shows that Au(III) is bonded to two Cl atoms and to two nitrogen atoms of a *N*-(2-methylphenyl)imidodicarbonimidic diamide ligand which acts as a bidentate ligand, giving rise to a slightly distorted cationic square planar complex. As mentioned above a third Cl^- functions as the anion to this cation. The value of the N-Au-N bond angle at the Au atom, N(9)-Au(1)-N(13) [90.0(3)º], agrees with the values observed in *cis*-dichloro(metforminuro)gold(III) dimethylacetamide [88.3(4)-92.3(2)º].[36] The Cl(2)-Au(1)-Cl(1) [91.95(8)˚], is also in agreement with the literature value of *cis*-

[36] P. Lemoine, B. Viossat, D. Nguyen-Huy, *Z. Kristallogr.*, **1998**, *213*, 726.

dichloro(metforminuro)gold(III) dimethylacetamide [92.26º]. The Au-Cl bond lengths are 2.267(2) Å and 2.272(2) Å and are larger than the Au-Cl bond distances in 2,2-bipyridinedigold(III) tetrafluoroborate [2.252(4) Å] [37] but in agreement with *cis*-[ethylenediamine disulfitoaurate(III)[38] anions [2.287(4) Å]. The Au-N bond lengths [1.982(8) Å for Au(1)-N(9) and 1.970(1) Å for Au(1)-N(13)] are comparable to the values in *cis*-dichloro(metforminuro)gold(III) dimethylacetamide[31] [1.94(1) Å and 1.98(1) Å]. The C-N bond lengths, C(12)-N(13) [1.32(2) Å], C(12)-N(11) [1.36(2) Å], N(11)-C(8) [1.38(1)Å] and C(8)-N(9) [1.293(2)Å], indicate a degree of delocalisation. These bond lengths have values between the value of standard C-N double bond [1.27 Å][34] and single C-N bond [1.41 Å].[34] The bond length, C(8)-N(9) [1.29(2)º], shows double bond character when compared to standard reported C-N bond values for a double bond [1.27 Å].[34] The C(8)-N(11) [1.38(1) Å] bond value is a true single bond. There is no significant difference in bond lengths of the C(12)-N(13) bond when the coordinating ligand is compared to the free ligand. The noteworthy angle is C(12)-N(11)-C(8) which shows an increase from the angle in the free *N*-(2-methylphenyl)imidodicarbonimidic diamide of 122.4(8)º compared to 129.7(8)º. This may be attributed to the constraint placed on the ligand by its coordination. The other noteworthy angle is N(7)-C(8)-N(11) at a value of 115.8(8)º which shows a significant decrease when compared to the value in the same bond in the free ligand [125.2(4)º]. This may be as a result of the bond length of the C(8)-N(7) bond [1.34(1) Å] which shows an increase when compared to the free ligand [1.283(5) Å], indicating a degree of double bond character and thus delocalisation. The biguanide ligand has the same nearly planar geometry as the free ligand but π-conjugation along a different backbone is observed in complex **22** [N(7)-C(8)-N(11)-C(12)-N(13)] than in the free ligand [N(13)-C(12)-N(11)-C(8)-N(9)]. The plane through the phenyl ring [C(1)-C(2)-C(3)-C(4)-C(5)-C(6)- C(10)] is at an angle of 70.65 (0.19)º with the plane Cl(1)-Au(1)-N(9)-C(8)-N(11)-C(12)-N(13)-Au(1)-Cl(2).

[37] E.J.L. McInnes, A.J. Welch, L.J. Yellowlees, *Acta Crystallogr.*, **1995**, *C51*, 2023.
[38] F.H. Allen, O. Kennard, D.G. Watson, L. Brammer, A.G. Orpen, and R. Taylor*, J. Chem. Soc.*, *Perkin Trans. 2*, **1987**, *S1*.

Table 4.12: Selected bond lengths (Å) and angles (°) of **22** with estimated standard uncertainty in parenthesis.

Bond lengths (Å)			
Au(1)-N (9)	1.982(8)	C(12)-N(14)	1.33(2)
Au(1)-N(13)	1.970(7)	C(12)-N(11)	1.36(2)
Au(1)-Cl(2)	2.267(2)	N(7)- C(8)	1.34(1)
Au(1)-Cl(1)	2.272(2)	N(7)-C(1)	1.43(1)
N(9)-C(8)	1.29(2)	N(11)-C(8)	1.38(1)
N(13)-C(12)	1.324(2)		
Bond angles (º)			
N(9)-Au(1)-N(13)	90.0(3)	N(14)-C(12)-N(11)	115.5(8)
Cl(2)-Au(1)-Cl(1)	91.95(8)	C(12)-N(11)-C(8)	129.7(8)
N(13)-C(12)-N(14)	122.4(8)	N(7)-C(8)-N(11)	115.8(8)

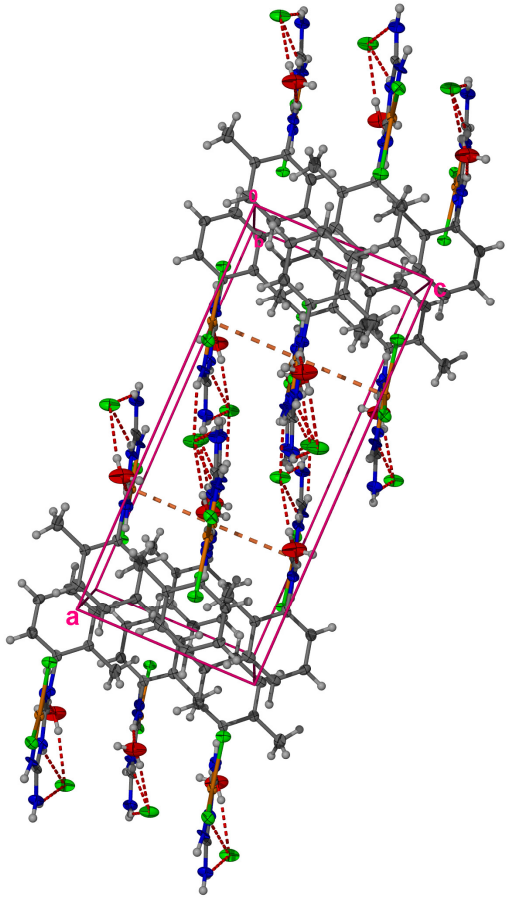

Figure 4.10: Crystal organization along the b-axis where the orange line dashed line indicates Au···Au interactions and the red lines (---) indicate hydrogen bonding.

The phenyl rings pack in layers along the a-axis which are alternated by the Au(III) layer. The closest contact for phenyl rings is 12.611 Å thus rendering π–stacking absent. The hydrogen bonds observed in the crystal lattice are N(11)-H(11)···Cl(3) [2.35(8)Å], N(14)-H(14B)···Cl(3) [2.45(9)Å], N(13)-H(13)···Cl(3) [2.36(8)Å]* (where * 1-X,Y-1/2,1/2-Z), N(7)-H(7)-O(4) [2.00(2)Å] and O(4)-H(4B)···Cl(3) [2.4 (1)º]. Hydrogen bonds ensure the crystalline cohesion.

4.3 Conclusions

In this chapter the formation of the dinuclear gold(I) complex bis[μ_2-bis(diphenylphosphino)methanedigold(I)] nitrate perdeuteromethanol, is reported. The complex was fully characterised by NMR spectroscopy, MS spectrometry and single crystal X-ray diffraction. The ^{13}C NMR revealed that in complex **20** the signal for the CH_2 carbon is observed at δ 27.4 significantly upfield from the same signal in the free ligand of δ 39.6. The structural analyses of complex **20** revealed the unexpected compound, bis[μ_2-bis(diphenylphosphino)methanedigold(I)] nitrate perdeuteromethanol, a dinuclear gold(I) complex thus co-crystallised with deuterated solvent, which we were first to report.[28] The crystal structure determinations also revealed that the nitrate anion and the deuterated methanol participate in hydrogen bonding and the cation is involved in intramolecular Au···Au interaction. These two types of interaction seem to govern the solid state packing of the complex.

We were first to report the X-ray structure of the free *N*-(2-methylphenyl)imidodicarbonimidic diamide water solvate, revealing the presence of 4 independent molecules per asymmetric unit displaying intra-and intermolecular hydrogen bonding. Delocalisation over the nitrogen backbone is observed in the molecule. Hydrogen bonding and π-stacking governs the crystal lattice organization.

The crystal structure of compounds **21** and **21A** showed a new imomium cation from *N*-(2-methylphenyl)imidodicarbonimidic diamide with a homoleptically rearranged $Au(C_6F_5)_2^-$ anion. The attempts to prepare gold(I) complexes with the diamide ligand thus also leads to the homoleptic rearranged products, **21** and **21A**.

The structures of both **21** and **21A** reveal the formation of an unique imonuim cation, with delocalisation over the central C-N backbone and with a hydrogen bond between the

central nitrogen and the hydrogen atom on the NH group next to the phenyl group of the neighbouring imonuim cation for **21**. The structure of **21A** displays additional delocalisation over the entire C-N backbone and a hydrogen bond *via* the terminal NH_2 group to a neighbouring cation. Solid state packing in both **21** and **21A** are governed by Au···Au interaction, π-stacking and hydrogen bonding.

The structure of the new cationic Au(III) complex of *N*-(2-methylphenyl)imidodicarbonimidic diamide was surprising, in that the ligand was not deprotonated as had been observed by Lemoine and co workers[37] in the structure of their neutral Au(III) complex, *cis*-dichloro(metforminuro)gold(III) dimethylacetamide. Complex **22** is square planar and again significant delocalisation is observed over the ligand backbone with hydrogen bonds that ensure the crystalline cohesion.

4.4 Experimental

4.4.1 General procedures and instruments

Experimental

Reactions were carried out under argon using standard Schlenk and vacuum line techniques. THF and diethyl ether were distilled under N_2 from sodium diphenyl ketyl, *n*-pentane from sodium, CH_2Cl_2 and methanol from $Mg(OCH_3)_2$, ethanol from $Mg(OEt)_2$ and acetone from 3Å molecular sieves. The NMR spectra were recorded on a Varian VXR 300 spectrometer (δ reported relative to the solvent resonance or external reference 85% H_3PO_4). The mass spectra were recorded on a VG-705EQ (FAB, 2-nitrobenzylalcholmatrix) or a Micromass Quattro Triple Quadrupole instrument (ES). Melting points were determined on a Stuart Scientific Melting Point Apparatus SMP3 and are uncorrected. The potassium tert-butoxide and $AgNO_3$ were purchased from Fluka while all the other reagents were purchased from Aldrich. The following gold(I) starting materials were synthesized using literature methods: chloro(triphenylphosphine)gold(I),[39] nitrato(triphenylphosphine)gold(I), [40] chloro(tetrahydrothiophene)gold(I), [41] chloro[bis(di-phenylphosphino)methane]gold(I)[42] and pentafluorophenyl(tetrahydrothiophene)gold(I).[43]

[39] M.I. Bruce, B.K. Nicholson, O. Bin Shawkataly, *Inorg. Synth,* **1989**, 324.
[40] L. Malatesta, L. Naldini, G. Simonetta, F. Cariati, *Coord. Chem. Rev.,* **1966**, *1*, 255.
[41] H.D. Kaesz, *Inorg. Synth*,, **1989**, *26*, 86.
[42] H Schmidbaur, A. Wohlleben, F. Wagner, O. Orama, G. Hutter, *Chem. Ber*., ***110***,1748.
[43] R. Usón, A. Laguna, M. Laguna, *Inorg. Synth*. **1989**, *26*, 85.

The methyllithium was standardised before use.[44] Elemental analysis was carried out at the Soil Science Department, University of the Stellenbosch. Prior to elemental analysis, the products were evacuated under high vacuum for 10 h.

4.4.2 Preparations and procedures

4.4.2.1 Preparation of bis[μ_2-bis(diphenylphosphino)methanedigold(I)] nitrate perdeuteromethanol, 20.

A suspension of $AgNO_3$ (0.68 g, 1.4 mmol) in ethanol (10 ml) was added to dppm$(AuCl)_2$ (0.61 g, 0.71 mmol) in dichloromethane (6 ml) and stirred for 2 h. The resulting solution was filtered with CH_2Cl_2 (60 ml). The filtrate was evaporated to dryness *in vacuo*, thus yielding microcrystalline material (0.85 g, 88 %) of **6**.

4.4.2.2 Preparation of N-(2-methylphenyl)imidodicarbonimidic diamide (penta-fluorophenyl)gold(I) diethyl ether, 21

The ligand, *N*-(2-methylphenyl)imidodicarbonimidic diamide (0.170 g, 0.89 mmol), was added to a solution of Au(C_6F_5)(tht) (0.403 g, 0.89 mmol) in diethyl ether (50 ml) and stirred at room temperature for 2 h. The resulting solution was then dried *in vacuo*, resulting in a white oily product that was washed with pentane (40 ml) to yield a colourless solid. The colourless product was then redissolved in diethyl ether (50 ml) and filtered through $MgSO_4$. The filtrate was then reduced to a colourless solid (0.59 g, 83 %) in high yield. Crystals were obtained by slow diffusion of *n*-pentane into a concentrated solution of **21** in diethyl ether at - 21 ºC.

4.4.2.3 Preparation of N-(2-methylphenyl)imidodicarbonimidic(pentafluoro-phenyl) gold(I), 21A.

The ligand, *N*-(2-methylphenyl)imidodicarbonimidic diamide (0.068 g, 0.35mmol), was added to a solution of AuC_6F_5(tht) (0.332 g, 0.71 mmol) in diethyl ether (50 ml) and stirred at room temperature for 2 h. The resulting solution was then dried *in vacuo*. The

[44] M.R. Winkle, J.M. Laansinger, R.C. Ronald, *J. Chem. Soc., Chem.Comm.*, **1980**, *87.*

colourless product was redissolved in diethyl ether (20 ml) and filtered through $MgSO_4$. The filtrate is then reduced to a colourless solid. Crystals were obtained from slow diffusion of *n*-pentane into a concentrated solution of **21A** in diethyl ether at - 21 ºC.

4.4.2.4 Preparation of cis-dichloro(N-(2-methylphenyl)imidodicarbonimidic-diamide)gold(III) chloride, 22

A solution of $Na[AuCl_4].2H_2O$ (0.54 g, 1.4 mmol) in methanol/H_2O (3:2) was added to *N*-(2-methylphenyl)imidodicarbonimidic diamide (0.24 g, 1.4 mmol) and stirred for 18 h. The product was suspended in acetonitrile, centrifuged and the excess liquid was decanted. The orange product was dried *in vacuo*, yielding 0.414 g (67 %) of **22**. Crystals were obtained from the concentrated solution in methanol at room temperature.

4.6 X-ray structure determinations

The crystal data collection and refinement details of compounds ***N-(2-methylphenyl)imidodicarbonimidic diamide***, **20, 21, 21A** and **22** are summarised in Tables 4.13 - 4.15. Data sets were collected on a Bruker SMART Apex CCD diffractometer with graphite monochromated MoK_α radiation (λ=0.71073 Å).[45] Data reduction was performed according to standard methods using the software package Bruker SAINT and data were treated with SADABS.[46,47,48] All the structures were solved using direct methods or the interpretation of a Patterson synthesis, which yielded the positions of the metal atoms, and conventional difference Fourier methods. All non-hydrogen atoms were refined anisotropically by full-matrix least squares calculations on F^2 using SHELX-97[49] within the X-seed environment.[50,51] Figures were generated with X-seed[50] and POV Ray for Windows, with the displacement ellipsoids at 50% probability level. Further information is available from Dr. S. Cronje at the Department of Chemistry and Polymer Science, Stellenbosch University.

---

[45] SMART Data Collection Software (version 5.629), Bruker AXS Inc. (Madison), WI, **2003**.
[46] SAINT, Data Reduction Software (version 6.45), Bruker AXS Inc. (Madison), WI, **2003**.
[47] R.H. Blessing, *Acta Crystallogr.,* **1995**, *A51*, 33.
[48] SADABS (version 2.05), Bruker AXS Inc. (Madison), WI, **2002**.
[49] G.M. Shelrick, SHELX-97. Program for Crystal Structure Analysis, University of Göttingen (Germany), **1997**.
[50] L.J. Barbour, *J. Supramol. Chem,*. **2003**, *1*, 189.
[51] J.L. Atwood, L.J. Barbour, *Cryst. Growth Des.,* **2003**, *3*, 3.

Table 4.13: Crystallographic data of *N*-(2-methylphenyl)imidodicarbonimidic diamide and compound **20**

Compound	***N-(2-methylphenyl)imidodicarbonimidic diamide***	**20**
Molecular formula	$C_{18}H_{27}N_{10}O$	$C_{52}H_{50}Au_2N_2O_6P_2$
Molecular weight	399.50	1358.7136
Wavelength (Å)	0.71073	0.71073
Crystal system	triclinic	monoclinic
Crystal dimensions	0.20 x 0.05 x 0.02 mm^3	$0.27 \times 0.19 \times 0.13$ mm^3
Crystal shape and	colourless blocks	colourless prism
Space group	$P\bar{1}$ (No. 2)	space group $P2_1/n$ (No. 14)
a (Å)	9.88(2)	11.6214(8)
b (Å)	14.581(2)	13.6313(9)
c (Å)	15.394(2)	16.432(1)
α (°)	73.449(2)	90
β (°)	80.604(2)	109.048(1)
γ (°)	89.982(2)	90
Volume ($Å^3$)	2094.7(5)	2460.5(3)
Z	8	2
d_{calcd} (g/cm^3)	1.267	1.894
μ (Mo-Ka) (mm^{-1})	0.086	6.143
Absorption correction	Semi-empirical from equivalents	Semi-empirical from equivalents
$F_{(000)}$	852	1320
θ-range for data	1.40 to26.43	1.89 to 26.39
Index range	-12<h<12, -18<k<18,-19<l<19	-14< h <14, -17< k <12, -20< l <18
No. of reflections	22251	14182
No. of unique	8519 unique(R_{int}=0.0560)	5019 unique (R_{int} =0.0251)
Max. and min.	0.9832 and 0.9983	0.2908 and 0.4977
Refinement parameters	285 parameters, 0 restraints.	309 parameters, 0 restraints.
Goodness of fit on F^2	1.715	1.064
Final R-indices	R_1 = 0.1231	R_1 = 0.0218
[I>2σ>(I)]	wR_2 = 0.2706	wR_2 = 0.0507
R indices (all data)	R_1 = 0.1620	R_1 = 0.0248
	wR_2 = 0.3022	wR_2 = 0.0517
Largest diff. peak and	-0.916 and 0.826	-0.456 and 1.637
Weigthing Scheme [a]	a = 0.10000	a = 0.0256 / b = 0.7357

[a] $wR_2 = \{\Sigma[w(F_o^2-F_c^2)^2]/\Sigma[w(F_o^2)^2]\}^{1/2}$; $w = 1/[\sigma^2(F_o^2)+(aP)^2+bP+d+\text{esin}\theta]$; $P = [f(\text{Max}(0 \text{ or } F_o^2)] + (1\text{-f}) F_c^2$

Table 4.14: Crystallographic data for compounds **21** and **21A**.

Compound	**21**	**21A**
Molecular formula	$C_{25}H_{23}AuF_{10}N_5O$	$C_{21}H_{13}AuF_{10}N_5$
Molecular weight	796.45	722. 33
Crystal system	triclinic	triclinic
Crystal dimensions (mm)	0.20 x 0.05 x 0.02 mm^3	0.09 x 0.06x 0.04 mm^3
Crystal shape and colour	Colourless needles	Colourless needles
Space group	$P\bar{1}$ (No. 2)	$P\bar{1}$ (No. 2)
a (Å)	9.671 (2)	8.889(2)
b (Å)	10.602(2)	9.657(2)
c (Å)	14.620(3)	13.533(3)
α (°)	76.191(3)	96.779(3)
β (°)	71.307(3)	102.511(3)
γ (°)	85.603(3)	92.000(3)
Volume ($Å^3$)	1379.0(5)	1124.0(4)
Z	2	2
d_{calcd} (g/cm^3)	1.918 g/cm^3	2.134 g/cm^3
μ (Mo-Ka) (mm^{-1})	5.431 mm^{-1}	6.648 mm^{-1}.
Absorption correction	Semi-empirical from equivalents	Semi-empirical from equivalents
F(000)	770	686
θ-range for data collection	1.51 to 28.39	1.55 to 26.46
Index range	$-12 < h < 12$, $-13 < k < 14$, $-18 < l < 18$	$-11 < h < 11$, $-12 < k < 12$, $-16 < l < 16$
No. of reflections	16217 reflections collected	12164 reflections collected
No. of unique reflections	6434 unique (R_{int}= 0.0261)	4592 unique (R_{int} =0.0236)
Max. and min. transmission	0.9832 and 0.9983	0.3833 and 0.5981
Refinement parameters / restraints	410 parameters, 0 restrains	166 parameters, 6 restraints
Goodness of fit on F^2	1.072	1.049
Final R-indices [I>2σ>(I)]	R_1 =0.0253	R_1= 0.0339
	wR_2= 0.0584	wR_2=0.0869
R indices (all data)	R_1 =0.0297	R_1 =0.0355
	wR_2 =0.0672	wR_2 =0.0881
Largest diff. peak and hole	-0.811 and 1.551	4.101 and -3.294
Weighting Scheme [a]	a= 0. 0399	a =0.0630/ b= 1.7226

[a] $wR_2 = \{\Sigma[w(F_o^2-F_c^2)^2]/\Sigma[w(F_o^2)^2]\}^{1/2}$; $w = 1/[\sigma^2(F_o^2)+(aP)^2+bP+d+\text{esin}\theta]$; $P = [f(\text{Max}(0 \text{ or } F_o^2)] + (1\text{-}f)\ F_c^2$

Table 4.15: Crystallographic data for compound **22**.

Compound	**22**
Molecular formula	$C_9H_{15}AuCl_3N_5O$
Molecular weight	512.58
Wavelength (Å)	0.71073
Crystal system	Monoclinic
Crystal dimensions (mm)	0.24 x 0.11x 0.03 mm^3
Crystal shape and colour	Yellow blocks
Space group	$P2_1/c$ (No.14)
a (Å)	16.501(3)
b (Å)	12.413(2)
c (Å)	7. 222(1)
α (°)	90
β (°)	90
γ(°)	90
Volume ($Å^3$)	1491(4)
Z	4
d_{calcd} (g/cm^3)	2.302 g/cm^3
m (Mo-Ka) (mm^{-1})	10.487 mm^{-1}
Absorption correction	Semi-empirical from equivalents (SADABS)
$F_{(000)}$	968
q-range for data collection (°)	-20< h < 18, -15 < k <15,-6< l< 9
Index range	1.23 to 26.47
No. of reflections collected	7986
No. of unique reflections	2489 unique ($R_{int=}$0.0442)
Max. and min. transmission	0.2978 and 0.8252
Refinement parameters / restraints	181 parameters/3 restraints.
Goodness of fit on F^2	1.072
Final R-indices [I>2s >(I)]	R_1=0.0596 wR_2 =0.1049
R indices (all data)	R_1=0.0455 wR_2= 0.0994
Largest diff. peak and hole ($e.A^{-3}$)	-1.789 and 3.611
Weighting Scheme [a]	a=0.0487 / b= 6.2802

[a] $wR_2 = \{\Sigma[w(F_o^2-F_c^2)^2]/\Sigma[w(F_o^2)^2]\}^{1/2}$; $w = 1/[\sigma^2(F_o^2)+(aP)^2+bP+d+\text{esin}\theta]$; $P = [f(\text{Max}(0 \text{ or } F_o^2)] + (1\text{-f}) F_c^2$